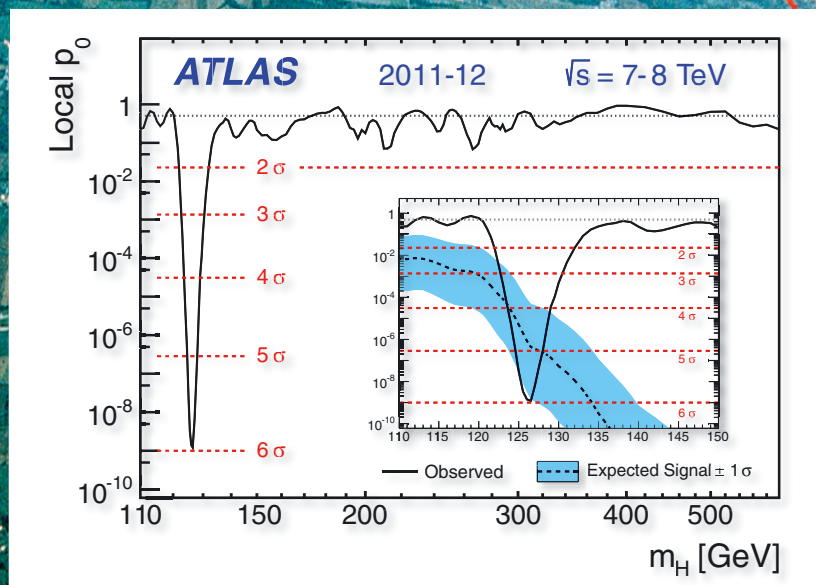
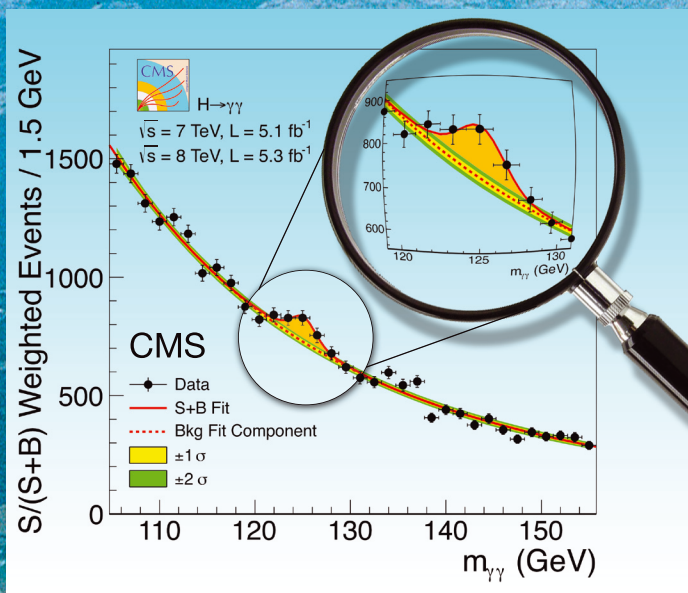


First observations of a new particle in the search for the Standard Model Higgs boson at the LHC



Two quotations from the experimental papers presented in this publication:

"... The search for the Higgs boson, the only elementary particle in the Standard Model that has not yet been observed, is one of the highlights of the Large Hadron Collider physics program."

- ATLAS Collaboration

"... The decay to two photons indicates that the new particle is a boson with spin different from one. The results presented here are consistent, ... with expectations for a standard model Higgs boson."

- CMS Collaboration

The discovery at CERN of a particle, most probably identifiable with the Scalar boson introduced by Brout and myself as part and parcel of a mechanism giving mass to gauge fields, is an impressive historic event. Writing these notes, I revive the intensity of these early collaborations with my companion in physics and lifelong friend Robert Brout who contributed so much to set the stage for this discovery but unfortunately passed away last year and missed its dramatic announcement.

Our approach was done in the quantum field theory framework. Shortly after, the same scheme was proposed independently by Higgs using the classical field approach. The mechanism proposed in these two approaches not only allowed for gauge field masses but also permitted the spontaneous generation of elementary fermion masses in chiral theories [such as $SU(2)_L \times U(1)_Y$] by absorbing the unobserved massless Nambu-Goldstone bosons in the massive gauge fields. This was realized in the Electroweak Theory proposed in 1967 by Weinberg.

The importance of the discovery of the Scalar boson is that it provides a direct verification of the mechanism, which for the first time led to a renormalizable and hence consistent quantum theory of charged gauge vector bosons. This was proven in 1971 by 't Hooft and Veltman, and a qualitative understanding of the issues involved emerges in comparing the two aforementioned approaches. The renormalizability of the mechanism opened the way to the modern view of unified laws of nature.

Not only does the discovery yield the missing link to the present Standard Model theory of elementary particles, but a detailed analysis of the decays, in particular of the decay of the Scalar to two photons which is sensitive to loops of intermediated charged particles, will possibly yield information about the spectrum beyond the Standard Model.

Prof. François Englert

A handwritten signature in black ink, appearing to be 'F. Englert', written in a cursive style.



SCHOOL of PHYSICS and ASTRONOMY

The University of Edinburgh
James Clerk Maxwell Building
The King's Buildings
Mayfield Road
Edinburgh EH9 3JZ

Telephone +44 (0)131 650 1000
or direct dial +44 (0)131 650 5249

Fax +44 (0)131 650 5902

Email info@ph.ed.ac.uk

www.ph.ed.ac.uk

Congratulations to both
Atlas and CMS Collaborations
and to the builders of the LHC
on a magnificent achievement!

Peter Higgs

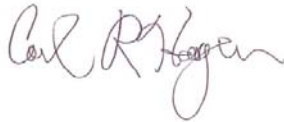
30 August 2012

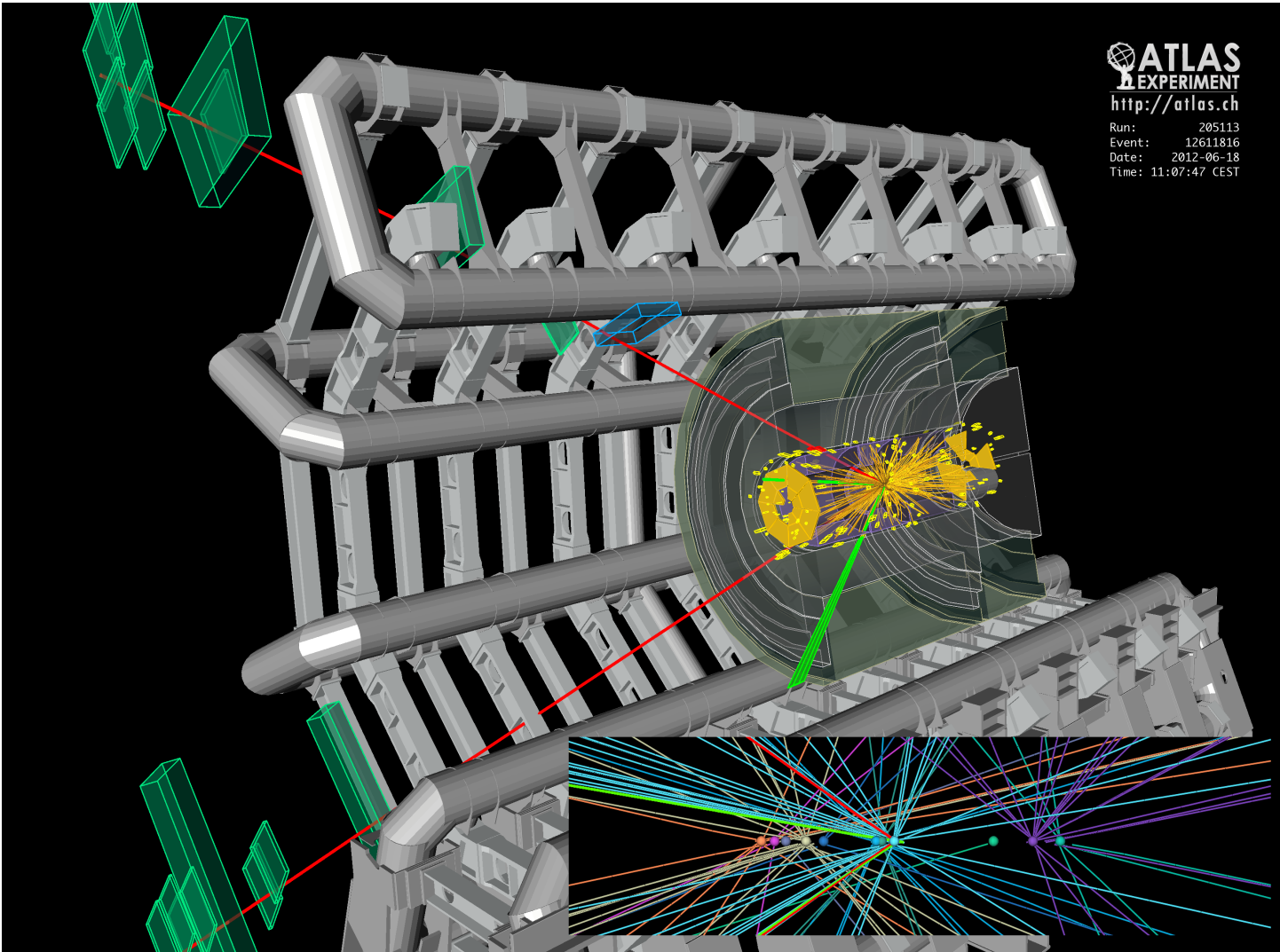
It is somewhat surreal to find that work we did nearly fifty years ago is once again at the centre of attention. This is a triumph for the standard model of particle physics, but even more for the experimenters. The achievement of the two great experimental collaborations reported here is quite magnificent. They have devoted decades to planning, designing, building and operating these huge pieces of precision engineering. It is great to know that the famous boson almost certainly exists, and we are eagerly waiting for detailed measurement of its properties.

Prof. Tom Kibble

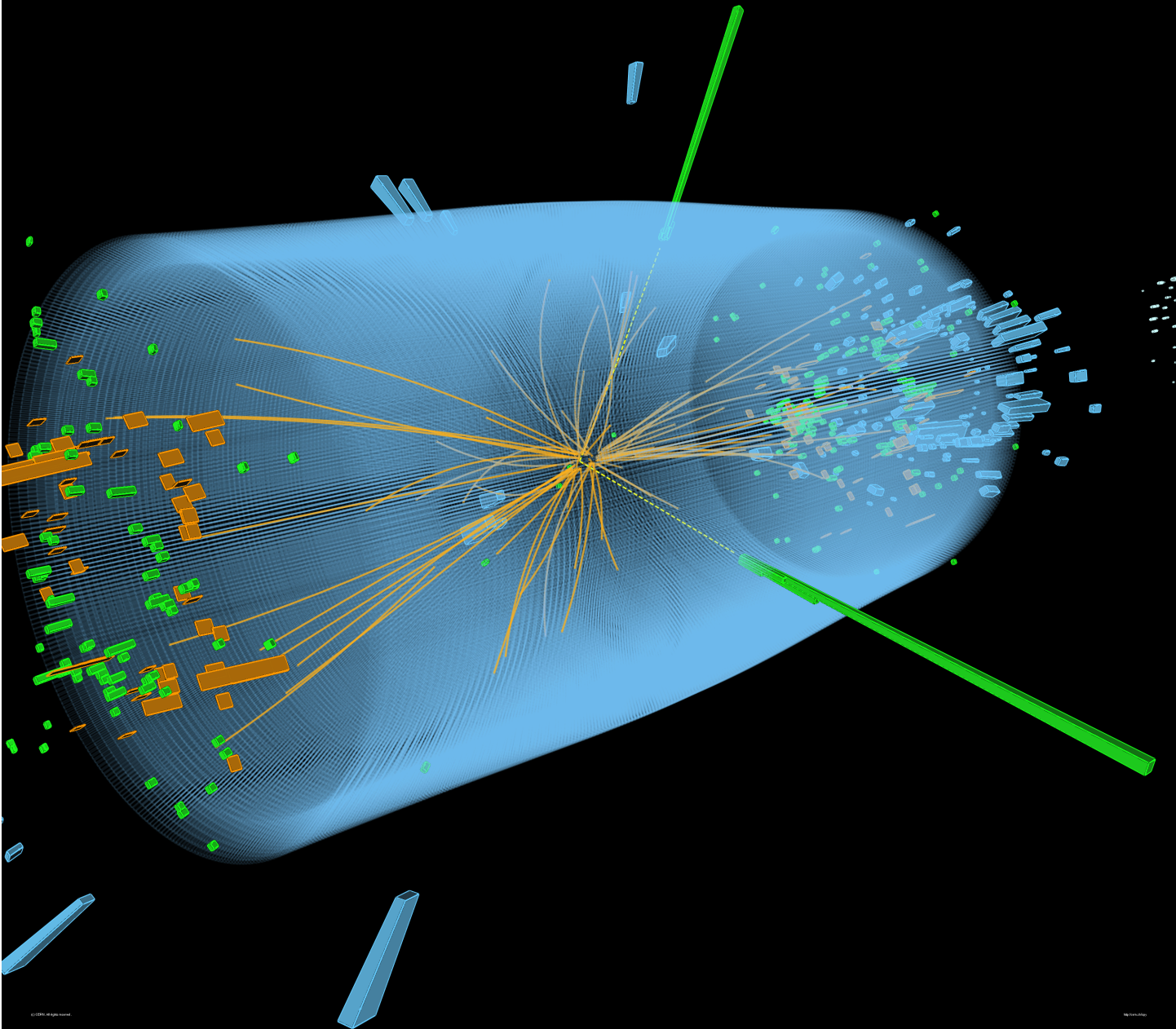
Prof. Carl R. Hagen

Prof. Gerald Guralnik

Handwritten signature of Tom Kibble in cursive script.Handwritten signature of Carl R. Hagen in cursive script.Handwritten signature of S. D. Guralnik in cursive script, with a horizontal line underneath.



ATLAS
EXPERIMENT
<http://atlas.ch>
Run: 205113
Event: 12611816
Date: 2012-06-18
Time: 11:07:47 CEST



Captions from CMS:

Front Cover, top figure:

Results from the CMS search for the Higgs boson decaying to two photons. The plot shows the diphoton mass spectrum, where the Higgs boson signal would manifest itself as a “bump” on top of a smoothly falling background. As the search is carried out in a number of diphoton categories of different quality and kinematic criteria, and thus with different signal-to-background ratios, the categories are not simply summed together. Instead, a weighted sum, emphasizing the contribution of categories with the best signal-to-background ratio, is shown. The inset is an artistic view of the same mass spectrum zoomed on the peak region.

Previous page, bottom figure:

CMS event display:

View of a Higgs boson $H \rightarrow \gamma\gamma$ candidate event.

The trajectories of the two photons are indicated in dotted yellow lines, while the height of the green towers at the end of dotted lines indicate the energy measured in the electromagnetic calorimeter. The orange lines show the trajectories of charged particles, as reconstructed in the CMS tracking detector, while the orange towers display the energy in the hadronic calorimeter.

=====
Captions from ATLAS:

Front cover, bottom figure:

Results of the ATLAS Standard Model Higgs boson searches.

The solid line shows the observed probability (local p_0) for background processes to be consistent with the data.

No significant deviation from the background expectation is observed anywhere in the explored mass region, except for $m_H \sim 126$ GeV.

The probability that the data are due to background for $m_H \sim 126$ GeV is 1.7×10^{-9} , corresponding to a signal significance of 5.9σ .

The insert shows a zoom of this region, together with the expected probability for a Standard Model Higgs boson at a given mass (dashed line with the $\pm 1\sigma$ uncertainty band).

Previous page, top figure:

ATLAS Event display:

Cut-away view of a Higgs boson $H \rightarrow ZZ \rightarrow e^+e^-\mu^+\mu^-$ candidate event.

The muons are indicated in red, penetrating through the detector to the muon chambers.

The electrons are picked out in green, associated with narrow clusters of energy in the electromagnetic calorimeter.

The inset shows the eleven reconstructed collision vertices, with the four lepton tracks coming from the same vertex.

Front Cover, background figure:

Aerial view of CERN indicating the scale of the Large Hadron Collider (LHC) ring. Image source for cover background © 2001 CERN



Observation of a new particle in the search for the Standard Model Higgs boson with the ATLAS detector at the LHC [☆]

ATLAS Collaboration ^{*}

This paper is dedicated to the memory of our ATLAS colleagues who did not live to see the full impact and significance of their contributions to the experiment.

ARTICLE INFO

Article history:

Received 31 July 2012

Received in revised form 8 August 2012

Accepted 11 August 2012

Available online 14 August 2012

Editor: W.-D. Schlatter

ABSTRACT

A search for the Standard Model Higgs boson in proton–proton collisions with the ATLAS detector at the LHC is presented. The datasets used correspond to integrated luminosities of approximately 4.8 fb^{-1} collected at $\sqrt{s} = 7 \text{ TeV}$ in 2011 and 5.8 fb^{-1} at $\sqrt{s} = 8 \text{ TeV}$ in 2012. Individual searches in the channels $H \rightarrow ZZ^{(*)} \rightarrow 4\ell$, $H \rightarrow \gamma\gamma$ and $H \rightarrow WW^{(*)} \rightarrow e\nu\mu\nu$ in the 8 TeV data are combined with previously published results of searches for $H \rightarrow ZZ^{(*)}$, $WW^{(*)}$, $b\bar{b}$ and $\tau^+\tau^-$ in the 7 TeV data and results from improved analyses of the $H \rightarrow ZZ^{(*)} \rightarrow 4\ell$ and $H \rightarrow \gamma\gamma$ channels in the 7 TeV data. Clear evidence for the production of a neutral boson with a measured mass of $126.0 \pm 0.4 \text{ (stat)} \pm 0.4 \text{ (sys)} \text{ GeV}$ is presented. This observation, which has a significance of 5.9 standard deviations, corresponding to a background fluctuation probability of 1.7×10^{-9} , is compatible with the production and decay of the Standard Model Higgs boson.

© 2012 CERN. Published by Elsevier B.V. All rights reserved.

1. Introduction

The Standard Model (SM) of particle physics [1–4] has been tested by many experiments over the last four decades and has been shown to successfully describe high energy particle interactions. However, the mechanism that breaks electroweak symmetry in the SM has not been verified experimentally. This mechanism [5–10], which gives mass to massive elementary particles, implies the existence of a scalar particle, the SM Higgs boson. The search for the Higgs boson, the only elementary particle in the SM that has not yet been observed, is one of the highlights of the Large Hadron Collider [11] (LHC) physics programme.

Indirect limits on the SM Higgs boson mass of $m_H < 158 \text{ GeV}$ at 95% confidence level (CL) have been set using global fits to precision electroweak results [12]. Direct searches at LEP [13], the Tevatron [14–16] and the LHC [17,18] have previously excluded, at 95% CL, a SM Higgs boson with mass below 600 GeV, apart from some mass regions between 116 GeV and 127 GeV.

Both the ATLAS and CMS Collaborations reported excesses of events in their 2011 datasets of proton–proton (pp) collisions at centre-of-mass energy $\sqrt{s} = 7 \text{ TeV}$ at the LHC, which were compatible with SM Higgs boson production and decay in the mass region 124–126 GeV, with significances of 2.9 and 3.1 standard deviations (σ), respectively [17,18]. The CDF and DØ experiments at the Tevatron have also recently reported a broad excess in the mass region

120–135 GeV; using the existing LHC constraints, the observed local significances for $m_H = 125 \text{ GeV}$ are 2.7σ for CDF [14], 1.1σ for DØ [15] and 2.8σ for their combination [16].

The previous ATLAS searches in $4.6\text{--}4.8 \text{ fb}^{-1}$ of data at $\sqrt{s} = 7 \text{ TeV}$ are combined here with new searches for $H \rightarrow ZZ^{(*)} \rightarrow 4\ell$, $H \rightarrow \gamma\gamma$ and $H \rightarrow WW^{(*)} \rightarrow e\nu\mu\nu$ in the $5.8\text{--}5.9 \text{ fb}^{-1}$ of pp collision data taken at $\sqrt{s} = 8 \text{ TeV}$ between April and June 2012.

The data were recorded with instantaneous luminosities up to $6.8 \times 10^{33} \text{ cm}^{-2} \text{ s}^{-1}$; they are therefore affected by multiple pp collisions occurring in the same or neighbouring bunch crossings (pile-up). In the 7 TeV data, the average number of interactions per bunch crossing was approximately 10; the average increased to approximately 20 in the 8 TeV data. The reconstruction, identification and isolation criteria used for electrons and photons in the 8 TeV data are improved, making the $H \rightarrow ZZ^{(*)} \rightarrow 4\ell$ and $H \rightarrow \gamma\gamma$ searches more robust against the increased pile-up. These analyses were re-optimised with simulation and frozen before looking at the 8 TeV data.

In the $H \rightarrow WW^{(*)} \rightarrow \ell\nu\ell\nu$ channel, the increased pile-up deteriorates the event missing transverse momentum, E_T^{miss} , resolution, which results in significantly larger Drell–Yan background in the same-flavour final states. Since the $e\mu$ channel provides most of the sensitivity of the search, only this final state is used in the analysis of the 8 TeV data. The kinematic region in which a SM Higgs boson with a mass between 110 GeV and 140 GeV is

[☆] © CERN for the benefit of the ATLAS Collaboration.

^{*} E-mail address: atlas.publications@cern.ch.

¹ The symbol ℓ stands for electron or muon.

searched for was kept blinded during the analysis optimisation, until satisfactory agreement was found between the observed and predicted numbers of events in control samples dominated by the principal backgrounds.

This Letter is organised as follows. The ATLAS detector is briefly described in Section 2. The simulation samples and the signal predictions are presented in Section 3. The analyses of the $H \rightarrow ZZ^{(*)} \rightarrow 4\ell$, $H \rightarrow \gamma\gamma$ and $H \rightarrow WW^{(*)} \rightarrow e\nu\mu\nu$ channels are described in Sections 4–6, respectively. The statistical procedure used to analyse the results is summarised in Section 7. The systematic uncertainties which are correlated between datasets and search channels are described in Section 8. The results of the combination of all channels are reported in Section 9, while Section 10 provides the conclusions.

2. The ATLAS detector

The ATLAS detector [19–21] is a multipurpose particle physics apparatus with forward-backward symmetric cylindrical geometry. The inner tracking detector (ID) consists of a silicon pixel detector, a silicon microstrip detector (SCT), and a straw-tube transition radiation tracker (TRT). The ID is surrounded by a thin superconducting solenoid which provides a 2 T magnetic field, and by high-granularity liquid-argon (LAr) sampling electromagnetic calorimetry. The electromagnetic calorimeter is divided into a central barrel (pseudorapidity² $|\eta| < 1.475$) and end-cap regions on either end of the detector ($1.375 < |\eta| < 2.5$ for the outer wheel and $2.5 < |\eta| < 3.2$ for the inner wheel). In the region matched to the ID ($|\eta| < 2.5$), it is radially segmented into three layers. The first layer has a fine segmentation in η to facilitate e/γ separation from π^0 and to improve the resolution of the shower position and direction measurements. In the region $|\eta| < 1.8$, the electromagnetic calorimeter is preceded by a presampler detector to correct for upstream energy losses. An iron-scintillator/tile calorimeter gives hadronic coverage in the central rapidity range ($|\eta| < 1.7$), while a LAr hadronic end-cap calorimeter provides coverage over $1.5 < |\eta| < 3.2$. The forward regions ($3.2 < |\eta| < 4.9$) are instrumented with LAr calorimeters for both electromagnetic and hadronic measurements. The muon spectrometer (MS) surrounds the calorimeters and consists of three large air-core superconducting magnets providing a toroidal field, each with eight coils, a system of precision tracking chambers, and fast detectors for triggering. The combination of all these systems provides charged particle measurements together with efficient and precise lepton and photon measurements in the pseudorapidity range $|\eta| < 2.5$. Jets and E_T^{miss} are reconstructed using energy deposits over the full coverage of the calorimeters, $|\eta| < 4.9$.

3. Signal and background simulation samples

The SM Higgs boson production processes considered in this analysis are the dominant gluon fusion ($gg \rightarrow H$, denoted ggF), vector-boson fusion ($qq' \rightarrow qq'H$, denoted VBF) and Higgs-strahlung ($qq' \rightarrow WH, ZH$, denoted WH/ZH). The small contribution from the associated production with a $t\bar{t}$ pair ($q\bar{q}/gg \rightarrow t\bar{t}H$, denoted $t\bar{t}H$) is taken into account only in the $H \rightarrow \gamma\gamma$ analysis.

For the ggF process, the signal cross section is computed at up to next-to-next-to-leading order (NNLO) in QCD [22–28]. Next-to-

Table 1

Event generators used to model the signal and background processes. “PYTHIA” indicates that PYTHIA6 and PYTHIA8 are used for simulations of $\sqrt{s} = 7$ TeV and $\sqrt{s} = 8$ TeV data, respectively.

Process	Generator
ggF, VBF $WH, ZH, t\bar{t}H$	POWHEG [57,58] + PYTHIA PYTHIA
W + jets, $Z/\gamma^* +$ jets $t\bar{t}, tW, tb$ tqb $q\bar{q} \rightarrow WW$ $gg \rightarrow WW$ $q\bar{q} \rightarrow ZZ$ $gg \rightarrow ZZ$ WZ $W\gamma$ + jets $W\gamma^*$ [65] $q\bar{q}/gg \rightarrow \gamma\gamma$	ALPGEN [59] + HERWIG MC@NLO [60] + HERWIG AcerMC [61] + PYTHIA MC@NLO + HERWIG gg2WW [62] + HERWIG POWHEG [63] + PYTHIA gg2ZZ [64] + HERWIG MadGraph + PYTHIA, HERWIG ALPGEN + HERWIG MadGraph + PYTHIA SHERPA

leading order (NLO) electroweak (EW) corrections are applied [29, 30], as well as QCD soft-gluon re-summations at up to next-to-next-to-leading logarithm (NNLL) [31]. These calculations, which are described in Refs. [32–35], assume factorisation between QCD and EW corrections. The transverse momentum, p_T , spectrum of the Higgs boson in the ggF process follows the HqT calculation [36], which includes QCD corrections at NLO and QCD soft-gluon re-summations up to NNLL; the effects of finite quark masses are also taken into account [37].

For the VBF process, full QCD and EW corrections up to NLO [38–41] and approximate NNLO QCD corrections [42] are used to calculate the cross section. Cross sections of the associated WH/ZH processes (VH) are calculated including QCD corrections up to NNLO [43–45] and EW corrections up to NLO [46]. The cross sections for the $t\bar{t}H$ process are estimated up to NLO QCD [47–51].

The total cross sections for SM Higgs boson production at the LHC with $m_H = 125$ GeV are predicted to be 17.5 pb for $\sqrt{s} = 7$ TeV and 22.3 pb for $\sqrt{s} = 8$ TeV [52,53].

The branching ratios of the SM Higgs boson as a function of m_H , as well as their uncertainties, are calculated using the HDECAY [54] and PROPHECY4F [55,56] programs and are taken from Refs. [52,53]. The interference in the $H \rightarrow ZZ^{(*)} \rightarrow 4\ell$ final states with identical leptons is taken into account [55,56,53].

The event generators used to model signal and background processes in samples of Monte Carlo (MC) simulated events are listed in Table 1. The normalisations of the generated samples are obtained from the state of the art calculations described above. Several different programs are used to generate the hard-scattering processes. To generate parton showers and their hadronisation, and to simulate the underlying event [66–68], PYTHIA6 [69] (for 7 TeV samples and 8 TeV samples produced with MadGraph [70,71] or AcerMC) or PYTHIA8 [72] (for other 8 TeV samples) are used. Alternatively, HERWIG [73] or SHERPA [74] are used to generate and hadronise parton showers, with the HERWIG underlying event simulation performed using JIMMY [75]. When PYTHIA6 or HERWIG are used, TAUOLA [76] and PHOTOS [77] are employed to describe tau lepton decays and additional photon radiation from charged leptons, respectively.

The following parton distribution function (PDF) sets are used: CT10 [78] for the POWHEG, MC@NLO, gg2WW and gg2ZZ samples; CTEQ6L1 [79] for the PYTHIA8, ALPGEN, AcerMC, MadGraph, HERWIG and SHERPA samples; and MRSTMcal [80] for the PYTHIA6 samples.

Acceptances and efficiencies are obtained mostly from full simulations of the ATLAS detector [81] using GEANT4 [82]. These simulations include a realistic modelling of the pile-up conditions observed in the data. Corrections obtained from measurements in

² ATLAS uses a right-handed coordinate system with its origin at the nominal interaction point (IP) in the centre of the detector, and the z-axis along the beam line. The x-axis points from the IP to the centre of the LHC ring, and the y-axis points upwards. Cylindrical coordinates (r, ϕ) are used in the transverse plane, ϕ being the azimuthal angle around the beam line. Observables labelled “transverse” are projected into the x–y plane. The pseudorapidity is defined in terms of the polar angle θ as $\eta = -\ln \tan(\theta/2)$.

data are applied to account for small differences between data and simulation (e.g. large samples of W , Z and J/ψ decays are used to derive scale factors for lepton reconstruction and identification efficiencies).

4. $H \rightarrow ZZ^{(*)} \rightarrow 4\ell$ channel

The search for the SM Higgs boson through the decay $H \rightarrow ZZ^{(*)} \rightarrow 4\ell$, where $\ell = e$ or μ , provides good sensitivity over a wide mass range (110–600 GeV), largely due to the excellent momentum resolution of the ATLAS detector. This analysis searches for Higgs boson candidates by selecting two pairs of isolated leptons, each of which is comprised of two leptons with the same flavour and opposite charge. The expected cross section times branching ratio for the process $H \rightarrow ZZ^{(*)} \rightarrow 4\ell$ with $m_H = 125$ GeV is 2.2 fb for $\sqrt{s} = 7$ TeV and 2.8 fb for $\sqrt{s} = 8$ TeV.

The largest background comes from continuum ($Z^{(*)}/\gamma^{(*)}(Z^{(*)}/\gamma^{(*)})$ production, referred to hereafter as $ZZ^{(*)}$. For low masses there are also important background contributions from Z + jets and $t\bar{t}$ production, where charged lepton candidates arise either from decays of hadrons with b - or c -quark content or from mis-identification of jets.

The 7 TeV data have been re-analysed and combined with the 8 TeV data. The analysis is improved in several aspects with respect to Ref. [83] to enhance the sensitivity to a low-mass Higgs boson. In particular, the kinematic selections are revised, and the 8 TeV data analysis benefits from improvements in the electron reconstruction and identification. The expected signal significances for a Higgs boson with $m_H = 125$ GeV are 1.6σ for the 7 TeV data (to be compared with 1.25σ in Ref. [83]) and 2.1σ for the 8 TeV data.

4.1. Event selection

The data are selected using single-lepton or dilepton triggers. For the single-muon trigger, the p_T threshold is 18 GeV for the 7 TeV data and 24 GeV for the 8 TeV data, while for the single-electron trigger the transverse energy, E_T , threshold varies from 20 GeV to 22 GeV for the 7 TeV data and is 24 GeV for the 8 TeV data. For the dielectron triggers, the thresholds are 12 GeV for both electrons. For the dimuon triggers, the thresholds for the 7 TeV data are 10 GeV for each muon, while for the 8 TeV data the thresholds are 13 GeV. An additional asymmetric dimuon trigger is used in the 8 TeV data with thresholds 18 GeV and 8 GeV for the leading and sub-leading muon, respectively.

Muon candidates are formed by matching reconstructed ID tracks with either a complete track or a track-segment reconstructed in the MS [84]. The muon acceptance is extended with respect to Ref. [83] using tracks reconstructed in the forward region of the MS ($2.5 < |\eta| < 2.7$), which is outside the ID coverage. If both an ID and a complete MS track are present, the two independent momentum measurements are combined; otherwise the information of the ID or the MS is used alone. Electron candidates must have a well-reconstructed ID track pointing to an electromagnetic calorimeter cluster and the cluster should satisfy a set of identification criteria [85] that require the longitudinal and transverse shower profiles to be consistent with those expected for electromagnetic showers. Tracks associated with electromagnetic clusters are fitted using a Gaussian-Sum Filter [86], which allows for bremsstrahlung energy losses to be taken into account.

Each electron (muon) must satisfy $p_T > 7$ GeV ($p_T > 6$ GeV) and be measured in the pseudorapidity range $|\eta| < 2.47$ ($|\eta| < 2.7$). All possible quadruplet combinations with same-flavour opposite-charge lepton pairs are then formed. The most energetic lepton in the quadruplet must satisfy $p_T > 20$ GeV, and the second (third)

lepton in p_T order must satisfy $p_T > 15$ GeV ($p_T > 10$ GeV). At least one of the leptons must satisfy the single-lepton trigger or one pair must satisfy the dilepton trigger requirements. The leptons are required to be separated from each other by $\Delta R = \sqrt{(\Delta\eta)^2 + (\Delta\phi)^2} > 0.1$ if they are of the same flavour and by $\Delta R > 0.2$ otherwise. The longitudinal impact parameters of the leptons along the beam axis are required to be within 10 mm of the reconstructed primary vertex. The primary vertex used for the event is defined as the reconstructed vertex with the highest $\sum p_T^2$ of associated tracks and is required to have at least three tracks with $p_T > 0.4$ GeV. To reject cosmic rays, muon tracks are required to have a transverse impact parameter, defined as the distance of closest approach to the primary vertex in the transverse plane, of less than 1 mm.

The same-flavour and opposite-charge lepton pair with an invariant mass closest to the Z boson mass (m_Z) in the quadruplet is referred to as the leading lepton pair. Its invariant mass, denoted by m_{12} , is required to be between 50 GeV and 106 GeV. The remaining same-flavour, opposite-charge lepton pair is the sub-leading lepton pair. Its invariant mass, m_{34} , is required to be in the range $m_{\min} < m_{34} < 115$ GeV, where the value of m_{\min} depends on the reconstructed four-lepton invariant mass, $m_{4\ell}$. The value of m_{\min} varies monotonically from 17.5 GeV at $m_{4\ell} = 120$ GeV to 50 GeV at $m_{4\ell} = 190$ GeV [87] and is constant above this value. All possible lepton pairs in the quadruplet that have the same flavour and opposite charge must satisfy $m_{\ell\ell} > 5$ GeV in order to reject backgrounds involving the production and decay of J/ψ mesons. If two or more quadruplets satisfy the above selection, the one with the highest value of m_{34} is selected. Four different analysis sub-channels, $4e$, $2e2\mu$, $2\mu2e$ and 4μ , arranged by the flavour of the leading lepton pair, are defined.

Non-prompt leptons from heavy flavour decays, electrons from photon conversions and jets mis-identified as electrons have broader transverse impact parameter distributions than prompt leptons from Z boson decays and/or are non-isolated. Thus, the Z + jets and $t\bar{t}$ background contributions are reduced by applying a cut on the transverse impact parameter significance, defined as the transverse impact parameter divided by its uncertainty, d_0/σ_{d_0} . This is required to be less than 3.5 (6.5) for muons (electrons). The electron impact parameter is affected by bremsstrahlung and thus has a broader distribution.

In addition, leptons must satisfy isolation requirements based on tracking and calorimetric information. The normalised track isolation discriminant is defined as the sum of the transverse momenta of tracks inside a cone of size $\Delta R = 0.2$ around the lepton direction, excluding the lepton track, divided by the lepton p_T . The tracks considered in the sum are those compatible with the lepton vertex and have $p_T > 0.4$ GeV ($p_T > 1$ GeV) in the case of electron (muon) candidates. Each lepton is required to have a normalised track isolation smaller than 0.15. The normalised calorimetric isolation for electrons is computed as the sum of the E_T of positive-energy topological clusters [88] with a reconstructed barycentre falling within a cone of size $\Delta R = 0.2$ around the candidate electron cluster, divided by the electron E_T . The algorithm for topological clustering suppresses noise by keeping cells with a significant energy deposit and their neighbours. The summed energy of the cells assigned to the electron cluster is excluded, while a correction is applied to account for the electron energy deposited outside the cluster. The ambient energy deposition in the event from pile-up and the underlying event is accounted for using a calculation of the median transverse energy density from low- p_T jets [89,90]. The normalised calorimetric isolation for electrons is required to be less than 0.20. The normalised calorimetric isolation discriminant for muons is defined by the ratio to the p_T of the muon of the E_T sum of the calorimeter cells inside a cone of size

$\Delta R = 0.2$ around the muon direction minus the energy deposited by the muon. Muons are required to have a normalised calorimetric isolation less than 0.30 (0.15 for muons without an associated ID track). For both the track- and calorimeter-based isolation, any contributions arising from other leptons of the quadruplet are subtracted.

The combined signal reconstruction and selection efficiencies for a SM Higgs with $m_H = 125$ GeV for the 7 TeV (8 TeV) data are 37% (36%) for the 4μ channel, 20% (22%) for the $2e2\mu/2\mu2e$ channels and 15% (20%) for the $4e$ channel.

The 4ℓ invariant mass resolution is improved by applying a Z -mass constrained kinematic fit to the leading lepton pair for $m_{4\ell} < 190$ GeV and to both lepton pairs for higher masses. The expected width of the reconstructed mass distribution is dominated by the experimental resolution for $m_H < 350$ GeV, and by the natural width of the Higgs boson for higher masses (30 GeV at $m_H = 400$ GeV). The typical mass resolutions for $m_H = 125$ GeV are 1.7 GeV, 1.7 GeV/2.2 GeV and 2.3 GeV for the 4μ , $2e2\mu/2\mu2e$ and $4e$ sub-channels, respectively.

4.2. Background estimation

The expected background yield and composition are estimated using the MC simulation normalised to the theoretical cross section for $ZZ^{(*)}$ production and by methods using control regions from data for the $Z + \text{jets}$ and $t\bar{t}$ processes. Since the background composition depends on the flavour of the sub-leading lepton pair, different approaches are taken for the $\ell\ell + \mu\mu$ and the $\ell\ell + ee$ final states. The transfer factors needed to extrapolate the background yields from the control regions defined below to the signal region are obtained from the MC simulation. The MC description of the selection efficiencies for the different background components has been verified with data.

The reducible $\ell\ell + \mu\mu$ background is dominated by $t\bar{t}$ and $Z + \text{jets}$ (mostly $Zb\bar{b}$) events. A control region is defined by removing the isolation requirement on the leptons in the sub-leading pair, and by requiring that at least one of the sub-leading muons fails the transverse impact parameter significance selection. These modifications remove $ZZ^{(*)}$ contributions, and allow both the $t\bar{t}$ and $Z + \text{jets}$ backgrounds to be estimated simultaneously using a fit to the m_{12} distribution. The $t\bar{t}$ background contribution is cross-checked by selecting a control sample of events with an opposite charge $e\mu$ pair with an invariant mass between 50 GeV and 106 GeV, accompanied by an opposite-charge muon pair. Events with a Z candidate decaying to a pair of electrons or muons in the aforementioned mass range are excluded. Isolation and transverse impact parameter significance requirements are applied only to the leptons of the $e\mu$ pair.

In order to estimate the reducible $\ell\ell + ee$ background, a control region is formed by relaxing the selection criteria for the electrons of the sub-leading pair. The different sources of electron background are then separated into categories consisting of non-prompt leptons from heavy flavour decays, electrons from photon conversions and jets mis-identified as electrons, using appropriate discriminating variables [91]. This method allows the sum of the $Z + \text{jets}$ and $t\bar{t}$ background contributions to be estimated. As a cross-check, the same method is also applied to a similar control region containing same-charge sub-leading electron pairs. An additional cross-check of the $\ell\ell + ee$ background estimation is performed by using a control region with same-charge sub-leading electron pairs, where the three highest p_T leptons satisfy all the analysis criteria whereas the selection cuts are relaxed for the remaining electrons. All the cross-checks yield consistent results.

The data-driven background estimates are summarised in Table 2. The distribution of m_{34} , for events selected by the analysis

Table 2

Summary of the estimated numbers of $Z + \text{jets}$ and $t\bar{t}$ background events, for the $\sqrt{s} = 7$ TeV and $\sqrt{s} = 8$ TeV data in the entire phase-space of the analysis after the kinematic selections described in the text. The backgrounds are combined for the $2\mu2e$ and $4e$ channels, as discussed in the text. The first uncertainty is statistical, while the second is systematic.

Background	Estimated numbers of events	
	$\sqrt{s} = 7$ TeV	$\sqrt{s} = 8$ TeV
4μ		
$Z + \text{jets}$	$0.3 \pm 0.1 \pm 0.1$	$0.5 \pm 0.1 \pm 0.2$
$t\bar{t}$	$0.02 \pm 0.02 \pm 0.01$	$0.04 \pm 0.02 \pm 0.02$
$2e2\mu$		
$Z + \text{jets}$	$0.2 \pm 0.1 \pm 0.1$	$0.4 \pm 0.1 \pm 0.1$
$t\bar{t}$	$0.02 \pm 0.01 \pm 0.01$	$0.04 \pm 0.01 \pm 0.01$
$2\mu2e$		
$Z + \text{jets}, t\bar{t}$	$2.6 \pm 0.4 \pm 0.4$	$4.9 \pm 0.8 \pm 0.7$
$4e$		
$Z + \text{jets}, t\bar{t}$	$3.1 \pm 0.6 \pm 0.5$	$3.9 \pm 0.7 \pm 0.8$

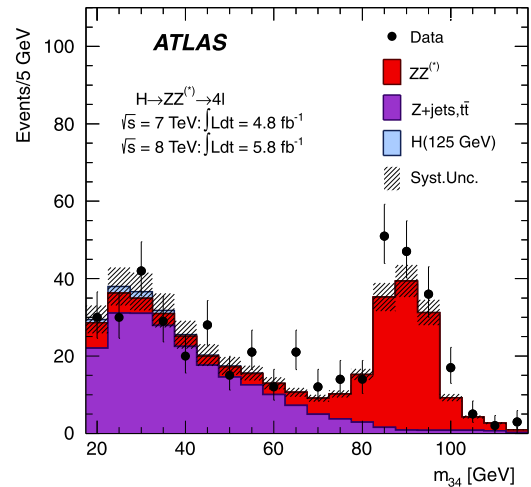


Fig. 1. Invariant mass distribution of the sub-leading lepton pair (m_{34}) for a sample defined by the presence of a Z boson candidate and an additional same-flavour electron or muon pair, for the combination of $\sqrt{s} = 7$ TeV and $\sqrt{s} = 8$ TeV data in the entire phase-space of the analysis after the kinematic selections described in the text. Isolation and transverse impact parameter significance requirements are applied to the leading lepton pair only. The MC is normalised to the data-driven background estimations. The relatively small contribution of a SM Higgs with $m_H = 125$ GeV in this sample is also shown.

except that the isolation and transverse impact parameter requirements for the sub-leading lepton pair are removed, is presented in Fig. 1.

4.3. Systematic uncertainties

The uncertainties on the integrated luminosities are determined to be 1.8% for the 7 TeV data and 3.6% for the 8 TeV data using the techniques described in Ref. [92].

The uncertainties on the lepton reconstruction and identification efficiencies and on the momentum scale and resolution are determined using samples of W , Z and J/ψ decays [85, 84]. The relative uncertainty on the signal acceptance due to the uncertainty on the muon reconstruction and identification efficiency is $\pm 0.7\%$ ($\pm 0.5\%/ \pm 0.5\%$) for the 4μ ($2e2\mu/2\mu2e$) channel for $m_{4\ell} = 600$ GeV and increases to $\pm 0.9\%$ ($\pm 0.8\%/ \pm 0.5\%$) for $m_{4\ell} = 115$ GeV. Similarly, the relative uncertainty on the signal acceptance due to the uncertainty on the electron reconstruction and identification efficiency is $\pm 2.6\%$ ($\pm 1.7\%/ \pm 1.8\%$) for the $4e$ ($2e2\mu/2\mu2e$) channel for $m_{4\ell} = 600$ GeV and reaches $\pm 8.0\%$

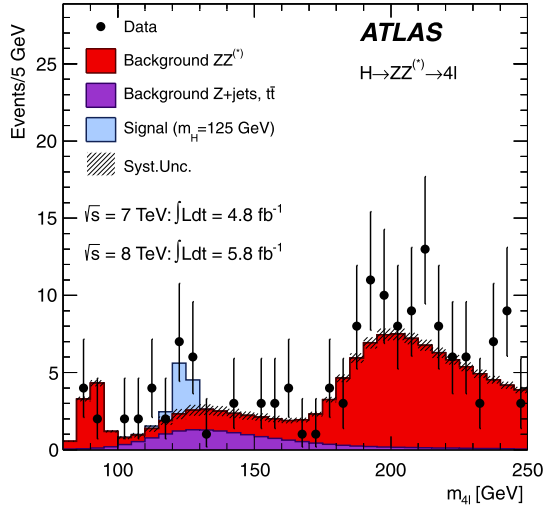


Fig. 2. The distribution of the four-lepton invariant mass, $m_{4\ell}$, for the selected candidates, compared to the background expectation in the 80–250 GeV mass range, for the combination of the $\sqrt{s} = 7$ TeV and $\sqrt{s} = 8$ TeV data. The signal expectation for a SM Higgs with $m_H = 125$ GeV is also shown.

Table 3

The numbers of expected signal ($m_H = 125$ GeV) and background events, together with the numbers of observed events in the data, in a window of size ± 5 GeV around 125 GeV, for the combined $\sqrt{s} = 7$ TeV and $\sqrt{s} = 8$ TeV data.

	Signal	$ZZ^{(*)}$	$Z + \text{jets}, t\bar{t}$	Observed
4μ	2.09 ± 0.30	1.12 ± 0.05	0.13 ± 0.04	6
$2e2\mu/2\mu2e$	2.29 ± 0.33	0.80 ± 0.05	1.27 ± 0.19	5
$4e$	0.90 ± 0.14	0.44 ± 0.04	1.09 ± 0.20	2

($\pm 2.3\%/\pm 7.6\%$) for $m_{4\ell} = 115$ GeV. The uncertainty on the electron energy scale results in an uncertainty of $\pm 0.7\%$ ($\pm 0.5\%/\pm 0.2\%$) on the mass scale of the $m_{4\ell}$ distribution for the $4e$ ($2e2\mu/2\mu2e$) channel. The impact of the uncertainties on the electron energy resolution and on the muon momentum resolution and scale are found to be negligible.

The theoretical uncertainties associated with the signal are described in detail in Section 8. For the SM $ZZ^{(*)}$ background, which is estimated from MC simulation, the uncertainty on the total yield due to the QCD scale uncertainty is $\pm 5\%$, while the effect of the PDF and α_s uncertainties is $\pm 4\%$ ($\pm 8\%$) for processes initiated by quarks (gluons) [53]. In addition, the dependence of these uncertainties on the four-lepton invariant mass spectrum has been taken into account as discussed in Ref. [53]. Though a small excess of events is observed for $m_{4\ell} > 160$ GeV, the measured $ZZ^{(*)} \rightarrow 4\ell$ cross section [93] is consistent with the SM theoretical prediction. The impact of not using the theoretical constraints on the $ZZ^{(*)}$ yield on the search for a Higgs boson with $m_H < 2m_Z$ has been studied in Ref. [87] and has been found to be negligible. The impact of the interference between a Higgs signal and the non-resonant $gg \rightarrow ZZ^{(*)}$ background is small and becomes negligible for $m_H < 2m_Z$ [94].

4.4. Results

The expected distributions of $m_{4\ell}$ for the background and for a Higgs boson signal with $m_H = 125$ GeV are compared to the data in Fig. 2. The numbers of observed and expected events in a window of ± 5 GeV around $m_H = 125$ GeV are presented for the combined 7 TeV and 8 TeV data in Table 3. The distribution of the m_{34} versus m_{12} invariant mass is shown in Fig. 3. The statistical interpretation of the excess of events near $m_{4\ell} = 125$ GeV in Fig. 2 is presented in Section 9.

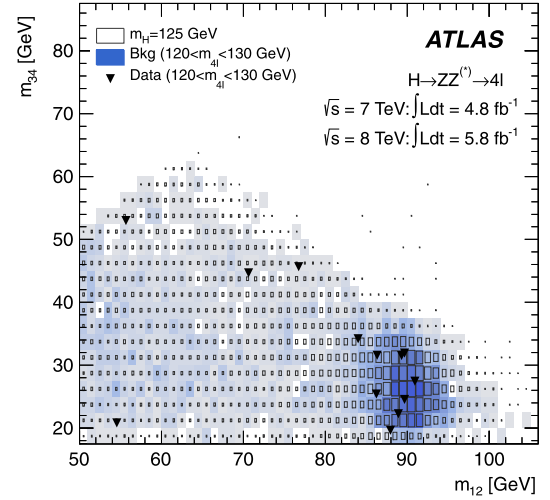


Fig. 3. Distribution of the m_{34} versus the m_{12} invariant mass, before the application of the Z-mass constrained kinematic fit, for the selected candidates in the $m_{4\ell}$ range 120–130 GeV. The expected distributions for a SM Higgs with $m_H = 125$ GeV (the sizes of the boxes indicate the relative density) and for the total background (the intensity of the shading indicates the relative density) are also shown.

5. $H \rightarrow \gamma\gamma$ channel

The search for the SM Higgs boson through the decay $H \rightarrow \gamma\gamma$ is performed in the mass range between 110 GeV and 150 GeV. The dominant background is SM diphoton production ($\gamma\gamma$); contributions also come from $\gamma + \text{jet}$ and $\text{jet} + \text{jet}$ production with one or two jets mis-identified as photons (γj and jj) and from the Drell–Yan process. The 7 TeV data have been re-analysed and the results combined with those from the 8 TeV data. Among other changes to the analysis, a new category of events with two jets is introduced, which enhances the sensitivity to the VBF process. Higgs boson events produced by the VBF process have two forward jets, originating from the two scattered quarks, and tend to be devoid of jets in the central region. Overall, the sensitivity of the analysis has been improved by about 20% with respect to that described in Ref. [95].

5.1. Event selection

The data used in this channel are selected using a diphoton trigger [96], which requires two clusters formed from energy depositions in the electromagnetic calorimeter. An E_T threshold of 20 GeV is applied to each cluster for the 7 TeV data, while for the 8 TeV data the thresholds are increased to 35 GeV on the leading (the highest E_T) cluster and to 25 GeV on the sub-leading (the next-highest E_T) cluster. In addition, loose criteria are applied to the shapes of the clusters to match the expectations for electromagnetic showers initiated by photons. The efficiency of the trigger is greater than 99% for events passing the final event selection.

Events are required to contain at least one reconstructed vertex with at least two associated tracks with $p_T > 0.4$ GeV, as well as two photon candidates. Photon candidates are reconstructed in the fiducial region $|\eta| < 2.37$, excluding the calorimeter barrel/endcap transition region $1.37 \leq |\eta| < 1.52$. Photons that convert to electron–positron pairs in the ID material can have one or two reconstructed tracks matched to the clusters in the calorimeter. The photon reconstruction efficiency is about 97% for $E_T > 30$ GeV.

In order to account for energy losses upstream of the calorimeter and energy leakage outside of the cluster, MC simulation results are used to calibrate the energies of the photon candidates; there are separate calibrations for unconverted and converted

candidates. The calibration is refined by applying η -dependent correction factors, which are of the order of $\pm 1\%$, determined from measured $Z \rightarrow e^+e^-$ events. The leading (sub-leading) photon candidate is required to have $E_T > 40$ GeV (30 GeV).

Photon candidates are required to pass identification criteria based on shower shapes in the electromagnetic calorimeter and on energy leakage into the hadronic calorimeter [97]. For the 7 TeV data, this information is combined in a neural network, tuned to achieve a similar jet rejection as the cut-based selection described in Ref. [95], but with higher photon efficiency. For the 8 TeV data, cut-based criteria are used to ensure reliable photon performance for recently-recorded data. This cut-based selection has been tuned to be robust against pile-up by relaxing requirements on shower shape criteria more susceptible to pile-up, and tightening others. The photon identification efficiencies, averaged over η , range from 85% to above 95% for the E_T range under consideration.

To further suppress the jet background, an isolation requirement is applied. The isolation transverse energy is defined as the sum of the transverse energy of positive-energy topological clusters, as described in Section 4, within a cone of size $\Delta R = 0.4$ around the photon candidate, excluding the region within 0.125×0.175 in $\Delta\eta \times \Delta\phi$ around the photon barycentre. The distributions of the isolation transverse energy in data and simulation have been found to be in good agreement using electrons from $Z \rightarrow e^+e^-$ events and photons from $Z \rightarrow \ell^+\ell^-\gamma$ events. Remaining small differences are taken into account as a systematic uncertainty. Photon candidates are required to have an isolation transverse energy of less than 4 GeV.

5.2. Invariant mass reconstruction

The invariant mass of the two photons is evaluated using the photon energies measured in the calorimeter, the azimuthal angle ϕ between the photons as determined from the positions of the photons in the calorimeter, and the values of η calculated from the position of the identified primary vertex and the impact points of the photons in the calorimeter.

The primary vertex of the hard interaction is identified by combining the following information in a global likelihood: the directions of flight of the photons as determined using the longitudinal segmentation of the electromagnetic calorimeter (calorimeter pointing), the parameters of the beam spot, and the $\sum p_T^2$ of the tracks associated with each reconstructed vertex. In addition, for the 7 TeV data analysis, the reconstructed conversion vertex is used in the likelihood for converted photons with tracks containing hits in the silicon layers of the ID. The calorimeter pointing is sufficient to ensure that the contribution of the opening angle between the photons to the mass resolution is negligible. Using the calorimeter pointing alone, the resolution of the vertex z coordinate is ~ 15 mm, improving to ~ 6 mm for events with two reconstructed converted photons. The tracking information from the ID improves the identification of the vertex of the hard interaction, which is needed for the jet selection in the 2-jet category.

With the selection described in Section 5.1, in the diphoton invariant mass range between 100 GeV and 160 GeV, 23 788 and 35 251 diphoton candidates are observed in the 7 TeV and 8 TeV data samples, respectively.

Data-driven techniques [98] are used to estimate the numbers of $\gamma\gamma$, γj and jj events in the selected sample. The contribution from the Drell–Yan background is determined from a sample of $Z \rightarrow e^+e^-$ decays in data where either one or both electrons pass the photon selection. The measured composition of the selected sample is approximately 74%, 22%, 3% and 1% for the $\gamma\gamma$, γj , jj and Drell–Yan processes, respectively, demonstrating the dominance of the irreducible diphoton production. This decomposition

is not directly used in the signal search; however, it is used to study the parameterisation of the background modelling.

5.3. Event categorisation

To increase the sensitivity to a Higgs boson signal, the events are separated into ten mutually exclusive categories having different mass resolutions and signal-to-background ratios. An exclusive category of events containing two jets improves the sensitivity to VBF. The other nine categories are defined by the presence or not of converted photons, η of the selected photons, and $p_{T\ell}$, the component³ of the diphoton p_T that is orthogonal to the axis defined by the difference between the two photon momenta [99,100].

Jets are reconstructed [101] using the anti- k_r algorithm [102] with radius parameter $R = 0.4$. At least two jets with $|\eta| < 4.5$ and $p_T > 25$ GeV are required in the 2-jet selection. In the analysis of the 8 TeV data, the p_T threshold is raised to 30 GeV for jets with $2.5 < |\eta| < 4.5$. For jets in the ID acceptance ($|\eta| < 2.5$), the fraction of the sum of the p_T of tracks, associated with the jet and matched to the selected primary vertex, with respect to the sum of the p_T of tracks associated with the jet (jet vertex fraction, JVF) is required to be at least 0.75. This requirement on the JVF reduces the number of jets from proton–proton interactions not associated with the primary vertex. Motivated by the VBF topology, three additional cuts are applied in the 2-jet selection: the difference of the pseudorapidity between the leading and sub-leading jets (tag jets) is required to be larger than 2.8, the invariant mass of the tag jets has to be larger than 400 GeV, and the azimuthal angle difference between the diphoton system and the system of the tag jets has to be larger than 2.6. About 70% of the signal events in the 2-jet category come from the VBF process.

The other nine categories are defined as follows: events with two unconverted photons are separated into *unconverted central* ($|\eta| < 0.75$ for both candidates) and *unconverted rest* (all other events), events with at least one converted photon are separated into *converted central* ($|\eta| < 0.75$ for both candidates), *converted transition* (at least one photon with $1.3 < |\eta| < 1.75$) and *converted rest* (all other events). Except for the *converted transition* category, each category is further divided by a cut at $p_{T\ell} = 60$ GeV into two categories, *low* $p_{T\ell}$ and *high* $p_{T\ell}$. MC studies show that signal events, particularly those produced via VBF or associated production (WH/ZH and $t\bar{t}H$), have on average larger $p_{T\ell}$ than background events. The number of data events in each category, as well as the sum of all the categories, which is denoted *inclusive*, are given in Table 4.

5.4. Signal modelling

The description of the Higgs boson signal is obtained from MC, as described in Section 3. The cross sections multiplied by the branching ratio into two photons are given in Table 4 for $m_H = 126.5$ GeV. The number of signal events produced via the ggF process is rescaled to take into account the expected destructive interference between the $gg \rightarrow \gamma\gamma$ continuum background and ggF [103], leading to a reduction of the production rate by 2–5% depending on m_H and the event category. For both the 7 TeV and 8 TeV MC samples, the fractions of ggF, VBF, WH , ZH and $t\bar{t}H$ production are approximately 88%, 7%, 3%, 2% and 0.5%, respectively, for $m_H = 126.5$ GeV.

In the simulation, the shower shape distributions are shifted slightly to improve the agreement with the data [97], and the

³ $p_{T\ell} = |(\mathbf{p}_1^{\gamma_1} + \mathbf{p}_1^{\gamma_2}) \times (\mathbf{p}_1^{\gamma_1} - \mathbf{p}_1^{\gamma_2})| / |\mathbf{p}_1^{\gamma_1} - \mathbf{p}_1^{\gamma_2}|$, where $\mathbf{p}_1^{\gamma_1}$ and $\mathbf{p}_1^{\gamma_2}$ are the transverse momenta of the two photons.

Table 4

Number of events in the data (N_D) and expected number of signal events (N_S) for $m_H = 126.5$ GeV from the $H \rightarrow \gamma\gamma$ analysis, for each category in the mass range 100–160 GeV. The mass resolution FWHM (see text) is also given for the 8 TeV data. The Higgs boson production cross section multiplied by the branching ratio into two photons ($\sigma \times B(H \rightarrow \gamma\gamma)$) is listed for $m_H = 126.5$ GeV. The statistical uncertainties on N_S and FWHM are less than 1%.

\sqrt{s}	7 TeV		8 TeV		FWHM [GeV]
	$\sigma \times B(H \rightarrow \gamma\gamma)$ [fb]				
Category	N_D	N_S	N_D	N_S	
Unconv. central, low $p_{T\tau}$	2054	10.5	2945	14.2	3.4
Unconv. central, high $p_{T\tau}$	97	1.5	173	2.5	3.2
Unconv. rest, low $p_{T\tau}$	7129	21.6	12 136	30.9	3.7
Unconv. rest, high $p_{T\tau}$	444	2.8	785	5.2	3.6
Conv. central, low $p_{T\tau}$	1493	6.7	2015	8.9	3.9
Conv. central, high $p_{T\tau}$	77	1.0	113	1.6	3.5
Conv. rest, low $p_{T\tau}$	8313	21.1	11 099	26.9	4.5
Conv. rest, high $p_{T\tau}$	501	2.7	706	4.5	3.9
Conv. transition	3591	9.5	5140	12.8	6.1
2-jet	89	2.2	139	3.0	3.7
All categories (inclusive)	23 788	79.6	35 251	110.5	3.9

photon energy resolution is broadened (by approximately 1% in the barrel calorimeter and 1.2–2.1% in the end-cap regions) to account for small differences observed between $Z \rightarrow e^+e^-$ data and MC events. The signal yields expected for the 7 TeV and 8 TeV data samples are given in Table 4. The overall selection efficiency is about 40%.

The shape of the invariant mass of the signal in each category is modelled by the sum of a Crystal Ball function [104], describing the core of the distribution with a width σ_{CB} , and a Gaussian contribution describing the tails (amounting to < 10%) of the mass distribution. The expected full-width-at-half-maximum (FWHM) is 3.9 GeV and σ_{CB} is 1.6 GeV for the inclusive sample. The resolution varies with event category (see Table 4); the FWHM is typically a factor 2.3 larger than σ_{CB} .

5.5. Background modelling

The background in each category is estimated from data by fitting the diphoton mass spectrum in the mass range 100–160 GeV with a selected model with free parameters of shape and normalisation. Different models are chosen for the different categories to achieve a good compromise between limiting the size of a potential bias while retaining good statistical power. A fourth-order Bernstein polynomial function [105] is used for the *unconverted rest* (low $p_{T\tau}$), *converted rest* (low $p_{T\tau}$) and *inclusive* categories, an exponential function of a second-order polynomial for the *unconverted central* (low $p_{T\tau}$), *converted central* (low $p_{T\tau}$) and *converted transition* categories, and an exponential function for all others.

Studies to determine the potential bias have been performed using large samples of simulated background events complemented by data-driven estimates. The background shapes in the simulation have been cross-checked using data from control regions. The potential bias for a given model is estimated, separately for each category, by performing a maximum likelihood fit to large samples of simulated background events in the mass range 100–160 GeV, of the sum of a signal plus the given background model. The signal shape is taken to follow the expectation for a SM Higgs boson; the signal yield is a free parameter of the fit. The potential bias is defined by the largest absolute signal yield obtained from the likelihood fit to the simulated background samples for hypothesised Higgs boson masses in the range 110–150 GeV. A pre-selection of background parameterisations is made by requiring that the potential bias, as defined above, is less than 20% of the statistical uncertainty on the fitted signal yield. The pre-

selected parameterisation in each category with the best expected sensitivity for $m_H = 125$ GeV is selected as the background model.

The largest absolute signal yield as defined above is taken as the systematic uncertainty on the background model. It amounts to $\pm(0.2\text{--}4.6)$ and $\pm(0.3\text{--}6.8)$ events, depending on the category for the 7 TeV and 8 TeV data samples, respectively. In the final fit to the data (see Section 5.7) a signal-like term is included in the likelihood function for each category. This term incorporates the estimated potential bias, thus providing a conservative estimate of the uncertainty due to the background modelling.

5.6. Systematic uncertainties

Hereafter, in cases where two uncertainties are quoted, they refer to the 7 TeV and 8 TeV data, respectively. The dominant experimental uncertainty on the signal yield ($\pm 8\%$, $\pm 11\%$) comes from the photon reconstruction and identification efficiency, which is estimated with data using electrons from Z decays and photons from $Z \rightarrow \ell^+\ell^-\gamma$ events. Pile-up modelling also affects the expected yields and contributes to the uncertainty ($\pm 4\%$). Further uncertainties on the signal yield are related to the trigger ($\pm 1\%$), photon isolation ($\pm 0.4\%$, $\pm 0.5\%$) and luminosity ($\pm 1.8\%$, $\pm 3.6\%$). Uncertainties due to the modelling of the underlying event are $\pm 6\%$ for VBF and $\pm 30\%$ for other production processes in the 2-jet category. Uncertainties on the predicted cross sections and branching ratio are summarised in Section 8.

The uncertainty on the expected fractions of signal events in each category is described in the following. The uncertainty on the knowledge of the material in front of the calorimeter is used to derive the amount of possible event migration between the converted and unconverted categories ($\pm 4\%$). The uncertainty from pile-up on the population of the converted and unconverted categories is $\pm 2\%$. The uncertainty from the jet energy scale (JES) amounts to up to $\pm 19\%$ for the 2-jet category, and up to $\pm 4\%$ for the other categories. Uncertainties from the JVF modelling are $\pm 12\%$ (for the 8 TeV data) for the 2-jet category, estimated from $Z + 2$ -jets events by comparing data and MC. Different PDFs and scale variations in the HqT calculations are used to derive possible event migration among categories ($\pm 9\%$) due to the modelling of the Higgs boson kinematics.

The total uncertainty on the mass resolution is $\pm 14\%$. The dominant contribution ($\pm 12\%$) comes from the uncertainty on the energy resolution of the calorimeter, which is determined from $Z \rightarrow e^+e^-$ events. Smaller contributions come from the imperfect knowledge of the material in front of the calorimeter, which affects the extrapolation of the calibration from electrons to photons ($\pm 6\%$), and from pile-up ($\pm 4\%$).

5.7. Results

The distributions of the invariant mass, $m_{\gamma\gamma}$, of the diphoton events, summed over all categories, are shown in Fig. 4(a) and (b). The result of a fit including a signal component fixed to $m_H = 126.5$ GeV and a background component described by a fourth-order Bernstein polynomial is superimposed.

The statistical analysis of the data employs an unbinned likelihood function constructed from those of the ten categories of the 7 TeV and 8 TeV data samples. To demonstrate the sensitivity of this likelihood analysis, Figs. 4(c) and (d) also show the mass spectrum obtained after weighting events with category-dependent factors reflecting the signal-to-background ratios. The weight w_i for events in category $i \in [1, 10]$ for the 7 TeV and 8 TeV data samples is defined to be $\ln(1 + S_i/B_i)$, where S_i is 90% of the expected signal for $m_H = 126.5$ GeV, and B_i is the integral, in

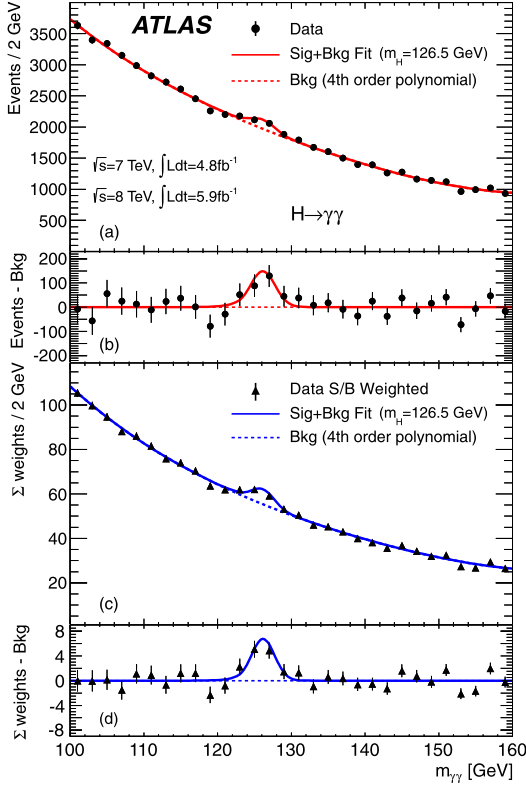


Fig. 4. The distributions of the invariant mass of diphoton candidates after all selections for the combined 7 TeV and 8 TeV data sample. The inclusive sample is shown in (a) and a weighted version of the same sample in (c); the weights are explained in the text. The result of a fit to the data of the sum of a signal component fixed to $m_H = 126.5$ GeV and a background component described by a fourth-order Bernstein polynomial is superimposed. The residuals of the data and weighted data with respect to the respective fitted background component are displayed in (b) and (d).

a window containing S_i , of a background-only fit to the data. The values S_i/B_i have only a mild dependence on m_H .

The statistical interpretation of the excess of events near $m_{\gamma\gamma} = 126.5$ GeV in Fig. 4 is presented in Section 9.

6. $H \rightarrow WW^{(*)} \rightarrow e\nu\mu\nu$ channel

The signature for this channel is two opposite-charge leptons with large transverse momentum and a large momentum imbalance in the event due to the escaping neutrinos. The dominant backgrounds are non-resonant WW , $t\bar{t}$, and Wt production, all of which have real W pairs in the final state. Other important backgrounds include Drell–Yan events ($pp \rightarrow Z/\gamma^{(*)} \rightarrow \ell\ell$) with E_T^{miss} that may arise from mismeasurement, W + jets events in which a jet produces an object reconstructed as the second electron or muon, and $W\gamma$ events in which the photon undergoes a conversion. Boson pair production ($W\gamma^{(*)}/WZ^{(*)}$ and $ZZ^{(*)}$) can also produce opposite-charge lepton pairs with additional leptons that are not detected.

The analysis of the 8 TeV data presented here is focused on the mass range $110 < m_H < 200$ GeV. It follows the procedure used for the 7 TeV data, described in Ref. [106], except that more stringent criteria are applied to reduce the W + jets background and some selections have been modified to mitigate the impact of the higher instantaneous luminosity at the LHC in 2012. In particular, the higher luminosity results in a larger Drell–Yan background to the same-flavour final states, due to the deterioration of the missing transverse momentum resolution. For this reason, and the fact that the $e\mu$ final state provides more than 85% of the sensitivity of

the search, the same-flavour final states have not been used in the analysis described here.

6.1. Event selection

For the 8 TeV $H \rightarrow WW^{(*)} \rightarrow e\nu\mu\nu$ search, the data are selected using inclusive single-muon and single-electron triggers. Both triggers require an isolated lepton with $p_T > 24$ GeV. Quality criteria are applied to suppress non-collision backgrounds such as cosmic-ray muons, beam-related backgrounds, and noise in the calorimeters. The primary vertex selection follows that described in Section 4. Candidates for the $H \rightarrow WW^{(*)} \rightarrow e\nu\mu\nu$ search are pre-selected by requiring exactly two opposite-charge leptons of different flavours, with p_T thresholds of 25 GeV for the leading lepton and 15 GeV for the sub-leading lepton. Events are classified into two exclusive lepton channels depending on the flavour of the leading lepton, where $e\mu$ (μe) refers to events with a leading electron (muon). The dilepton invariant mass is required to be greater than 10 GeV.

The lepton selection and isolation have more stringent requirements than those used for the $H \rightarrow ZZ^{(*)} \rightarrow 4\ell$ analysis (see Section 4), to reduce the larger background from non-prompt leptons in the $\ell\nu\ell\nu$ final state. Electron candidates are selected using a combination of tracking and calorimetric information [85]; the criteria are optimised for background rejection, at the expense of some reduced efficiency. Muon candidates are restricted to those with matching MS and ID tracks [84], and therefore are reconstructed over $|\eta| < 2.5$. The isolation criteria require the scalar sums of the p_T of charged particles and of calorimeter topological clusters within $\Delta R = 0.3$ of the lepton direction (excluding the lepton itself) each to be less than 0.12–0.20 times the lepton p_T . The exact value differs between the criteria for tracks and calorimeter clusters, for both electrons and muons, and depends on the lepton p_T . Jet selections follow those described in Section 5.3, except that the JVF is required to be greater than 0.5.

Since two neutrinos are present in the signal final state, events are required to have large E_T^{miss} . $\mathbf{E}_T^{\text{miss}}$ is the negative vector sum of the transverse momenta of the reconstructed objects, including muons, electrons, photons, jets, and clusters of calorimeter cells not associated with these objects. The quantity $E_{T,\text{rel}}^{\text{miss}}$ used in this analysis is required to be greater than 25 GeV and is defined as: $E_{T,\text{rel}}^{\text{miss}} = E_T^{\text{miss}} \sin \Delta\phi_{\text{min}}$, where $\Delta\phi_{\text{min}}$ is $\min(\Delta\phi, \frac{\pi}{2})$, and E_T^{miss} is the magnitude of the vector $\mathbf{E}_T^{\text{miss}}$. Here, $\Delta\phi$ is the angle between $\mathbf{E}_T^{\text{miss}}$ and the transverse momentum of the nearest lepton or jet with $p_T > 25$ GeV. Compared to E_T^{miss} , $E_{T,\text{rel}}^{\text{miss}}$ has increased rejection power for events in which the E_T^{miss} is generated by a neutrino in a jet or the mismeasurement of an object, since in those events the $\mathbf{E}_T^{\text{miss}}$ tends to point in the direction of the object. After the lepton isolation and $E_{T,\text{rel}}^{\text{miss}}$ requirements that define the pre-selected sample, the multijet background is negligible and the Drell–Yan background is much reduced. The Drell–Yan contribution becomes very small after the topological selections, described below, are applied.

The background rate and composition depend significantly on the jet multiplicity, as does the signal topology. Without accompanying jets, the signal originates almost entirely from the ggF process and the background is dominated by WW events. In contrast, when produced in association with two or more jets, the signal contains a much larger contribution from the VBF process compared to the ggF process, and the background is dominated by $t\bar{t}$ production. Therefore, to maximise the sensitivity to SM Higgs events, further selection criteria depending on the jet multiplicity are applied to the pre-selected sample. The data are subdivided into 0-jet, 1-jet and 2-jet search channels according to the number

of jets in the final state, with the 2-jet channel also including higher jet multiplicities.

Owing to spin correlations in the $WW^{(*)}$ system arising from the spin-0 nature of the SM Higgs boson and the V-A structure of the W boson decay vertex, the charged leptons tend to emerge from the primary vertex pointing in the same direction [107]. This kinematic feature is exploited for all jet multiplicities by requiring that $|\Delta\phi_{\ell\ell}| < 1.8$, and the dilepton invariant mass, $m_{\ell\ell}$, be less than 50 GeV for the 0-jet and 1-jet channels. For the 2-jet channel, the $m_{\ell\ell}$ upper bound is increased to 80 GeV.

In the 0-jet channel, the magnitude $p_T^{\ell\ell}$ of the transverse momentum of the dilepton system, $\mathbf{p}_T^{\ell\ell} = \mathbf{p}_T^{\ell 1} + \mathbf{p}_T^{\ell 2}$, is required to be greater than 30 GeV. This improves the rejection of the Drell–Yan background.

In the 1-jet channel, backgrounds from top quark production are suppressed by rejecting events containing a b -tagged jet, as determined using a b -tagging algorithm that uses a neural network and exploits the topology of weak decays of b - and c -hadrons [108]. The total transverse momentum, p_T^{tot} , defined as the magnitude of the vector sum $\mathbf{p}_T^{\text{tot}} = \mathbf{p}_T^{\ell 1} + \mathbf{p}_T^{\ell 2} + \mathbf{p}_T^j + \mathbf{E}_T^{\text{miss}}$, is required to be smaller than 30 GeV to suppress top background events that have jets with p_T below the threshold defined for jet counting. In order to reject the background from $Z \rightarrow \tau\tau$, the $\tau\tau$ invariant mass, $m_{\tau\tau}$, is computed under the assumptions that the reconstructed leptons are τ lepton decay products. In addition the neutrinos produced in these decays are assumed to be the only source of E_T^{miss} and to be collinear with the leptons [109]. Events with $|m_{\tau\tau} - m_Z| < 25$ GeV are rejected if the collinear approximation yields a physical solution.

The 2-jet selection follows the 1-jet selection described above, with the p_T^{tot} definition modified to include all selected jets. Motivated by the VBF topology, several additional criteria are applied to the tag jets, defined as the two highest- p_T jets in the event. These are required to be separated in rapidity by a distance $|\Delta y_{jj}| > 3.8$ and to have an invariant mass, m_{jj} , larger than 500 GeV. Events with an additional jet with $p_T > 20$ GeV between the tag jets ($y_{j1} < y < y_{j2}$) are rejected.

A transverse mass variable, m_T [110], is used to test for the presence of a signal for all jet multiplicities. This variable is defined as:

$$m_T = \sqrt{(E_T^{\ell\ell} + E_T^{\text{miss}})^2 - |\mathbf{p}_T^{\ell\ell} + \mathbf{E}_T^{\text{miss}}|^2},$$

where $E_T^{\ell\ell} = \sqrt{|\mathbf{p}_T^{\ell\ell}|^2 + m_{\ell\ell}^2}$. The statistical analysis of the data uses a fit to the m_T distribution in the signal region after the $\Delta\phi_{\ell\ell}$ requirement (see Section 6.4), which results in increased sensitivity compared to the analysis described in Ref. [111].

For a SM Higgs boson with $m_H = 125$ GeV, the cross section times branching ratio to the $e\nu\mu\nu$ final state is 88 fb for $\sqrt{s} = 7$ TeV, increasing to 112 fb at $\sqrt{s} = 8$ TeV. The combined acceptance times efficiency of the 8 TeV 0-jet and 1-jet selection relative to the ggF production cross section times branching ratio is about 7.4%. The acceptance times efficiency of the 8 TeV 2-jet selection relative to the VBF production cross section times branching ratio is about 14%. Both of these figures are based on the number of events selected before the final m_T criterion is applied (as described in Section 6.4).

6.2. Background normalisation and control samples

The leading backgrounds from SM processes producing two isolated high- p_T leptons are WW and top (in this section, “top” background always includes both $t\bar{t}$ and single top, unless otherwise noted). These are estimated using partially data-driven techniques

based on normalising the MC predictions to the data in control regions dominated by the relevant background source. The W + jets background is estimated from data for all jet multiplicities. Only the small backgrounds from Drell–Yan and diboson processes other than WW , as well as the WW background for the 2-jet analysis, are estimated using MC simulation.

The control and validation regions are defined by selections similar to those used for the signal region but with some criteria reversed or modified to obtain signal-depleted samples enriched in a particular background. The term “validation region” distinguishes these regions from the control regions that are used to directly normalise the backgrounds. Some control regions have significant contributions from backgrounds other than the targeted one, which introduces dependencies among the background estimates. These correlations are fully incorporated in the fit to the m_T distribution. In the following sections, each background estimate is described after any others on which it depends. Hence, the largest background (WW) is described last.

6.2.1. W + jets background estimation

The W + jets background contribution is estimated using a control sample of events where one of the two leptons satisfies the identification and isolation criteria described in Section 6.1, and the other lepton fails these criteria but satisfies a loosened selection (denoted “anti-identified”). Otherwise, events in this sample are required to pass all the signal selections. The dominant contribution to this sample comes from W + jets events in which a jet produces an object that is reconstructed as a lepton. This object may be either a true electron or muon from the decay of a heavy quark, or else a product of the fragmentation identified as a lepton candidate.

The contamination in the signal region is obtained by scaling the number of events in the data control sample by a transfer factor. The transfer factor is defined here as the ratio of the number of identified lepton candidates passing all selections to the number of anti-identified leptons. It is calculated as a function of the anti-identified lepton p_T using a data sample dominated by QCD jet production (dijet sample) after subtracting the residual contributions from leptons produced by leptonic W and Z decays, as estimated from data. The small remaining lepton contamination, which includes $W\gamma^{(*)}/WZ^{(*)}$ events, is subtracted using MC simulation.

The processes producing the majority of same-charge dilepton events, W + jets, $W\gamma^{(*)}/WZ^{(*)}$ and $Z^{(*)}Z^{(*)}$, are all backgrounds in the opposite-charge signal region. W + jets and $W\gamma^{(*)}$ backgrounds are particularly important in a search optimised for a low Higgs boson mass hypothesis. Therefore, the normalisation and kinematic features of same-charge dilepton events are used to validate the predictions of these backgrounds. The predicted number of same-charge events after the $E_{T,\text{rel}}^{\text{miss}}$ and zero-jet requirements is 216 ± 7 (stat) ± 42 (syst), while 182 events are observed in the data. Satisfactory agreement between data and simulation is observed in various kinematic distributions, including those of $\Delta\phi_{\ell\ell}$ (see Fig. 5(a)) and the transverse mass.

6.2.2. Top control sample

In the 0-jet channel, the top quark background prediction is first normalised using events satisfying the pre-selection criteria described in Section 6.1. This sample is selected without jet multiplicity or b -tagging requirements, and the majority of events contain top quarks. Non-top contributions are subtracted using predictions from simulation, except for W + jets, which is estimated using data. After this normalisation is performed, the fraction of events with zero jets that pass all selections is evaluated. This fraction is small (about 3%), since the top quark decay $t \rightarrow Wb$

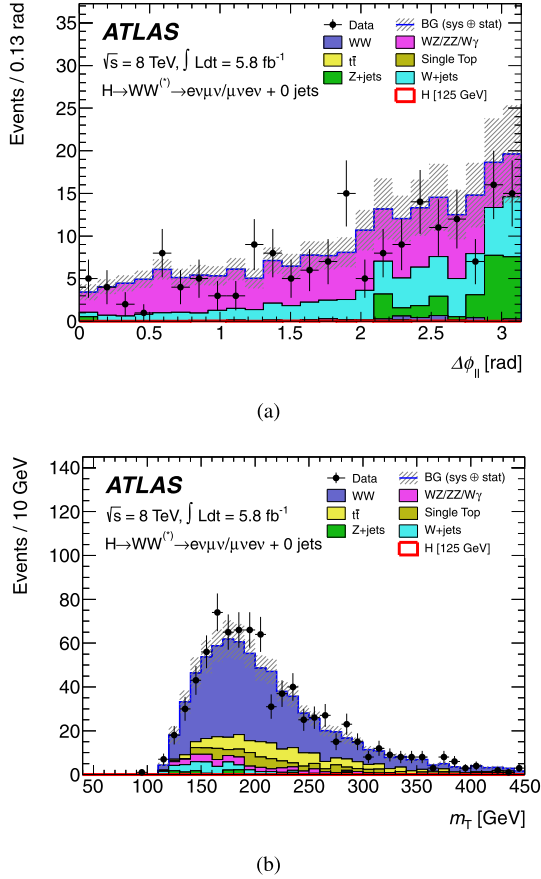


Fig. 5. Validation and control distributions for the $H \rightarrow WW^{(*)} \rightarrow e\nu\mu\nu$ analysis. (a) $\Delta\phi_{\ell\ell}$ distribution in the same-charge validation region after the $E_{T,\text{rel}}^{\text{miss}}$ and zero-jet requirements. (b) m_T distribution in the WW control region for the 0-jet channel. The $e\mu$ and μe final states are combined. The hashed area indicates the total uncertainty on the background prediction. The expected signal for $m_H = 125 \text{ GeV}$ is negligible and therefore not visible.

has a branching ratio of nearly 1. Predictions of this fraction from MC simulation are sensitive to theoretical uncertainties such as the modelling of initial- and final-state radiation, as well as experimental uncertainties, especially that on the jet energy scale. To reduce the impact of these uncertainties, the top quark background determination uses data from a b -tagged control region in which the one-to-two jet ratio is compared to the MC simulation [112]. The resulting correction factor to a purely MC-based background estimate after all selections amounts to 1.11 ± 0.06 (stat).

In the 1-jet and 2-jet analyses, the top quark background predictions are normalised to the data using control samples defined by reversing the b -jet veto and removing the requirements on $\Delta\phi_{\ell\ell}$ and $m_{\ell\ell}$. The $|\Delta y_{jj}|$ and m_{jj} requirements are included in the definition of the 2-jet control region. The resulting samples are dominated by top quark events. The small contributions from other sources are taken into account using MC simulation and the data-driven W + jets estimate. Good agreement between data and MC simulation is observed for the total numbers of events and the shapes of the m_T distributions. The resulting normalisation factors are 1.11 ± 0.05 for the 1-jet control region and 1.01 ± 0.26 for the 2-jet control region. Only the statistical uncertainties are quoted.

6.2.3. WW control sample

The MC predictions of the WW background in the 0-jet and 1-jet analyses, summed over lepton flavours, are normalised using control regions defined with the same selections as for the signal

region except that the $\Delta\phi_{\ell\ell}$ requirement is removed and the upper bound on $m_{\ell\ell}$ is replaced with a lower bound: $m_{\ell\ell} > 80 \text{ GeV}$. The numbers of events and the shape of the m_T distribution in the control regions are in good agreement between data and MC, as shown in Fig. 5(b). WW production contributes about 70% of the events in the 0-jet control region and about 45% in the 1-jet region. Contaminations from sources other than WW are derived as for the signal region, including the data-driven W + jets and top estimates. The resulting normalisation factors with their associated statistical uncertainties are 1.06 ± 0.06 for the 0-jet control region and 0.99 ± 0.15 for the 1-jet control region.

6.3. Systematic uncertainties

The systematic uncertainties that have the largest impact on the sensitivity of the search are the theoretical uncertainties associated with the signal. These are described in Section 9. The main experimental uncertainties are associated with the JES, the jet energy resolution (JER), pile-up, E_T^{miss} , the b -tagging efficiency, the W + jets transfer factor, and the integrated luminosity. The largest uncertainties on the backgrounds include WW normalisation and modelling, top normalisation, and $W\gamma^{(*)}$ normalisation. The 2-jet systematic uncertainties are dominated by the statistical uncertainties in the data and the MC simulation, and are therefore not discussed further.

Variations of the jet energy scale within the systematic uncertainties can cause events to migrate between the jet bins. The uncertainty on the JES varies from $\pm 2\%$ to $\pm 9\%$ as a function of jet p_T and η for jets with $p_T > 25 \text{ GeV}$ and $|\eta| < 4.5$ [101]. The largest impact of this uncertainty on the total signal (background) yield amounts to 7% (4%) in the 0-jet (1-jet) bin. The uncertainty on the JER is estimated from *in situ* measurements and it impacts mostly the 1-jet channel, where its effect on the total signal and background yields is 4% and 2%, respectively. An additional contribution to the JES uncertainty arises from pile-up, and is estimated to vary between $\pm 1\%$ and $\pm 5\%$ for multiple pp collisions in the same bunch crossing and up to $\pm 10\%$ for neighbouring bunch crossings. This uncertainty affects mainly the 1-jet channel, where its impact on the signal and background yields is 4% and 2%, respectively. JES and lepton momentum scale uncertainties are propagated to the E_T^{miss} measurement. Additional contributions to the E_T^{miss} uncertainties arise from jets with $p_T < 20 \text{ GeV}$ and from low-energy calorimeter deposits not associated with reconstructed physics objects [113]. The impact of the E_T^{miss} uncertainty on the total signal and background yields is $\sim 3\%$. The efficiency of the b -tagging algorithm is calibrated using samples containing muons reconstructed in the vicinity of jets [114]. The uncertainty on the b -jet tagging efficiency varies between $\pm 5\%$ and $\pm 18\%$ as a function of the jet p_T , and its impact on the total background yield is 10% for the 1-jet channel. The uncertainty in the W + jets transfer factor is dominated by differences in jet properties between dijet and W + jets events as observed in MC simulations. The total uncertainty on this background is approximately $\pm 40\%$, resulting in an uncertainty on the total background yield of 5%. The uncertainty on the integrated luminosity is $\pm 3.6\%$.

A fit to the distribution of m_T is performed in order to obtain the signal yield for each mass hypothesis (see Section 6.4). Most theoretical and experimental uncertainties do not produce statistically significant changes to the m_T distribution. The uncertainties that do produce significant changes of the distribution of m_T have no appreciable effect on the final results, with the exception of those associated with the WW background. In this case, an uncertainty is included to take into account differences in the distribution of m_T and normalisation observed between the MCFM [115], MC@NLO + HERWIG and POWHEG + PYTHIA

Table 5

The expected numbers of signal ($m_H = 125$ GeV) and background events after all selections, including a cut on the transverse mass of $0.75m_H < m_T < m_H$ for $m_H = 125$ GeV. The observed numbers of events in data are also displayed. The $e\mu$ and μe channels are combined. The uncertainties shown are the combination of the statistical and all systematic uncertainties, taking into account the constraints from control samples. For the 2-jet analysis, backgrounds with fewer than 0.01 expected events are marked with ‘-’.

	0-jet	1-jet	2-jet
Signal	20 ± 4	5 ± 2	0.34 ± 0.07
WW	101 ± 13	12 ± 5	0.10 ± 0.14
$WZ^{(*)}/ZZ/W\gamma^{(*)}$	12 ± 3	1.9 ± 1.1	0.10 ± 0.10
$t\bar{t}$	8 ± 2	6 ± 2	0.15 ± 0.10
$tW/tb/tqb$	3.4 ± 1.5	3.7 ± 1.6	-
$Z/\gamma^* + \text{jets}$	1.9 ± 1.3	0.10 ± 0.10	-
$W + \text{jets}$	15 ± 7	2 ± 1	-
Total background	142 ± 16	26 ± 6	0.35 ± 0.18
Observed	185	38	0

generators. The potential impact of interference between resonant (Higgs-mediated) and non-resonant $gg \rightarrow WW$ diagrams [116] for $m_T > m_H$ was investigated and found to be negligible. The effect of the WW normalisation, modelling, and shape systematics on the total background yield is 9% for the 0-jet channel and 19% for the 1-jet channel. The uncertainty on the shape of the total background is dominated by the uncertainties on the normalisations of the individual backgrounds. The main uncertainties on the top background in the 0-jet analysis include those associated with interference effects between $t\bar{t}$ and single top, initial state and final state radiation, b -tagging, and JER. The impact on the total background yield in the 0-jet bin is 3%. For the 1-jet analysis, the impact of the top background on the total yield is 14%. Theoretical uncertainties on the $W\gamma$ background normalisation are evaluated for each jet bin using the procedure described in Ref. [117]. They are $\pm 11\%$ for the 0-jet bin and $\pm 50\%$ for the 1-jet bin. For $W\gamma^*$ with $m_{\ell\ell} < 7$ GeV, a k -factor of 1.3 ± 0.3 is applied to the MadGraph LO prediction based on the comparison with the MCFM NLO calculation. The k -factor for $W\gamma^*/WZ^{(*)}$ with $m_{\ell\ell} > 7$ GeV is 1.5 ± 0.5 . These uncertainties affect mostly the 1-jet channel, where their impact on the total background yield is approximately 4%.

6.4. Results

Table 5 shows the numbers of events expected from a SM Higgs boson with $m_H = 125$ GeV and from the backgrounds, as well as the numbers of candidates observed in data, after application of all selection criteria plus an additional cut on m_T of $0.75m_H < m_T < m_H$. The uncertainties shown in Table 5 include the systematic uncertainties discussed in Section 6.3, constrained by the use of the control regions discussed in Section 6.2. An excess of events relative to the background expectation is observed in the data.

Fig. 6 shows the distribution of the transverse mass after all selection criteria in the 0-jet and 1-jet channels combined, and for both lepton channels together.

The statistical analysis of the data employs a binned likelihood function constructed as the product of Poisson probability terms for the $e\mu$ channel and the μe channel. The mass-dependent cuts on m_T described above are not used. Instead, the 0-jet (1-jet) signal regions are subdivided into five (three) m_T bins. For the 2-jet signal region, only the results integrated over m_T are used, due to the small number of events in the final sample. The statistical interpretation of the observed excess of events is presented in Section 9.

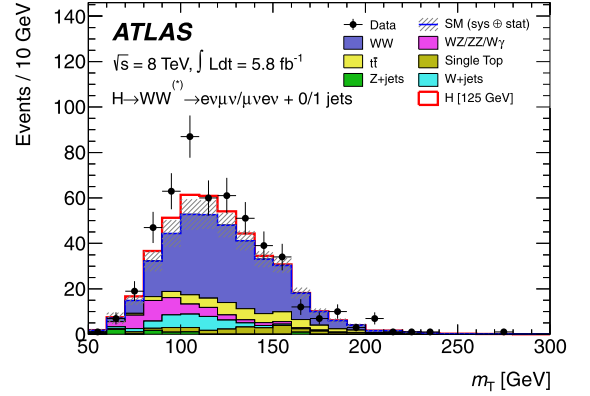


Fig. 6. Distribution of the transverse mass, m_T , in the 0-jet and 1-jet analyses with both $e\mu$ and μe channels combined, for events satisfying all selection criteria. The expected signal for $m_H = 125$ GeV is shown stacked on top of the background prediction. The $W + \text{jets}$ background is estimated from data, and WW and top background MC predictions are normalised to the data using control regions. The hashed area indicates the total uncertainty on the background prediction.

7. Statistical procedure

The statistical procedure used to interpret the data is described in Refs. [17,118–121]. The parameter of interest is the global signal strength factor μ , which acts as a scale factor on the total number of events predicted by the Standard Model for the Higgs boson signal. This factor is defined such that $\mu = 0$ corresponds to the background-only hypothesis and $\mu = 1$ corresponds to the SM Higgs boson signal in addition to the background. Hypothesised values of μ are tested with a statistic $\lambda(\mu)$ based on the profile likelihood ratio [122]. This test statistic extracts the information on the signal strength from a full likelihood fit to the data. The likelihood function includes all the parameters that describe the systematic uncertainties and their correlations.

Exclusion limits are based on the CL_s prescription [123]; a value of μ is regarded as excluded at 95% CL when CL_s is less than 5%. A SM Higgs boson with mass m_H is considered excluded at 95% confidence level (CL) when $\mu = 1$ is excluded at that mass. The significance of an excess in the data is first quantified with the local p_0 , the probability that the background can produce a fluctuation greater than or equal to the excess observed in data. The equivalent formulation in terms of number of standard deviations, Z_l , is referred to as the local significance. The global probability for the most significant excess to be observed anywhere in a given search region is estimated with the method described in Ref. [124]. The ratio of the global to the local probabilities, the trials factor used to correct for the “look elsewhere” effect, increases with the range of Higgs boson mass hypotheses considered, the mass resolutions of the channels involved in the combination, and the significance of the excess.

The statistical tests are performed in steps of values of the hypothesised Higgs boson mass m_H . The asymptotic approximation [122] upon which the results are based has been validated with the method described in Ref. [17].

The combination of individual search sub-channels for a specific Higgs boson decay, and the full combination of all search channels, are based on the global signal strength factor μ and on the identification of the nuisance parameters that correspond to the correlated sources of systematic uncertainty described in Section 8.

8. Correlated systematic uncertainties

The individual search channels that enter the combination are summarised in Table 6.

Table 6
Summary of the individual channels entering the combination. The transition points between separately optimised m_H regions are indicated where applicable. In channels sensitive to associated production of the Higgs boson, V indicates a W or Z boson. The symbols \otimes and \oplus represent direct products and sums over sets of selection requirements, respectively.

Higgs boson decay	Subsequent decay	Sub-channels	m_H range [GeV]	$\int L dt$ [fb^{-1}]	Ref.
2011 $\sqrt{s} = 7$ TeV					
$H \rightarrow ZZ^{(*)}$	4ℓ	$\{4e, 2e2\mu, 2\mu2e, 4\mu\}$	110–600	4.8	[87]
	$\ell\nu\ell\nu$	$\{ee, \mu\mu\} \otimes \{\text{low, high pile-up}\}$	200–280–600	4.7	[125]
	$\ell\ell q\bar{q}$	$\{b\text{-tagged, untagged}\}$	200–300–600	4.7	[126]
$H \rightarrow \gamma\gamma$	–	10 categories $\{p_{Tt} \otimes \eta_\gamma \otimes \text{conversion}\} \oplus \{2\text{-jet}\}$	110–150	4.8	[127]
$H \rightarrow WW^{(*)}$	$\ell\nu\ell\nu$	$\{ee, e\mu/\mu e, \mu\mu\} \otimes \{0\text{-jet, 1-jet, 2-jet}\} \otimes \{\text{low, high pile-up}\}$	110–200–300–600	4.7	[106]
	$\ell\nu qq'$	$\{e, \mu\} \otimes \{0\text{-jet, 1-jet, 2-jet}\}$	300–600	4.7	[128]
$H \rightarrow \tau\tau$	$\tau_{\text{lep}}\tau_{\text{lep}}$	$\{e\mu\} \otimes \{0\text{-jet}\} \oplus \{\ell\ell\} \otimes \{1\text{-jet, 2-jet, } VH\}$	110–150	4.7	[129]
	$\tau_{\text{lep}}\tau_{\text{had}}$	$\{e, \mu\} \otimes \{0\text{-jet}\} \otimes \{E_T^{\text{miss}} < 20 \text{ GeV}, E_T^{\text{miss}} \geq 20 \text{ GeV}\}$	110–150	4.7	
	$\tau_{\text{had}}\tau_{\text{had}}$	$\{1\text{-jet}\}$	110–150	4.7	
$VH \rightarrow Vbb$	$Z \rightarrow \nu\nu$	$E_T^{\text{miss}} \in \{120\text{--}160, 160\text{--}200, \geq 200 \text{ GeV}\}$	110–130	4.6	[130]
	$W \rightarrow \ell\nu$	$p_T^W \in \{< 50, 50\text{--}100, 100\text{--}200, \geq 200 \text{ GeV}\}$	110–130	4.7	
	$Z \rightarrow \ell\ell$	$p_T^Z \in \{< 50, 50\text{--}100, 100\text{--}200, \geq 200 \text{ GeV}\}$	110–130	4.7	
2012 $\sqrt{s} = 8$ TeV					
$H \rightarrow ZZ^{(*)}$	4ℓ	$\{4e, 2e2\mu, 2\mu2e, 4\mu\}$	110–600	5.8	[87]
$H \rightarrow \gamma\gamma$	–	10 categories $\{p_{Tt} \otimes \eta_\gamma \otimes \text{conversion}\} \oplus \{2\text{-jet}\}$	110–150	5.9	[127]
$H \rightarrow WW^{(*)}$	$e\nu\mu\nu$	$\{e\mu, \mu e\} \otimes \{0\text{-jet, 1-jet, 2-jet}\}$	110–200	5.8	[131]

The main uncorrelated systematic uncertainties are described in Sections 4–6 for the $H \rightarrow ZZ^{(*)} \rightarrow 4\ell$, $H \rightarrow \gamma\gamma$ and $H \rightarrow WW^{(*)} \rightarrow \ell\nu\ell\nu$ channels and in Ref. [17] for the other channels. They include the background normalisations or background model parameters from control regions or sidebands, the Monte Carlo simulation statistical uncertainties and the theoretical uncertainties affecting the background processes.

The main sources of correlated systematic uncertainties are the following.

1. *Integrated luminosity*: The uncertainty on the integrated luminosity is considered as fully correlated among channels and amounts to $\pm 3.9\%$ for the 7 TeV data [132,133], except for the $H \rightarrow ZZ^{(*)} \rightarrow 4\ell$ and $H \rightarrow \gamma\gamma$ channels which were re-analysed; the uncertainty is $\pm 1.8\%$ [92] for these channels. The uncertainty is $\pm 3.6\%$ for the 8 TeV data.

2. *Electron and photon trigger identification*: The uncertainties in the trigger and identification efficiencies are treated as fully correlated for electrons and photons.

3. *Electron and photon energy scales*: The electron and photon energy scales in the $H \rightarrow ZZ^{(*)} \rightarrow 4\ell$ and $H \rightarrow \gamma\gamma$ channels are described by five parameters, which provide a detailed account of the sources of systematic uncertainty. They are related to the calibration method, the presampler energy scale in the barrel and end-cap calorimeters, and the material description upstream of the calorimeters.

4. *Muon reconstruction*: The uncertainties affecting muons are separated into those related to the ID and MS, in order to obtain a better description of the correlated effects among channels using different muon identification criteria and different ranges of muon p_T .

5. *Jet energy scale and missing transverse energy*: The jet energy scale and jet energy resolution are affected by uncertainties which depend on the p_T , η , and flavour of the jet. A simplified scheme is used in which independent JES and JER nuisance parameters are associated with final states with significantly different kinematic selections and sensitivity to scattering processes with different kinematic distributions or flavour composition. This scheme includes a specific treatment for b -jets. The sensitivity of the results to various assumptions about the correlation between these sources of uncertainty has been found to be negligible. An uncorrelated component of the uncertainty on E_T^{miss} is included, in

addition to the JES uncertainty, which is due to low energy jet activity not associated with reconstructed physics objects.

6. *Theory uncertainties*: Correlated theoretical uncertainties affect mostly the signal predictions. The QCD scale uncertainties for $m_H = 125$ GeV amount to $^{+7\%}_{-8\%}$ for the ggF process, $\pm 1\%$ for the VBF and WH/ZH processes, and $^{+4\%}_{-9\%}$ for the $t\bar{t}H$ process [52,53]; the small dependence of these uncertainties on m_H is taken into account. The uncertainties on the predicted branching ratios amount to $\pm 5\%$. The uncertainties related to the parton distribution functions amount to $\pm 8\%$ for the predominantly gluon-initiated ggF and $t\bar{t}H$ processes, and $\pm 4\%$ for the predominantly quark-initiated VBF and WH/ZH processes [78,134–136]. The theoretical uncertainty associated with the exclusive Higgs boson production process with additional jets in the $H \rightarrow \gamma\gamma$, $H \rightarrow WW^{(*)} \rightarrow \ell\nu\ell\nu$ and $H \rightarrow \tau^+\tau^-$ channels is estimated using the prescription of Refs. [53,117,118], with the noticeable difference that an explicit calculation of the gluon-fusion process at NLO using MCFM [137] in the 2-jet category reduces the uncertainty on this non-negligible contribution to 25%. An additional theoretical uncertainty on the signal normalisation of $\pm 150\% \times (m_H/\text{TeV})^3$ (e.g. $\pm 4\%$ for $m_H = 300$ GeV) accounts for effects related to off-shell Higgs boson production and interference with other SM processes [53].

Sources of systematic uncertainty that affect both the 7 TeV and the 8 TeV data are taken as fully correlated. The uncertainties on background estimates based on control samples in the data are considered uncorrelated between the 7 TeV and 8 TeV data.

9. Results

The addition of the 8 TeV data for the $H \rightarrow ZZ^{(*)} \rightarrow 4\ell$, $H \rightarrow \gamma\gamma$ and $H \rightarrow WW^{(*)} \rightarrow e\nu\mu\nu$ channels, as well as the improvements to the analyses of the 7 TeV data in the first two of these channels, bring a significant gain in sensitivity in the low-mass region with respect to the previous combined search [17].

9.1. Excluded mass regions

The combined 95% CL exclusion limits on the production of the SM Higgs boson, expressed in terms of the signal strength parameter μ , are shown in Fig. 7(a) as a function of m_H . The expected 95% CL exclusion region covers the m_H range from 110 GeV to

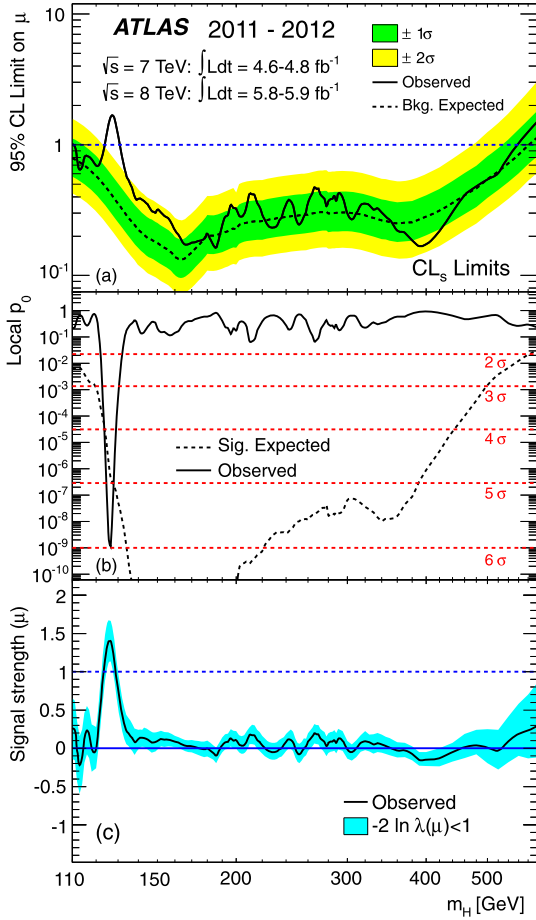


Fig. 7. Combined search results: (a) The observed (solid) 95% CL limits on the signal strength as a function of m_H and the expectation (dashed) under the background-only hypothesis. The dark and light shaded bands show the $\pm 1\sigma$ and $\pm 2\sigma$ uncertainties on the background-only expectation. (b) The observed (solid) local p_0 as a function of m_H and the expectation (dashed) for a SM Higgs boson signal hypothesis ($\mu = 1$) at the given mass. (c) The best-fit signal strength $\hat{\mu}$ as a function of m_H . The band indicates the approximate 68% CL interval around the fitted value.

582 GeV. The observed 95% CL exclusion regions are 111–122 GeV and 131–559 GeV. Three mass regions are excluded at 99% CL, 113–114, 117–121 and 132–527 GeV, while the expected exclusion range at 99% CL is 113–532 GeV.

9.2. Observation of an excess of events

An excess of events is observed near $m_H = 126$ GeV in the $H \rightarrow ZZ^{(*)} \rightarrow 4\ell$ and $H \rightarrow \gamma\gamma$ channels, both of which provide fully reconstructed candidates with high resolution in invariant mass, as shown in Figs. 8(a) and 8(b). These excesses are confirmed by the highly sensitive but low-resolution $H \rightarrow WW^{(*)} \rightarrow \ell\nu\ell\nu$ channel, as shown in Fig. 8(c).

The observed local p_0 values from the combination of channels, using the asymptotic approximation, are shown as a function of m_H in Fig. 7(b) for the full mass range and in Fig. 9 for the low mass range.

The largest local significance for the combination of the 7 and 8 TeV data is found for a SM Higgs boson mass hypothesis of $m_H = 126.5$ GeV, where it reaches 6.0σ , with an expected value in the presence of a SM Higgs boson signal at that mass of 4.9σ (see also Table 7). For the 2012 data alone, the maximum local significance for the $H \rightarrow ZZ^{(*)} \rightarrow 4\ell$, $H \rightarrow \gamma\gamma$ and $H \rightarrow WW^{(*)} \rightarrow$

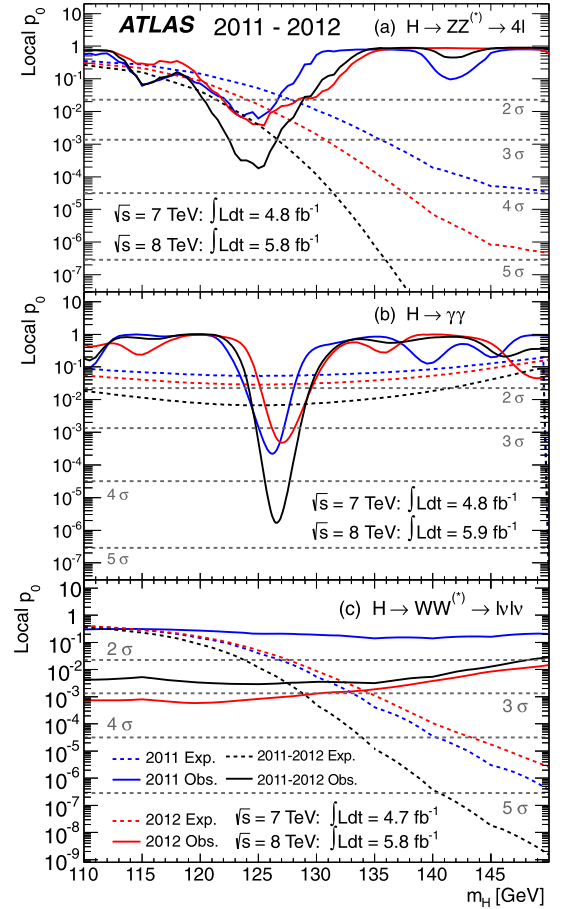


Fig. 8. The observed local p_0 as a function of the hypothesised Higgs boson mass for the (a) $H \rightarrow ZZ^{(*)} \rightarrow 4\ell$, (b) $H \rightarrow \gamma\gamma$ and (c) $H \rightarrow WW^{(*)} \rightarrow \ell\nu\ell\nu$ channels. The dashed curves show the expected local p_0 under the hypothesis of a SM Higgs boson signal at that mass. Results are shown separately for the $\sqrt{s} = 7$ TeV data (dark, blue in the web version), the $\sqrt{s} = 8$ TeV data (light, red in the web version), and their combination (black).

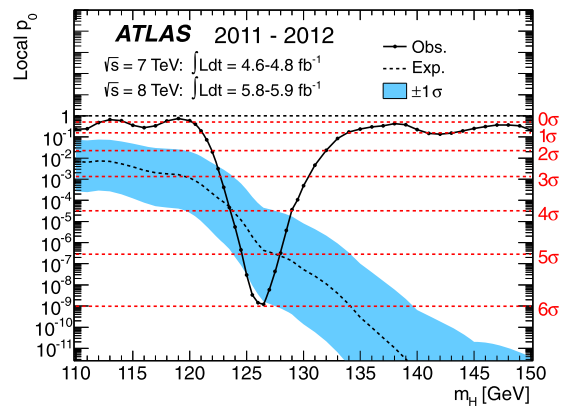


Fig. 9. The observed (solid) local p_0 as a function of m_H in the low mass range. The dashed curve shows the expected local p_0 under the hypothesis of a SM Higgs boson signal at that mass with its $\pm 1\sigma$ band. The horizontal dashed lines indicate the p -values corresponding to significances of 1 to 6σ .

$\ell\nu\ell\nu$ channels combined is 4.9σ , and occurs at $m_H = 126.5$ GeV (3.8σ expected).

The significance of the excess is mildly sensitive to uncertainties in the energy resolutions and energy scale systematic uncertainties for photons and electrons; the effect of the muon energy scale systematic uncertainties is negligible. The presence of these

Table 7
Characterisation of the excess in the $H \rightarrow ZZ^{(*)} \rightarrow 4\ell$, $H \rightarrow \gamma\gamma$ and $H \rightarrow WW^{(*)} \rightarrow \ell\nu\ell\nu$ channels and the combination of all channels listed in Table 6. The mass value m_{\max} for which the local significance is maximum, the maximum observed local significance Z_l and the expected local significance $E(Z_l)$ in the presence of a SM Higgs boson signal at m_{\max} are given. The best fit value of the signal strength parameter $\hat{\mu}$ at $m_H = 126$ GeV is shown with the total uncertainty. The expected and observed mass ranges excluded at 95% CL (99% CL, indicated by a *) are also given, for the combined $\sqrt{s} = 7$ TeV and $\sqrt{s} = 8$ TeV data.

Search channel	Dataset	m_{\max} [GeV]	Z_l [σ]	$E(Z_l)$ [σ]	$\hat{\mu}(m_H = 126 \text{ GeV})$	Expected exclusion [GeV]	Observed exclusion [GeV]
$H \rightarrow ZZ^{(*)} \rightarrow 4\ell$	7 TeV	125.0	2.5	1.6	1.4 ± 1.1		
	8 TeV	125.5	2.6	2.1	1.1 ± 0.8		
	7 & 8 TeV	125.0	3.6	2.7	1.2 ± 0.6	124–164, 176–500	131–162, 170–460
$H \rightarrow \gamma\gamma$	7 TeV	126.0	3.4	1.6	2.2 ± 0.7		
	8 TeV	127.0	3.2	1.9	1.5 ± 0.6		
	7 & 8 TeV	126.5	4.5	2.5	1.8 ± 0.5	110–140	112–123, 132–143
$H \rightarrow WW^{(*)} \rightarrow \ell\nu\ell\nu$	7 TeV	135.0	1.1	3.4	0.5 ± 0.6		
	8 TeV	120.0	3.3	1.0	1.9 ± 0.7		
	7 & 8 TeV	125.0	2.8	2.3	1.3 ± 0.5	124–233	137–261
Combined	7 TeV	126.5	3.6	3.2	1.2 ± 0.4		
	8 TeV	126.5	4.9	3.8	1.5 ± 0.4		
	7 & 8 TeV	126.5	6.0	4.9	1.4 ± 0.3	110–582 113–532 (*)	111–122, 131–559 113–114, 117–121, 132–527 (*)

uncertainties, evaluated as described in Ref. [138], reduces the local significance to 5.9σ .

The global significance of a local 5.9σ excess anywhere in the mass range 110–600 GeV is estimated to be approximately 5.1σ , increasing to 5.3σ in the range 110–150 GeV, which is approximately the mass range not excluded at the 99% CL by the LHC combined SM Higgs boson search [139] and the indirect constraints from the global fit to precision electroweak measurements [12].

9.3. Characterising the excess

The mass of the observed new particle is estimated using the profile likelihood ratio $\lambda(m_H)$ for $H \rightarrow ZZ^{(*)} \rightarrow 4\ell$ and $H \rightarrow \gamma\gamma$, the two channels with the highest mass resolution. The signal strength is allowed to vary independently in the two channels, although the result is essentially unchanged when restricted to the SM hypothesis $\mu = 1$. The leading sources of systematic uncertainty come from the electron and photon energy scales and resolutions. The resulting estimate for the mass of the observed particle is 126.0 ± 0.4 (stat) ± 0.4 (sys) GeV.

The best-fit signal strength $\hat{\mu}$ is shown in Fig. 7(c) as a function of m_H . The observed excess corresponds to $\hat{\mu} = 1.4 \pm 0.3$ for $m_H = 126$ GeV, which is consistent with the SM Higgs boson hypothesis $\mu = 1$. A summary of the individual and combined best-fit values of the strength parameter for a SM Higgs boson mass hypothesis of 126 GeV is shown in Fig. 10, while more information about the three main channels is provided in Table 7.

In order to test which values of the strength and mass of a signal hypothesis are simultaneously consistent with the data, the profile likelihood ratio $\lambda(\mu, m_H)$ is used. In the presence of a strong signal, it will produce closed contours around the best-fit point $(\hat{\mu}, \hat{m}_H)$, while in the absence of a signal the contours will be upper limits on μ for all values of m_H .

Asymptotically, the test statistic $-2 \ln \lambda(\mu, m_H)$ is distributed as a χ^2 distribution with two degrees of freedom. The resulting 68% and 95% CL contours for the $H \rightarrow \gamma\gamma$ and $H \rightarrow WW^{(*)} \rightarrow \ell\nu\ell\nu$ channels are shown in Fig. 11, where the asymptotic approximations have been validated with ensembles of pseudo-experiments. Similar contours for the $H \rightarrow ZZ^{(*)} \rightarrow 4\ell$ channel are also shown in Fig. 11, although they are only approximate confidence intervals due to the smaller number of candidates in this channel. These contours in the (μ, m_H) plane take into account uncertainties in the energy scale and resolution.

The probability for a single Higgs boson-like particle to produce resonant mass peaks in the $H \rightarrow ZZ^{(*)} \rightarrow 4\ell$ and $H \rightarrow \gamma\gamma$

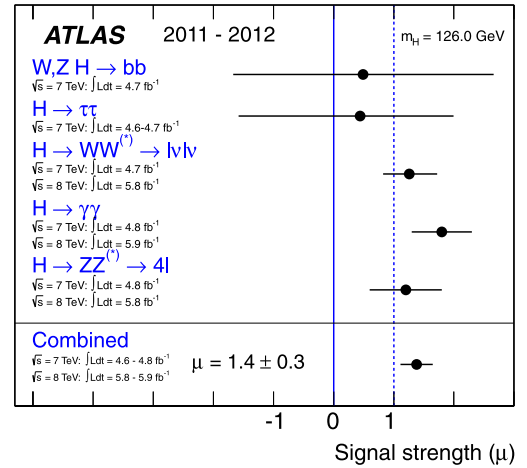


Fig. 10. Measurements of the signal strength parameter μ for $m_H = 126$ GeV for the individual channels and their combination.

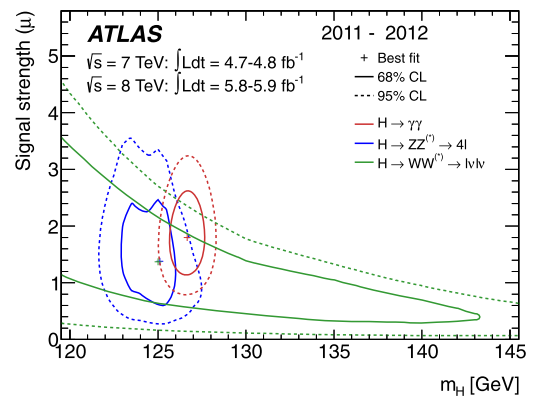


Fig. 11. Confidence intervals in the (μ, m_H) plane for the $H \rightarrow ZZ^{(*)} \rightarrow 4\ell$, $H \rightarrow \gamma\gamma$, and $H \rightarrow WW^{(*)} \rightarrow \ell\nu\ell\nu$ channels, including all systematic uncertainties. The markers indicate the maximum likelihood estimates $(\hat{\mu}, \hat{m}_H)$ in the corresponding channels (the maximum likelihood estimates for $H \rightarrow ZZ^{(*)} \rightarrow 4\ell$ and $H \rightarrow WW^{(*)} \rightarrow \ell\nu\ell\nu$ coincide).

channels separated by more than the observed mass difference, allowing the signal strengths to vary independently, is about 8%.

The contributions from the different production modes in the $H \rightarrow \gamma\gamma$ channel have been studied in order to assess any tension between the data and the ratios of the production cross

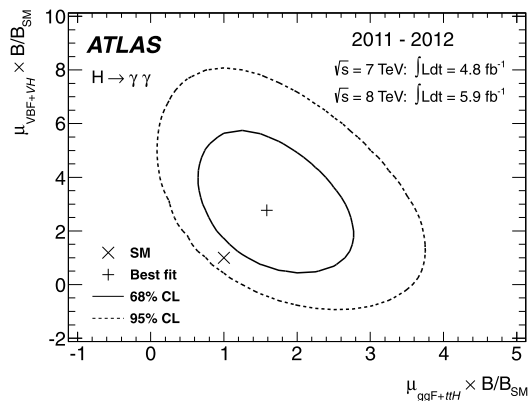


Fig. 12. Likelihood contours for the $H \rightarrow \gamma\gamma$ channel in the $(\mu_{ggF+t\bar{t}H}, \mu_{VBF+VH})$ plane including the branching ratio factor B/B_{SM} . The quantity $\mu_{ggF+t\bar{t}H}$ (μ_{VBF+VH}) is a common scale factor for the ggF and $t\bar{t}H$ (VBF and VH) production cross sections. The best fit to the data (+) and 68% (full) and 95% (dashed) CL contours are also indicated, as well as the SM expectation (\times).

sections predicted in the Standard Model. A new signal strength parameter μ_i is introduced for each production mode, defined by $\mu_i = \sigma_i/\sigma_{i,SM}$. In order to determine the values of (μ_i, μ_j) that are simultaneously consistent with the data, the profile likelihood ratio $\lambda(\mu_i, \mu_j)$ is used with the measured mass treated as a nuisance parameter.

Since there are four Higgs boson production modes at the LHC, two-dimensional contours require either some μ_i to be fixed, or multiple μ_i to be related in some way. Here, μ_{ggF} and $\mu_{t\bar{t}H}$ have been grouped together as they scale with the $t\bar{t}H$ coupling in the SM, and are denoted by the common parameter $\mu_{ggF+t\bar{t}H}$. Similarly, μ_{VBF} and μ_{VH} have been grouped together as they scale with the WWH/ZZH coupling in the SM, and are denoted by the common parameter μ_{VBF+VH} . Since the distribution of signal events among the 10 categories of the $H \rightarrow \gamma\gamma$ search is sensitive to these factors, constraints in the plane of $\mu_{ggF+t\bar{t}H} \times B/B_{SM}$ and $\mu_{VBF+VH} \times B/B_{SM}$, where B is the branching ratio for $H \rightarrow \gamma\gamma$, can be obtained (Fig. 12). Theoretical uncertainties are included so that the consistency with the SM expectation can be quantified. The data are compatible with the SM expectation at the 1.5σ level.

10. Conclusion

Searches for the Standard Model Higgs boson have been performed in the $H \rightarrow ZZ^{(*)} \rightarrow 4\ell$, $H \rightarrow \gamma\gamma$ and $H \rightarrow WW^{(*)} \rightarrow e\nu\mu\nu$ channels with the ATLAS experiment at the LHC using 5.8–5.9 fb^{-1} of pp collision data recorded during April to June 2012 at a centre-of-mass energy of 8 TeV. These results are combined with earlier results [17], which are based on an integrated luminosity of 4.6–4.8 fb^{-1} recorded in 2011 at a centre-of-mass energy of 7 TeV, except for the $H \rightarrow ZZ^{(*)} \rightarrow 4\ell$ and $H \rightarrow \gamma\gamma$ channels, which have been updated with the improved analyses presented here.

The Standard Model Higgs boson is excluded at 95% CL in the mass range 111–559 GeV, except for the narrow region 122–131 GeV. In this region, an excess of events with significance 5.9σ , corresponding to $p_0 = 1.7 \times 10^{-9}$, is observed. The excess is driven by the two channels with the highest mass resolution, $H \rightarrow ZZ^{(*)} \rightarrow 4\ell$ and $H \rightarrow \gamma\gamma$, and the equally sensitive but low-resolution $H \rightarrow WW^{(*)} \rightarrow \ell\nu\ell\nu$ channel. Taking into account the entire mass range of the search, 110–600 GeV, the global significance of the excess is 5.1σ , which corresponds to $p_0 = 1.7 \times 10^{-7}$.

These results provide conclusive evidence for the discovery of a new particle with mass 126.0 ± 0.4 (stat) ± 0.4 (sys) GeV. The signal strength parameter μ has the value 1.4 ± 0.3 at the fitted mass,

which is consistent with the SM Higgs boson hypothesis $\mu = 1$. The decays to pairs of vector bosons whose net electric charge is zero identify the new particle as a neutral boson. The observation in the diphoton channel disfavors the spin-1 hypothesis [140, 141]. Although these results are compatible with the hypothesis that the new particle is the Standard Model Higgs boson, more data are needed to assess its nature in detail.

Acknowledgements

The results reported in this Letter would not have been possible without the outstanding performance of the LHC. We warmly thank CERN and the entire LHC exploitation team, including the operation, technical and infrastructure groups, and all the people who have contributed to the conception, design and construction of this superb accelerator. We thank also the support staff at our institutions without whose excellent contributions ATLAS could not have been successfully constructed or operated so efficiently.

We acknowledge the support of ANPCyT, Argentina; YerPhI, Armenia; ARC, Australia; BMWF, Austria; ANAS, Azerbaijan; SSTC, Belarus; CNPq and FAPESP, Brazil; NSERC, NRC and CFI, Canada; CERN; CONICYT, Chile; CAS, MOST and NSFC, China; COLCIENCIAS, Colombia; MSMT CR, MPO CR and VSC CR, Czech Republic; DNRF, DNSRC and Lundbeck Foundation, Denmark; EPLANET and ERC, European Union; IN2P3-CNRS, CEA-DSM/IRFU, France; GNAS, Georgia; BMBF, DFG, HGF, MPG and AvH Foundation, Germany; GSRT, Greece; ISF, MINERVA, GIF, DIP and Benoziyo Center, Israel; INFN, Italy; MEXT and JSPS, Japan; CNRST, Morocco; FOM and NWO, Netherlands; RCN, Norway; MNiSW, Poland; GRICES and FCT, Portugal; MERYS (MECTS), Romania; MES of Russia and ROSATOM, Russian Federation; JINR; MSTD, Serbia; MSSR, Slovakia; ARRS and MVZT, Slovenia; DST/NRF, South Africa; MICINN, Spain; SRC and Wallenberg Foundation, Sweden; SER, SNSF and Cantons of Bern and Geneva, Switzerland; NSC, Taiwan; TAEK, Turkey; STFC, the Royal Society and Leverhulme Trust, United Kingdom; DOE and NSF, United States of America.

The crucial computing support from all WLCG partners is acknowledged gratefully, in particular from CERN and the ATLAS Tier-1 facilities at TRIUMF (Canada), NDGF (Denmark, Norway, Sweden), CC-IN2P3 (France), KIT/GridKA (Germany), INFN-CNAF (Italy), NL-T1 (Netherlands), PIC (Spain), ASGC (Taiwan), RAL (UK) and BNL (USA) and in the Tier-2 facilities worldwide.

Open access

This article is published Open Access at sciencedirect.com. It is distributed under the terms of the Creative Commons Attribution License 3.0, which permits unrestricted use, distribution, and reproduction in any medium, provided the original authors and source are credited.

References

- [1] S.L. Glashow, Nucl. Phys. 22 (4) (1961) 579.
- [2] S. Weinberg, Phys. Rev. Lett. 19 (1967) 1264.
- [3] A. Salam, in: N. Svartholm (Ed.), Proceedings of the Eighth Nobel Symposium, Almqvist & Wiksell, 1968, p. 367.
- [4] G. 't Hooft, M. Veltman, Nucl. Phys. B 44 (1972) 189.
- [5] F. Englert, R. Brout, Phys. Rev. Lett. 13 (1964) 321.
- [6] P.W. Higgs, Phys. Lett. 12 (1964) 132.
- [7] P.W. Higgs, Phys. Rev. Lett. 13 (1964) 508.
- [8] G.S. Guralnik, C.R. Hagen, T.W.B. Kibble, Phys. Rev. Lett. 13 (1964) 585.
- [9] P.W. Higgs, Phys. Rev. 145 (1966) 1156.
- [10] T.W.B. Kibble, Phys. Rev. 155 (1967) 1554.
- [11] L. Evans, P. Bryant (Eds.), LHC Machine, JINST, vol. 3, 2008, p. S08001.
- [12] ALEPH, CDF, DØ, DELPHI, L3, OPAL, SLD Collaborations, the LEP Electroweak Working Group, the Tevatron Electroweak Working Group,

- the SLD Electroweak and Heavy Flavour Groups, CERN-PH-EP-2010-095, arXiv:1012.2367 [hep-ex], 2010.
- [13] ALEPH, DELPHI, L3 and OPAL Collaborations, Phys. Lett. B 565 (2003) 61.
- [14] CDF Collaboration, T. Aaltonen, et al. Phys. Rev. Lett. (2012), in press, arXiv:1207.1707 [hep-ex].
- [15] DØ Collaboration, V.M. Abazov, et al. Phys. Rev. Lett. (2012), submitted for publication, arXiv:1207.6631 [hep-ex].
- [16] CDF Collaboration, DØ Collaboration, Phys. Rev. Lett. (2012), submitted for publication, arXiv:1207.6436 [hep-ex].
- [17] ATLAS Collaboration, Phys. Rev. D 86 (2012) 032003.
- [18] CMS Collaboration, Phys. Lett. B 710 (2012) 26.
- [19] ATLAS Collaboration, ATLAS: Letter of intent for a general-purpose pp experiment at the large hadron collider at CERN, CERN-LHCC-92-004 (1992).
- [20] ATLAS Collaboration, The ATLAS Collaboration, ATLAS Technical Proposal for a General-Purpose pp Experiment at the Large Hadron Collider at CERN, CERN-LHCC-94-43 (1994).
- [21] ATLAS Collaboration, JINST 3 (2008) S08003.
- [22] H. Georgi, S. Glashow, M. Machacek, D.V. Nanopoulos, Phys. Rev. Lett. 40 (1978) 692.
- [23] A. Djouadi, M. Spira, P.M. Zerwas, Phys. Lett. B 264 (1991) 440.
- [24] S. Dawson, Nucl. Phys. B 359 (1991) 283.
- [25] M. Spira, A. Djouadi, D. Graudenz, P.M. Zerwas, Nucl. Phys. B 453 (1995) 17.
- [26] R. Harlander, W.B. Kilgore, Phys. Rev. Lett. 88 (2002) 201801.
- [27] C. Anastasiou, K. Melnikov, Nucl. Phys. B 646 (2002) 220.
- [28] V. Ravindran, J. Smith, W.L. van Neerven, Nucl. Phys. B 665 (2003) 325.
- [29] U. Aglietti, R. Bonciani, G. Degrossi, A. Vicini, Phys. Lett. B 595 (2004) 432.
- [30] S. Actis, G. Passarino, C. Sturm, S. Uccirati, Phys. Lett. B 670 (2008) 12.
- [31] S. Catani, D. de Florian, M. Grazzini, P. Nason, JHEP 0307 (2003) 028.
- [32] C. Anastasiou, R. Boughezal, F. Petriello, JHEP 0904 (2009) 003.
- [33] D. de Florian, M. Grazzini, Higgs production at the LHC: Updated cross sections at $\sqrt{s} = 8$ TeV, arXiv:1206.4133 [hep-ph].
- [34] C. Anastasiou, S. Buehler, F. Herzog, A. Lazopoulos, JHEP 1204 (2012) 004.
- [35] J. Baglio, A. Djouadi, JHEP 1103 (2011) 055.
- [36] D. de Florian, G. Ferrera, M. Grazzini, D. Tommasini, JHEP 1111 (2011) 064.
- [37] P.S.E. Bagnaschi, G. Degrossi, A. Vicini, JHEP 1202 (2012) 88.
- [38] R. Cahn, S. Dawson, Phys. Lett. B 136 (1984) 196; R. Cahn, S. Dawson, Phys. Lett. B 138 (1984) 464 (Erratum).
- [39] M. Ciccolini, A. Denner, S. Dittmaier, Phys. Rev. Lett. 99 (2007) 161803.
- [40] M. Ciccolini, A. Denner, S. Dittmaier, Phys. Rev. D 77 (2008) 013002.
- [41] K. Arnold, M. Bahr, G. Bozzi, F. Campanario, C. Englert, Comput. Phys. Commun. 180 (2009) 1661.
- [42] P. Bolzoni, F. Maltoni, S.-O. Moch, M. Zaro, Phys. Rev. Lett. 105 (2010) 011801.
- [43] S. Glashow, D.V. Nanopoulos, A. Yildiz, Phys. Rev. D 18 (1978) 1724.
- [44] T. Han, S. Willenbrock, Phys. Lett. B 273 (1991) 167.
- [45] O. Brein, A. Djouadi, R. Harlander, Phys. Lett. B 579 (2004) 149.
- [46] M.L. Ciccolini, S. Dittmaier, M. Kramer, Phys. Rev. D 68 (2003) 073003.
- [47] Z. Kunszt, Nucl. Phys. B 247 (1984) 339.
- [48] W. Beenakker, et al., Phys. Rev. Lett. 87 (2001) 201805.
- [49] W. Beenakker, et al., Nucl. Phys. B 653 (2003) 151.
- [50] S. Dawson, L.H. Orr, L. Reina, D. Wackerroth, Phys. Rev. D 67 (2003) 071503.
- [51] S. Dawson, C. Jackson, L.H. Orr, L. Reina, D. Wackerroth, Phys. Rev. D 68 (2003) 034022.
- [52] S. Dittmaier, C. Mariotti, G. Passarino, R. Tanaka (Eds.), LHC Higgs Cross Section Working Group, Handbook of LHC Higgs cross sections: 1. Inclusive observables, CERN-2011-002, arXiv:1101.0593 [hep-ph], 2011.
- [53] S. Dittmaier, C. Mariotti, G. Passarino, R. Tanaka (Eds.), LHC Higgs Cross Section Working Group, Handbook of LHC Higgs Cross Sections: 2. Differential Distributions, CERN-2012-002, arXiv:1201.3084 [hep-ph], 2012.
- [54] A. Djouadi, J. Kalinowski, M. Spira, Comput. Phys. Commun. 108 (1998) 56.
- [55] A. Bredenstein, A. Denner, S. Dittmaier, M.M. Weber, Phys. Rev. D 74 (2006) 013004.
- [56] A. Bredenstein, A. Denner, S. Dittmaier, M.M. Weber, JHEP 0702 (2007) 080.
- [57] S. Alioli, P. Nason, C. Oleari, E. Re, JHEP 0904 (2009) 002.
- [58] P. Nason, C. Oleari, JHEP 1002 (2010) 037.
- [59] M.L. Mangano, et al., JHEP 0307 (2003) 001.
- [60] S. Frixione, B.R. Webber, JHEP 0206 (2002) 029; S. Frixione, P. Nason, B.R. Webber, JHEP 0308 (2003) 007; S. Frixione, E. Laenen, P. Motylinski, B.R. Webber, JHEP 0603 (2006) 092; S. Frixione, E. Laenen, P. Motylinski, C. White, B.R. Webber, JHEP 0807 (2008) 029; S. Frixione, F. Stoeckli, P. Torrielli, B.R. Webber, JHEP 1101 (2011) 053.
- [61] B.P. Kersevan, E. Richter-Was, The Monte Carlo event generator AcerMC version 2.0 with interfaces to PYTHIA 6.2 and HERWIG 6.5, arXiv:hep-ph/0405247.
- [62] T. Binoth, M. Ciccolini, N. Kauer, M. Krämer, JHEP 0612 (2006) 046.
- [63] T. Melia, P. Nason, R. Rontsch, G. Zanderighi, JHEP 1111 (2011) 078.
- [64] T. Binoth, N. Kauer, P. Mertsch, Gluon-induced QCD Corrections to $pp \rightarrow ZZ \rightarrow \ell\ell\ell\bar{\nu}$, arXiv:0807.0024 [hep-ph].
- [65] R.C. Gray, C. Kilic, M. Park, S. Somalwar, S. Thomas, Backgrounds to Higgs boson searches from $W\gamma^* \rightarrow l\nu(l)$ asymmetric internal conversion, arXiv:1110.1368 [hep-ph].
- [66] ATLAS Collaborations, New ATLAS event generator tunes to 2010 data, ATL-PHYS-PUB-2011-008, <http://cdsweb.cern.ch/record/1345343>, 2011.
- [67] ATLAS Collaborations, ATLAS tunes of PYTHIA 6 and Pythia 8 for MC11, ATL-PHYS-PUB-2011-009, <http://cdsweb.cern.ch/record/1363300>, 2011.
- [68] ATLAS Collaborations, Further ATLAS tunes of PYTHIA6 and Pythia 8, ATL-PHYS-PUB-2011-014, <http://cdsweb.cern.ch/record/1400677>, 2011.
- [69] T. Sjöstrand, S. Mrenna, P. Skands, JHEP 0605 (2006) 026.
- [70] J. Alwall, et al., JHEP 0709 (2007) 028.
- [71] J. Alwall, M. Herquet, F. Maltoni, O. Mattelaer, T. Stelzer, JHEP 1106 (2011) 128.
- [72] T. Sjöstrand, S. Mrenna, P. Skands, Comput. Phys. Commun. 178 (2008) 852.
- [73] G. Corcella, I. Knowles, G. Marchesini, S. Moretti, K. Odagiri, et al., JHEP 0101 (2001) 010.
- [74] T. Gleisberg, et al., JHEP 0902 (2009) 007.
- [75] J.M. Butterworth, J.R. Forshaw, M.H. Seymour, Z. Phys. C 72 (1996) 637.
- [76] S. Jadach, Z. Was, R. Decker, J.H. Kuhn, Comput. Phys. Commun. 76 (1993) 361.
- [77] P. Golonka, Z. Was, Eur. Phys. J. C 45 (2006) 97.
- [78] H.-L. Lai, et al., Phys. Rev. D 82 (2010) 074024.
- [79] P.M. Nadolsky, et al., Phys. Rev. D 78 (2008) 013004.
- [80] A. Sherstnev, R.S. Thorne, Eur. Phys. J. C 55 (2009) 553.
- [81] ATLAS Collaboration, Eur. Phys. J. C 70 (2010) 823.
- [82] S. Agostinelli, et al., Nucl. Instrum. Meth. A 506 (2003) 250.
- [83] ATLAS Collaboration, Phys. Lett. B 710 (2012) 383.
- [84] ATLAS Collaboration, Muon reconstruction efficiency in reprocessed 2010 LHC proton-proton collision data recorded with the ATLAS detector, ATLAS-CONF-2011-063, 2011, <http://cdsweb.cern.ch/record/1345743>.
- [85] ATLAS Collaboration, Eur. Phys. J. C 72 (2012) 1909.
- [86] ATLAS Collaboration, Improved electron reconstruction in ATLAS using the Gaussian Sum Filter-based model for bremsstrahlung, <http://cdsweb.cern.ch/record/1449796>.
- [87] ATLAS Collaboration, Observation of an excess of events in the search for the Standard Model Higgs boson in the $H \rightarrow ZZ^{(*)} \rightarrow 4\ell$ channel with the ATLAS detector, ATLAS-CONF-2012-092, 2012, <http://cdsweb.cern.ch/record/1460411>.
- [88] W. Lampl, S. Laplace, D. Lelas, P. Loch, H. Ma, S. Menke, S. Rajagopalan, D. Rousseau, S. Snyder, G. Unal, Calorimeter clustering algorithms: Description and performance, ATL-LARG-PUB-2008-002, 2008, <http://cdsweb.cern.ch/record/1099735>.
- [89] M. Cacciari, G.P. Salam, Phys. Lett. B 659 (2008) 119.
- [90] M. Cacciari, G.P. Salam, G. Soyez, Eur. Phys. J. C 72 (2012) 1896.
- [91] ATLAS Collaboration, Phys. Lett. B 707 (2012) 438.
- [92] ATLAS Collaboration, Improved luminosity determination in pp collisions at $\sqrt{s} = 7$ TeV using the ATLAS detector at the LHC, ATLAS-CONF-2012-080, 2012, <http://cdsweb.cern.ch/record/1460392>.
- [93] ATLAS Collaboration, Measurement of the total ZZ production cross section in the four-lepton channel using 5.8 fb^{-1} of ATLAS data at $\sqrt{s} = 8$ TeV, ATLAS-CONF-2012-090, 2012, <http://cdsweb.cern.ch/record/1460409>.
- [94] N. Kauer, G. Passarino, Inadequacy of zero-width approximation for a light Higgs boson signal, arXiv:1206.4803 [hep-ph].
- [95] ATLAS Collaboration, Phys. Rev. Lett. 108 (2012) 111803.
- [96] ATLAS Collaboration, Eur. Phys. J. C 72 (2012) 1849.
- [97] ATLAS Collaboration, Phys. Rev. D 83 (2011) 052005.
- [98] ATLAS Collaboration, Phys. Lett. B 705 (2011) 452.
- [99] OPAL Collaboration, K. Ackerstaff, et al., Eur. Phys. J. C 4 (1998) 47.
- [100] M. Vesterinen, T.R. Wyatt, Nucl. Instrum. Meth. A 602 (2009) 432.
- [101] ATLAS Collaboration, Eur. Phys. J. C (2011), submitted for publication, arXiv:1112.6426 [hep-ex].
- [102] M. Cacciari, G.P. Salam, G. Soyez, JHEP 0804 (2008) 063.
- [103] L.J. Dixon, M.S. Siu, Phys. Rev. Lett. 90 (2003) 252001.
- [104] J. Gaiser, Charmonium spectroscopy from radiative decays of the J/ψ and ψ' , Ph.D. Thesis No. SLAC-R-255, 1982.
- [105] S.N. Bernstein, Comm. Soc. Math. Kharkov 13 (1912) 1.
- [106] ATLAS Collaboration, Phys. Lett. B 716 (2012) 62, in this issue.
- [107] M. Dittmar, H. Dreiner, Phys. Rev. D 55 (2007) 167.
- [108] ATLAS Collaboration, Commissioning of the ATLAS high-performance b -tagging algorithms in the 7 TeV collision data, ATLAS-CONF-2011-102, 2011, <http://cdsweb.cern.ch/record/1369219>.
- [109] R.K. Ellis, et al., Nucl. Phys. B 297 (1988) 221.
- [110] A.J. Barr, B. Gripaios, C.G. Lester, JHEP 0907 (2009) 072.
- [111] ATLAS Collaboration, Phys. Rev. Lett. 108 (2012) 111802.
- [112] ATLAS Collaboration, Eur. Phys. J. C 71 (2011) 1728.
- [113] ATLAS Collaboration, Eur. Phys. J. C 72 (2012) 1844.
- [114] ATLAS Collaboration, Measurement of the b -tag efficiency in a sample of jets containing muons with 5 fb^{-1} of data from the ATLAS detector, ATLAS-CONF-2012-043, 2012, <http://cdsweb.cern.ch/record/1435197>.
- [115] J.M. Campbell, R.K. Ellis, C. Williams, JHEP 1107 (2011) 018.
- [116] J. Campbell, R. Ellis, C. Williams, JHEP 1110 (2011) 005.

- [117] I. Stewart, F. Tackmann, Phys. Rev. D 85 (2012) 034011.
- [118] ATLAS Collaboration, CMS Collaboration, Procedure for the LHC Higgs boson search combination in Summer 2011, ATL-PHYS-PUB-2011-011, CERN-CMS-NOTE-2011-005, 2011, <http://cdsweb.cern.ch/record/1375842>.
- [119] L. Moneta, K. Belasco, K.S. Cranmer, S. Kreiss, A. Lazzaro, et al., The RooStats Project, PoS ACAT2010 (2010) 057, arXiv:1009.1003 [physics.data-an].
- [120] K. Cranmer, G. Lewis, L. Moneta, A. Shibata, W. Verkerke, HistFactory: A tool for creating statistical models for use with RooFit and RooStats, CERN-OPEN-2012-016, 2012, <http://cdsweb.cern.ch/record/1456844>.
- [121] W. Verkerke, D. Kirkby, The RooFit toolkit for data modeling, Tech. Rep., SLAC, Stanford, CA, June 2003, arXiv:physics/0306116 [physics.data-an].
- [122] G. Cowan, K. Cranmer, E. Gross, O. Vitells, Eur. Phys. J. C 71 (2011) 1554.
- [123] A.L. Read, J. Phys. G 28 (2002) 2693.
- [124] E. Gross, O. Vitells, Eur. Phys. J. C 70 (2010) 525.
- [125] ATLAS Collaboration, Phys. Lett. B (2012), submitted for publication, arXiv:1205.6744 [hep-ex].
- [126] ATLAS Collaboration, Phys. Lett. B (2012), submitted for publication, arXiv:1206.2443 [hep-ex].
- [127] ATLAS Collaboration, Observation of an excess of events in the search for the Standard Model Higgs boson in the gamma-gamma channel with the ATLAS detector, ATLAS-CONF-2012-091, 2012, <http://cdsweb.cern.ch/record/1460410>.
- [128] ATLAS Collaboration, Phys. Lett. B (2012), submitted for publication, arXiv:1206.6074 [hep-ex].
- [129] ATLAS Collaboration, JHEP (2012), in press, arXiv:1206.5971 [hep-ex].
- [130] ATLAS Collaboration, Phys. Lett. B (2012), submitted for publication, arXiv:1207.0210 [hep-ex].
- [131] ATLAS Collaboration, Observation of an excess of events in the search for the Standard Model Higgs Boson in the $H \rightarrow WW^{(*)} \rightarrow \ell\nu\ell\nu$ channel with the ATLAS detector, ATLAS-CONF-2012-098, 2012, <http://cdsweb.cern.ch/record/1462530>.
- [132] ATLAS Collaboration, Eur. Phys. J. C 71 (2011) 1630.
- [133] ATLAS Collaboration, Luminosity determination in pp collisions at $\sqrt{s} = 7$ TeV using the ATLAS detector in 2011, ATLAS-CONF-2011-116, 2011, <http://cdsweb.cern.ch/record/1376384>.
- [134] M. Botje, J. Butterworth, A. Cooper-Sarkar, A. de Roeck, J. Feltesse, et al., The PDF4LHC Working Group interim recommendations, arXiv:1101.0538 [hep-ph].
- [135] A. Martin, W. Stirling, R. Thorne, G. Watt, Eur. Phys. J. C 63 (2009) 189.
- [136] R.D. Ball, et al., Nucl. Phys. B 849 (2011) 296.
- [137] J.M. Campbell, R.K. Ellis, G. Zanderighi, JHEP 0610 (2006) 028.
- [138] ATLAS Collaboration, Observation of an excess of events in the search for the Standard Model Higgs boson with the ATLAS detector at the LHC, ATLAS-CONF-2012-093, 2012, <http://cdsweb.cern.ch/record/1460439>.
- [139] ATLAS Collaboration, CMS Collaboration, Combined Standard Model Higgs boson searches with up to 2.3 fb^{-1} of pp, collisions at $\sqrt{s} = 7$ TeV at the LHC, ATLAS-CONF-2011-157, CMS-PAS-HIG-11-023, 2011, <http://cdsweb.cern.ch/record/1399599>.
- [140] L.D. Landau, Dokl. Akad. Nauk USSR 60 (1948) 207.
- [141] C.N. Yang, Phys. Rev. 77 (1950) 242.

ATLAS Collaboration

G. Aad⁴⁸, T. Abajyan²¹, B. Abbott¹¹¹, J. Abdallah¹², S. Abdel Khalek¹¹⁵, A.A. Abdelalim⁴⁹, O. Abdinov¹¹, R. Aben¹⁰⁵, B. Abi¹¹², M. Abolins⁸⁸, O.S. AbouZeid¹⁵⁸, H. Abramowicz¹⁵³, H. Abreu¹³⁶, B.S. Acharya^{164a,164b}, L. Adamczyk³⁸, D.L. Adams²⁵, T.N. Addy⁵⁶, J. Adelman¹⁷⁶, S. Adomeit⁹⁸, P. Adragna⁷⁵, T. Adye¹²⁹, S. Aefsky²³, J.A. Aguilar-Saavedra^{124b,a}, M. Agustoni¹⁷, M. Aharrouche⁸¹, S.P. Ahlen²², F. Ahles⁴⁸, A. Ahmad¹⁴⁸, M. Ahsan⁴¹, G. Aielli^{133a,133b}, T. Akdogan^{19a}, T.P.A. Åkesson⁷⁹, G. Akimoto¹⁵⁵, A.V. Akimov⁹⁴, M.S. Alam², M.A. Alam⁷⁶, J. Albert¹⁶⁹, S. Albrand⁵⁵, M. Aleksa³⁰, I.N. Aleksandrov⁶⁴, F. Alessandria^{89a}, C. Alexa^{26a}, G. Alexander¹⁵³, G. Alexandre⁴⁹, T. Alexopoulos¹⁰, M. Alhroob^{164a,164c}, M. Aliev¹⁶, G. Alimonti^{89a}, J. Alison¹²⁰, B.M.M. Allbrooke¹⁸, P.P. Allport⁷³, S.E. Allwood-Spiers⁵³, J. Almond⁸², A. Aloisio^{102a,102b}, R. Alon¹⁷², A. Alonso⁷⁹, F. Alonso⁷⁰, A. Altheimer³⁵, B. Alvarez Gonzalez⁸⁸, M.G. Alviggi^{102a,102b}, K. Amako⁶⁵, C. Amelung²³, V.V. Ammosov^{128,*}, S.P. Amor Dos Santos^{124a}, A. Amorim^{124a,b}, N. Amram¹⁵³, C. Anastopoulos³⁰, L.S. Ancu¹⁷, N. Andari¹¹⁵, T. Andeen³⁵, C.F. Anders^{58b}, G. Anders^{58a}, K.J. Anderson³¹, A. Andreazza^{89a,89b}, V. Andrei^{58a}, M.-L. Andrieux⁵⁵, X.S. Anduaga⁷⁰, S. Angelidakis⁹, P. Anger⁴⁴, A. Angerami³⁵, F. Anghinolfi³⁰, A. Anisenkov¹⁰⁷, N. Anjos^{124a}, A. Annovi⁴⁷, A. Antonaki⁹, M. Antonelli⁴⁷, A. Antonov⁹⁶, J. Antos^{144b}, F. Anulli^{132a}, M. Aoki¹⁰¹, S. Aoun⁸³, L. Aperio Bella⁵, R. Apolle^{118,c}, G. Arabidze⁸⁸, I. Aracena¹⁴³, Y. Arai⁶⁵, A.T.H. Arce⁴⁵, S. Arfaoui¹⁴⁸, J.-F. Arguin⁹³, E. Arik^{19a,*}, M. Arik^{19a}, A.J. Armbruster⁸⁷, O. Arnaez⁸¹, V. Arnal⁸⁰, C. Arnault¹¹⁵, A. Artamonov⁹⁵, G. Artoni^{132a,132b}, D. Arutinov²¹, S. Asai¹⁵⁵, S. Ask²⁸, B. Åsman^{146a,146b}, L. Asquith⁶, K. Assamagan²⁵, A. Astbury¹⁶⁹, M. Atkinson¹⁶⁵, B. Aubert⁵, E. Auge¹¹⁵, K. Augsten¹²⁷, M. Aourseu^{145a}, G. Avolio¹⁶³, R. Avramidou¹⁰, D. Axen¹⁶⁸, G. Azuelos^{93,d}, Y. Azuma¹⁵⁵, M.A. Baak³⁰, G. Baccaglioni^{89a}, C. Bacci^{134a,134b}, A.M. Bach¹⁵, H. Bachacou¹³⁶, K. Bachas³⁰, M. Backes⁴⁹, M. Backhaus²¹, J. Backus Mayes¹⁴³, E. Badescu^{26a}, P. Bagnaia^{132a,132b}, S. Bahinipati³, Y. Bai^{33a}, D.C. Bailey¹⁵⁸, T. Bain¹⁵⁸, J.T. Baines¹²⁹, O.K. Baker¹⁷⁶, M.D. Baker²⁵, S. Baker⁷⁷, P. Balek¹²⁶, E. Banas³⁹, P. Banerjee⁹³, Sw. Banerjee¹⁷³, D. Banfi³⁰, A. Bangert¹⁵⁰, V. Bansal¹⁶⁹, H.S. Bansil¹⁸, L. Barak¹⁷², S.P. Baranov⁹⁴, A. Barbaro Galtieri¹⁵, T. Barber⁴⁸, E.L. Barberio⁸⁶, D. Barberis^{50a,50b}, M. Barbero²¹, D.Y. Bardin⁶⁴, T. Barillari⁹⁹, M. Barisonzi¹⁷⁵, T. Barklow¹⁴³, N. Barlow²⁸, B.M. Barnett¹²⁹, R.M. Barnett¹⁵, A. Baroncelli^{134a}, G. Barone⁴⁹, A.J. Barr¹¹⁸, F. Barreiro⁸⁰, J. Barreiro Guimarães da Costa⁵⁷, P. Barrillon¹¹⁵, R. Bartoldus¹⁴³, A.E. Barton⁷¹, V. Bartsch¹⁴⁹, A. Basye¹⁶⁵, R.L. Bates⁵³, L. Batkova^{144a}, J.R. Batley²⁸, A. Battaglia¹⁷, M. Battistin³⁰, F. Bauer¹³⁶, H.S. Bawa^{143,e}, S. Beale⁹⁸, T. Beau⁷⁸, P.H. Beauchemin¹⁶¹, R. Beccherle^{50a}, P. Bechtel²¹, H.P. Beck¹⁷, A.K. Becker¹⁷⁵, S. Becker⁹⁸, M. Beckingham¹³⁸, K.H. Becks¹⁷⁵, A.J. Beddall^{19c}, A. Beddall^{19c}, S. Bedikian¹⁷⁶, V.A. Bednyakov⁶⁴, C.P. Bee⁸³, L.J. Beemster¹⁰⁵, M. Begel²⁵, S. Behar Harpaz¹⁵², P.K. Behera⁶², M. Beimforde⁹⁹,

C. Belanger-Champagne⁸⁵, P.J. Bell⁴⁹, W.H. Bell⁴⁹, G. Bella¹⁵³, L. Bellagamba^{20a}, M. Bellomo³⁰,
 A. Belloni⁵⁷, O. Beloborodova^{107,f}, K. Belotskiy⁹⁶, O. Beltramello³⁰, O. Benary¹⁵³, D. Benckekroun^{135a},
 K. Bendtz^{146a,146b}, N. Benekos¹⁶⁵, Y. Benhammou¹⁵³, E. Benhar Noccioli⁴⁹, J.A. Benitez Garcia^{159b},
 D.P. Benjamin⁴⁵, M. Benoit¹¹⁵, J.R. Bensinger²³, K. Benslama¹³⁰, S. Bentvelsen¹⁰⁵, D. Berge³⁰,
 E. Bergeaas Kuutmann⁴², N. Berger⁵, F. Berghaus¹⁶⁹, E. Berglund¹⁰⁵, J. Beringer¹⁵, P. Bernat⁷⁷,
 R. Bernhard⁴⁸, C. Bernius²⁵, F.U. Bernlochner¹⁶⁹, T. Berry⁷⁶, C. Bertella⁸³, A. Bertin^{20a,20b},
 F. Bertolucci^{122a,122b}, M.I. Besana^{89a,89b}, G.J. Besjes¹⁰⁴, N. Besson¹³⁶, S. Bethke⁹⁹, W. Bhimji⁴⁶,
 R.M. Bianchi³⁰, M. Bianco^{72a,72b}, O. Biebel⁹⁸, S.P. Bieniek⁷⁷, K. Bierwagen⁵⁴, J. Biesiada¹⁵,
 M. Biglietti^{134a}, H. Bilokon⁴⁷, M. Bindi^{20a,20b}, S. Binet¹¹⁵, A. Bingul^{19c}, C. Bini^{132a,132b}, C. Biscarat¹⁷⁸,
 B. Bittner⁹⁹, K.M. Black²², R.E. Blair⁶, J.-B. Blanchard¹³⁶, G. Blanchot³⁰, T. Blazek^{144a}, I. Bloch⁴²,
 C. Blocker²³, J. Blocki³⁹, A. Blondel⁴⁹, W. Blum⁸¹, U. Blumenschein⁵⁴, G.J. Bobbink¹⁰⁵,
 V.B. Bobrovnikov¹⁰⁷, S.S. Bocchetta⁷⁹, A. Bocci⁴⁵, C.R. Boddy¹¹⁸, M. Boehler⁴⁸, J. Boek¹⁷⁵, N. Boelaert³⁶,
 J.A. Bogaerts³⁰, A. Bogdanchikov¹⁰⁷, A. Bogouch^{90,*}, C. Bohm^{146a}, J. Bohm¹²⁵, V. Boisvert⁷⁶, T. Bold³⁸,
 V. Boldea^{26a}, N.M. Bolnet¹³⁶, M. Bomben⁷⁸, M. Bona⁷⁵, M. Boonekamp¹³⁶, S. Bordini⁷⁸, C. Borer¹⁷,
 A. Borisov¹²⁸, G. Borissov⁷¹, I. Borjanovic^{13a}, M. Borri⁸², S. Borroni⁸⁷, V. Bortolotto^{134a,134b}, K. Bos¹⁰⁵,
 D. Boscherini^{20a}, M. Bosman¹², H. Boterenbrood¹⁰⁵, J. Bouchami⁹³, J. Boudreau¹²³,
 E.V. Bouhova-Thacker⁷¹, D. Boumediene³⁴, C. Bourdarios¹¹⁵, N. Bousson⁸³, A. Boveia³¹, J. Boyd³⁰,
 I.R. Boyko⁶⁴, I. Bozovic-Jelisavcic^{13b}, J. Bracinik¹⁸, P. Branchini^{134a}, G.W. Brandenburg⁵⁷, A. Brandt⁸,
 G. Brandt¹¹⁸, O. Brandt⁵⁴, U. Bratzler¹⁵⁶, B. Brau⁸⁴, J.E. Brau¹¹⁴, H.M. Braun^{175,*}, S.F. Brazzale^{164a,164c},
 B. Brelier¹⁵⁸, J. Bremer³⁰, K. Brendlinger¹²⁰, R. Brenner¹⁶⁶, S. Bressler¹⁷², D. Britton⁵³, F.M. Brochu²⁸,
 I. Brock²¹, R. Brock⁸⁸, F. Broggi^{89a}, C. Bromberg⁸⁸, J. Bronner⁹⁹, G. Brooijmans³⁵, T. Brooks⁷⁶,
 W.K. Brooks^{32b}, G. Brown⁸², H. Brown⁸, P.A. Bruckman de Renstrom³⁹, D. Bruncko^{144b}, R. Bruneliere⁴⁸,
 S. Brunet⁶⁰, A. Bruni^{20a}, G. Bruni^{20a}, M. Bruschi^{20a}, T. Buanes¹⁴, Q. Buat⁵⁵, F. Bucci⁴⁹, J. Buchanan¹¹⁸,
 P. Buchholz¹⁴¹, R.M. Buckingham¹¹⁸, A.G. Buckley⁴⁶, S.I. Buda^{26a}, I.A. Budagov⁶⁴, B. Budick¹⁰⁸,
 V. Büscher⁸¹, L. Bugge¹¹⁷, O. Bulekov⁹⁶, A.C. Bundock⁷³, M. Bunse⁴³, T. Buran¹¹⁷, H. Burckhart³⁰,
 S. Burdin⁷³, T. Burgess¹⁴, S. Burke¹²⁹, E. Busato³⁴, P. Bussey⁵³, C.P. Buszello¹⁶⁶, B. Butler¹⁴³,
 J.M. Butler²², C.M. Buttar⁵³, J.M. Butterworth⁷⁷, W. Buttinger²⁸, S. Cabrera Urbán¹⁶⁷, D. Caforio^{20a,20b},
 O. Cakir^{4a}, P. Calafiura¹⁵, G. Calderini⁷⁸, P. Calfayan⁹⁸, R. Calkins¹⁰⁶, L.P. Caloba^{24a}, R. Caloi^{132a,132b},
 D. Calvet³⁴, S. Calvet³⁴, R. Camacho Toro³⁴, P. Camarri^{133a,133b}, D. Cameron¹¹⁷, L.M. Caminada¹⁵,
 R. Caminal Armadans¹², S. Campana³⁰, M. Campanelli⁷⁷, V. Canale^{102a,102b}, F. Canelli^{31,g},
 A. Canepa^{159a}, J. Cantero⁸⁰, R. Cantrill⁷⁶, L. Capasso^{102a,102b}, M.D.M. Capeans Garrido³⁰, I. Caprini^{26a},
 M. Caprini^{26a}, D. Capriotti⁹⁹, M. Capua^{37a,37b}, R. Caputo⁸¹, R. Cardarelli^{133a}, T. Carli³⁰, G. Carlino^{102a},
 L. Carminati^{89a,89b}, B. Caron⁸⁵, S. Caron¹⁰⁴, E. Carquin^{32b}, G.D. Carrillo-Montoya¹⁷³, A.A. Carter⁷⁵,
 J.R. Carter²⁸, J. Carvalho^{124a,h}, D. Casadei¹⁰⁸, M.P. Casado¹², M. Cascella^{122a,122b}, C. Caso^{50a,50b,*},
 A.M. Castaneda Hernandez^{173,i}, E. Castaneda-Miranda¹⁷³, V. Castillo Gimenez¹⁶⁷, N.F. Castro^{124a},
 G. Cataldi^{72a}, P. Catastini⁵⁷, A. Catinaccio³⁰, J.R. Catmore³⁰, A. Cattai³⁰, G. Cattani^{133a,133b},
 S. Caughron⁸⁸, V. Cavaliere¹⁶⁵, P. Cavalleri⁷⁸, D. Cavalli^{89a}, M. Cavalli-Sforza¹², V. Cavasinni^{122a,122b},
 F. Ceradini^{134a,134b}, A.S. Cerqueira^{24b}, A. Cerri³⁰, L. Cerrito⁷⁵, F. Cerutti⁴⁷, S.A. Cetin^{19b}, A. Chafaq^{135a},
 D. Chakraborty¹⁰⁶, I. Chalupkova¹²⁶, K. Chan³, P. Chang¹⁶⁵, B. Chapleau⁸⁵, J.D. Chapman²⁸,
 J.W. Chapman⁸⁷, E. Chareyre⁷⁸, D.G. Charlton¹⁸, V. Chavda⁸², C.A. Chavez Barajas³⁰, S. Cheatham⁸⁵,
 S. Chekanov⁶, S.V. Chekulaev^{159a}, G.A. Chelkov⁶⁴, M.A. Chelstowska¹⁰⁴, C. Chen⁶³, H. Chen²⁵,
 S. Chen^{33c}, X. Chen¹⁷³, Y. Chen³⁵, Y. Cheng³¹, A. Cheplakov⁶⁴, R. Cherkaoui El Moursli^{135e},
 V. Chernyatin²⁵, E. Cheu⁷, S.L. Cheung¹⁵⁸, L. Chevalier¹³⁶, G. Chiefari^{102a,102b}, L. Chikovani^{51a,*},
 J.T. Childers³⁰, A. Chilingarov⁷¹, G. Chiodini^{72a}, A.S. Chisholm¹⁸, R.T. Chislett⁷⁷, A. Chitan^{26a},
 M.V. Chizhov⁶⁴, G. Choudalakis³¹, S. Chouridou¹³⁷, I.A. Christidi⁷⁷, A. Christov⁴⁸,
 D. Chromek-Burckhart³⁰, M.L. Chu¹⁵¹, J. Chudoba¹²⁵, G. Ciapetti^{132a,132b}, A.K. Ciftci^{4a}, R. Ciftci^{4a},
 D. Cinca³⁴, V. Cindro⁷⁴, C. Ciocca^{20a,20b}, A. Ciocio¹⁵, M. Cirilli⁸⁷, P. Cirkovic^{13b}, Z.H. Citron¹⁷²,
 M. Citterio^{89a}, M. Ciubancan^{26a}, A. Clark⁴⁹, P.J. Clark⁴⁶, R.N. Clarke¹⁵, W. Cleland¹²³, J.C. Clemens⁸³,
 B. Clement⁵⁵, C. Clement^{146a,146b}, Y. Coadou⁸³, M. Cobl^{164a,164c}, A. Coccaro¹³⁸, J. Cochran⁶³,
 L. Coffey²³, J.G. Cogan¹⁴³, J. Coggeshall¹⁶⁵, E. Cogneras¹⁷⁸, J. Colas⁵, S. Cole¹⁰⁶, A.P. Colijn¹⁰⁵,
 N.J. Collins¹⁸, C. Collins-Tooth⁵³, J. Collot⁵⁵, T. Colombo^{119a,119b}, G. Colon⁸⁴, G. Compostella⁹⁹,
 P. Conde Muiño^{124a}, E. Coniavitis¹⁶⁶, M.C. Conidi¹², S.M. Consonni^{89a,89b}, V. Consorti⁴⁸,

S. Constantinescu^{26a}, C. Conta^{119a,119b}, G. Conti⁵⁷, F. Conventi^{102a,j}, M. Cooke¹⁵, B.D. Cooper⁷⁷, A.M. Cooper-Sarkar¹¹⁸, N.J. Cooper-Smith⁷⁶, K. Copic¹⁵, T. Cornelissen¹⁷⁵, M. Corradi^{20a}, F. Corriveau^{85,k}, A. Cortes-Gonzalez¹⁶⁵, G. Cortiana⁹⁹, G. Costa^{89a}, M.J. Costa¹⁶⁷, D. Costanzo¹³⁹, D. Côté³⁰, L. Courneyea¹⁶⁹, G. Cowan⁷⁶, C. Cowden²⁸, B.E. Cox⁸², K. Cranmer¹⁰⁸, F. Crescioli^{122a,122b}, M. Cristinziani²¹, G. Crosetti^{37a,37b}, S. Crépé-Renaudin⁵⁵, C.-M. Cuciuc^{26a}, C. Cuenca Almenar¹⁷⁶, T. Cuhadar Donszelmann¹³⁹, M. Curatolo⁴⁷, C.J. Curtis¹⁸, C. Cuthbert¹⁵⁰, P. Cwetanski⁶⁰, H. Czirr¹⁴¹, P. Czodrowski⁴⁴, Z. Czyczula¹⁷⁶, S. D'Auria⁵³, M. D'Onofrio⁷³, A. D'Orazio^{132a,132b}, M.J. Da Cunha Sargedas De Sousa^{124a}, C. Da Via⁸², W. Dabrowski³⁸, A. Dafinca¹¹⁸, T. Dai⁸⁷, C. Dallapiccola⁸⁴, M. Dam³⁶, M. Dameri^{50a,50b}, D.S. Damiani¹³⁷, H.O. Danielsson³⁰, V. Dao⁴⁹, G. Darbo^{50a}, G.L. Darlea^{26b}, J.A. Dassoulas⁴², W. Davey²¹, T. Davidek¹²⁶, N. Davidson⁸⁶, R. Davidson⁷¹, E. Davies^{118,c}, M. Davies⁹³, O. Davignon⁷⁸, A.R. Davison⁷⁷, Y. Davygora^{58a}, E. Dawe¹⁴², I. Dawson¹³⁹, R.K. Daya-Ishmukhametova²³, K. De⁸, R. de Asmundis^{102a}, S. De Castro^{20a,20b}, S. De Cecco⁷⁸, J. de Graat⁹⁸, N. De Groot¹⁰⁴, P. de Jong¹⁰⁵, C. De La Taille¹¹⁵, H. De la Torre⁸⁰, F. De Lorenzi⁶³, L. de Mora⁷¹, L. De Nooij¹⁰⁵, D. De Pedis^{132a}, A. De Salvo^{132a}, U. De Sanctis^{164a,164c}, A. De Santo¹⁴⁹, J.B. De Vivie De Regie¹¹⁵, G. De Zorzi^{132a,132b}, W.J. Dearnaley⁷¹, R. Debbé²⁵, C. Debenedetti⁴⁶, B. Dechenaux⁵⁵, D.V. Dedovich⁶⁴, J. Degenhardt¹²⁰, C. Del Papa^{164a,164c}, J. Del Peso⁸⁰, T. Del Prete^{122a,122b}, T. Delemontex⁵⁵, M. Deliyergiyev⁷⁴, A. Dell'Acqua³⁰, L. Dell'Asta²², M. Della Pietra^{102a,j}, D. della Volpe^{102a,102b}, M. Delmastro⁵, P. Delpierre⁸³, P.A. Delsart⁵⁵, C. Deluca¹⁰⁵, S. Demers¹⁷⁶, M. Demichev⁶⁴, B. Demirköz^{12,l}, J. Deng¹⁶³, S.P. Denisov¹²⁸, D. Derendarz³⁹, J.E. Derkaoui^{135d}, F. Derue⁷⁸, P. Dervan⁷³, K. Desch²¹, E. Devetak¹⁴⁸, P.O. Deviveiros¹⁰⁵, A. Dewhurst¹²⁹, B. DeWilde¹⁴⁸, S. Dhaliwal¹⁵⁸, R. Dhullipudi^{25,m}, A. Di Ciaccio^{133a,133b}, L. Di Ciaccio⁵, C. Di Donato^{102a,102b}, A. Di Girolamo³⁰, B. Di Girolamo³⁰, S. Di Luise^{134a,134b}, A. Di Mattia¹⁷³, B. Di Micco³⁰, R. Di Nardo⁴⁷, A. Di Simone^{133a,133b}, R. Di Sipio^{20a,20b}, M.A. Diaz^{32a}, E.B. Diehl⁸⁷, J. Dietrich⁴², T.A. Dietzsch^{58a}, S. Diglio⁸⁶, K. Dindar Yagci⁴⁰, J. Dingfelder²¹, F. Dinut^{26a}, C. Dionisi^{132a,132b}, P. Dita^{26a}, S. Dita^{26a}, F. Dittus³⁰, F. Djama⁸³, T. Djobava^{51b}, M.A.B. do Vale^{24c}, A. Do Valle Wemans^{124a,n}, T.K.O. Doan⁵, M. Dobbs⁸⁵, R. Dobinson^{30,*}, D. Dobos³⁰, E. Dobson^{30,o}, J. Dodd³⁵, C. Doglioni⁴⁹, T. Doherty⁵³, Y. Doi^{65,*}, J. Dolejsi¹²⁶, I. Dolenc⁷⁴, Z. Dolezal¹²⁶, B.A. Dolgoshein^{96,*}, T. Dohmae¹⁵⁵, M. Donadelli^{24d}, J. Donini³⁴, J. Dopke³⁰, A. Doria^{102a}, A. Dos Anjos¹⁷³, A. Dotti^{122a,122b}, M.T. Dova⁷⁰, J.D. Dowell¹⁸, A.D. Doxiadis¹⁰⁵, A.T. Doyle⁵³, N. Dressnandt¹²⁰, M. Dris¹⁰, J. Dubbert⁹⁹, S. Dube¹⁵, E. Duchovni¹⁷², G. Duckeck⁹⁸, D. Duda¹⁷⁵, A. Dudarev³⁰, F. Dudziak⁶³, M. Dührssen³⁰, I.P. Duerdoth⁸², L. Dufлот¹¹⁵, M.-A. Dufour⁸⁵, L. Duguid⁷⁶, M. Dunford^{58a}, H. Duran Yildiz^{4a}, R. Duxfield¹³⁹, M. Dwuznik³⁸, F. Dydak³⁰, M. Düren⁵², W.L. Ebenstein⁴⁵, J. Ebke⁹⁸, S. Eckweiler⁸¹, K. Edmonds⁸¹, W. Edson², C.A. Edwards⁷⁶, N.C. Edwards⁵³, W. Ehrenfeld⁴², T. Eifert¹⁴³, G. Eigen¹⁴, K. Einsweiler¹⁵, E. Eisenhandler⁷⁵, T. Ekelof¹⁶⁶, M. El Kacimi^{135c}, M. Ellert¹⁶⁶, S. Elles⁵, F. Ellinghaus⁸¹, K. Ellis⁷⁵, N. Ellis³⁰, J. Elmsheuser⁹⁸, M. Elsing³⁰, D. Emeliyanov¹²⁹, R. Engelmann¹⁴⁸, A. Engl⁹⁸, B. Epp⁶¹, J. Erdmann⁵⁴, A. Ereditato¹⁷, D. Eriksson^{146a}, J. Ernst², M. Ernst²⁵, J. Ernwein¹³⁶, D. Errede¹⁶⁵, S. Errede¹⁶⁵, E. Ertel⁸¹, M. Escalier¹¹⁵, H. Esch⁴³, C. Escobar¹²³, X. Espinal Curull¹², B. Esposito⁴⁷, F. Etienne⁸³, A.I. Etienvre¹³⁶, E. Etzion¹⁵³, D. Evangelakou⁵⁴, H. Evans⁶⁰, L. Fabbri^{20a,20b}, C. Fabre³⁰, R.M. Fakhruddinov¹²⁸, S. Falciano^{132a}, Y. Fang¹⁷³, M. Fanti^{89a,89b}, A. Farbin⁸, A. Farilla^{134a}, J. Farley¹⁴⁸, T. Farooque¹⁵⁸, S. Farrell¹⁶³, S.M. Farrington¹⁷⁰, P. Farthouat³⁰, F. Fassi¹⁶⁷, P. Fassnacht³⁰, D. Fassouliotis⁹, B. Fatholahzadeh¹⁵⁸, A. Favareto^{89a,89b}, L. Fayard¹¹⁵, S. Fazio^{37a,37b}, R. Febbraro³⁴, P. Federic^{144a}, O.L. Fedin¹²¹, W. Fedorko⁸⁸, M. Fehling-Kaschek⁴⁸, L. Felgioni⁸³, D. Fellmann⁶, C. Feng^{33d}, E.J. Feng⁶, A.B. Fenyuk¹²⁸, J. Ferencei^{144b}, W. Fernando⁶, S. Ferrag⁵³, J. Ferrando⁵³, V. Ferrara⁴², A. Ferrari¹⁶⁶, P. Ferrari¹⁰⁵, R. Ferrari^{119a}, D.E. Ferreira de Lima⁵³, A. Ferrer¹⁶⁷, D. Ferrere⁴⁹, C. Ferretti⁸⁷, A. Ferretto Parodi^{50a,50b}, M. Fiascaris³¹, F. Fiedler⁸¹, A. Filipčič⁷⁴, F. Filthaut¹⁰⁴, M. Fincke-Keeler¹⁶⁹, M.C.N. Fiolhais^{124a,h}, L. Fiorini¹⁶⁷, A. Firan⁴⁰, G. Fischer⁴², M.J. Fisher¹⁰⁹, M. Flechl⁴⁸, I. Fleck¹⁴¹, J. Fleckner⁸¹, P. Fleischmann¹⁷⁴, S. Fleischmann¹⁷⁵, T. Flick¹⁷⁵, A. Floderus⁷⁹, L.R. Flores Castillo¹⁷³, M.J. Flowerdew⁹⁹, T. Fonseca Martin¹⁷, A. Formica¹³⁶, A. Forti⁸², D. Fortin^{159a}, D. Fournier¹¹⁵, A.J. Fowler⁴⁵, H. Fox⁷¹, P. Francavilla¹², M. Franchini^{20a,20b}, S. Franchino^{119a,119b}, D. Francis³⁰, T. Frank¹⁷², M. Franklin⁵⁷, S. Franz³⁰, M. Fraternali^{119a,119b}, S. Fratina¹²⁰, S.T. French²⁸, C. Friedrich⁴², F. Friedrich⁴⁴, R. Froeschl³⁰, D. Froidevaux³⁰, J.A. Frost²⁸, C. Fukunaga¹⁵⁶, E. Fullana Torregrosa³⁰,

B.G. Fulson¹⁴³, J. Fuster¹⁶⁷, C. Gabaldon³⁰, O. Gabizon¹⁷², S. Gadatsch¹⁰⁵, T. Gadfort²⁵, S. Gadomski⁴⁹,
 G. Gagliardi^{50a,50b}, P. Gagnon⁶⁰, C. Galea⁹⁸, B. Galhardo^{124a}, E.J. Gallas¹¹⁸, V. Gallo¹⁷, B.J. Gallop¹²⁹,
 P. Gallus¹²⁵, K.K. Gan¹⁰⁹, Y.S. Gao^{143,e}, A. Gaponenko¹⁵, F. Garberon¹⁷⁶, M. Garcia-Sciveres¹⁵,
 C. García¹⁶⁷, J.E. García Navarro¹⁶⁷, R.W. Gardner³¹, N. Garelli³⁰, H. Garitaonandia¹⁰⁵, V. Garonne³⁰,
 C. Gatti⁴⁷, G. Gaudio^{119a}, B. Gaur¹⁴¹, L. Gauthier¹³⁶, P. Gauzzi^{132a,132b}, I.L. Gavrilenko⁹⁴, C. Gay¹⁶⁸,
 G. Gaycken²¹, E.N. Gazis¹⁰, P. Ge^{33d}, Z. Gece¹⁶⁸, C.N.P. Gee¹²⁹, D.A.A. Geerts¹⁰⁵, Ch. Geich-Gimbel²¹,
 K. Gellerstedt^{146a,146b}, C. Gemme^{50a}, A. Gemmell⁵³, M.H. Genest⁵⁵, S. Gentile^{132a,132b}, M. George⁵⁴,
 S. George⁷⁶, P. Gerlach¹⁷⁵, A. Gershon¹⁵³, C. Geweniger^{58a}, H. Ghazlane^{135b}, N. Ghodbane³⁴,
 B. Giacobbe^{20a}, S. Giagu^{132a,132b}, V. Giakoumopoulou⁹, V. Giangiobbe¹², F. Gianotti³⁰, B. Gibbard²⁵,
 A. Gibson¹⁵⁸, S.M. Gibson³⁰, M. Gilchriese¹⁵, O. Gildemeister³⁰, D. Gillberg²⁹, A.R. Gillman¹²⁹,
 D.M. Gingrich^{3,d}, J. Ginzburg¹⁵³, N. Giokaris⁹, M.P. Giordani^{164c}, R. Giordano^{102a,102b}, F.M. Giorgi¹⁶,
 P. Giovannini⁹⁹, P.F. Giraud¹³⁶, D. Giugni^{89a}, M. Giunta⁹³, P. Giusti^{20a}, B.K. Gjelsten¹¹⁷, L.K. Gladilin⁹⁷,
 C. Glasman⁸⁰, J. Glatzer²¹, A. Glazov⁴², K.W. Glitza¹⁷⁵, G.L. Glonti⁶⁴, J.R. Goddard⁷⁵, J. Godfrey¹⁴²,
 J. Godlewski³⁰, M. Goebel⁴², T. Göpfert⁴⁴, C. Goeringer⁸¹, C. Gössling⁴³, S. Goldfarb⁸⁷, T. Golling¹⁷⁶,
 A. Gomes^{124a,b}, L.S. Gomez Fajardo⁴², R. Gonçalo⁷⁶, J. Goncalves Pinto Firmino Da Costa⁴², L. Gonella²¹,
 S. González de la Hoz¹⁶⁷, G. Gonzalez Parra¹², M.L. Gonzalez Silva²⁷, S. Gonzalez-Sevilla⁴⁹,
 J.J. Goodson¹⁴⁸, L. Goossens³⁰, P.A. Gorbounov⁹⁵, H.A. Gordon²⁵, I. Gorelov¹⁰³, G. Gorfine¹⁷⁵,
 B. Gorini³⁰, E. Gorini^{72a,72b}, A. Gorišek⁷⁴, E. Gornicki³⁹, B. Gosdzik⁴², A.T. Goshaw⁶, M. Gosselink¹⁰⁵,
 M.I. Gostkin⁶⁴, I. Gough Eschrich¹⁶³, M. Gouighri^{135a}, D. Goujdami^{135c}, M.P. Goulette⁴⁹,
 A.G. Goussiou¹³⁸, C. Goy⁵, S. Gozpinar²³, I. Grabowska-Bold³⁸, P. Grafström^{20a,20b}, K.-J. Grahn⁴²,
 E. Gramstad¹¹⁷, F. Grancagnolo^{72a}, S. Grancagnolo¹⁶, V. Grassi¹⁴⁸, V. Gratchev¹²¹, N. Grau³⁵,
 H.M. Gray³⁰, J.A. Gray¹⁴⁸, E. Graziani^{134a}, O.G. Grebenyuk¹²¹, T. Greenshaw⁷³, Z.D. Greenwood^{25,m},
 K. Gregersen³⁶, I.M. Gregor⁴², P. Grenier¹⁴³, J. Griffiths⁸, N. Grigalashvili⁶⁴, A.A. Grillo¹³⁷,
 S. Grinstein¹², Ph. Gris³⁴, Y.V. Grishkevich⁹⁷, J.-F. Grivaz¹¹⁵, E. Gross¹⁷², J. Grosse-Knetter⁵⁴,
 J. Groth-Jensen¹⁷², K. Grybel¹⁴¹, D. Guest¹⁷⁶, C. Guicheney³⁴, T. Guillemin¹¹⁵, S. Guindon⁵⁴, U. Gul⁵³,
 J. Gunther¹²⁵, B. Guo¹⁵⁸, J. Guo³⁵, P. Gutierrez¹¹¹, N. Guttman¹⁵³, O. Gutzwiller¹⁷³, C. Guyot¹³⁶,
 C. Gwenlan¹¹⁸, C.B. Gwilliam⁷³, A. Haas¹⁴³, S. Haas³⁰, C. Haber¹⁵, H.K. Hadavand⁸, D.R. Hadley¹⁸,
 P. Haefner²¹, F. Hahn³⁰, S. Haider³⁰, Z. Hajduk³⁹, H. Hakobyan¹⁷⁷, D. Hall¹¹⁸, J. Haller⁵⁴,
 K. Hamacher¹⁷⁵, P. Hamal¹¹³, K. Hamano⁸⁶, M. Hamer⁵⁴, A. Hamilton^{145b,p}, S. Hamilton¹⁶¹, L. Han^{33b},
 K. Hanagaki¹¹⁶, K. Hanawa¹⁶⁰, M. Hance¹⁵, C. Handel⁸¹, P. Hanke^{58a}, J.R. Hansen³⁶, J.B. Hansen³⁶,
 J.D. Hansen³⁶, P.H. Hansen³⁶, P. Hansson¹⁴³, K. Hara¹⁶⁰, A.S. Hard¹⁷³, G.A. Hare¹³⁷, T. Harenberg¹⁷⁵,
 S. Harkusha⁹⁰, D. Harper⁸⁷, R.D. Harrington⁴⁶, O.M. Harris¹³⁸, J. Hartert⁴⁸, F. Hartjes¹⁰⁵,
 T. Haruyama⁶⁵, A. Harvey⁵⁶, S. Hasegawa¹⁰¹, Y. Hasegawa¹⁴⁰, S. Hassani¹³⁶, S. Haug¹⁷, M. Hauschild³⁰,
 R. Hauser⁸⁸, M. Havranek²¹, C.M. Hawkes¹⁸, R.J. Hawkins³⁰, A.D. Hawkins⁷⁹, T. Hayakawa⁶⁶,
 T. Hayashi¹⁶⁰, D. Hayden⁷⁶, C.P. Hays¹¹⁸, H.S. Hayward⁷³, S.J. Haywood¹²⁹, S.J. Head¹⁸, V. Hedberg⁷⁹,
 L. Heelan⁸, S. Heim⁸⁸, B. Heinemann¹⁵, S. Heisterkamp³⁶, L. Helary²², C. Heller⁹⁸, M. Heller³⁰,
 S. Hellman^{146a,146b}, D. Hellmich²¹, C. Hensens¹², R.C.W. Henderson⁷¹, M. Henke^{58a}, A. Henrichs⁵⁴,
 A.M. Henriques Correia³⁰, S. Henrot-Versille¹¹⁵, C. Hensel⁵⁴, T. Henß¹⁷⁵, C.M. Hernandez⁸,
 Y. Hernández Jiménez¹⁶⁷, R. Herrberg¹⁶, G. Herten⁴⁸, R. Hertenberger⁹⁸, L. Hervas³⁰, G.G. Hesketh⁷⁷,
 N.P. Hessey¹⁰⁵, E. Higón-Rodríguez¹⁶⁷, J.C. Hill²⁸, K.H. Hiller⁴², S. Hillert²¹, S.J. Hillier¹⁸, I. Hinchliffe¹⁵,
 E. Hines¹²⁰, M. Hirose¹¹⁶, F. Hirsch⁴³, D. Hirschbuehl¹⁷⁵, J. Hobbs¹⁴⁸, N. Hod¹⁵³, M.C. Hodgkinson¹³⁹,
 P. Hodgson¹³⁹, A. Hoecker³⁰, M.R. Hoferkamp¹⁰³, J. Hoffman⁴⁰, D. Hoffmann⁸³, M. Hohlfeld⁸¹,
 M. Holder¹⁴¹, S.O. Holmgren^{146a}, T. Holy¹²⁷, J.L. Holzbauer⁸⁸, T.M. Hong¹²⁰,
 L. Hooft van Huysduynen¹⁰⁸, S. Horner⁴⁸, J.-Y. Hostachy⁵⁵, S. Hou¹⁵¹, A. Hoummada^{135a}, J. Howard¹¹⁸,
 J. Howarth⁸², I. Hristova¹⁶, J. Hrivnac¹¹⁵, T. Hryn'ova⁵, P.J. Hsu⁸¹, S.-C. Hsu¹⁵, D. Hu³⁵, Z. Hubacek¹²⁷,
 F. Hubaut⁸³, F. Huegging²¹, A. Huettmann⁴², T.B. Huffman¹¹⁸, E.W. Hughes³⁵, G. Hughes⁷¹,
 M. Huhtinen³⁰, M. Hurwitz¹⁵, N. Huseynov^{64,q}, J. Huston⁸⁸, J. Huth⁵⁷, G. Iacobucci⁴⁹, G. Iakovidis¹⁰,
 M. Ibbotson⁸², I. Ibragimov¹⁴¹, L. Iconomidou-Fayard¹¹⁵, J. Idarraga¹¹⁵, P. Iengo^{102a}, O. Igonkina¹⁰⁵,
 Y. Ikegami⁶⁵, M. Ikeno⁶⁵, D. Iliadis¹⁵⁴, N. Ilic¹⁵⁸, T. Ince⁹⁹, J. Inigo-Golfín³⁰, P. Ioannou⁹, M. Iodice^{134a},
 K. Iordanidou⁹, V. Ippolito^{132a,132b}, A. Irls Quiles¹⁶⁷, C. Isaksson¹⁶⁶, M. Ishino⁶⁷, M. Ishitsuka¹⁵⁷,
 R. Ishmukhametov¹⁰⁹, C. Issever¹¹⁸, S. Istin^{19a}, A.V. Ivashin¹²⁸, W. Iwanski³⁹, H. Iwasaki⁶⁵, J.M. Izen⁴¹,
 V. Izzo^{102a}, B. Jackson¹²⁰, J.N. Jackson⁷³, P. Jackson¹, M.R. Jaekel³⁰, V. Jain⁶⁰, K. Jakobs⁴⁸,

S. Jakobsen³⁶, T. Jakoubek¹²⁵, J. Jakubek¹²⁷, D.O. Jamin¹⁵¹, D.K. Jana¹¹¹, E. Jansen⁷⁷, H. Jansen³⁰, A. Jantsch⁹⁹, M. Janus⁴⁸, G. Jarlskog⁷⁹, L. Jeanty⁵⁷, I. Jen-La Plante³¹, D. Jennens⁸⁶, P. Jenni³⁰, A.E. Loevschall-Jensen³⁶, P. Jež³⁶, S. Jézéquel⁵, M.K. Jha^{20a}, H. Ji¹⁷³, W. Ji⁸¹, J. Jia¹⁴⁸, Y. Jiang^{33b}, M. Jimenez Belenguer⁴², S. Jin^{33a}, O. Jinnouchi¹⁵⁷, M.D. Joergensen³⁶, D. Joffe⁴⁰, M. Johansen^{146a,146b}, K.E. Johansson^{146a}, P. Johansson¹³⁹, S. Johnert⁴², K.A. Johns⁷, K. Jon-And^{146a,146b}, G. Jones¹⁷⁰, R.W.L. Jones⁷¹, T.J. Jones⁷³, C. Joram³⁰, P.M. Jorge^{124a}, K.D. Joshi⁸², J. Jovicevic¹⁴⁷, T. Jovin^{13b}, X. Ju¹⁷³, C.A. Jung⁴³, R.M. Jungst³⁰, V. Juranek¹²⁵, P. Jussel⁶¹, A. Juste Rozas¹², S. Kabana¹⁷, M. Kaci¹⁶⁷, A. Kaczmarska³⁹, P. Kadlecik³⁶, M. Kado¹¹⁵, H. Kagan¹⁰⁹, M. Kagan⁵⁷, E. Kajomovitz¹⁵², S. Kalinin¹⁷⁵, L.V. Kalinovskaya⁶⁴, S. Kama⁴⁰, N. Kanaya¹⁵⁵, M. Kaneda³⁰, S. Kaneti²⁸, T. Kanno¹⁵⁷, V.A. Kantserov⁹⁶, J. Kanzaki⁶⁵, B. Kaplan¹⁰⁸, A. Kapliy³¹, J. Kaplon³⁰, D. Kar⁵³, M. Karagounis²¹, K. Karakostas¹⁰, M. Karnevskiy⁴², V. Kartvelishvili⁷¹, A.N. Karyukhin¹²⁸, L. Kashif¹⁷³, G. Kasieczka^{58b}, R.D. Kass¹⁰⁹, A. Kastanas¹⁴, M. Kataoka⁵, Y. Kataoka¹⁵⁵, E. Katsoufis¹⁰, J. Katzy⁴², V. Kaushik⁷, K. Kawagoe⁶⁹, T. Kawamoto¹⁵⁵, G. Kawamura⁸¹, M.S. Kayl¹⁰⁵, S. Kazama¹⁵⁵, V.A. Kazanin¹⁰⁷, M.Y. Kazarinov⁶⁴, R. Keeler¹⁶⁹, P.T. Keener¹²⁰, R. Kehoe⁴⁰, M. Keil⁵⁴, G.D. Kekelidze⁶⁴, J.S. Keller¹³⁸, M. Kenyon⁵³, O. Kepka¹²⁵, N. Kerschen³⁰, B.P. Kerševan⁷⁴, S. Kersten¹⁷⁵, K. Kessoku¹⁵⁵, J. Keung¹⁵⁸, F. Khalil-zada¹¹, H. Khandanyan^{146a,146b}, A. Khanov¹¹², D. Kharchenko⁶⁴, A. Khodinov⁹⁶, A. Khomich^{58a}, T.J. Khoo²⁸, G. Khorauli²¹, A. Khoroshilov¹⁷⁵, V. Khovanskiy⁹⁵, E. Khramov⁶⁴, J. Khubua^{51b}, H. Kim^{146a,146b}, S.H. Kim¹⁶⁰, N. Kimura¹⁷¹, O. Kind¹⁶, B.T. King⁷³, M. King⁶⁶, R.S.B. King¹¹⁸, J. Kirk¹²⁹, A.E. Kiryunin⁹⁹, T. Kishimoto⁶⁶, D. Kisielewska³⁸, T. Kitamura⁶⁶, T. Kittelmann¹²³, K. Kiuchi¹⁶⁰, E. Kladiva^{144b}, M. Klein⁷³, U. Klein⁷³, K. Kleinknecht⁸¹, M. Klemetti⁸⁵, A. Klier¹⁷², P. Klimek^{146a,146b}, A. Klimentov²⁵, R. Klingenberg⁴³, J.A. Klinger⁸², E.B. Klinkby³⁶, T. Klioutchnikova³⁰, P.F. Klok¹⁰⁴, S. Klous¹⁰⁵, E.-E. Kluge^{58a}, T. Kluge⁷³, P. Kluit¹⁰⁵, S. Kluth⁹⁹, E. Kneringer⁶¹, E.B.F.G. Knoop⁸³, A. Knue⁵⁴, B.R. Ko⁴⁵, T. Kobayashi¹⁵⁵, M. Kobel⁴⁴, M. Kocian¹⁴³, P. Kodys¹²⁶, K. Köneke³⁰, A.C. König¹⁰⁴, S. Koenig⁸¹, L. Köpke⁸¹, F. Koetsveld¹⁰⁴, P. Koevesarki²¹, T. Koffas²⁹, E. Koffeman¹⁰⁵, L.A. Kogan¹¹⁸, S. Kohlmann¹⁷⁵, F. Kohn⁵⁴, Z. Kohout¹²⁷, T. Kohriki⁶⁵, T. Koi¹⁴³, G.M. Kolachev^{107,*}, H. Kolanoski¹⁶, V. Kolesnikov⁶⁴, I. Koletsou^{89a}, J. Koll⁸⁸, A.A. Komar⁹⁴, Y. Komori¹⁵⁵, T. Kondo⁶⁵, T. Kono^{42,r}, A.I. Kononov⁴⁸, R. Konoplich^{108,s}, N. Konstantinidis⁷⁷, R. Kopeliansky¹⁵², S. Koperny³⁸, K. Korcyl³⁹, K. Kordas¹⁵⁴, A. Korn¹¹⁸, A. Korol¹⁰⁷, I. Korolkov¹², E.V. Korolkova¹³⁹, V.A. Korotkov¹²⁸, O. Kortner⁹⁹, S. Kortner⁹⁹, V.V. Kostyukhin²¹, S. Kotov⁹⁹, V.M. Kotov⁶⁴, A. Kotwal⁴⁵, C. Kourkoumelis⁹, V. Kouskoura¹⁵⁴, A. Koutsman^{159a}, R. Kowalewski¹⁶⁹, T.Z. Kowalski³⁸, W. Kozanecki¹³⁶, A.S. Kozhin¹²⁸, V. Kral¹²⁷, V.A. Kramarenko⁹⁷, G. Kramberger⁷⁴, M.W. Krasny⁷⁸, A. Krasznahorkay¹⁰⁸, J.K. Kraus²¹, S. Kreiss¹⁰⁸, F. Krejci¹²⁷, J. Kretzschmar⁷³, N. Krieger⁵⁴, P. Krieger¹⁵⁸, K. Kroeninger⁵⁴, H. Kroha⁹⁹, J. Kroll¹²⁰, J. Kroseberg²¹, J. Krstic^{13a}, U. Kruchonak⁶⁴, H. Krüger²¹, T. Kruker¹⁷, N. Krumnack⁶³, Z.V. Krumshteyn⁶⁴, A. Kruse¹⁷³, T. Kubota⁸⁶, S. Kuday^{4a}, S. Kuehn⁴⁸, A. Kugel^{58c}, T. Kuhl⁴², D. Kuhn⁶¹, V. Kukhtin⁶⁴, Y. Kulchitsky⁹⁰, S. Kuleshov^{32b}, C. Kummer⁹⁸, M. Kuna⁷⁸, J. Kunkle¹²⁰, A. Kupco¹²⁵, H. Kurashige⁶⁶, M. Kurata¹⁶⁰, Y.A. Kurochkin⁹⁰, V. Kus¹²⁵, E.S. Kuwertz¹⁴⁷, M. Kuze¹⁵⁷, J. Kvita¹⁴², R. Kwee¹⁶, A. La Rosa⁴⁹, L. La Rotonda^{37a,37b}, L. Labarga⁸⁰, J. Labbe⁵, S. Lablak^{135a}, C. Lacasta¹⁶⁷, F. Lacava^{132a,132b}, J. Lacey²⁹, H. Lacker¹⁶, D. Lacour⁷⁸, V.R. Lacuesta¹⁶⁷, E. Ladygin⁶⁴, R. Lafaye⁵, B. Laforge⁷⁸, T. Lagouri¹⁷⁶, S. Lai⁴⁸, E. Laisne⁵⁵, M. Lamanna³⁰, L. Lambourne⁷⁷, C.L. Lampen⁷, W. Lampl⁷, E. Lancon¹³⁶, U. Landgraf⁴⁸, M.P.J. Landon⁷⁵, V.S. Lang^{58a}, C. Lange⁴², A.J. Lankford¹⁶³, F. Lanni²⁵, K. Lantzsck¹⁷⁵, S. Laplace⁷⁸, C. Lapoire²¹, J.F. Laporte¹³⁶, T. Lari^{89a}, A. Larter¹¹⁸, M. Lassnig³⁰, P. Laurelli⁴⁷, V. Lavorini^{37a,37b}, W. Lavrijsen¹⁵, P. Laycock⁷³, T. Lazovich⁵⁷, O. Le Dortz⁷⁸, E. Le Guirriec⁸³, E. Le Menedeu¹², T. LeCompte⁶, F. Ledroit-Guillon⁵⁵, H. Lee¹⁰⁵, J.S.H. Lee¹¹⁶, S.C. Lee¹⁵¹, L. Lee¹⁷⁶, M. Lefebvre¹⁶⁹, M. Legendre¹³⁶, F. Legger⁹⁸, C. Leggett¹⁵, M. Lehmann²¹, G. Lehmann Miotto³⁰, X. Lei⁷, M.A.L. Leite^{24d}, R. Leitner¹²⁶, D. Lellouch¹⁷², B. Lemmer⁵⁴, V. Lendermann^{58a}, K.J.C. Leney^{145b}, T. Lenz¹⁰⁵, G. Lenzen¹⁷⁵, B. Lenzi³⁰, K. Leonhardt⁴⁴, S. Leontsinis¹⁰, F. Lepold^{58a}, C. Leroy⁹³, J.-R. Lessard¹⁶⁹, C.G. Lester²⁸, C.M. Lester¹²⁰, J. Levêque⁵, D. Levin⁸⁷, L.J. Levinson¹⁷², A. Lewis¹¹⁸, G.H. Lewis¹⁰⁸, A.M. Leyko²¹, M. Leyton¹⁶, B. Li⁸³, H. Li¹⁴⁸, H.L. Li³¹, S. Li^{33b,t}, X. Li⁸⁷, Z. Liang^{118,u}, H. Liao³⁴, B. Liberti^{133a}, P. Lichard³⁰, M. Lichtnecker⁹⁸, K. Lie¹⁶⁵, W. Liebig¹⁴, C. Limbach²¹, A. Limosani⁸⁶, M. Limper⁶², S.C. Lin^{151,v}, F. Linde¹⁰⁵, J.T. Linnemann⁸⁸, E. Lipeles¹²⁰, A. Lipniacka¹⁴, T.M. Liss¹⁶⁵, D. Lissauer²⁵, A. Lister⁴⁹, A.M. Litke¹³⁷, C. Liu²⁹, D. Liu¹⁵¹, H. Liu⁸⁷, J.B. Liu⁸⁷, K. Liu^{33b,w}, L. Liu⁸⁷, M. Liu^{33b}, Y. Liu^{33b}, M. Livan^{119a,119b}, S.S.A. Livermore¹¹⁸,

A. Lleres⁵⁵, J. Llorente Merino⁸⁰, S.L. Lloyd⁷⁵, E. Lobodzinska⁴², P. Loch⁷, W.S. Lockman¹³⁷,
 T. Loddenkoetter²¹, F.K. Loebinger⁸², A. Loginov¹⁷⁶, C.W. Loh¹⁶⁸, T. Lohse¹⁶, K. Lohwasser⁴⁸,
 M. Lokajicek¹²⁵, V.P. Lombardo⁵, J.D. Long⁸⁷, R.E. Long⁷¹, L. Lopes^{124a}, D. Lopez Mateos⁵⁷, J. Lorenz⁹⁸,
 N. Lorenzo Martinez¹¹⁵, M. Losada¹⁶², P. Loscutoff¹⁵, F. Lo Sterzo^{132a,132b}, M.J. Losty^{159a,*}, X. Lou⁴¹,
 A. Lounis¹¹⁵, K.F. Loureiro¹⁶², J. Love⁶, P.A. Love⁷¹, A.J. Lowe^{143,e}, F. Lu^{33a}, H.J. Lubatti¹³⁸,
 C. Luci^{132a,132b}, A. Lucotte⁵⁵, A. Ludwig⁴⁴, D. Ludwig⁴², I. Ludwig⁴⁸, J. Ludwig⁴⁸, F. Luehring⁶⁰,
 G. Luijckx¹⁰⁵, W. Lukas⁶¹, L. Luminari^{132a}, E. Lund¹¹⁷, B. Lund-Jensen¹⁴⁷, B. Lundberg⁷⁹,
 J. Lundberg^{146a,146b}, O. Lundberg^{146a,146b}, J. Lundquist³⁶, M. Lungwitz⁸¹, D. Lynn²⁵, E. Lytken⁷⁹,
 H. Ma²⁵, L.L. Ma¹⁷³, G. Maccarrone⁴⁷, A. Macchiolo⁹⁹, B. Maček⁷⁴, J. Machado Miguens^{124a},
 R. Mackeprang³⁶, R.J. Madaras¹⁵, H.J. Maddocks⁷¹, W.F. Mader⁴⁴, R. Maenner^{58c}, T. Maeno²⁵,
 P. Mättig¹⁷⁵, S. Mättig⁸¹, L. Magnoni¹⁶³, E. Magradze⁵⁴, K. Mahboubi⁴⁸, J. Mahlstedt¹⁰⁵,
 S. Mahmoud⁷³, G. Mahout¹⁸, C. Maiani¹³⁶, C. Maidantchik^{24a}, A. Maio^{124a,b}, S. Majewski²⁵,
 Y. Makida⁶⁵, N. Makovec¹¹⁵, P. Mal¹³⁶, B. Malaescu³⁰, Pa. Malecki³⁹, P. Malecki³⁹, V.P. Maleev¹²¹,
 F. Malek⁵⁵, U. Mallik⁶², D. Malon⁶, C. Malone¹⁴³, S. Maltezos¹⁰, V. Malyshev¹⁰⁷, S. Malyukov³⁰,
 R. Mameghani⁹⁸, J. Mamuzic^{13b}, A. Manabe⁶⁵, L. Mandelli^{89a}, I. Mandić⁷⁴, R. Mandrysch¹⁶,
 J. Maneira^{124a}, A. Manfredini⁹⁹, P.S. Mangeard⁸⁸, L. Manhaes de Andrade Filho^{24b},
 J.A. Manjarres Ramos¹³⁶, A. Mann⁵⁴, P.M. Manning¹³⁷, A. Manousakis-Katsikakis⁹, B. Mansoulie¹³⁶,
 A. Mapelli³⁰, L. Mapelli³⁰, L. March¹⁶⁷, J.F. Marchand²⁹, F. Marchese^{133a,133b}, G. Marchiori⁷⁸,
 M. Marcisovsky¹²⁵, C.P. Marino¹⁶⁹, F. Marroquim^{24a}, Z. Marshall³⁰, F.K. Martens¹⁵⁸, L.F. Marti¹⁷,
 S. Marti-Garcia¹⁶⁷, B. Martin³⁰, B. Martin⁸⁸, J.P. Martin⁹³, T.A. Martin¹⁸, V.J. Martin⁴⁶,
 B. Martin dit Latour⁴⁹, S. Martin-Haugh¹⁴⁹, M. Martinez¹², V. Martinez Outschoorn⁵⁷,
 A.C. Martyniuk¹⁶⁹, M. Marx⁸², F. Marzano^{132a}, A. Marzin¹¹¹, L. Masetti⁸¹, T. Mashimo¹⁵⁵,
 R. Mashinistov⁹⁴, J. Masik⁸², A.L. Maslennikov¹⁰⁷, I. Massa^{20a,20b}, G. Massaro¹⁰⁵, N. Massol⁵,
 P. Mastrandrea¹⁴⁸, A. Mastroberardino^{37a,37b}, T. Masubuchi¹⁵⁵, P. Matricon¹¹⁵, H. Matsunaga¹⁵⁵,
 T. Matsushita⁶⁶, C. Mattraversi^{118,c}, J. Maurer⁸³, S.J. Maxfield⁷³, A. Mayne¹³⁹, R. Mazini¹⁵¹, M. Mazur²¹,
 L. Mazzaferro^{133a,133b}, M. Mazzanti^{89a}, J. Mc Donald⁸⁵, S.P. Mc Kee⁸⁷, A. McCarn¹⁶⁵, R.L. McCarthy¹⁴⁸,
 T.G. McCarthy²⁹, N.A. McCubbin¹²⁹, K.W. McFarlane^{56,*}, J.A. McFayden¹³⁹, G. Mchedlidze^{51b},
 T. McLaughlan¹⁸, S.J. McMahon¹²⁹, R.A. McPherson^{169,k}, A. Meade⁸⁴, J. Mechnich¹⁰⁵, M. Mechtel¹⁷⁵,
 M. Medinnis⁴², R. Meera-Lebbai¹¹¹, T. Meguro¹¹⁶, R. Mehdiyev⁹³, S. Mehlhase³⁶, A. Mehta⁷³,
 K. Meier^{58a}, B. Meirose⁷⁹, C. Melachrinou³¹, B.R. Mellado Garcia¹⁷³, F. Meloni^{89a,89b},
 L. Mendoza Navas¹⁶², Z. Meng^{151,x}, A. Mengarelli^{20a,20b}, S. Menke⁹⁹, E. Meoni¹⁶¹, K.M. Mercurio⁵⁷,
 P. Mermod⁴⁹, L. Merola^{102a,102b}, C. Meroni^{89a}, F.S. Merritt³¹, H. Merritt¹⁰⁹, A. Messina^{30,y},
 J. Metcalfe²⁵, A.S. Mete¹⁶³, C. Meyer⁸¹, C. Meyer³¹, J.-P. Meyer¹³⁶, J. Meyer¹⁷⁴, J. Meyer⁵⁴,
 T.C. Meyer³⁰, S. Michal³⁰, L. Micu^{26a}, R.P. Middleton¹²⁹, S. Migas⁷³, L. Mijović¹³⁶, G. Mikenberg¹⁷²,
 M. Mikestikova¹²⁵, M. Mikuž⁷⁴, D.W. Miller³¹, R.J. Miller⁸⁸, W.J. Mills¹⁶⁸, C. Mills⁵⁷, A. Milov¹⁷²,
 D.A. Milstead^{146a,146b}, D. Milstein¹⁷², A.A. Minaenko¹²⁸, M. Miñano Moya¹⁶⁷, I.A. Minashvili⁶⁴,
 A.I. Mincer¹⁰⁸, B. Mindur³⁸, M. Mineev⁶⁴, Y. Ming¹⁷³, L.M. Mir¹², G. Mirabelli^{132a}, J. Mitrevski¹³⁷,
 V.A. Mitsou¹⁶⁷, S. Mitsui⁶⁵, P.S. Miyagawa¹³⁹, J.U. Mjörnmark⁷⁹, T. Moa^{146a,146b}, V. Moeller²⁸,
 K. Mönig⁴², N. Möser²¹, S. Mohapatra¹⁴⁸, W. Mohr⁴⁸, R. Moles-Valls¹⁶⁷, A. Molfetas³⁰, J. Monk⁷⁷,
 E. Monnier⁸³, J. Montejo Berlingen¹², F. Monticelli⁷⁰, S. Monzani^{20a,20b}, R.W. Moore³, G.F. Moorhead⁸⁶,
 C. Mora Herrera⁴⁹, A. Moraes⁵³, N. Morange¹³⁶, J. Morel⁵⁴, G. Morello^{37a,37b}, D. Moreno⁸¹,
 M. Moreno Llácer¹⁶⁷, P. Morettini^{50a}, M. Morgenstern⁴⁴, M. Morii⁵⁷, A.K. Morley³⁰, G. Mornacchi³⁰,
 J.D. Morris⁷⁵, L. Morvaj¹⁰¹, H.G. Moser⁹⁹, M. Mosidze^{51b}, J. Moss¹⁰⁹, R. Mount¹⁴³, E. Mountricha^{10,z},
 S.V. Mouraviev^{94,*}, E.J.W. Moyse⁸⁴, F. Mueller^{58a}, J. Mueller¹²³, K. Mueller²¹, T.A. Müller⁹⁸,
 T. Mueller⁸¹, D. Muenstermann³⁰, Y. Munwes¹⁵³, W.J. Murray¹²⁹, I. Mussche¹⁰⁵, E. Musto^{102a,102b},
 A.G. Myagkov¹²⁸, M. Myska¹²⁵, O. Nackenhorst⁵⁴, J. Nadal¹², K. Nagai¹⁶⁰, R. Nagai¹⁵⁷, K. Nagano⁶⁵,
 A. Nagarkar¹⁰⁹, Y. Nagasaka⁵⁹, M. Nagel⁹⁹, A.M. Nairz³⁰, Y. Nakahama³⁰, K. Nakamura¹⁵⁵,
 T. Nakamura¹⁵⁵, I. Nakano¹¹⁰, G. Nanava²¹, A. Napier¹⁶¹, R. Narayan^{58b}, M. Nash^{77,c}, T. Nattermann²¹,
 T. Naumann⁴², G. Navarro¹⁶², H.A. Neal⁸⁷, P.Yu. Nechaeva⁹⁴, T.J. Neep⁸², A. Negri^{119a,119b}, G. Negri³⁰,
 M. Negrini^{20a}, S. Nektarijevic⁴⁹, A. Nelson¹⁶³, T.K. Nelson¹⁴³, S. Nemecek¹²⁵, P. Nemethy¹⁰⁸,
 A.A. Nepomuceno^{24a}, M. Nessi^{30,aa}, M.S. Neubauer¹⁶⁵, M. Neumann¹⁷⁵, A. Neusiedl⁸¹, R.M. Neves¹⁰⁸,
 P. Nevski²⁵, F.M. Newcomer¹²⁰, P.R. Newman¹⁸, V. Nguyen Thi Hong¹³⁶, R.B. Nickerson¹¹⁸,

R. Nicolaidou¹³⁶, B. Nicquevert³⁰, F. Niedercorn¹¹⁵, J. Nielsen¹³⁷, N. Nikiforou³⁵, A. Nikiforov¹⁶, V. Nikolaenko¹²⁸, I. Nikolic-Audit⁷⁸, K. Nikolics⁴⁹, K. Nikolopoulos¹⁸, H. Nilsen⁴⁸, P. Nilsson⁸, Y. Ninomiya¹⁵⁵, A. Nisati^{132a}, R. Nisius⁹⁹, T. Nobe¹⁵⁷, L. Nodulman⁶, M. Nomachi¹¹⁶, I. Nomidis¹⁵⁴, S. Norberg¹¹¹, M. Nordberg³⁰, P.R. Norton¹²⁹, J. Novakova¹²⁶, M. Nozaki⁶⁵, L. Nozka¹¹³, I.M. Nugent^{159a}, A.-E. Nuncio-Quiroz²¹, G. Nunes Hanninger⁸⁶, T. Nunnemann⁹⁸, E. Nurse⁷⁷, B.J. O'Brien⁴⁶, D.C. O'Neil¹⁴², V. O'Shea⁵³, L.B. Oakes⁹⁸, F.G. Oakham^{29,d}, H. Oberlack⁹⁹, J. Ocariz⁷⁸, A. Ochi⁶⁶, S. Oda⁶⁹, S. Odaka⁶⁵, J. Odier⁸³, H. Ogren⁶⁰, A. Oh⁸², S.H. Oh⁴⁵, C.C. Ohm³⁰, T. Ohshima¹⁰¹, W. Okamura¹¹⁶, H. Okawa²⁵, Y. Okumura³¹, T. Okuyama¹⁵⁵, A. Olariu^{26a}, A.G. Olchevski⁶⁴, S.A. Olivares Pino^{32a}, M. Oliveira^{124a,h}, D. Oliveira Damazio²⁵, E. Oliver Garcia¹⁶⁷, D. Olivito¹²⁰, A. Olszewski³⁹, J. Olszowska³⁹, A. Onofre^{124a,ab}, P.U.E. Onyisi³¹, C.J. Oram^{159a}, M.J. Oreglia³¹, Y. Oren¹⁵³, D. Orestano^{134a,134b}, N. Orlando^{72a,72b}, I. Orlov¹⁰⁷, C. Oropeza Barrera⁵³, R.S. Orr¹⁵⁸, B. Osculati^{50a,50b}, R. Ospanov¹²⁰, C. Osuna¹², G. Otero y Garzon²⁷, J.P. Ottersbach¹⁰⁵, M. Ouchrif^{135d}, E.A. Ouellette¹⁶⁹, F. Ould-Saada¹¹⁷, A. Ouraou¹³⁶, Q. Ouyang^{33a}, A. Ovcharova¹⁵, M. Owen⁸², S. Owen¹³⁹, V.E. Ozcan^{19a}, N. Ozturk⁸, A. Pacheco Pages¹², C. Padilla Aranda¹², S. Pagan Griso¹⁵, E. Paganis¹³⁹, C. Pahl⁹⁹, F. Paige²⁵, P. Pais⁸⁴, K. Pajchel¹¹⁷, G. Palacino^{159b}, C.P. Paleari⁷, S. Palestini³⁰, D. Pallin³⁴, A. Palma^{124a}, J.D. Palmer¹⁸, Y.B. Pan¹⁷³, E. Panagiotopoulou¹⁰, J.G. Panduro Vazquez⁷⁶, P. Pani¹⁰⁵, N. Panikashvili⁸⁷, S. Panitkin²⁵, D. Pantea^{26a}, A. Papadelis^{146a}, Th.D. Papadopoulou¹⁰, A. Paramonov⁶, D. Paredes Hernandez³⁴, W. Park^{25,ac}, M.A. Parker²⁸, F. Parodi^{50a,50b}, J.A. Parsons³⁵, U. Parzefall⁴⁸, S. Pashapour⁵⁴, E. Pasqualucci^{132a}, S. Passaggio^{50a}, A. Passeri^{134a}, F. Pastore^{134a,134b,*}, Fr. Pastore⁷⁶, G. Pásztor^{49,ad}, S. Pataria¹⁷⁵, N. Patel¹⁵⁰, J.R. Pater⁸², S. Patricelli^{102a,102b}, T. Pauly³⁰, M. Pecsny^{144a}, S. Pedraza Lopez¹⁶⁷, M.I. Pedraza Morales¹⁷³, S.V. Peleganchuk¹⁰⁷, D. Pelikan¹⁶⁶, H. Peng^{33b}, B. Penning³¹, A. Penson³⁵, J. Penwell⁶⁰, M. Perantoni^{24a}, K. Perez^{35,ae}, T. Perez Cavalcanti⁴², E. Perez Codina^{159a}, M.T. Pérez García-Estañ¹⁶⁷, V. Perez Reale³⁵, L. Perini^{89a,89b}, H. Pernegger³⁰, R. Perrino^{72a}, P. Perrodo⁵, V.D. Peshekhonov⁶⁴, K. Peters³⁰, B.A. Petersen³⁰, J. Petersen³⁰, T.C. Petersen³⁶, E. Petit⁵, A. Petridis¹⁵⁴, C. Petridou¹⁵⁴, E. Petrolo^{132a}, F. Petrucci^{134a,134b}, D. Petschall⁴², M. Petteni¹⁴², R. Pezoa^{32b}, A. Phan⁸⁶, P.W. Phillips¹²⁹, G. Piacquadio³⁰, A. Picazio⁴⁹, E. Piccaro⁷⁵, M. Piccinini^{20a,20b}, S.M. Piec⁴², R. Piegai²⁷, D.T. Pignotti¹⁰⁹, J.E. Pilcher³¹, A.D. Pilkington⁸², J. Pina^{124a,b}, M. Pinamonti^{164a,164c}, A. Pinder¹¹⁸, J.L. Pinfold³, B. Pinto^{124a}, C. Pizio^{89a,89b}, M. Plamondon¹⁶⁹, M.-A. Pleier²⁵, E. Plotnikova⁶⁴, A. Poblaguev²⁵, S. Poddar^{58a}, F. Podlyski³⁴, L. Poggioli¹¹⁵, D. Pohl²¹, M. Pohl⁴⁹, G. Polesello^{119a}, A. Policicchio^{37a,37b}, R. Polifka¹⁵⁸, A. Polini^{20a}, J. Poll⁷⁵, V. Polychronakos²⁵, D. Pomeroy²³, K. Pommès³⁰, L. Pontecorvo^{132a}, B.G. Pope⁸⁸, G.A. Popeneciu^{26a}, D.S. Popovic^{13a}, A. Poppleton³⁰, X. Portell Bueso³⁰, G.E. Pospelov⁹⁹, S. Pospisil¹²⁷, I.N. Potrap⁹⁹, C.J. Potter¹⁴⁹, C.T. Potter¹¹⁴, G. Poulard³⁰, J. Poveda⁶⁰, V. Pozdnyakov⁶⁴, R. Prabhu⁷⁷, P. Pralavorio⁸³, A. Pranko¹⁵, S. Prasad³⁰, R. Pravahan²⁵, S. Prell⁶³, K. Pretzl¹⁷, D. Price⁶⁰, J. Price⁷³, L.E. Price⁶, D. Prieur¹²³, M. Primavera^{72a}, K. Prokofiev¹⁰⁸, F. Prokoshin^{32b}, S. Protopopescu²⁵, J. Proudfoot⁶, X. Prudent⁴⁴, M. Przybycien³⁸, H. Przysiezniak⁵, S. Psoroulas²¹, E. Ptacek¹¹⁴, E. Pueschel⁸⁴, J. Purdham⁸⁷, M. Purohit^{25,ac}, P. Puzo¹¹⁵, Y. Pylypchenko⁶², J. Qian⁸⁷, A. Quadt⁵⁴, D.R. Quarrie¹⁵, W.B. Quayle¹⁷³, F. Quinonez^{32a}, M. Raas¹⁰⁴, S. Raddum¹¹⁷, V. Radeka²⁵, V. Radescu⁴², P. Radloff¹¹⁴, T. Rador^{19a}, F. Ragusa^{89a,89b}, G. Rahal¹⁷⁸, A.M. Rahimi¹⁰⁹, D. Rahm²⁵, S. Rajagopalan²⁵, M. Rammensee⁴⁸, M. Rammes¹⁴¹, A.S. Randle-Conde⁴⁰, K. Randrianarivony²⁹, F. Rauscher⁹⁸, T.C. Rave⁴⁸, M. Raymond³⁰, A.L. Read¹¹⁷, D.M. Rebuszi^{119a,119b}, A. Redelbach¹⁷⁴, G. Redlinger²⁵, R. Reece¹²⁰, K. Reeves⁴¹, E. Reinherz-Aronis¹⁵³, A. Reinsch¹¹⁴, I. Reisinger⁴³, C. Rembser³⁰, Z.L. Ren¹⁵¹, A. Renaud¹¹⁵, M. Rescigno^{132a}, S. Resconi^{89a}, B. Resende¹³⁶, P. Reznicek⁹⁸, R. Rezvani¹⁵⁸, R. Richter⁹⁹, E. Richter-Was^{5,af}, M. Ridel⁷⁸, M. Rijpstra¹⁰⁵, M. Rijssenbeek¹⁴⁸, A. Rimoldi^{119a,119b}, L. Rinaldi^{20a}, R.R. Rios⁴⁰, I. Riu¹², G. Rivoltella^{89a,89b}, F. Rizatdinova¹¹², E. Rizvi⁷⁵, S.H. Robertson^{85,k}, A. Robichaud-Veronneau¹¹⁸, D. Robinson²⁸, J.E.M. Robinson⁸², A. Robson⁵³, J.G. Rocha de Lima¹⁰⁶, C. Roda^{122a,122b}, D. Roda Dos Santos³⁰, A. Roe⁵⁴, S. Roe³⁰, O. Røhne¹¹⁷, S. Rolli¹⁶¹, A. Romaniouk⁹⁶, M. Romano^{20a,20b}, G. Romeo²⁷, E. Romero Adam¹⁶⁷, N. Rompotis¹³⁸, L. Roos⁷⁸, E. Ros¹⁶⁷, S. Rosati^{132a}, K. Rosbach⁴⁹, A. Rose¹⁴⁹, M. Rose⁷⁶, G.A. Rosenbaum¹⁵⁸, E.I. Rosenberg⁶³, P.L. Rosendahl¹⁴, O. Rosenthal¹⁴¹, L. Rossetlet⁴⁹, V. Rossetti¹², E. Rossi^{132a,132b}, L.P. Rossi^{50a}, M. Rotaru^{26a}, I. Roth¹⁷², J. Rothberg¹³⁸, D. Rousseau¹¹⁵, C.R. Royon¹³⁶, A. Rozanov⁸³, Y. Rozen¹⁵², X. Ruan^{33a,ag}, F. Rubbo¹², I. Rubinskiy⁴², N. Ruckstuhl¹⁰⁵, V.I. Rud⁹⁷, C. Rudolph⁴⁴, G. Rudolph⁶¹, F. Rühr⁷, A. Ruiz-Martinez⁶³,

L. Romyantsev⁶⁴, Z. Rurikova⁴⁸, N.A. Rusakovich⁶⁴, J.P. Rutherford⁷, P. Ruzicka¹²⁵, Y.F. Ryabov¹²¹,
 M. Rybar¹²⁶, G. Rybkin¹¹⁵, N.C. Ryder¹¹⁸, A.F. Saavedra¹⁵⁰, I. Sadeh¹⁵³, H.F.-W. Sadrozinski¹³⁷,
 R. Sadykov⁶⁴, F. Safai Tehrani^{132a}, H. Sakamoto¹⁵⁵, G. Salamanna⁷⁵, A. Salamon^{133a}, M. Saleem¹¹¹,
 D. Salek³⁰, D. Salihagic⁹⁹, A. Salnikov¹⁴³, J. Salt¹⁶⁷, B.M. Salvachua Ferrando⁶, D. Salvatore^{37a,37b},
 F. Salvatore¹⁴⁹, A. Salvucci¹⁰⁴, A. Salzburger³⁰, D. Sampsonidis¹⁵⁴, B.H. Samset¹¹⁷, A. Sanchez^{102a,102b},
 V. Sanchez Martinez¹⁶⁷, H. Sandaker¹⁴, H.G. Sander⁸¹, M.P. Sanders⁹⁸, M. Sandhoff¹⁷⁵, T. Sandoval²⁸,
 C. Sandoval¹⁶², R. Sandstroem⁹⁹, D.P.C. Sankey¹²⁹, A. Sansoni⁴⁷, C. Santamarina Rios⁸⁵, C. Santoni³⁴,
 R. Santonico^{133a,133b}, H. Santos^{124a}, J.G. Saraiva^{124a}, T. Sarangi¹⁷³, E. Sarkisyan-Grinbaum⁸,
 F. Sarri^{122a,122b}, G. Sartisohn¹⁷⁵, O. Sasaki⁶⁵, Y. Sasaki¹⁵⁵, N. Sasao⁶⁷, I. Satsounkevitch⁹⁰,
 G. Sauvage^{5,*}, E. Sauvan⁵, J.B. Sauvan¹¹⁵, P. Savard^{158,d}, V. Savinov¹²³, D.O. Savu³⁰, L. Sawyer^{25,m},
 D.H. Saxon⁵³, J. Saxon¹²⁰, C. Sbarra^{20a}, A. Sbrizzi^{20a,20b}, D.A. Scannicchio¹⁶³, M. Scarcella¹⁵⁰,
 J. Schaarschmidt¹¹⁵, P. Schacht⁹⁹, D. Schaefer¹²⁰, U. Schäfer⁸¹, A. Schaelicke⁴⁶, S. Schaepe²¹,
 S. Schaezel^{58b}, A.C. Schaffer¹¹⁵, D. Schaile⁹⁸, R.D. Schamberger¹⁴⁸, A.G. Schamov¹⁰⁷, V. Scharf^{58a},
 V.A. Schegelsky¹²¹, D. Scheirich⁸⁷, M. Schernau¹⁶³, M.I. Scherzer³⁵, C. Schiavi^{50a,50b}, J. Schieck⁹⁸,
 M. Schioppa^{37a,37b}, S. Schlenker³⁰, P. Schmid³⁰, E. Schmidt⁴⁸, K. Schmieden²¹, C. Schmitt⁸¹,
 S. Schmitt^{58b}, M. Schmitz²¹, B. Schneider¹⁷, U. Schnoor⁴⁴, L. Schoeffel¹³⁶, A. Schoening^{58b},
 A.L.S. Schorlemmer⁵⁴, M. Schott³⁰, D. Schouten^{159a}, J. Schovancova¹²⁵, M. Schram⁸⁵, C. Schroeder⁸¹,
 N. Schroer^{58c}, M.J. Schultens²¹, J. Schultes¹⁷⁵, H.-C. Schultz-Coulon^{58a}, H. Schulz¹⁶, M. Schumacher⁴⁸,
 B.A. Schumm¹³⁷, Ph. Schune¹³⁶, C. Schwanenberger⁸², A. Schwartzman¹⁴³, Ph. Schwegler⁹⁹,
 Ph. Schwemling⁷⁸, R. Schwienhorst⁸⁸, R. Schwierz⁴⁴, J. Schwindling¹³⁶, T. Schwindt²¹, M. Schwoerer⁵,
 G. Sciolla²³, W.G. Scott¹²⁹, J. Searcy¹¹⁴, G. Sedov⁴², E. Sedykh¹²¹, S.C. Seidel¹⁰³, A. Seiden¹³⁷,
 F. Seifert⁴⁴, J.M. Seixas^{24a}, G. Sekhniaidze^{102a}, S.J. Sekula⁴⁰, K.E. Selbach⁴⁶, D.M. Seliverstov¹²¹,
 B. Sellden^{146a}, G. Sellers⁷³, M. Seman^{144b}, N. Semprini-Cesari^{20a,20b}, C. Serfon⁹⁸, L. Serin¹¹⁵,
 L. Serkin⁵⁴, R. Seuster^{159a}, H. Severini¹¹¹, A. Sfyrla³⁰, E. Shabalina⁵⁴, M. Shamim¹¹⁴, L.Y. Shan^{33a},
 J.T. Shank²², Q.T. Shao⁸⁶, M. Shapiro¹⁵, P.B. Shatalov⁹⁵, K. Shaw^{164a,164c}, D. Sherman¹⁷⁶, P. Sherwood⁷⁷,
 S. Shimizu¹⁰¹, M. Shimojima¹⁰⁰, T. Shin⁵⁶, M. Shiyakova⁶⁴, A. Shmeleva⁹⁴, M.J. Shochet³¹, D. Short¹¹⁸,
 S. Shrestha⁶³, E. Shulga⁹⁶, M.A. Shupe⁷, P. Sicho¹²⁵, A. Sidoti^{132a}, F. Siegert⁴⁸, Dj. Sijacki^{13a},
 O. Silbert¹⁷², J. Silva^{124a}, Y. Silver¹⁵³, D. Silverstein¹⁴³, S.B. Silverstein^{146a}, V. Simak¹²⁷, O. Simard¹³⁶,
 Lj. Simic^{13a}, S. Simion¹¹⁵, E. Simioni⁸¹, B. Simmons⁷⁷, R. Simoniello^{89a,89b}, M. Simonyan³⁶,
 P. Sinervo¹⁵⁸, N.B. Sinev¹¹⁴, V. Sipica¹⁴¹, G. Siragusa¹⁷⁴, A. Sircar²⁵, A.N. Sisakyan^{64,*},
 S.Yu. Sivoklokov⁹⁷, J. Sjölin^{146a,146b}, T.B. Sjursen¹⁴, L.A. Skinnari¹⁵, H.P. Skottowe⁵⁷, K. Skovpen¹⁰⁷,
 P. Skubic¹¹¹, M. Slater¹⁸, T. Slavicek¹²⁷, K. Sliwa¹⁶¹, V. Smakhtin¹⁷², B.H. Smart⁴⁶, L. Smestad¹¹⁷,
 S.Yu. Smirnov⁹⁶, Y. Smirnov⁹⁶, L.N. Smirnova⁹⁷, O. Smirnova⁷⁹, B.C. Smith⁵⁷, D. Smith¹⁴³, K.M. Smith⁵³,
 M. Smizanska⁷¹, K. Smolek¹²⁷, A.A. Snesarev⁹⁴, S.W. Snow⁸², J. Snow¹¹¹, S. Snyder²⁵, R. Sobie^{169,k},
 J. Sodomka¹²⁷, A. Soffer¹⁵³, C.A. Solans¹⁶⁷, M. Solar¹²⁷, J. Solc¹²⁷, E.Yu. Soldatov⁹⁶, U. Soldevila¹⁶⁷,
 E. Solfaroli Camillocci^{132a,132b}, A.A. Solodkov¹²⁸, O.V. Solovyanov¹²⁸, V. Solovyev¹²¹, N. Soni¹,
 V. Sopko¹²⁷, B. Sopko¹²⁷, M. Sosebee⁸, R. Soualah^{164a,164c}, A. Soukharev¹⁰⁷, S. Spagnolo^{72a,72b},
 F. Spanò⁷⁶, W.R. Spearman⁵⁷, R. Spighi^{20a}, G. Spigo³⁰, R. Spiwoks³⁰, M. Spousta^{126,ah}, T. Spreitzer¹⁵⁸,
 B. Spurlock⁸, R.D. St. Denis⁵³, J. Stahlman¹²⁰, R. Stamen^{58a}, E. Stanecka³⁹, R.W. Stanek⁶,
 C. Stanescu^{134a}, M. Stanescu-Bellu⁴², M.M. Stanitzki⁴², S. Stapnes¹¹⁷, E.A. Starchenko¹²⁸, J. Stark⁵⁵,
 P. Staroba¹²⁵, P. Starovoitov⁴², R. Staszewski³⁹, A. Staude⁹⁸, P. Stavina^{144a,*}, G. Steele⁵³, P. Steinbach⁴⁴,
 P. Steinberg²⁵, I. Stekl¹²⁷, B. Stelzer¹⁴², H.J. Stelzer⁸⁸, O. Stelzer-Chilton^{159a}, H. Stenzel⁵², S. Stern⁹⁹,
 G.A. Stewart³⁰, J.A. Stillings²¹, M.C. Stockton⁸⁵, K. Stoerig⁴⁸, G. Stoicea^{26a}, S. Stonjek⁹⁹, P. Strachota¹²⁶,
 A.R. Stradling⁸, A. Straessner⁴⁴, J. Strandberg¹⁴⁷, S. Strandberg^{146a,146b}, A. Strandlie¹¹⁷, M. Strang¹⁰⁹,
 E. Strauss¹⁴³, M. Strauss¹¹¹, P. Strizenec^{144b}, R. Ströhmer¹⁷⁴, D.M. Strom¹¹⁴, J.A. Strong^{76,*},
 R. Stroynowski⁴⁰, B. Stugu¹⁴, I. Stumer^{25,*}, J. Stupak¹⁴⁸, P. Sturm¹⁷⁵, N.A. Styles⁴², D.A. Soh^{151,u},
 D. Su¹⁴³, H.S. Subramania³, R. Subramaniam²⁵, A. Succurro¹², Y. Sugaya¹¹⁶, C. Suhr¹⁰⁶, M. Suk¹²⁶,
 V.V. Sulin⁹⁴, S. Sultansoy^{4d}, T. Sumida⁶⁷, X. Sun⁵⁵, J.E. Sundermann⁴⁸, K. Suruliz¹³⁹, G. Susinno^{37a,37b},
 M.R. Sutton¹⁴⁹, Y. Suzuki⁶⁵, Y. Suzuki⁶⁶, M. Svatos¹²⁵, S. Swedish¹⁶⁸, I. Sykora^{144a}, T. Sykora¹²⁶,
 J. Sánchez¹⁶⁷, D. Ta¹⁰⁵, K. Tackmann⁴², A. Taffard¹⁶³, R. Tafirout^{159a}, N. Taiblum¹⁵³, Y. Takahashi¹⁰¹,
 H. Takai²⁵, R. Takashima⁶⁸, H. Takeda⁶⁶, T. Takeshita¹⁴⁰, Y. Takubo⁶⁵, M. Talby⁸³, A. Talyshev^{107,f},
 M.C. Tamsett²⁵, K.G. Tan⁸⁶, J. Tanaka¹⁵⁵, R. Tanaka¹¹⁵, S. Tanaka¹³¹, S. Tanaka⁶⁵, A.J. Tanasijczuk¹⁴²,

K. Tani⁶⁶, N. Tannoury⁸³, S. Tapprogge⁸¹, D. Tardif¹⁵⁸, S. Tarem¹⁵², F. Tarrade²⁹, G.F. Tartarelli^{89a},
 P. Tas¹²⁶, M. Tasevsky¹²⁵, E. Tassi^{37a,37b}, M. Tatarkhanov¹⁵, Y. Tayalati^{135d}, C. Taylor⁷⁷, F.E. Taylor⁹²,
 G.N. Taylor⁸⁶, W. Taylor^{159b}, M. Teinturier¹¹⁵, F.A. Teischinger³⁰, M. Teixeira Dias Castanheira⁷⁵,
 P. Teixeira-Dias⁷⁶, K.K. Temming⁴⁸, H. Ten Kate³⁰, P.K. Teng¹⁵¹, S. Terada⁶⁵, K. Terashi¹⁵⁵, J. Terron⁸⁰,
 M. Testa⁴⁷, R.J. Teuscher^{158,k}, J. Therhaag²¹, T. Theveneaux-Pelzer⁷⁸, S. Thoma⁴⁸, J.P. Thomas¹⁸,
 E.N. Thompson³⁵, P.D. Thompson¹⁸, P.D. Thompson¹⁵⁸, A.S. Thompson⁵³, L.A. Thomsen³⁶,
 E. Thomson¹²⁰, M. Thomson²⁸, W.M. Thong⁸⁶, R.P. Thun⁸⁷, F. Tian³⁵, M.J. Tibbetts¹⁵, T. Tic¹²⁵,
 V.O. Tikhomirov⁹⁴, Y.A. Tikhonov^{107,f}, S. Timoshenko⁹⁶, E. Tiouchichine⁸³, P. Tipton¹⁷⁶, S. Tisserant⁸³,
 T. Todorov⁵, S. Todorova-Nova¹⁶¹, B. Toggerson¹⁶³, J. Tojo⁶⁹, S. Tokár^{144a}, K. Tokushuku⁶⁵,
 K. Tollefson⁸⁸, M. Tomoto¹⁰¹, L. Tompkins³¹, K. Toms¹⁰³, A. Tonoyan¹⁴, C. Topfel¹⁷, N.D. Topilin⁶⁴,
 I. Torchiani³⁰, E. Torrence¹¹⁴, H. Torres⁷⁸, E. Torr  Pastor¹⁶⁷, J. Toth^{83.ad}, F. Touchard⁸³, D.R. Tovey¹³⁹,
 T. Trefzger¹⁷⁴, L. Tremblet³⁰, A. Tricoli³⁰, I.M. Trigger^{159a}, G. Trilling¹⁵, S. Trincaz-Duvoid⁷⁸,
 M.F. Tripiana⁷⁰, N. Triplett²⁵, W. Trischuk¹⁵⁸, B. Trocm ⁵⁵, C. Troncon^{89a}, M. Trotter-McDonald¹⁴²,
 M. Trzebinski³⁹, A. Trzupek³⁹, C. Tsarouchas³⁰, J.C.-L. Tseng¹¹⁸, M. Tsiakiris¹⁰⁵, P.V. Tsiareshka⁹⁰,
 D. Tsiou^{5.ai}, G. Tsipolitis¹⁰, S. Tsiskaridze¹², V. Tsiskaridze⁴⁸, E.G. Tskhadadze^{51a}, I.I. Tsukerman⁹⁵,
 V. Tsulaia¹⁵, J.-W. Tsung²¹, S. Tsuno⁶⁵, D. Tsybychev¹⁴⁸, A. Tua¹³⁹, A. Tudorache^{26a}, V. Tudorache^{26a},
 J.M. Tuggle³¹, M. Turala³⁹, D. Turecek¹²⁷, I. Turk Cakir^{4e}, E. Turlay¹⁰⁵, R. Turra^{89a,89b}, P.M. Tuts³⁵,
 A. Tykhonov⁷⁴, M. Tylmad^{146a,146b}, M. Tyndel¹²⁹, G. Tzanakos⁹, K. Uchida²¹, I. Ueda¹⁵⁵, R. Ueno²⁹,
 M. Uglan ¹⁴, M. Uhlenbrock²¹, M. Uhrmacher⁵⁴, F. Ukegawa¹⁶⁰, G. Unal³⁰, A. Undrus²⁵, G. Unel¹⁶³,
 Y. Unno⁶⁵, D. Urbaniec³⁵, P. Urquijo²¹, G. Usai⁸, M. Uslenghi^{119a,119b}, L. Vacavant⁸³, V. Vacek¹²⁷,
 B. Vachon⁸⁵, S. Vahsen¹⁵, J. Valenta¹²⁵, S. Valentinietti^{20a,20b}, A. Valero¹⁶⁷, S. Valkar¹²⁶,
 E. Valladolid Gallego¹⁶⁷, S. Vallecorsa¹⁵², J.A. Valls Ferrer¹⁶⁷, R. Van Berg¹²⁰, P.C. Van Der Deijl¹⁰⁵,
 R. van der Geer¹⁰⁵, H. van der Graaf¹⁰⁵, R. Van Der Leeuw¹⁰⁵, E. van der Poel¹⁰⁵, D. van der Ster³⁰,
 N. van Eldik³⁰, P. van Gemmeren⁶, I. van Vulpen¹⁰⁵, M. Vanadia⁹⁹, W. Vandelli³⁰, R. Vanguri¹²⁰,
 A. Vaniachine⁶, P. Vankov⁴², F. Vannucci⁷⁸, R. Vari^{132a}, T. Varol⁸⁴, D. Varouchas¹⁵, A. Vartapetian⁸,
 K.E. Varvell¹⁵⁰, V.I. Vassilakopoulos⁵⁶, F. Vazeille³⁴, T. Vazquez Schroeder⁵⁴, G. Vegni^{89a,89b},
 J.J. Veillet¹¹⁵, F. Veloso^{124a}, R. Veness³⁰, S. Veneziano^{132a}, A. Ventura^{72a,72b}, D. Ventura⁸⁴,
 M. Venturi⁴⁸, N. Venturi¹⁵⁸, V. Vercesi^{119a}, M. Verducci¹³⁸, W. Verkerke¹⁰⁵, J.C. Vermeulen¹⁰⁵,
 A. Vest⁴⁴, M.C. Vetterli^{142,d}, I. Vichou¹⁶⁵, T. Vickey^{145b,aj}, O.E. Vickey Boeriu^{145b}, G.H.A. Viehhauser¹¹⁸,
 S. Viel¹⁶⁸, M. Villa^{20a,20b}, M. Villaplana Perez¹⁶⁷, E. Vilucchi⁴⁷, M.G. Vincter²⁹, E. Vinek³⁰,
 V.B. Vinogradov⁶⁴, M. Virchaux^{136,*}, J. Virzi¹⁵, O. Vitells¹⁷², M. Viti⁴², I. Vivarelli⁴⁸, F. Vives Vaque³,
 S. Vlachos¹⁰, D. Vladoiu⁹⁸, M. Vlasak¹²⁷, A. Vogel²¹, P. Vokac¹²⁷, G. Volpi⁴⁷, M. Volpi⁸⁶, G. Volpini^{89a},
 H. von der Schmitt⁹⁹, H. von Radziewski⁴⁸, E. von Toerne²¹, V. Vorobel¹²⁶, V. Vorwerk¹², M. Vos¹⁶⁷,
 R. Voss³⁰, T.T. Voss¹⁷⁵, J.H. Vosseveld⁷³, N. Vranjes¹³⁶, M. Vranjes Milosavljevic¹⁰⁵, V. Vrba¹²⁵,
 M. Vreeswijk¹⁰⁵, T. Vu Anh⁴⁸, R. Vuillermet³⁰, I. Vukotic³¹, W. Wagner¹⁷⁵, P. Wagner¹²⁰, H. Wahlen¹⁷⁵,
 S. Wahrenmund⁴⁴, J. Wakabayashi¹⁰¹, S. Walch⁸⁷, J. Walder⁷¹, R. Walker⁹⁸, W. Walkowiak¹⁴¹, R. Wall¹⁷⁶,
 P. Waller⁷³, B. Walsh¹⁷⁶, C. Wang⁴⁵, F. Wang¹⁷³, H. Wang¹⁷³, H. Wang^{33b.ak}, J. Wang¹⁵¹, J. Wang⁵⁵,
 R. Wang¹⁰³, S.M. Wang¹⁵¹, T. Wang²¹, A. Warburton⁸⁵, C.P. Ward²⁸, D.R. Wardrope⁷⁷, M. Warsinsky⁴⁸,
 A. Washbrook⁴⁶, C. Wasicki⁴², I. Watanabe⁶⁶, P.M. Watkins¹⁸, A.T. Watson¹⁸, I.J. Watson¹⁵⁰,
 M.F. Watson¹⁸, G. Watts¹³⁸, S. Watts⁸², A.T. Waugh¹⁵⁰, B.M. Waugh⁷⁷, M.S. Weber¹⁷, P. Weber⁵⁴,
 J.S. Webster³¹, A.R. Weidberg¹¹⁸, P. Weigell⁹⁹, J. Weingarten⁵⁴, C. Weiser⁴⁸, P.S. Wells³⁰, T. Wenaus²⁵,
 D. Wendland¹⁶, Z. Weng^{151,u}, T. Wengler³⁰, S. Wenig³⁰, N. Wermes²¹, M. Werner⁴⁸, P. Werner³⁰,
 M. Werth¹⁶³, M. Wessels^{58a}, J. Wetter¹⁶¹, C. Weydert⁵⁵, K. Whalen²⁹, S.J. Wheeler-Ellis¹⁶³, A. White⁸,
 M.J. White⁸⁶, S. White^{122a,122b}, S.R. Whitehead¹¹⁸, D. Whiteson¹⁶³, D. Whittington⁶⁰, F. Wicek¹¹⁵,
 D. Wicke¹⁷⁵, F.J. Wickens¹²⁹, W. Wiedenmann¹⁷³, M. Wielers¹²⁹, P. Wienemann²¹, C. Wiglesworth⁷⁵,
 L.A.M. Wiik-Fuchs⁴⁸, P.A. Wijeratne⁷⁷, A. Wildauer⁹⁹, M.A. Wildt^{42,r}, I. Wilhelm¹²⁶, H.G. Wilkens³⁰,
 J.Z. Will⁹⁸, E. Williams³⁵, H.H. Williams¹²⁰, W. Willis³⁵, S. Willocq⁸⁴, J.A. Wilson¹⁸, M.G. Wilson¹⁴³,
 A. Wilson⁸⁷, I. Wingerter-Seez⁵, S. Winkelmann⁴⁸, F. Winklmeier³⁰, M. Wittgen¹⁴³, S.J. Wollstadt⁸¹,
 M.W. Wolter³⁹, H. Wolters^{124a,h}, W.C. Wong⁴¹, G. Wooden⁸⁷, B.K. Wosiek³⁹, J. Wotschack³⁰,
 M.J. Woudstra⁸², K.W. Wozniak³⁹, K. Wraight⁵³, M. Wright⁵³, B. Wrona⁷³, S.L. Wu¹⁷³, X. Wu⁴⁹,
 Y. Wu^{33b,al}, E. Wulf³⁵, B.M. Wynne⁴⁶, S. Xella³⁶, M. Xiao¹³⁶, S. Xie⁴⁸, C. Xu^{33b,z}, D. Xu¹³⁹,
 B. Yabsley¹⁵⁰, S. Yacoob^{145a,am}, M. Yamada⁶⁵, H. Yamaguchi¹⁵⁵, Y. Yamaguchi¹⁵⁵, A. Yamamoto⁶⁵,

K. Yamamoto⁶³, S. Yamamoto¹⁵⁵, T. Yamamura¹⁵⁵, T. Yamanaka¹⁵⁵, T. Yamazaki¹⁵⁵, Y. Yamazaki⁶⁶, Z. Yan²², H. Yang⁸⁷, H. Yang¹⁷³, U.K. Yang⁸², Y. Yang¹⁰⁹, Z. Yang^{146a,146b}, S. Yanush⁹¹, L. Yao^{33a}, Y. Yao¹⁵, Y. Yasu⁶⁵, G.V. Ybeles Smit¹³⁰, J. Ye⁴⁰, S. Ye²⁵, M. Yilmaz^{4c}, R. Yoosofmiya¹²³, K. Yorita¹⁷¹, R. Yoshida⁶, K. Yoshihara¹⁵⁵, C. Young¹⁴³, C.J. Young¹¹⁸, S. Youssef²², D. Yu²⁵, J. Yu⁸, J. Yu¹¹², L. Yuan⁶⁶, A. Yurkewicz¹⁰⁶, M. Byszewski³⁰, B. Zabinski³⁹, R. Zaidan⁶², A.M. Zaitsev¹²⁸, Z. Zajacova³⁰, L. Zanello^{132a,132b}, D. Zanzi⁹⁹, A. Zaytsev²⁵, C. Zeitnitz¹⁷⁵, M. Zeman¹²⁵, A. Zemla³⁹, C. Zender²¹, O. Zenin¹²⁸, T. Ženiš^{144a}, Z. Zinonos^{122a,122b}, D. Zerwas¹¹⁵, G. Zevi della Porta⁵⁷, D. Zhang^{33b,ak}, H. Zhang⁸⁸, J. Zhang⁶, X. Zhang^{33d}, Z. Zhang¹¹⁵, L. Zhao¹⁰⁸, Z. Zhao^{33b}, A. Zhemchugov⁶⁴, J. Zhong¹¹⁸, B. Zhou⁸⁷, N. Zhou¹⁶³, Y. Zhou¹⁵¹, C.G. Zhu^{33d}, H. Zhu⁴², J. Zhu⁸⁷, Y. Zhu^{33b}, X. Zhuang⁹⁸, V. Zhuravlov⁹⁹, D. Zieminska⁶⁰, N.I. Zimin⁶⁴, R. Zimmermann²¹, S. Zimmermann²¹, S. Zimmermann⁴⁸, M. Ziolkowski¹⁴¹, R. Zitoun⁵, L. Živković³⁵, V.V. Zmouchko^{128,*}, G. Zobernig¹⁷³, A. Zoccoli^{20a,20b}, M. zur Nedden¹⁶, V. Zutshi¹⁰⁶, L. Zwalinski³⁰

¹ School of Chemistry and Physics, University of Adelaide, Adelaide, Australia

² Physics Department, SUNY Albany, Albany, NY, United States

³ Department of Physics, University of Alberta, Edmonton, AB, Canada

⁴ ^(a) Department of Physics, Ankara University, Ankara; ^(b) Department of Physics, Dumlupinar University, Kutahya; ^(c) Department of Physics, Gazi University, Ankara; ^(d) Division of Physics, TOBB University of Economics and Technology, Ankara; ^(e) Turkish Atomic Energy Authority, Ankara, Turkey

⁵ LAPP, CNRS/IN2P3 and Université de Savoie, Annecy-le-Vieux, France

⁶ High Energy Physics Division, Argonne National Laboratory, Argonne, IL, United States

⁷ Department of Physics, University of Arizona, Tucson, AZ, United States

⁸ Department of Physics, The University of Texas at Arlington, Arlington, TX, United States

⁹ Physics Department, University of Athens, Athens, Greece

¹⁰ Physics Department, National Technical University of Athens, Zografou, Greece

¹¹ Institute of Physics, Azerbaijan Academy of Sciences, Baku, Azerbaijan

¹² Institut de Física d'Altes Energies and Departament de Física de la Universitat Autònoma de Barcelona and ICREA, Barcelona, Spain

¹³ ^(a) Institute of Physics, University of Belgrade, Belgrade; ^(b) Vinca Institute of Nuclear Sciences, University of Belgrade, Belgrade, Serbia

¹⁴ Department for Physics and Technology, University of Bergen, Bergen, Norway

¹⁵ Physics Division, Lawrence Berkeley National Laboratory and University of California, Berkeley, CA, United States

¹⁶ Department of Physics, Humboldt University, Berlin, Germany

¹⁷ Albert Einstein Center for Fundamental Physics and Laboratory for High Energy Physics, University of Bern, Bern, Switzerland

¹⁸ School of Physics and Astronomy, University of Birmingham, Birmingham, United Kingdom

¹⁹ ^(a) Department of Physics, Bogazici University, Istanbul; ^(b) Division of Physics, Dogus University, Istanbul; ^(c) Department of Physics Engineering, Gaziantep University, Gaziantep;

^(d) Department of Physics, Istanbul Technical University, Istanbul, Turkey

²⁰ ^(a) INFN Sezione di Bologna; ^(b) Dipartimento di Fisica, Università di Bologna, Bologna, Italy

²¹ Physikalisches Institut, University of Bonn, Bonn, Germany

²² Department of Physics, Boston University, Boston, MA, United States

²³ Department of Physics, Brandeis University, Waltham, MA, United States

²⁴ ^(a) Universidade Federal do Rio De Janeiro COPPE/EE/IF, Rio de Janeiro; ^(b) Federal University of Juiz de Fora (UFJF), Juiz de Fora; ^(c) Federal University of Sao Joao del Rei (UFSJ), Sao Joao del Rei; ^(d) Instituto de Física, Universidade de Sao Paulo, Sao Paulo, Brazil

²⁵ Physics Department, Brookhaven National Laboratory, Upton, NY, United States

²⁶ ^(a) National Institute of Physics and Nuclear Engineering, Bucharest; ^(b) University Politehnica Bucharest, Bucharest; ^(c) West University in Timisoara, Timisoara, Romania

²⁷ Departamento de Física, Universidad de Buenos Aires, Buenos Aires, Argentina

²⁸ Cavendish Laboratory, University of Cambridge, Cambridge, United Kingdom

²⁹ Department of Physics, Carleton University, Ottawa, ON, Canada

³⁰ CERN, Geneva, Switzerland

³¹ Enrico Fermi Institute, University of Chicago, Chicago, IL, United States

³² ^(a) Departamento de Física, Pontificia Universidad Católica de Chile, Santiago; ^(b) Departamento de Física, Universidad Técnica Federico Santa María, Valparaíso, Chile

³³ ^(a) Institute of High Energy Physics, Chinese Academy of Sciences, Beijing; ^(b) Department of Modern Physics, University of Science and Technology of China, Anhui; ^(c) Department of Physics, Nanjing University, Jiangsu; ^(d) School of Physics, Shandong University, Shandong, China

³⁴ Laboratoire de Physique Corpusculaire, Clermont Université and Université Blaise Pascal and CNRS/IN2P3, Clermont-Ferrand, France

³⁵ Nevis Laboratory, Columbia University, Irvington, NY, United States

³⁶ Niels Bohr Institute, University of Copenhagen, Copenhagen, Denmark

³⁷ ^(a) INFN Gruppo Collegato di Cosenza; ^(b) Dipartimento di Fisica, Università della Calabria, Arcavata di Rende, Italy

³⁸ AGH University of Science and Technology, Faculty of Physics and Applied Computer Science, Krakow, Poland

³⁹ The Henryk Niewodniczanski Institute of Nuclear Physics, Polish Academy of Sciences, Krakow, Poland

⁴⁰ Physics Department, Southern Methodist University, Dallas, TX, United States

⁴¹ Physics Department, University of Texas at Dallas, Richardson, TX, United States

⁴² DESY, Hamburg and Zeuthen, Germany

⁴³ Institut für Experimentelle Physik IV, Technische Universität Dortmund, Dortmund, Germany

⁴⁴ Institut für Kern- und Teilchenphysik, Technical University Dresden, Dresden, Germany

⁴⁵ Department of Physics, Duke University, Durham, NC, United States

⁴⁶ SUPA – School of Physics and Astronomy, University of Edinburgh, Edinburgh, United Kingdom

⁴⁷ INFN Laboratori Nazionali di Frascati, Frascati, Italy

⁴⁸ Fakultät für Mathematik und Physik, Albert-Ludwigs-Universität, Freiburg, Germany

⁴⁹ Section de Physique, Université de Genève, Geneva, Switzerland

⁵⁰ ^(a) INFN Sezione di Genova; ^(b) Dipartimento di Fisica, Università di Genova, Genova, Italy

⁵¹ ^(a) E. Andronikashvili Institute of Physics, Tbilisi State University, Tbilisi; ^(b) High Energy Physics Institute, Tbilisi State University, Tbilisi, Georgia

⁵² II Physikalisches Institut, Justus-Liebig-Universität Giessen, Giessen, Germany

⁵³ SUPA – School of Physics and Astronomy, University of Glasgow, Glasgow, United Kingdom

⁵⁴ II Physikalisches Institut, Georg-August-Universität, Göttingen, Germany

⁵⁵ Laboratoire de Physique Subatomique et de Cosmologie, Université Joseph Fourier and CNRS/IN2P3 and Institut National Polytechnique de Grenoble, Grenoble, France

⁵⁶ Department of Physics, Hampton University, Hampton, VA, United States

- 57 Laboratory for Particle Physics and Cosmology, Harvard University, Cambridge, MA, United States
- 58 ^(a) Kirchhoff-Institut für Physik, Ruprecht-Karls-Universität Heidelberg, Heidelberg; ^(b) Physikalisches Institut, Ruprecht-Karls-Universität Heidelberg, Heidelberg; ^(c) ZITI Institut für technische Informatik, Ruprecht-Karls-Universität Heidelberg, Mannheim, Germany
- 59 Faculty of Applied Information Science, Hiroshima Institute of Technology, Hiroshima, Japan
- 60 Department of Physics, Indiana University, Bloomington, IN, United States
- 61 Institut für Astro- und Teilchenphysik, Leopold-Franzens-Universität, Innsbruck, Austria
- 62 University of Iowa, Iowa City, IA, United States
- 63 Department of Physics and Astronomy, Iowa State University, Ames, IA, United States
- 64 Joint Institute for Nuclear Research, JINR Dubna, Dubna, Russia
- 65 KEK, High Energy Accelerator Research Organization, Tsukuba, Japan
- 66 Graduate School of Science, Kobe University, Kobe, Japan
- 67 Faculty of Science, Kyoto University, Kyoto, Japan
- 68 Kyoto University of Education, Kyoto, Japan
- 69 Department of Physics, Kyushu University, Fukuoka, Japan
- 70 Instituto de Física La Plata, Universidad Nacional de La Plata and CONICET, La Plata, Argentina
- 71 Physics Department, Lancaster University, Lancaster, United Kingdom
- 72 ^(a) INFN Sezione di Lecce; ^(b) Dipartimento di Matematica e Fisica, Università del Salento, Lecce, Italy
- 73 Oliver Lodge Laboratory, University of Liverpool, Liverpool, United Kingdom
- 74 Department of Physics, Jožef Stefan Institute and University of Ljubljana, Ljubljana, Slovenia
- 75 School of Physics and Astronomy, Queen Mary University of London, London, United Kingdom
- 76 Department of Physics, Royal Holloway University of London, Surrey, United Kingdom
- 77 Department of Physics and Astronomy, University College London, London, United Kingdom
- 78 Laboratoire de Physique Nucléaire et de Hautes Energies, UPMC and Université Paris-Diderot and CNRS/IN2P3, Paris, France
- 79 Fysiska institutionen, Lunds universitet, Lund, Sweden
- 80 Departamento de Física Teórica C-15, Universidad Autónoma de Madrid, Madrid, Spain
- 81 Institut für Physik, Universität Mainz, Mainz, Germany
- 82 School of Physics and Astronomy, University of Manchester, Manchester, United Kingdom
- 83 CPPM, Aix-Marseille Université and CNRS/IN2P3, Marseille, France
- 84 Department of Physics, University of Massachusetts, Amherst, MA, United States
- 85 Department of Physics, McGill University, Montreal, QC, Canada
- 86 School of Physics, University of Melbourne, Victoria, Australia
- 87 Department of Physics, The University of Michigan, Ann Arbor, MI, United States
- 88 Department of Physics and Astronomy, Michigan State University, East Lansing, MI, United States
- 89 ^(a) INFN Sezione di Milano; ^(b) Dipartimento di Fisica, Università di Milano, Milano, Italy
- 90 B.I. Stepanov Institute of Physics, National Academy of Sciences of Belarus, Minsk, Belarus
- 91 National Scientific and Educational Centre for Particle and High Energy Physics, Minsk, Belarus
- 92 Department of Physics, Massachusetts Institute of Technology, Cambridge, MA, United States
- 93 Group of Particle Physics, University of Montreal, Montreal, QC, Canada
- 94 P.N. Lebedev Institute of Physics, Academy of Sciences, Moscow, Russia
- 95 Institute for Theoretical and Experimental Physics (ITEP), Moscow, Russia
- 96 Moscow Engineering and Physics Institute (MEPhI), Moscow, Russia
- 97 Skobeltsyn Institute of Nuclear Physics, Lomonosov Moscow State University, Moscow, Russia
- 98 Fakultät für Physik, Ludwig-Maximilians-Universität München, München, Germany
- 99 Max-Planck-Institut für Physik (Werner-Heisenberg-Institut), München, Germany
- 100 Nagasaki Institute of Applied Science, Nagasaki, Japan
- 101 Graduate School of Science and Kobayashi-Maskawa Institute, Nagoya University, Nagoya, Japan
- 102 ^(a) INFN Sezione di Napoli; ^(b) Dipartimento di Scienze Fisiche, Università di Napoli, Napoli, Italy
- 103 Department of Physics and Astronomy, University of New Mexico, Albuquerque, NM, United States
- 104 Institute for Mathematics, Astrophysics and Particle Physics, Radboud University Nijmegen/Nikhef, Nijmegen, Netherlands
- 105 Nikhef National Institute for Subatomic Physics and University of Amsterdam, Amsterdam, Netherlands
- 106 Department of Physics, Northern Illinois University, DeKalb, IL, United States
- 107 Budker Institute of Nuclear Physics, SB RAS, Novosibirsk, Russia
- 108 Department of Physics, New York University, New York, NY, United States
- 109 Ohio State University, Columbus, OH, United States
- 110 Faculty of Science, Okayama University, Okayama, Japan
- 111 Homer L. Dodge Department of Physics and Astronomy, University of Oklahoma, Norman, OK, United States
- 112 Department of Physics, Oklahoma State University, Stillwater, OK, United States
- 113 Palacký University, RCPTM, Olomouc, Czech Republic
- 114 Center for High Energy Physics, University of Oregon, Eugene, OR, United States
- 115 LAL, Université Paris-Sud and CNRS/IN2P3, Orsay, France
- 116 Graduate School of Science, Osaka University, Osaka, Japan
- 117 Department of Physics, University of Oslo, Oslo, Norway
- 118 Department of Physics, Oxford University, Oxford, United Kingdom
- 119 ^(a) INFN Sezione di Pavia; ^(b) Dipartimento di Fisica, Università di Pavia, Pavia, Italy
- 120 Department of Physics, University of Pennsylvania, Philadelphia PA, United States
- 121 Petersburg Nuclear Physics Institute, Gatchina, Russia
- 122 ^(a) INFN Sezione di Pisa; ^(b) Dipartimento di Fisica E. Fermi, Università di Pisa, Pisa, Italy
- 123 Department of Physics and Astronomy, University of Pittsburgh, Pittsburgh, PA, United States
- 124 ^(a) Laboratório de Instrumentação e Física Experimental de Partículas – LIP, Lisboa, Portugal; ^(b) Departamento de Física Teórica y del Cosmos and CAFPE, Universidad de Granada, Granada, Spain
- 125 Institute of Physics, Academy of Sciences of the Czech Republic, Praha, Czech Republic
- 126 Faculty of Mathematics and Physics, Charles University in Prague, Praha, Czech Republic
- 127 Czech Technical University in Prague, Praha, Czech Republic
- 128 State Research Center Institute for High Energy Physics, Protvino, Russia
- 129 Particle Physics Department, Rutherford Appleton Laboratory, Didcot, United Kingdom
- 130 Physics Department, University of Regina, Regina, SK, Canada
- 131 Ritsumeikan University, Kusatsu, Shiga, Japan
- 132 ^(a) INFN Sezione di Roma I; ^(b) Dipartimento di Fisica, Università La Sapienza, Roma, Italy
- 133 ^(a) INFN Sezione di Roma Tor Vergata; ^(b) Dipartimento di Fisica, Università di Roma Tor Vergata, Roma, Italy

- ¹³⁴ ^(a) INFN Sezione di Roma Tre; ^(b) Dipartimento di Fisica, Università Roma Tre, Roma, Italy
- ¹³⁵ ^(a) Faculté des Sciences Ain Chock, Réseau Universitaire de Physique des Hautes Energies – Université Hassan II, Casablanca; ^(b) Centre National de l’Energie des Sciences Techniques Nucleaires, Rabat; ^(c) Faculté des Sciences Semlalia, Université Cadi Ayyad, LPHEA-Marrakech; ^(d) Faculté des Sciences, Université Mohamed Premier and LPTPM, Oujda; ^(e) Faculté des sciences, Université Mohammed V-Agdal, Rabat, Morocco
- ¹³⁶ DSM/IRFU (Institut de Recherches sur les Lois Fondamentales de l’Univers), CEA Saclay (Commissariat a l’Energie Atomique), Gif-sur-Yvette, France
- ¹³⁷ Santa Cruz Institute for Particle Physics, University of California Santa Cruz, Santa Cruz, CA, United States
- ¹³⁸ Department of Physics, University of Washington, Seattle, WA, United States
- ¹³⁹ Department of Physics and Astronomy, University of Sheffield, Sheffield, United Kingdom
- ¹⁴⁰ Department of Physics, Shinshu University, Nagano, Japan
- ¹⁴¹ Fachbereich Physik, Universität Siegen, Siegen, Germany
- ¹⁴² Department of Physics, Simon Fraser University, Burnaby, BC, Canada
- ¹⁴³ SLAC National Accelerator Laboratory, Stanford, CA, United States
- ¹⁴⁴ ^(a) Faculty of Mathematics, Physics & Informatics, Comenius University, Bratislava, Slovak Republic; ^(b) Department of Subnuclear Physics, Institute of Experimental Physics of the Slovak Academy of Sciences, Kosice, Slovak Republic
- ¹⁴⁵ ^(a) Department of Physics, University of Johannesburg, Johannesburg; ^(b) School of Physics, University of the Witwatersrand, Johannesburg, South Africa
- ¹⁴⁶ ^(a) Department of Physics, Stockholm University; ^(b) The Oskar Klein Centre, Stockholm, Sweden
- ¹⁴⁷ Physics Department, Royal Institute of Technology, Stockholm, Sweden
- ¹⁴⁸ Departments of Physics & Astronomy and Chemistry, Stony Brook University, Stony Brook, NY, United States
- ¹⁴⁹ Department of Physics and Astronomy, University of Sussex, Brighton, United Kingdom
- ¹⁵⁰ School of Physics, University of Sydney, Sydney, Australia
- ¹⁵¹ Institute of Physics, Academia Sinica, Taipei, Taiwan
- ¹⁵² Department of Physics, Technion: Israel Institute of Technology, Haifa, Israel
- ¹⁵³ Raymond and Beverly Sackler School of Physics and Astronomy, Tel Aviv University, Tel Aviv, Israel
- ¹⁵⁴ Department of Physics, Aristotle University of Thessaloniki, Thessaloniki, Greece
- ¹⁵⁵ International Center for Elementary Particle Physics and Department of Physics, The University of Tokyo, Tokyo, Japan
- ¹⁵⁶ Graduate School of Science and Technology, Tokyo Metropolitan University, Tokyo, Japan
- ¹⁵⁷ Department of Physics, Tokyo Institute of Technology, Tokyo, Japan
- ¹⁵⁸ Department of Physics, University of Toronto, Toronto, ON, Canada
- ¹⁵⁹ ^(a) TRIUMF, Vancouver, BC; ^(b) Department of Physics and Astronomy, York University, Toronto, ON, Canada
- ¹⁶⁰ Faculty of Pure and Applied Sciences, University of Tsukuba, Tsukuba, Japan
- ¹⁶¹ Department of Physics and Astronomy, Tufts University, Medford, MA, United States
- ¹⁶² Centro de Investigaciones, Universidad Antonio Narino, Bogota, Colombia
- ¹⁶³ Department of Physics and Astronomy, University of California Irvine, Irvine, CA, United States
- ¹⁶⁴ ^(a) INFN Gruppo Collegato di Udine; ^(b) ICTP, Trieste; ^(c) Dipartimento di Chimica, Fisica e Ambiente, Università di Udine, Udine, Italy
- ¹⁶⁵ Department of Physics, University of Illinois, Urbana, IL, United States
- ¹⁶⁶ Department of Physics and Astronomy, University of Uppsala, Uppsala, Sweden
- ¹⁶⁷ Instituto de Física Corpuscular (IFIC) and Departamento de Física Atómica, Molecular y Nuclear and Departamento de Ingeniería Electrónica and Instituto de Microelectrónica de Barcelona (IMB-CNM), University of Valencia and CSIC, Valencia, Spain
- ¹⁶⁸ Department of Physics, University of British Columbia, Vancouver, BC, Canada
- ¹⁶⁹ Department of Physics and Astronomy, University of Victoria, Victoria, BC, Canada
- ¹⁷⁰ Department of Physics, University of Warwick, Coventry, United Kingdom
- ¹⁷¹ Waseda University, Tokyo, Japan
- ¹⁷² Department of Particle Physics, The Weizmann Institute of Science, Rehovot, Israel
- ¹⁷³ Department of Physics, University of Wisconsin, Madison, WI, United States
- ¹⁷⁴ Fakultät für Physik und Astronomie, Julius-Maximilians-Universität, Würzburg, Germany
- ¹⁷⁵ Fachbereich C Physik, Bergische Universität Wuppertal, Wuppertal, Germany
- ¹⁷⁶ Department of Physics, Yale University, New Haven, CT, United States
- ¹⁷⁷ Yerevan Physics Institute, Yerevan, Armenia
- ¹⁷⁸ Centre de Calcul de l’Institut National de Physique Nucléaire et de Physique des Particules (IN2P3), Villeurbanne, France

^a Also at Laboratório de Instrumentação e Física Experimental de Partículas – LIP, Lisboa, Portugal.

^b Also at Faculdade de Ciências and CFNUL, Universidade de Lisboa, Lisboa, Portugal.

^c Also at Particle Physics Department, Rutherford Appleton Laboratory, Didcot, United Kingdom.

^d Also at TRIUMF, Vancouver, BC, Canada.

^e Also at Department of Physics, California State University, Fresno, CA, United States.

^f Also at Novosibirsk State University, Novosibirsk, Russia.

^g Also at Fermilab, Batavia, IL, United States.

^h Also at Department of Physics, University of Coimbra, Coimbra, Portugal.

ⁱ Also at Department of Physics, UASLP, San Luis Potosi, Mexico.

^j Also at Università di Napoli Parthenope, Napoli, Italy.

^k Also at Institute of Particle Physics (IPP), Canada.

^l Also at Department of Physics, Middle East Technical University, Ankara, Turkey.

^m Also at Louisiana Tech University, Ruston, LA, United States.

ⁿ Also at Dep Física and CEFITEC of Faculdade de Ciências e Tecnologia, Universidade Nova de Lisboa, Caparica, Portugal.

^o Also at Department of Physics and Astronomy, University College London, London, United Kingdom.

^p Also at Department of Physics, University of Cape Town, Cape Town, South Africa.

^q Also at Institute of Physics, Azerbaijan Academy of Sciences, Baku, Azerbaijan.

^r Also at Institut für Experimentalphysik, Universität Hamburg, Hamburg, Germany.

^s Also at Manhattan College, New York, NY, United States.

^t Also at CPPM, Aix-Marseille Université and CNRS/IN2P3, Marseille, France.

^u Also at School of Physics and Engineering, Sun Yat-sen University, Guanzhou, China.

^v Also at Academia Sinica Grid Computing, Institute of Physics, Academia Sinica, Taipei, Taiwan.

^w Also at Laboratoire de Physique Nucléaire et de Hautes Energies, UPMC and Université Paris-Diderot and CNRS/IN2P3, Paris, France.

^x Also at School of Physics, Shandong University, Shandong, China.

^y Also at Dipartimento di Fisica, Università La Sapienza, Roma, Italy.

^z Also at DSM/IRFU (Institut de Recherches sur les Lois Fondamentales de l’Univers), CEA Saclay (Commissariat a l’Energie Atomique), Gif-sur-Yvette, France.

^{aa} Also at Section de Physique, Université de Genève, Geneva, Switzerland.

- ^{ab} Also at Departamento de Fisica, Universidade de Minho, Braga, Portugal.
- ^{ac} Also at Department of Physics and Astronomy, University of South Carolina, Columbia, SC, United States.
- ^{ad} Also at Institute for Particle and Nuclear Physics, Wigner Research Centre for Physics, Budapest, Hungary.
- ^{ae} Also at California Institute of Technology, Pasadena, CA, United States.
- ^{af} Also at Institute of Physics, Jagiellonian University, Krakow, Poland.
- ^{ag} Also at LAL, Université Paris-Sud and CNRS/IN2P3, Orsay, France.
- ^{ah} Also at Nevis Laboratory, Columbia University, Irvington, NY, United States.
- ^{ai} Also at Department of Physics and Astronomy, University of Sheffield, Sheffield, United Kingdom.
- ^{aj} Also at Department of Physics, Oxford University, Oxford, United Kingdom.
- ^{ak} Also at Institute of Physics, Academia Sinica, Taipei, Taiwan.
- ^{al} Also at Department of Physics, The University of Michigan, Ann Arbor, MI, United States.
- ^{am} Also at Discipline of Physics, University of KwaZulu-Natal, Durban, South Africa.
- * Deceased.



Observation of a new boson at a mass of 125 GeV with the CMS experiment at the LHC [☆]

CMS Collaboration ^{*}

CERN, Switzerland

This paper is dedicated to the memory of our colleagues who worked on CMS but have since passed away. In recognition of their many contributions to the achievement of this observation.

ARTICLE INFO

Article history:

Received 31 July 2012

Received in revised form 9 August 2012

Accepted 11 August 2012

Available online 18 August 2012

Editor: W.-D. Schlatter

Keywords:

CMS

Physics

Higgs

ABSTRACT

Results are presented from searches for the standard model Higgs boson in proton–proton collisions at $\sqrt{s} = 7$ and 8 TeV in the Compact Muon Solenoid experiment at the LHC, using data samples corresponding to integrated luminosities of up to 5.1 fb^{-1} at 7 TeV and 5.3 fb^{-1} at 8 TeV. The search is performed in five decay modes: $\gamma\gamma$, ZZ, W^+W^- , $\tau^+\tau^-$, and $b\bar{b}$. An excess of events is observed above the expected background, with a local significance of 5.0 standard deviations, at a mass near 125 GeV, signalling the production of a new particle. The expected significance for a standard model Higgs boson of that mass is 5.8 standard deviations. The excess is most significant in the two decay modes with the best mass resolution, $\gamma\gamma$ and ZZ; a fit to these signals gives a mass of $125.3 \pm 0.4(\text{stat.}) \pm 0.5(\text{syst.}) \text{ GeV}$. The decay to two photons indicates that the new particle is a boson with spin different from one.

© 2012 CERN. Published by Elsevier B.V. All rights reserved.

1. Introduction

The standard model (SM) of elementary particles provides a remarkably accurate description of results from many accelerator and non-accelerator based experiments. The SM comprises quarks and leptons as the building blocks of matter, and describes their interactions through the exchange of force carriers: the photon for electromagnetic interactions, the W and Z bosons for weak interactions, and the gluons for strong interactions. The electromagnetic and weak interactions are unified in the electroweak theory. Although the predictions of the SM have been extensively confirmed, the question of how the W and Z gauge bosons acquire mass whilst the photon remains massless is still open.

Nearly fifty years ago it was proposed [1–6] that spontaneous symmetry breaking in gauge theories could be achieved through the introduction of a scalar field. Applying this mechanism to the electroweak theory [7–9] through a complex scalar doublet field leads to the generation of the W and Z masses, and to the prediction of the existence of the SM Higgs boson (H). The scalar field also gives mass to the fundamental fermions through the Yukawa interaction. The mass m_H of the SM Higgs boson is not predicted by theory. However, general considerations [10–13] suggest that

m_H should be smaller than $\sim 1 \text{ TeV}$, while precision electroweak measurements imply that $m_H < 152 \text{ GeV}$ at 95% confidence level (CL) [14]. Over the past twenty years, direct searches for the Higgs boson have been carried out at the LEP collider, leading to a lower bound of $m_H > 114.4 \text{ GeV}$ at 95% CL [15], and at the Tevatron proton–antiproton collider, excluding the mass range 162–166 GeV at 95% CL [16] and detecting an excess of events, recently reported in [17–19], in the range 120–135 GeV.

The discovery or exclusion of the SM Higgs boson is one of the primary scientific goals of the Large Hadron Collider (LHC) [20]. Previous direct searches at the LHC were based on data from proton–proton collisions corresponding to an integrated luminosity of 5 fb^{-1} collected at a centre-of-mass energy $\sqrt{s} = 7 \text{ TeV}$. The CMS experiment excluded at 95% CL a range of masses from 127 to 600 GeV [21]. The ATLAS experiment excluded at 95% CL the ranges 111.4–116.6, 119.4–122.1 and 129.2–541 GeV [22]. Within the remaining allowed mass region, an excess of events near 125 GeV was reported by both experiments. In 2012 the proton–proton centre-of-mass energy was increased to 8 TeV and by the end of June an additional integrated luminosity of more than 5 fb^{-1} had been recorded by each of these experiments, thereby enhancing significantly the sensitivity of the search for the Higgs boson.

This Letter reports the results of a search for the SM Higgs boson using samples collected by the CMS experiment, comprising data recorded at $\sqrt{s} = 7$ and 8 TeV. The search is performed in

[☆] © CERN for the benefit of the CMS Collaboration.

^{*} E-mail address: cms-publication-committee-chair@cern.ch.

five decay modes, $H \rightarrow \gamma\gamma$, ZZ , W^+W^- , $\tau^+\tau^-$, and $b\bar{b}$, in the low-mass range from 110 up to 160 GeV. In this mass range the Higgs boson production cross section is predicted to have values between 23 (29) and 10 (14) pb at $\sqrt{s} = 7$ (8) TeV [23]. The natural width of the SM Higgs boson over the same range is less than 100 MeV and the width of any observed peak would be entirely dominated by instrumental mass resolution. In what follows, ℓ stands for electrons or muons, $H \rightarrow W^+W^-$ is denoted as $H \rightarrow WW$, $H \rightarrow \tau^+\tau^-$ as $H \rightarrow \tau\tau$, and $H \rightarrow b\bar{b}$ as $H \rightarrow bb$. For the final states ZZ and WW in the low-mass region, one or more of the Z or W bosons is off mass shell.

With respect to the published analyses [24–28], most analyses have been re-optimized, incorporating improvements in reconstruction performance and event selection, and mitigating the more challenging conditions due to the higher LHC intensities in 2012. The new analyses presented herein, of 8 TeV samples, and of 7 TeV samples featuring modified event selection criteria, were performed in a “blind” way: the algorithms and selection procedures were formally approved and fixed before the results from data in the signal region were examined. In the previously published analyses similar but less formal procedures were followed.

Within the context of this search for the SM Higgs boson, we report the observation of an excess of events above the expected background, consistent with the production of a new particle with mass near 125 GeV. The observed local significance is 5.0 standard deviations (σ), compared with an expected significance of 5.8σ . The evidence is strongest in the two final states with the best mass resolution, namely $H \rightarrow \gamma\gamma$ with a significance of 4.1σ and $H \rightarrow ZZ$ (with the Z bosons decaying to electrons or muons) with a significance of 3.2σ . The decay to two photons indicates that the new particle is a boson with spin different from one.

2. The CMS experiment

The possibility of detection of the SM Higgs boson played a crucial role in the conceptual design of the CMS experiment as a benchmark to test the performance of the detector [29–31]. Since the SM Higgs boson mass is not predicted by theory and its production cross section and natural width vary widely over the allowed mass range, a search was envisaged over a large range of masses and in diverse decay modes: pairs of photons, Z bosons, W bosons, τ leptons, and b quarks. Planning in view of the analysis of all these channels ensured a detector capable of observing a Higgs boson over a broad mass range and able to detect most potential signals of new physics.

The central feature of the CMS apparatus [32] is a superconducting solenoid of 6 m internal diameter, which provides a magnetic field of 3.8 T. Within the field volume are a silicon pixel and strip tracker, a lead tungstate crystal electromagnetic calorimeter (ECAL), and a brass/scintillator hadron calorimeter (HCAL). Muons are measured in gas-ionization detectors embedded in the steel flux-return yoke. Extensive forward calorimeters complement the coverage provided by the barrel and endcap detectors.

Charged particles are tracked within the pseudorapidity range $|\eta| < 2.5$, where $\eta = -\ln[\tan(\theta/2)]$, and θ is the polar angle measured from the positive z axis (along the anticlockwise beam direction). The silicon pixel tracker comprises 66 million $100 \times 150 \mu\text{m}^2$ pixels, arranged in three barrel layers and two disks at each end. The silicon strip tracker, organized in ten barrel layers and twelve disks at each end, comprises 9.3 million strips with pitch between 80 and $180 \mu\text{m}$, with a total silicon surface area of 198 m^2 . The tracker has a track-finding efficiency larger than 99% for muons with transverse momentum p_T greater than 1 GeV and a transverse momentum resolution between 1.5 and 2.5% for charged

tracks of $p_T \sim 100$ GeV in the central region ($|\eta| < 1.5$). Measurements of the impact parameters of charged tracks and secondary vertices are used to identify jets that are likely to contain the hadronisation and decay products of b quarks (“ b jets”). A b -jet tagging efficiency of more than 50% is achieved with a rejection factor for light-quark jets of ~ 200 , as measured in $t\bar{t}$ events in data [33]. The dimuon mass resolution at the Υ mass, dominated by instrumental effects, is measured to be 0.6% in the barrel region [34], consistent with the design goal.

The ECAL is a fine-grained hermetic calorimeter consisting of 75848 lead tungstate crystals, arranged in a quasi-projective geometry and distributed in a barrel region ($|\eta| < 1.48$) and two endcaps that extend up to $|\eta| = 3.0$. The front-face cross section of the crystals is $22 \times 22 \text{ mm}^2$ in the barrel region and $28.6 \times 28.6 \text{ mm}^2$ in the endcaps. Preshower detectors consisting of two planes of silicon sensors interleaved with a total of three radiation lengths of lead absorber are located in front of the endcaps. Electromagnetic showers are very narrow in lead tungstate (Molière radius of 21 mm), helping in particle identification and in the implementation of isolation criteria. In the central barrel region the energy resolution of electrons that do not radiate substantially in the tracker material indicates that the resolution of unconverted photons is consistent with design goals. For such photons the diphoton mass resolution is 1.1 GeV at a mass of 125 GeV.

The HCAL barrel and endcaps are sampling calorimeters consisting of brass and scintillator plates, covering $|\eta| < 3.0$. Their thickness varies from 7 to 11 interaction lengths, depending on η ; a scintillator “tail catcher” placed outside the coil of the solenoid, just in front of the innermost muon detector, extends the instrumented thickness to more than 10 interaction lengths everywhere. Iron forward calorimeters with quartz fibers, read out by photomultipliers, extend the calorimeter coverage up to $|\eta| = 5.0$.

Muons are measured in the range $|\eta| < 2.4$, with detection planes based on three technologies: drift tubes ($|\eta| < 1.2$), cathode strip chambers ($0.9 < |\eta| < 2.4$), and resistive plate chambers ($|\eta| < 1.6$). The first two technologies provide a precise position measurement and trigger whilst the third provides precise timing information as well as a second and independent trigger. The muon system consists of four stations in the barrel and endcaps, designed to ensure robust triggering and detection of muons over a large angular range. In the barrel region each muon station consists of twelve drift-tube layers, except for the outermost station, which has eight layers. In the endcaps, each muon station consists of six detection planes. The precision of the r - ϕ measurement is $100 \mu\text{m}$ in the drift tubes and varies from 60 to $140 \mu\text{m}$ in the cathode strip chambers.

The CMS trigger and data acquisition systems ensure that potentially interesting events are recorded with high efficiency. The first level (L1) trigger, comprising the calorimeter, muon, and global trigger processors, uses coarse-granularity information to select the most interesting events in less than $4 \mu\text{s}$. The detector data are pipelined to ensure negligible deadtime up to a L1 rate of 100 kHz. After L1 triggering, data are transferred from the readout electronics of all subdetectors, through the readout network, to the high-level-trigger processor farm, which operates offline-quality reconstruction algorithms to decrease the event rate to around 0.5 kHz, before data storage.

The CMS experiment employs a highly distributed computing infrastructure, with a primary Tier-0 centre at CERN, supplemented by seven Tier-1, more than 50 Tier-2, and many Tier-3 centres at national laboratories and universities throughout the world. The CMS software running on this high-performance computing system executes numerous tasks, including the reconstruction and analysis of the collected data, as well as the generation and detailed detector simulation of Monte Carlo (MC) event samples.

3. Event reconstruction

The CMS “particle-flow” event description algorithm [35,36] is used to reconstruct and identify each single particle with an optimized combination of all subdetector information. In this process, the identification of the particle (photon, electron, muon, charged hadron, neutral hadron) plays an important role in the determination of the particle momentum. The reconstructed particles are henceforth referred to as objects.

Jets are reconstructed by clustering the particle-flow objects with the anti- k_T algorithm [37] using a distance parameter of 0.5. Additional selection criteria are applied to each event to remove spurious features originating from isolated noise patterns in certain HCAL regions, and from anomalous signals caused by particles depositing energy in the silicon avalanche photodiodes used in the ECAL barrel region. The average number of pp interactions per LHC bunch crossing is estimated to be about 9 and 19 in the 7 TeV (2011) and 8 TeV (2012) data sets, respectively. Energy from overlapping pp interactions (“pileup”), and from the underlying event, is subtracted using the FASTJET technique [38–40], which is based on the calculation of the η -dependent transverse momentum density, evaluated on an event-by-event basis.

The jet momentum is determined as the vector sum of all particle momenta in the jet. Jet energy corrections are derived from simulation studies and from in situ measurements using the energy balance of dijet and Z/γ + jet events [41]. These corrections are between 5% and 10% of the true momentum over the entire p_T spectrum and detector acceptance. The jet momentum resolution achieved is $\sigma(p_T)/p_T = 85\%/\sqrt{p_T/\text{GeV}} \oplus 4\%$ for central jets. A selection is applied to separate jets originating in the primary interaction from those due to energy deposits associated with pileup. The discrimination is based on the differences in the jet shapes, in the relative multiplicity of charged and neutral components, and in the fraction of transverse momentum carried by the hardest components. Within the tracker acceptance the jet tracks are also required to be consistent with originating at the primary vertex.

The missing transverse energy vector is taken as the negative vector sum of all particle transverse momenta, and its magnitude is referred to as E_T^{miss} . The typical missing transverse energy resolution is around $0.5\sqrt{\sum E_T}$ GeV [42], where $\sum E_T$ is the scalar sum of all particle transverse momenta in GeV.

The energy deposited in the ECAL is clustered both with general clustering algorithms [43] and with algorithms that constrain the clusters in η and ϕ to the shapes expected from electrons and photons with high p_T [44]. These specialised algorithms are used to cluster electromagnetic showers without any hypothesis regarding whether the particle originating from the interaction point was a photon or an electron; doing this for electrons from $Z \rightarrow ee$ events provides a measurement of the photon trigger, reconstruction, and identification efficiencies, as well as of the photon energy scale and resolution. The width of the reconstructed Z resonance is used to quantify the performance of the ECAL, using decays to two electrons whose energies are measured using the ECAL alone, with only their directions being determined from the tracks. In the 7 TeV data set, the dielectron mass resolution at the Z boson mass is 1.56 GeV in the barrel and 2.57 GeV in the endcaps, while in the 8 TeV sample, reconstructed with preliminary calibration constants, the corresponding values are 1.61 and 3.75 GeV. For electrons, the reconstruction combines the clusters in the ECAL and the trajectory in the silicon tracker [45]. Trajectories in the tracker volume are reconstructed using a model of electron energy loss and fitted with a Gaussian sum filter [46]. The electron momentum is determined from the combination of ECAL and tracker measurements.

Table 1

Summary of the subchannels, or categories, used in the analysis of each decay mode.

Decay mode	Production tagging	No. of subchannels	m_H range (GeV)	Int. Lum. (fb^{-1})	
				7 TeV	8 TeV
$\gamma\gamma$	untagged	4	110–150	5.1	5.3
	dijet (VBF)	1 or 2			
ZZ	untagged	3	110–160	5.1	5.3
	WW	4			
$\tau\tau$	untagged	16	110–145	4.9	5.1
	dijet (VBF)	4			
bb	lepton, E_T^{miss} (VH)	10	110–135	5.0	5.1

Muon candidates are reconstructed with two algorithms, one in which the tracks in the silicon detector are matched to segments in the muon chambers, and another in which a combined fit is performed to the signals found in both the silicon tracker and muon systems [43]. The efficiency to reconstruct a muon of $p_T > 5$ GeV is larger than 95%, while the probability to misidentify a hadron as a muon is below 0.1%. For $p_T > 200$ GeV the precision of the momentum measurement improves when the silicon tracker signals are complemented with the information from the muon chambers.

Selection based on isolation of lepton and photon objects is used extensively. A requirement is placed on the scalar sum of the transverse momenta of the particles reconstructed within a distance ΔR_{max} of the object, sometimes normalised to the p_T of the object. The distance ΔR is defined as $\Delta R = \sqrt{(\Delta\eta)^2 + (\Delta\phi)^2}$, where $\Delta\eta$ and $\Delta\phi$ are the pseudorapidity and azimuthal angle differences between the particle direction and the object direction. Typically ΔR_{max} is chosen to be 0.3 or 0.4.

The measurement of the integrated luminosity in CMS is based on a pixel cluster counting method, which exploits the large number of silicon pixels, and hence their low occupancy in a pp collision [47]. The cross section normalisation is derived from van der Meer scans [48]. The uncertainties in the luminosity measurements are 2.2% and 4.4% for the 7 TeV and 8 TeV data sets, respectively.

4. Searches for the standard model Higgs boson

Initial phenomenological discussions of Higgs boson production and decay can be found in Refs. [49–56]. Four main mechanisms are predicted for Higgs boson production in pp collisions: the gluon–gluon fusion mechanism, which has the largest cross section, followed in turn by vector-boson fusion (VBF), associated WH and ZH production (VH), and production in association with top quarks ($t\bar{t}H$). The cross sections for the individual production mechanisms and the decay branching fractions, together with their uncertainties, have been computed following Refs. [57–101] and are compiled in Refs. [23,102].

The particular set of sensitive decay modes of the SM Higgs boson depends strongly on m_H . The results presented in this Letter are based on the five most sensitive decay modes in the low-mass region: $H \rightarrow \gamma\gamma$; $H \rightarrow ZZ$ followed by ZZ decays to 4ℓ ; $H \rightarrow WW$ followed by decays to $2\ell 2\nu$; $H \rightarrow \tau\tau$ followed by at least one leptonic τ decay; and $H \rightarrow b\bar{b}$ followed by b-quark fragmentation into jets. This list is presented in Table 1 and comprises the full set of decay modes and subchannels, or categories, for which both the 7 and 8 TeV data sets have been analysed. Other lower sensitivity subchannels ($t\bar{t}H$, $H \rightarrow b\bar{b}$; W/ZH, $H \rightarrow \tau\tau$; W/ZH, $H \rightarrow WW \rightarrow 2\ell 2\nu$; $H \rightarrow ZZ \rightarrow 2\ell 2q$) have also been studied, so far only in the 7 TeV data, and are not included here. Adding these analyses in the combination results in an improvement of 0.1σ in the overall expected local significance at $m_H = 125$ GeV.

For a given value of m_H , the search sensitivity depends on the production cross section, the decay branching fraction into the chosen final state, the signal selection efficiency, the mass resolution, and the level of background from identical or similar final-state topologies.

Samples of MC events used to represent signal and background are fully simulated using `GEANT4` [103]. The simulations include pileup interactions matching the distribution of the number of such interactions observed in data. The description of the Higgs boson signal is obtained from MC simulation using, for most of the decay modes and production processes, the next-to-leading-order (NLO) matrix-element generator `POWHEG` [104,105], interfaced with `PYTHIA 6.4` [106]. For the dominant gluon–gluon fusion process, the transverse momentum spectrum of the Higgs boson in the 7 TeV MC samples is reweighted to the next-to-next-to-leading-logarithmic (NNLL) + NLO distribution computed with `HqT` [71,72,107] and `FEHiPro` [108,109], except in the $H \rightarrow ZZ$ analysis, where the effect is marginal. The agreement of the p_T spectrum in the simulation at 8 TeV with the NNLL + NLO distribution makes reweighting unnecessary. The improved agreement is due to a modification in the `POWHEG` setup recommended in Ref. [102]. The simulation of associated-production signal samples uses `PYTHIA` and all signal samples for $H \rightarrow bb$ are made using `POWHEG` interfaced to `HERWIG++` [110]. Samples used for background studies are generated with `PYTHIA`, `POWHEG`, and `MADGRAPH` [111], and the normalisations are obtained from the best available NNLO or NLO calculations. The uncertainty in the signal cross section related to the choice of parton distribution functions is determined with the `PDF4LHC` prescription [96–100].

The overall statistical methodology [112] used in this Letter was developed by the CMS and ATLAS Collaborations in the context of the LHC Higgs Combination Group. A more concise summary of CMS usage in the search for a Higgs boson is given in Ref. [21]. The modified frequentist criterion CL_s [113,114] is used for the calculation of exclusion limits. Systematic uncertainties are incorporated as nuisance parameters and are treated according to the frequentist paradigm. The combination of searches requires simultaneous analysis of the data selected by all individual analyses, accounting for all statistical and systematic uncertainties and their correlations. The probability for a background fluctuation to be at least as large as the observed maximum excess is termed the local p -value, and that for an excess *anywhere* in a specified mass range the global p -value. This probability can be evaluated by generating sets of simulated data incorporating all correlations between analyses optimized for different Higgs boson masses. The global p -value (for the specified region) is greater than the local p -value, and this fact is often referred to as the look-elsewhere effect (LEE) [115]. Both the local and global p -values can be expressed as a corresponding number of standard deviations using the one-sided Gaussian tail convention. The magnitude of a possible Higgs boson signal is characterised by the production cross section times the relevant branching fractions, relative to the SM expectation, denoted σ/σ_{SM} and referred to as the signal strength. The results presented in this Letter are obtained using asymptotic formulae [116], including updates recently introduced in the `ROOTSTATS` package [117].

Fig. 1 shows the expected local p -values in the mass range 110–145 GeV for the five decay modes reported here. The expected significance of a SM Higgs boson signal at $m_H = 125$ GeV when the five decay modes are combined is 5.6σ . The highest sensitivity in this mass range is achieved in the ZZ , $\gamma\gamma$, and WW channels. Because of the excellent mass resolution (1–2 GeV) achieved in the $\gamma\gamma$ and ZZ channels, they play a special role in the low-mass region, where the natural width of the SM Higgs boson is predicted to be less than 100 MeV. The expected signature in these channels

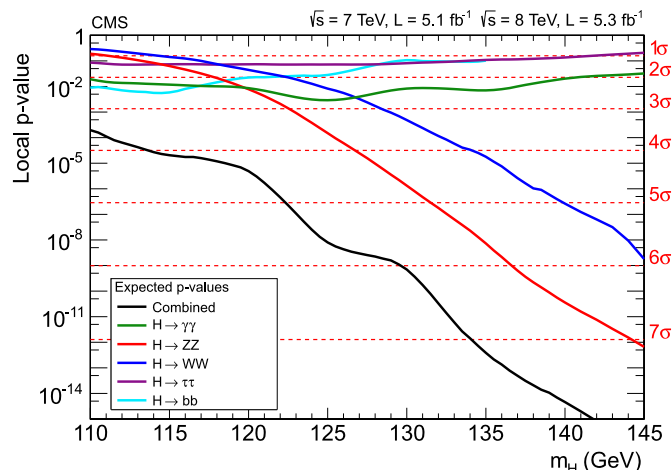


Fig. 1. Expected local p -values for a SM Higgs boson as a function of m_H , for the decay modes $\gamma\gamma$, ZZ , WW , $\tau\tau$, and bb and their combination.

is therefore a narrow resonance above background, with a width consistent with the detector resolution.

5. Decay modes with high mass resolution

5.1. $H \rightarrow \gamma\gamma$

In the $H \rightarrow \gamma\gamma$ analysis a search is made for a narrow peak in the diphoton invariant mass distribution in the range 110–150 GeV, on a large irreducible background from QCD production of two photons. There is also a reducible background where one or more of the reconstructed photon candidates originate from misidentification of jet fragments. Early detailed studies indicated this to be one of the most promising channels in the search for a SM Higgs boson in the low-mass range [118].

To enhance the sensitivity of the analysis, candidate diphoton events are separated into mutually exclusive categories of different expected signal-to-background ratios, based on the properties of the reconstructed photons and on the presence of two jets satisfying criteria aimed at selecting events in which a Higgs boson is produced through the VBF process. The analysis uses multivariate techniques for the selection and classification of the events. As an independent cross-check, an analysis is also performed that is almost identical to the one described in Ref. [24], using simpler criteria based on the properties of the reconstructed photons to select and classify events. The multivariate analysis achieves 15% higher sensitivity than the cross-check analysis.

The reconstructed primary vertex that most probably corresponds to the interaction vertex of the diphoton candidate is identified using the kinematic properties of the tracks associated with that vertex and their correlation with the diphoton kinematics. In addition, if either of the photons converts and the tracks from the conversion are reconstructed and identified, the direction of the converted photon contributes to the identification of the hard-scattering vertex. More details can be found in Ref. [24].

The event selection requires two photon candidates satisfying p_T requirements and “loose” photon identification criteria. These photons must be reconstructed within the fiducial region, $|\eta| < 2.5$, excluding the barrel–endcap transition region, $1.44 < |\eta| < 1.57$. A p_T threshold of $m_{\gamma\gamma}/3$ ($m_{\gamma\gamma}/4$) is applied to the photon leading (subleading) in p_T , where $m_{\gamma\gamma}$ is the diphoton invariant mass. Scaling the p_T thresholds in this way avoids distortion of the shape of the $m_{\gamma\gamma}$ distribution. In the case of events passing the dijet selection, the requirement on the leading photon

Table 2
Expected numbers of SM Higgs boson events ($m_H = 125$ GeV) and estimated background (at $m_{\gamma\gamma} = 125$ GeV) for all event categories of the 7 and 8 TeV data sets. There are two dijet-tagged categories for the 8 TeV data as described in the text, and for both data sets the remaining untagged events are separated into four categories labelled here BDT 0–3, BDT 0 having the largest expected signal-to-background ratio. The composition of the SM Higgs boson signal in terms of the production processes, and its mass resolution, are also given.

Event categories		SM Higgs boson expected signal ($m_H = 125$ GeV)						Background $m_{\gamma\gamma} = 125$ GeV (events/GeV)	
		Events	ggH	VBF	VH	ttH	σ_{eff} (GeV)		FWHM/2.35 (GeV)
7 TeV, 5.1 fb ⁻¹	BDT 0	3.2	61%	17%	19%	3%	1.21	1.14	3.3 ± 0.4
	BDT 1	16.3	88%	6%	6%	–	1.26	1.08	37.5 ± 1.3
	BDT 2	21.5	92%	4%	4%	–	1.59	1.32	74.8 ± 1.9
	BDT 3	32.8	92%	4%	4%	–	2.47	2.07	193.6 ± 3.0
	Dijet tag	2.9	27%	72%	1%	–	1.73	1.37	1.7 ± 0.2
8 TeV, 5.3 fb ⁻¹	BDT 0	6.1	68%	12%	16%	4%	1.38	1.23	7.4 ± 0.6
	BDT 1	21.0	87%	6%	6%	1%	1.53	1.31	54.7 ± 1.5
	BDT 2	30.2	92%	4%	4%	–	1.94	1.55	115.2 ± 2.3
	BDT 3	40.0	92%	4%	4%	–	2.86	2.35	256.5 ± 3.4
	Dijet tight	2.6	23%	77%	–	–	2.06	1.57	1.3 ± 0.2
	Dijet loose	3.0	53%	45%	2%	–	1.95	1.48	3.7 ± 0.4

is increased to $m_{\gamma\gamma}/2$, further reducing background with negligible loss of signal.

Jet selection criteria are applied to the two jets of largest p_T in the event within $|\eta| < 4.7$. The jet selection requirements are optimized using simulated VBF signal and diphoton background events. The p_T thresholds for the two jets are 30 and 20 GeV, and their η separation is required to be greater than 3.5. The dijet invariant mass is required to be greater than 350 and 250 GeV for the 7 and 8 TeV data sets, respectively. The lower dijet invariant mass requirement for the 8 TeV data set reflects the fact that for the analysis of that data set, the dijet event category is divided into two to increase the search sensitivity. This division creates a second “tight” dijet-tagged category in which the dijet invariant mass must be greater than 500 GeV and both jets must have $p_T > 30$ GeV. Two additional selection criteria, relating the dijet to the diphoton system, are applied: the difference between the average pseudorapidity of the two jets and the pseudorapidity of the diphoton system is required to be less than 2.5, and the difference in azimuthal angle between the diphoton system and the dijet system is required to be greater than 2.6 radians.

A multivariate regression is used to extract the photon energy and a photon-by-photon estimate of the uncertainty in that measurement. The calibration of the photon energy scale uses the Z boson mass as a reference; ECAL showers coming from electrons in $Z \rightarrow ee$ events are clustered and reconstructed in exactly the same way as photon showers. The photon selection efficiency, energy resolution, and associated systematic uncertainties are estimated from data, using $Z \rightarrow ee$ events to derive data/simulation correction factors. The jet reconstruction efficiency, the efficiency to correctly locate the vertex position, and the trigger efficiency, together with the corresponding systematic uncertainties, are also evaluated from data.

For the multivariate analysis, a boosted decision tree (BDT) [119,120] is trained to give a high output value (score) for signal-like events and for events with good diphoton invariant mass resolution, based on the following observables: (i) the photon quality determined from electromagnetic shower shape and isolation variables; (ii) the expected mass resolution; (iii) the per-event estimate of the probability of locating the diphoton vertex within 10 mm of its true location along the beam direction; and (iv) kinematic characteristics of the photons and the diphoton system. The kinematic variables are constructed so as to contain no information about the invariant mass of the diphoton system. The diphoton events not satisfying the dijet selection are classified into five categories based on the output of the BDT, with category boundaries optimized for sensitivity to a SM Higgs boson. Events in the category with small-

est expected signal-to-background ratio are rejected, leaving four categories of events. Dijet-tagged events with BDT scores smaller than the threshold for the fourth category are also rejected. Simulation studies indicate that the background in the selected event categories is dominated by the irreducible background from QCD production of two photons and that fewer than 30% of the diphoton events used in the analysis contain one or more misidentified photons (predominantly from $\gamma + \text{jet}$ production).

Table 2 shows the expected number of signal events in each event category for a SM Higgs boson (of $m_H = 125$ GeV), and the background at $m_{\gamma\gamma} = 125$ GeV, estimated from the fit described below. The estimated mass resolution is also shown, measured both by σ_{eff} , half the minimum width containing 68% of the signal events, and by the full width at half maximum (FWHM). A large variation in the expected signal-to-background ratio between the categories can be seen, although as a consequence of the optimization of the category boundaries the expected signal significances in each category are rather similar. The differences in the relative signal-to-background ratio between the categories are almost independent of m_H .

The background is estimated from data, without the use of MC simulation, by fitting the diphoton invariant mass distribution in each of the categories in a range ($100 < m_{\gamma\gamma} < 180$ GeV) extending slightly above and below that in which the search is performed. The choices of the function used to model the background and of the fit range are made based on a study of the possible bias in the measured signal strength. Polynomial functions are used. The degree is chosen by requiring that the potential bias be at least a factor of 5 smaller than the statistical accuracy of the fit prediction. The required polynomial degree ranges from 3 to 5.

A further independent analysis (referred to as the sideband background model) is performed using a different approach to the background modelling. Its sensitivity is very similar to that of the standard analysis. It employs a fit to the output of an additional BDT that takes as input the diphoton invariant mass and the diphoton BDT output, and uses a background model derived from the sidebands of the invariant mass distribution. A fit to the diphoton invariant mass distribution is used to obtain the background normalisation. This fit is of a power law and excludes a window of width $\pm 2\% \times m_H$ around the mass hypothesis. The methodology allows a systematic uncertainty to be assigned to the fit shape.

The expected 95% CL upper limit on the signal strength $\sigma/\sigma_{\text{SM}}$, in the background-only hypothesis, for the combined 7 and 8 TeV data, is less than 1.0 in the range $110 < m_H < 140$ GeV, with a value of 0.76 at $m_H = 125$ GeV. The observed limit indicates the

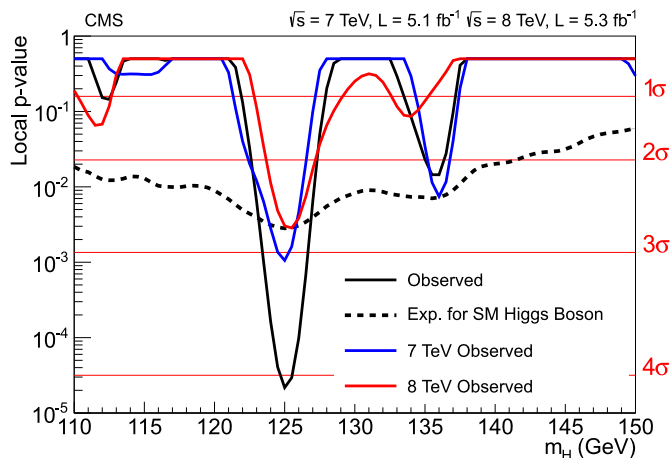


Fig. 2. The local p -value as a function of m_H in the $\gamma\gamma$ decay mode for the combined 7 and 8 TeV data sets. The additional lines show the values for the two data sets taken individually. The dashed line shows the expected local p -value for the combined data sets, should a SM Higgs boson exist with mass m_H .

presence of a significant excess at $m_H = 125$ GeV in both the 7 and 8 TeV data. The features of the observed limit are confirmed by the independent sideband-background-model and cross-check analyses. The local p -value is shown as a function of m_H in Fig. 2 for the 7 and 8 TeV data, and for their combination. The expected (observed) local p -value for a SM Higgs boson of mass 125 GeV corresponds to $2.8(4.1)\sigma$. In the sideband-background-model and cross-check analyses, the observed local p -values for $m_H = 125$ GeV correspond to 4.6 and 3.7σ , respectively. The best-fit signal strength for a SM Higgs boson mass hypothesis of 125 GeV is $\sigma/\sigma_{\text{SM}} = 1.6 \pm 0.4$.

In order to illustrate, in the $m_{\gamma\gamma}$ distribution, the significance given by the statistical methods, it is necessary to take into account the large differences in the expected signal-to-background ratios of the event categories shown in Table 2. The events are weighted according to the category in which they fall. A weight proportional to $S/(S+B)$ is used, as suggested in Ref. [121], where S and B are the number of signal and background events, respectively, calculated from the simultaneous signal-plus-background fit to all categories (with varying overall signal strength) and integrating over a $2\sigma_{\text{eff}}$ wide window, in each category, centred on 125 GeV. Fig. 3 shows the data, the signal model, and the background model, all weighted. The weights are normalised such that the integral of the weighted signal model matches the number of signal events given by the best fit. The unweighted distribution, using the same binning but in a more restricted mass range, is shown as an inset. The excess at 125 GeV is evident in both the weighted and unweighted distributions.

5.2. $H \rightarrow ZZ$

In the $H \rightarrow ZZ \rightarrow 4\ell$ decay mode a search is made for a narrow four-lepton mass peak in the presence of a small continuum background. Early detailed studies outlined the promise of this mode over a wide range of Higgs boson masses [122]. Only the search in the range 110–160 GeV is reported here. Since there are differences in the reducible background rates and mass resolutions between the subchannels $4e$, 4μ , and $2e2\mu$, they are analysed separately. The background sources include an irreducible four-lepton contribution from direct ZZ production via $q\bar{q}$ and gluon-gluon processes. Reducible contributions arise from $Z + b\bar{b}$ and $t\bar{t}$ production where the final states contain two isolated leptons and two b -quark jets producing secondary leptons. Additional background

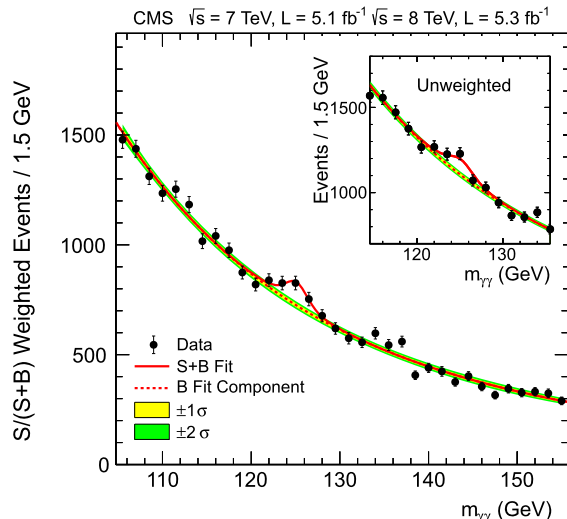


Fig. 3. The diphoton invariant mass distribution with each event weighted by the $S/(S+B)$ value of its category. The lines represent the fitted background and signal, and the coloured bands represent the ± 1 and ± 2 standard deviation uncertainties in the background estimate. The inset shows the central part of the unweighted invariant mass distribution. (For interpretation of the references to colour in this figure legend, the reader is referred to the web version of this Letter.)

arises from $Z + \text{jets}$ and $WZ + \text{jets}$ events where jets are misidentified as leptons. Compared to the analysis reported in Ref. [25], the present analysis employs improved muon reconstruction, improved lepton identification and isolation, and a kinematic discriminant exploiting the decay kinematics expected for the signal events. An algorithm to recover final-state radiation (FSR) photons has also been deployed.

Electrons are required to have $p_T > 7$ GeV and $|\eta| < 2.5$. The corresponding requirements for muons are $p_T > 5$ GeV and $|\eta| < 2.4$. Electrons are selected using a multivariate identifier trained using a sample of $W + \text{jets}$ events, and the working point is optimized using $Z + \text{jets}$ events. Both muons and electrons are required to be isolated. The combined reconstruction and selection efficiency is measured using electrons and muons in Z boson decays. Muon reconstruction and identification efficiency for muons with $p_T < 15$ GeV is measured using J/ψ decays.

The electron or muon pairs from Z boson decays are required to originate from the same primary vertex. This is ensured by requiring that the significance of the impact parameter with respect to the event vertex satisfy $|S_{\text{IP}}| < 4$ for each lepton, where $S_{\text{IP}} = l/\sigma_l$, l is the three-dimensional lepton impact parameter at the point of closest approach to the vertex, and σ_l its uncertainty.

Final-state radiation from the leptons is recovered and included in the computation of the lepton-pair invariant mass. The FSR recovery is tuned using simulated samples of $ZZ \rightarrow 4\ell$ and tested on data samples of Z boson decays to electrons and muons. Photons reconstructed within $|\eta| < 2.4$ are considered as possibly due to FSR. The photons must satisfy the following requirements. They must be within $\Delta R < 0.07$ of a muon and have $p_T^\gamma > 2$ GeV (most photon showers within this distance of an electron having already been automatically clustered with the electron shower); or if their distance from a lepton is in the range $0.07 < \Delta R < 0.5$, they must satisfy $p_T^\gamma > 4$ GeV, and be isolated within $\Delta R = 0.3$. Such photon candidates are combined with the lepton if the resulting three-body invariant mass is less than 100 GeV and closer to the Z boson mass than the mass before the addition of the photon.

The event selection requires two pairs of same-flavour, oppositely charged leptons. The pair with invariant mass closest to the Z boson mass is required to have a mass in the range 40–120 GeV

Table 3

The number of selected events, compared to the expected background yields and expected number of signal events ($m_H = 125$ GeV) for each final state in the $H \rightarrow ZZ$ analysis. The estimates of the $Z + X$ background are based on data. These results are given for the mass range from 110 to 160 GeV. The total background and the observed numbers of events are also shown for the three bins ("signal region") of Fig. 4 where an excess is seen ($121.5 < m_{4\ell} < 130.5$ GeV).

Channel	4e	4 μ	2e2 μ	4 ℓ
ZZ background	2.7 ± 0.3	5.7 ± 0.6	7.2 ± 0.8	15.6 ± 1.4
Z + X	$1.2^{+1.1}_{-0.8}$	$0.9^{+0.7}_{-0.6}$	$2.3^{+1.8}_{-1.4}$	$4.4^{+2.2}_{-1.7}$
All backgrounds (110 < $m_{4\ell}$ < 160 GeV)	4.0 ± 1.0	6.6 ± 0.9	9.7 ± 1.8	20 ± 3
Observed (110 < $m_{4\ell}$ < 160 GeV)	6	6	9	21
Signal ($m_H = 125$ GeV)	1.36 ± 0.22	2.74 ± 0.32	3.44 ± 0.44	7.54 ± 0.78
All backgrounds (signal region)	0.7 ± 0.2	1.3 ± 0.1	1.9 ± 0.3	3.8 ± 0.5
Observed (signal region)	1	3	5	9

and the other pair is required to have a mass in the range 12–120 GeV. The ZZ background is evaluated from MC simulation studies. Two different approaches are employed to estimate the reducible and instrumental backgrounds from data. Both start by selecting events in a background control region, well separated from the signal region, by relaxing the isolation and identification criteria for two same-flavour reconstructed leptons. In the first approach, the additional pair of leptons is required to have the same charge (to avoid signal contamination) while in the second, two opposite-charge leptons failing the isolation and identification criteria are required. In addition, a control region with three passing leptons and one failing lepton is used to estimate contributions from backgrounds with three prompt leptons and one misidentified lepton. The event rates measured in the background control region are extrapolated to the signal region using the measured probability for a reconstructed lepton to pass the isolation and identification requirements. This probability is measured in an independent sample. Within uncertainties, comparable background counts in the signal region are estimated by both methods.

The number of selected ZZ \rightarrow 4 ℓ candidate events in the mass range $110 < m_{4\ell} < 160$ GeV, in each of the three final states, is given in Table 3, where $m_{4\ell}$ is the four-lepton invariant mass. The number of predicted background events, in each of the three final states, and their uncertainties are also given, together with the number of signal events expected from a SM Higgs boson of $m_H = 125$ GeV. The $m_{4\ell}$ distribution is shown in Fig. 4. There is a clear peak at the Z boson mass where the decay $Z \rightarrow 4\ell$ is reconstructed. This feature of the data is well reproduced by the background estimation. The figure also shows an excess of events above the expected background around 125 GeV. The total background and the numbers of events observed in the three bins where an excess is seen are also shown in Table 3. The combined signal reconstruction and selection efficiency, with respect to the $m_H = 125$ GeV generated signal with $m_{\ell\ell} > 1$ GeV as the only cut, is 18% for the 4e channel, 40% for the 4 μ channel, and 27% for the 2e2 μ channel.

The kinematics of the $H \rightarrow ZZ \rightarrow 4\ell$ process in its centre-of-mass frame, for a given invariant mass of the four-lepton system, is fully described by five angles and the invariant masses of the two lepton pairs [123–125]. These seven variables provide significant discriminating power between signal and background. The momentum of the ZZ system may further differentiate signal from background, but would introduce dependence on the production mechanism, and on the modelling of the QCD effects, and is therefore not considered here. A kinematic discriminant is constructed based on the probability ratio of the signal and background hypotheses, $K_D = \mathcal{P}_{\text{sig}}/(\mathcal{P}_{\text{sig}} + \mathcal{P}_{\text{bkg}})$, as described in Ref. [126]. The likelihood ratio is defined for each value of $m_{4\ell}$. For the signal, the phase-space and Z propagator terms [127] are included in a fully analytic parameterization [124], while the background probability

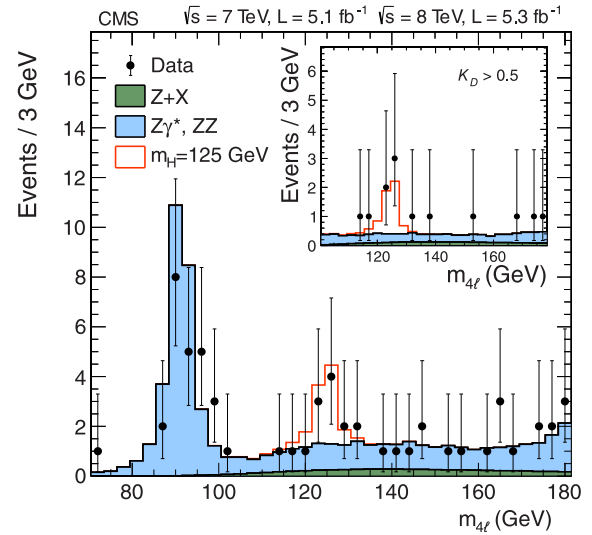


Fig. 4. Distribution of the four-lepton invariant mass for the $ZZ \rightarrow 4\ell$ analysis. The points represent the data, the filled histograms represent the background, and the open histogram shows the signal expectation for a Higgs boson of mass $m_H = 125$ GeV, added to the background expectation. The inset shows the $m_{4\ell}$ distribution after selection of events with $K_D > 0.5$, as described in the text.

is tabulated using a simulation of the $q\bar{q} \rightarrow ZZ/Z\gamma$ process. The statistical analysis only includes events with $m_{4\ell} > 100$ GeV.

Fig. 5 (upper) shows the distribution of K_D versus $m_{4\ell}$ for events selected in the 4 ℓ subchannels. The colour-coded regions show the expected background. Fig. 5 (lower) shows the same two-dimensional distribution of events, but this time superimposed on the expected event density from a SM Higgs boson ($m_H = 125$ GeV). A clustering of events is observed around 125 GeV with a large value of K_D , where the background expectation is low and the signal expectation is high, corresponding to the excess seen in the one-dimensional mass distribution. The $m_{4\ell}$ distribution of events satisfying $K_D > 0.5$ is shown in the inset in Fig. 4.

There are three final states and two data sets (7 and 8 TeV), and thus the statistical treatment requires six simultaneous two-dimensional maximum-likelihood fits for each value of m_H , in the variables $m_{4\ell}$ and K_D . Systematic uncertainties are evaluated from data for the trigger efficiency and for the combined lepton reconstruction, identification, and isolation efficiencies, as described in [128]. Systematic uncertainties in the energy/momentum calibration and in the energy resolution are estimated from data. Additional systematic uncertainties arise from limited statistical precision in the reducible background control regions.

The expected 95% CL upper limit on the signal strength $\sigma/\sigma_{\text{SM}}$, in the background-only hypothesis, for the combined 7 and 8 TeV

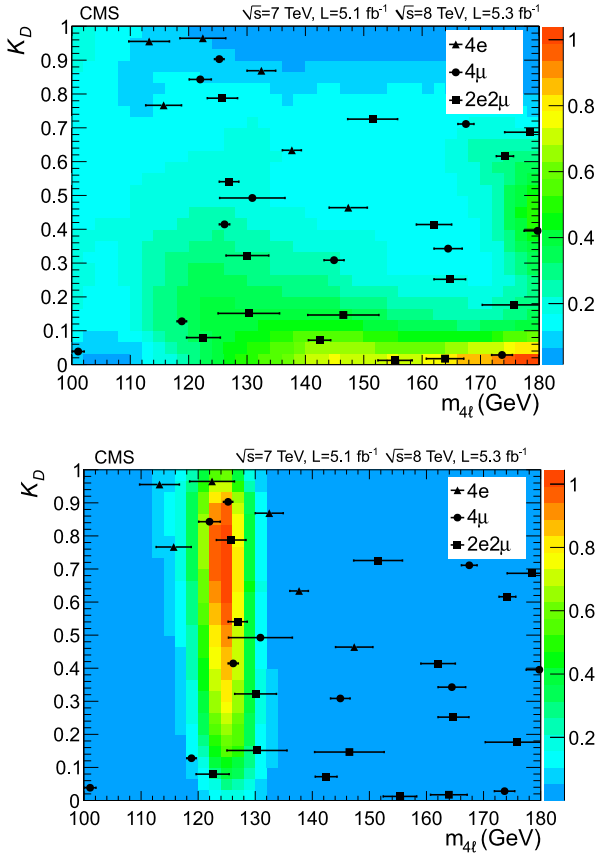


Fig. 5. The distribution of events selected in the 4ℓ subchannels for the kinematic discriminant K_D versus $m_{4\ell}$. Events in the three final states are marked by filled symbols (defined in the legend). The horizontal error bars indicate the estimated mass resolution. In the upper plot the colour-coded regions show the background expectation; in the lower plot the colour-coded regions show the event density expected from a SM Higgs boson ($m_H = 125$ GeV) (both in arbitrary units). (For interpretation of the references to colour in this figure legend, the reader is referred to the web version of this Letter.)

data, falls steeply between 110 and 140 GeV, and has a value of 0.6 at $m_H = 125$ GeV. The observed upper limit indicates the presence of a significant excess in the range $120 < m_H < 130$ GeV. The local p -value is shown as a function of m_H in Fig. 6 for the 7 and 8 TeV data, and for their combination. The minimum local p -value in the data occurs at $m_H = 125.6$ GeV and has a significance of 3.2σ (expected 3.8σ). The combined best-fit signal strength for a SM Higgs boson mass hypothesis of 125.6 GeV is $\sigma/\sigma_{SM} = 0.7^{+0.4}_{-0.3}$.

6. Decay modes with low mass resolution

6.1. $H \rightarrow WW$

The decay mode $H \rightarrow WW$ is highly sensitive to a SM Higgs boson in the mass range around the WW threshold of 160 GeV. With the development of tools for lepton identification and E_T^{miss} reconstruction optimized for LHC pileup conditions, it is possible to extend the sensitivity down to 120 GeV. This decay mode is analysed by selecting events in which both W bosons decay leptonically, resulting in a signature with two isolated, oppositely charged leptons (electrons or muons) and large E_T^{miss} due to the undetected neutrinos [129,130]. A p_T threshold of 20 (10) GeV is applied to the lepton leading (subleading) in p_T . The analysis of the 7 TeV data is described in Ref. [26] and remains unchanged, while the 8 TeV analysis was modified to cope with more difficult conditions induced by the higher pileup of the 2012 data taking.

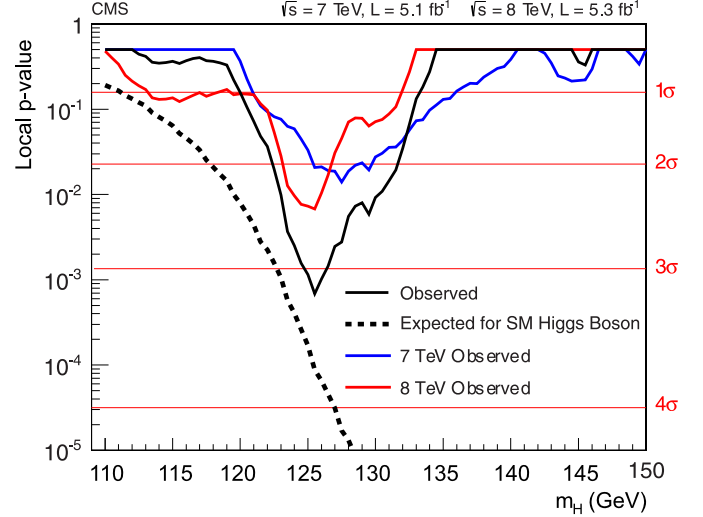


Fig. 6. The observed local p -value for the ZZ decay mode as a function of the SM Higgs boson mass. The dashed line shows the expected local p -values for a SM Higgs boson with a mass m_H .

Events are classified according to the number of jets (0, 1, or 2) with $p_T > 30$ GeV and within $|\eta| < 4.7$ ($|\eta| < 5.0$ for the 7 TeV data set), and further separated into same-flavour (ee and $\mu\mu$) or different-flavour ($e\mu$) categories. Events with more than two jets are rejected. To improve the sensitivity of the analysis, the selection criteria are optimized separately for the different event categories since they are characterised by different dominating backgrounds. The zero-jet $e\mu$ category has the best signal sensitivity. Its main backgrounds are irreducible nonresonant WW production and reducible $W + \text{jets}$ processes, where a jet is misidentified as a lepton. The one-jet $e\mu$ and zero-jet same-flavour categories only contribute to the signal sensitivity at the 10% level because of larger backgrounds, from top-quark decays and Drell-Yan production, respectively. Event selection in the two-jet category is optimized for the VBF production mechanism. This category has the highest expected signal-to-background ratio, but its contribution to the overall sensitivity is small owing to the lower cross section relative to inclusive production.

The projected E_T^{miss} variable [26] is used to reduce the Drell-Yan background arising from events where the E_T^{miss} vector is aligned with the lepton p_T , as well as events with mismeasured E_T^{miss} associated with poorly reconstructed leptons and jets. The projected E_T^{miss} is defined as the transverse component of the E_T^{miss} vector with respect to the closest lepton direction, if it is closer than $\pi/2$ in azimuthal angle, or the full E_T^{miss} otherwise. Since pileup degrades the projected E_T^{miss} resolution, the minimum of two different projected E_T^{miss} definitions is used: the first includes all particle candidates in the event, while the second uses only the charged particle candidates associated with the primary vertex. In the 8 TeV analysis, the minimum projected E_T^{miss} defined in this way is then required to be above a threshold that varies by category. For $m_H > 140$ GeV, projected E_T^{miss} is required to be greater than 20 GeV in the $e\mu$ channel, and greater than 45 GeV in the same-flavour channels. For $m_H \leq 140$ GeV in the same-flavour channels, where it is more difficult to separate the signal from the Drell-Yan background, a multivariate selection is used, combining kinematic and topological variables. In the two-jet category, a simple selection of $E_T^{\text{miss}} > 45$ GeV is applied. To further reduce the Drell-Yan background in the same-flavour final states, events with a dilepton mass within 15 GeV of the Z boson mass are rejected.

Table 4

Observed number of events, background estimates, and signal predictions for $m_H = 125$ GeV in each category of the WW analysis of the 8 TeV data set. All the selection requirements have been applied. The combined experimental and theoretical, systematic and statistical uncertainties are shown. The $Z\gamma$ process includes the dimuon, dielectron, and $\tau\tau \rightarrow \ell\ell$ final states.

Category:	0-jet $e\mu$	0-jet $\ell\ell$	1-jet $e\mu$	1-jet $\ell\ell$	2-jet $e\mu$	2-jet $\ell\ell$
WW	87.6 ± 9.5	60.4 ± 6.7	19.5 ± 3.7	9.7 ± 1.9	0.4 ± 0.1	0.3 ± 0.1
WZ + ZZ + $Z\gamma$	2.2 ± 0.2	37.7 ± 12.5	2.4 ± 0.3	8.7 ± 4.9	0.1 ± 0.0	3.1 ± 1.8
Top	9.3 ± 2.7	1.9 ± 0.5	22.3 ± 2.0	9.5 ± 1.1	3.4 ± 1.9	2.0 ± 1.2
W + jets	19.1 ± 7.2	10.8 ± 4.3	11.7 ± 4.6	3.9 ± 1.7	0.3 ± 0.3	0.0 ± 0.0
$W\gamma^{(*)}$	6.0 ± 2.3	4.6 ± 2.5	5.9 ± 3.2	1.3 ± 1.2	0.0 ± 0.0	0.0 ± 0.0
All backgrounds	124.2 ± 12.4	115.5 ± 15.0	61.7 ± 7.0	33.1 ± 5.7	4.1 ± 1.9	5.4 ± 2.2
Signal ($m_H = 125$ GeV)	23.9 ± 5.2	14.9 ± 3.3	10.3 ± 3.0	4.4 ± 1.3	1.5 ± 0.2	0.8 ± 0.1
Data	158	123	54	43	6	7

The background from low-mass resonances is rejected by requiring a dilepton invariant mass greater than 12 GeV.

To suppress the top-quark background, a “top tagging” technique based on soft-muon and b-jet tagging is applied. The first method is designed to veto events containing muons in b jets coming from decays of top quarks. The second method uses a b-jet tagging algorithm, which looks within jets for tracks with large impact parameters. The algorithm is applied also in the case of zero-jet events, which may contain low- p_T jets below the selection threshold. To reduce the background from WZ production, events with a third lepton passing the identification and isolation requirements are rejected.

Yields for the dominant backgrounds are estimated using control regions in the data. The W + jets contribution is derived from data using a “tight-loose” sample in which one lepton passes the standard criteria and the other does not, but instead satisfies a “loose” set of requirements. The efficiency ϵ_{loose} for a jet that satisfies the loose selection to pass the tight selection is determined using data from an independent loose lepton-trigger sample dominated by jets. The background contamination is then estimated using the events of the “tight-loose” sample weighted by $\epsilon_{\text{loose}}/(1 - \epsilon_{\text{loose}})$. The normalisation of the top-quark background is estimated by counting the number of top-tagged events and applying the corresponding top-tagging efficiency. The nonresonant WW contribution is normalised by using events with a dilepton mass larger than 100 GeV, where the Higgs boson signal contamination is negligible, extrapolated to the signal region using simulated samples. The same-flavour Drell-Yan background is normalised using the number of events observed with a dilepton mass within 7.5 GeV of the Z boson mass, after subtracting the non-Drell-Yan contribution. Other minor backgrounds from WZ, ZZ, and $W\gamma$ are estimated from simulation.

The 7 TeV data are analysed by training a BDT for each Higgs boson mass hypothesis in the zero-jet and one-jet event categories, while a simple selection strategy is employed in the VBF category [26]. In the BDT analysis, the Higgs boson signal is separated from the background by using a binned maximum-likelihood fit to the classifier distribution. The 8 TeV analysis is based on a simple selection strategy optimized for each mass hypothesis, where additional kinematic and topological requirements are applied to improve the signal-to-background ratio. One of the most sensitive variables to discriminate between $H \rightarrow WW$ decays and nonresonant WW production is the dilepton invariant mass $m_{\ell\ell}$. This quantity is shown in Fig. 7 for the zero-jet $e\mu$ category after the full selection for $m_H = 125$ GeV, except for the selection on $m_{\ell\ell}$ itself. Table 4 shows for the 8 TeV analysis the number of events selected in data, background estimates, and signal predictions for $m_H = 125$ GeV in each analysis category after applying all the selection requirements. About 97% of the signal events selected

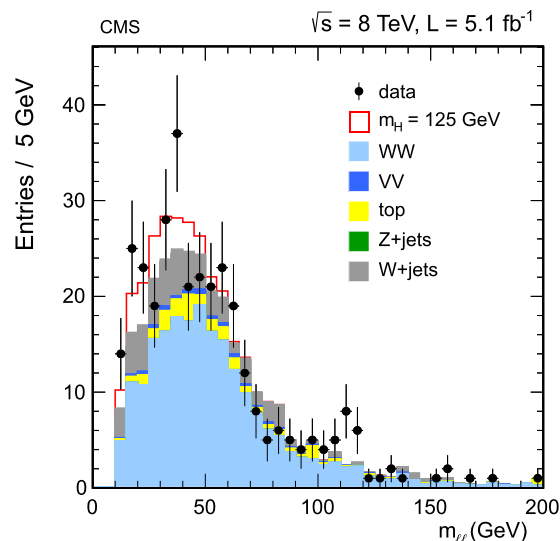


Fig. 7. Distribution of $m_{\ell\ell}$ for the zero-jet $e\mu$ category in the $H \rightarrow WW$ search at 8 TeV. The signal expected from a Higgs boson with a mass $m_H = 125$ GeV is shown added to the background.

in the zero-jet $e\mu$ category are expected to be produced by the gluon-gluon fusion process, whereas 83% of the signal in the two-jet $e\mu$ category is expected to be produced by the VBF process. The 95% CL expected and observed limits for the combination of the 7 and 8 TeV analyses are shown in Fig. 8. A broad excess is observed that is consistent with a SM Higgs boson of mass 125 GeV. This is illustrated by the dotted curve in Fig. 8 showing the median expected limit in the presence of a SM Higgs boson with $m_H = 125$ GeV. The expected significance for a SM Higgs of mass 125 GeV is 2.4σ and the observed significance is 1.6σ .

6.2. $H \rightarrow \tau\tau$

The decay mode $H \rightarrow \tau\tau$ is searched for in four exclusive sub-channels, corresponding to different decays of the τ pair: $e\mu$, $\mu\mu$, $e\tau_h$, and $\mu\tau_h$, where electrons and muons arise from leptonic τ decays, and τ_h denotes hadronic τ decays. The latter are reconstructed by selecting τ decays consistent with the hypothesis of three charged pions, or one charged pion and up to two neutral pions [131]. The search is made in the mass range 110–145 GeV, and a signal should appear as a broad excess in the distribution of the τ -pair invariant mass $m_{\tau\tau}$.

The sensitivity of the search is improved by classifying the events according to jet multiplicity and the transverse momentum of the reconstructed τ . The multiplicity of jets with $p_T > 30$ GeV

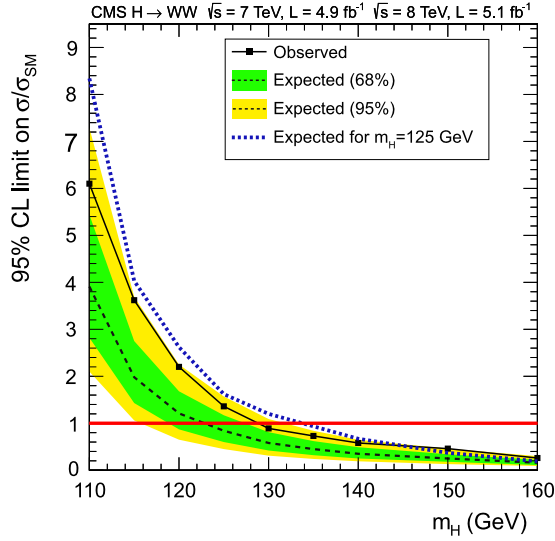


Fig. 8. The 95% CL limit on $\sigma/\sigma_{\text{SM}}$ for a Higgs boson decaying, via a W boson pair, to two leptons and two neutrinos, for the combined 7 and 8 TeV data sets. The symbol $\sigma/\sigma_{\text{SM}}$ denotes the production cross section times the relevant branching fractions, relative to the SM expectation. The background-only expectations are represented by their median (dashed line) and by the 68% and 95% CL bands. The dotted curve shows the median expected limit for a SM Higgs boson with $m_H = 125$ GeV.

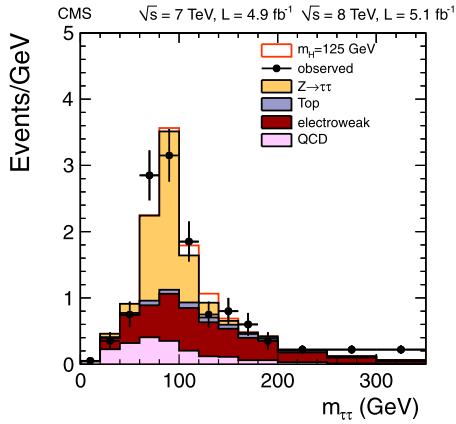


Fig. 9. Distribution of $m_{\tau\tau}$ in the combined 7 and 8 TeV data sets for the $\mu\tau_h$ VBF category of the $H \rightarrow \tau\tau$ search. The signal expected from a SM Higgs boson ($m_H = 125$ GeV) is added to the background.

reflects the production mechanism: events with zero or one jet are likely to come from the gluon–gluon fusion process, while events with two jets are candidates for VBF production. Events including b jets with $p_T > 20$ GeV are removed from zero- and one-jet categories. The signal purities in the zero- and one-jet categories are increased, and the $m_{\tau\tau}$ resolution is improved, by separating events into low- and high- p_T subchannels. The high- p_T subchannels are defined by $p_T^{\tau_h} > 40$ GeV in channels with a hadronic τ decay, and $p_T^\mu > 35$ (30) GeV in the $e\mu$ ($\mu\mu$) channel. The mass $m_{\tau\tau}$ is reconstructed with an algorithm [132] combining the visible τ decay products and the missing transverse energy, achieving a resolution of about 20% on $m_{\tau\tau}$. Fig. 9 shows as an example the reconstructed $m_{\tau\tau}$ distribution in the $\mu\tau_h$ VBF category for the combined 7 and 8 TeV data samples.

Backgrounds in the $e\mu$ and $\mu\mu$ channels arise from $t\bar{t}$ and Drell–Yan production, while W and Z production with a misidentified τ_h candidate from an electron, muon, or jet dominates in the hadronic channels. Backgrounds from $Z \rightarrow \tau\tau$ decays are modelled with $Z \rightarrow \mu\mu$ events in data where each muon is replaced

Table 5

Numbers of expected and observed events in the most sensitive event categories (VBF) in the $H \rightarrow \tau\tau$ analysis for the 7 and 8 TeV data sets. The expected signal yields for a SM Higgs boson with $m_H = 125$ GeV are also shown. Combined statistical and systematic uncertainties in each estimate are reported.

Subchannel	$e\tau_h$	$\mu\tau_h$	$e\mu$	$\mu\mu$
$Z \rightarrow \tau\tau$	53 ± 5	100 ± 9	56 ± 12	5.3 ± 0.4
QCD	35 ± 7	41 ± 9	7.4 ± 1.4	–
W + jets	46 ± 10	72 ± 15	–	–
Z + jets	13 ± 2	2.5 ± 0.6	–	–
$Z \rightarrow \mu\mu$	–	–	–	70 ± 8
$t\bar{t}$	7.0 ± 1.7	14 ± 3	24 ± 2	6.7 ± 1.5
Dibosons	1.2 ± 0.9	2.9 ± 2.1	11 ± 2	2.4 ± 0.9
All backgrounds	156 ± 13	233 ± 20	99 ± 13	85 ± 9
Signal ($m_H = 125$ GeV)	4.3 ± 0.6	7.7 ± 1.1	3.5 ± 0.4	0.8 ± 0.1
Data	142	263	110	83

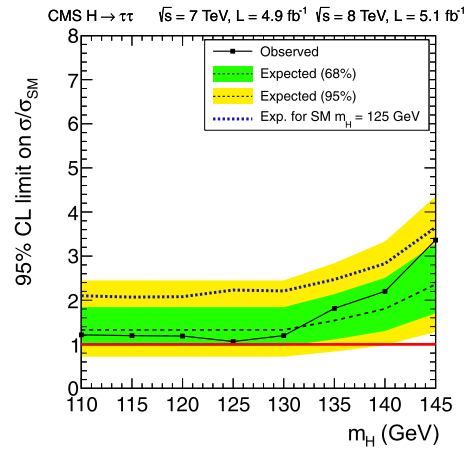


Fig. 10. The 95% CL limit on the signal strength $\sigma/\sigma_{\text{SM}}$ for a Higgs boson decaying to τ pairs, for the combined 7 and 8 TeV data sets. The symbol $\sigma/\sigma_{\text{SM}}$ denotes the production cross section times the relevant branching fractions, relative to the SM expectation. The background-only expectations are represented by their median (dashed line) and by the 68% and 95% CL bands. The dotted curve shows the median expected limit for a SM Higgs boson with $m_H = 125$ GeV.

with particles from simulated decays of a τ with the same momentum as the muon. Reducible backgrounds, comprising W + jets, QCD multijet production, and residual $Z \rightarrow ee$ events, are estimated from the data [27]. An improved signal-to-background ratio is achieved by including explicitly in the event selection for the VBF production mechanism the pseudorapidity separation between forward jets and the large invariant mass of the dijet system. Table 5 shows the numbers of expected and observed events in the most sensitive event categories (VBF) for the 7 and 8 TeV data sets. The expected signal yields for a SM Higgs boson with $m_H = 125$ GeV are also shown.

To search for the presence of a Higgs boson signal in the selected events, a binned maximum-likelihood fit to $m_{\tau\tau}$ is performed jointly across the four final states, each with five event categories. Systematic uncertainties are represented by nuisance parameters in the fitting process. The expected and observed 95% CL limits on the signal strength for the combination of all categories are shown in Fig. 10. The expected and observed limits are 1.3 and 1.1 times the SM Higgs boson cross section at mass 125 GeV, respectively. The expected significance for a SM Higgs boson of mass 125 GeV is 1.4σ , and the observed value is zero.

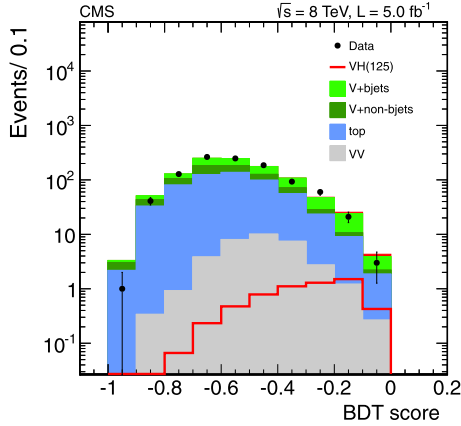


Fig. 11. Distribution of BDT scores for the high- p_T subchannel of the $Z(\nu\nu)H(bb)$ search in the 8 TeV data set after all selection criteria have been applied. The signal expected from a Higgs boson ($m_H = 125$ GeV), including $W(\ell\nu)H$ events where the charged lepton is not reconstructed, is shown added to the background and also overlaid for comparison with the diboson background.

6.3. $H \rightarrow bb$

For $m_H \leq 135$ GeV, the decay $H \rightarrow bb$ has the largest branching fraction of the five search modes, but the inclusive signal is overwhelmed by QCD production of bottom quarks. The analysis is therefore designed to search for the associated production of the Higgs boson in events where a dijet resonance is produced at high p_T in association with a W or Z boson; this largely suppresses the QCD background. Five independent search channels are explored corresponding to different decays of the vector boson: $Z(\ell\ell)H$, $Z(\nu\nu)H$, and $W(\ell\nu)H$. Events are further separated into two categories based on the p_T of the vector boson, ranging from 50–100 GeV for the lowest bin in the $Z(\ell\ell)$ search, to greater than 170 GeV for the highest bin in the $W(\ell\nu)$ search. For the $Z(\nu\nu)$ search, two subchannels are defined as $120 < E_T^{\text{miss}} < 160$ GeV and $E_T^{\text{miss}} > 160$ GeV. The two jets comprising the candidate Higgs boson decay are required to be identified as b jets, and the dijet system must satisfy a p_T threshold that is optimized within each channel: greater than 120 GeV for WH , 160 GeV for $Z(\nu\nu)H$, and no explicit threshold for $Z(\ell\ell)H$.

Dominant backgrounds arise from production of vector bosons in association with jets, pair- or single-production of top quarks, and diboson production (WW , WZ , ZZ) with one of the bosons decaying hadronically. Significant background rejection is achieved in general by requiring large p_T for the dijet, while also requiring that there be minimal additional jet activity and that the vector boson and dijet be back to back in azimuth. The effect on the signal efficiency of this selection due to higher-order electroweak [133] and QCD [91] corrections is accounted for in the systematic uncertainties. Further signal discrimination is obtained from the dijet invariant mass, which is expected to peak near m_H . A multivariate regression algorithm to better estimate b -jet p_T is trained on jets in simulated signal events and achieves a final dijet mass resolution of 8–9% for $m_H = 125$ GeV. The performance of the regression algorithm is checked in data using W/Z + jets and $t\bar{t}$ events.

A search for the signal is made in the distribution of scores of a BDT trained at discrete mass points. Input variables to the BDT algorithm exploit kinematic and topological information about the vector boson and dijet systems, and the colour-singlet nature of the Higgs boson [134]. The distribution of scores in simulated background events is checked using control regions in the data designed to enrich individual background contributions. Fig. 11 shows as an example the BDT scores for the high- p_T subchannel

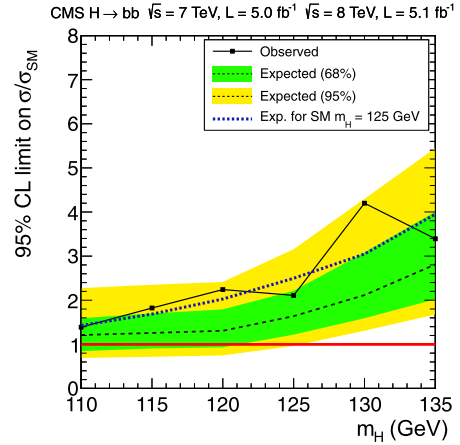


Fig. 12. The 95% CL limit on the signal strength $\sigma/\sigma_{\text{SM}}$ for a Higgs boson decaying to two b quarks, for the combined 7 and 8 TeV data sets. The symbol $\sigma/\sigma_{\text{SM}}$ denotes the production cross section times the relevant branching fractions, relative to the SM expectation. The background-only expectations are represented by their median (dashed line) and by the 68% and 95% CL bands. The dotted curve shows the median expected limit for a SM Higgs boson with $m_H = 125$ GeV.

of the $Z(\nu\nu)H$ channel in the 8 TeV data set, after all selection criteria have been applied.

The rates for the dominant backgrounds arising from production of W/Z + jets and top-quark pairs are estimated in data [28], while contributions from single-top and diboson production are estimated from simulation studies. The signal is then searched for as an excess in the BDT score distribution using the predicted shapes for signal and background events, for Higgs boson masses in the range 110–135 GeV.

Combined results for expected and observed 95% CL limits obtained from the 7 and 8 TeV data sets are displayed in Fig. 12. The expected and observed limits are 1.6 and 2.1 times the SM Higgs boson cross section at mass 125 GeV. The expected local p -value for a SM Higgs of mass 125 GeV corresponds to 1.9σ , while the observed value corresponds to 0.7σ .

7. Combined results

The individual results for the channels analysed for the five decay modes, summarised in Table 1, are combined using the methods outlined in Section 4. The combination assumes the relative branching fractions predicted by the SM and takes into account the experimental statistical and systematic uncertainties as well as the theoretical uncertainties, which are dominated by the imperfect knowledge of the QCD scale and parton distribution functions. The CL_s is shown in Fig. 13 as a function of the Higgs boson mass hypothesis. The observed values are shown by the solid points. The dashed line indicates the median of the expected results for the background-only hypothesis, with the green (dark) and yellow (light) bands indicating the ranges in which the CL_s values are expected to lie in 68% and 95% of the experiments under the background-only hypothesis. The probabilities for an observation, in the absence of a signal, to lie above or below the 68% (95%) band are 16% (2.5%) each. The thick horizontal lines indicate CL_s values of 0.05, 0.01, and 0.001. The mass regions where the observed CL_s values are below these lines are excluded with the corresponding $(1 - CL_s)$ confidence levels. Our previously published results exclude the SM Higgs boson from 127 to 600 GeV [21]. In the search described here, the SM Higgs boson is excluded at 95% CL in the range $110 < m_H < 121.5$ GeV. In the range $121.5 < m_H < 128$ GeV a significant excess is seen and the SM Higgs boson cannot be excluded at 95% CL.

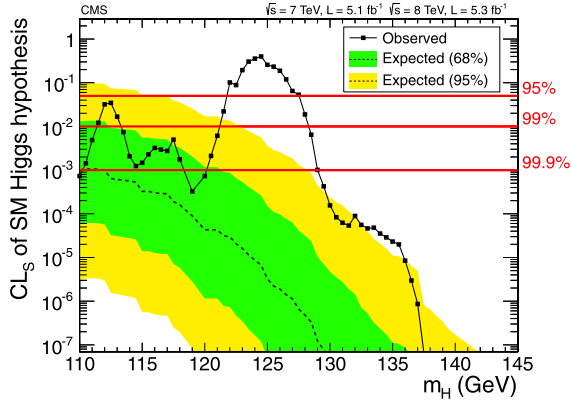


Fig. 13. The CL_s values for the SM Higgs boson hypothesis as a function of the Higgs boson mass in the range 110–145 GeV. The background-only expectations are represented by their median (dashed line) and by the 68% and 95% CL bands. (For interpretation of the references to colour, the reader is referred to the web version of this Letter.)

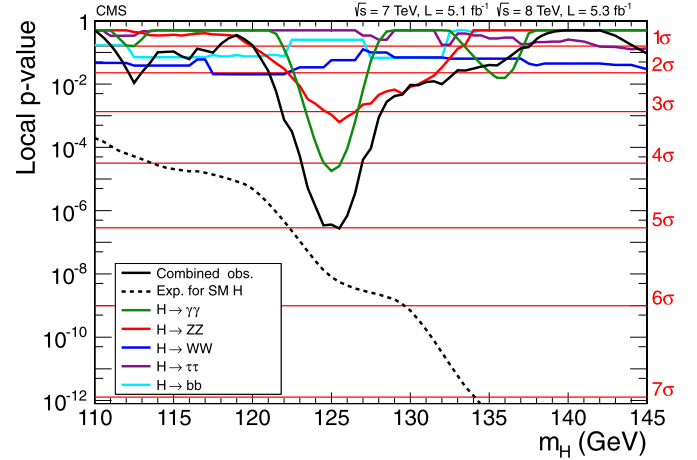


Fig. 15. The observed local p -value for the five decay modes and the overall combination as a function of the SM Higgs boson mass. The dashed line shows the expected local p -values for a SM Higgs boson with a mass m_H .

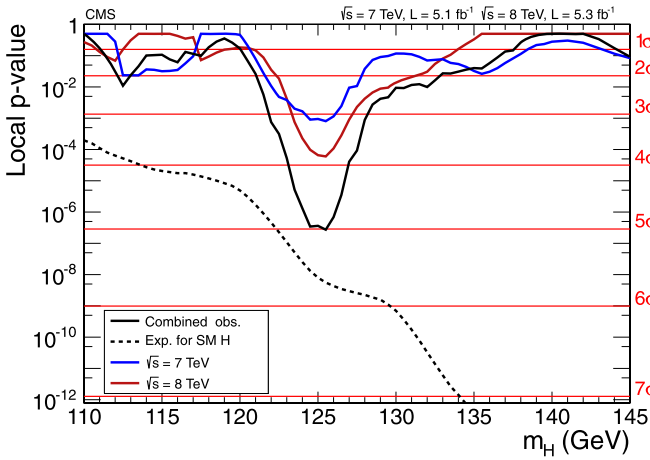


Fig. 14. The observed local p -value for 7 TeV and 8 TeV data, and their combination as a function of the SM Higgs boson mass. The dashed line shows the expected local p -values for a SM Higgs boson with a mass m_H .

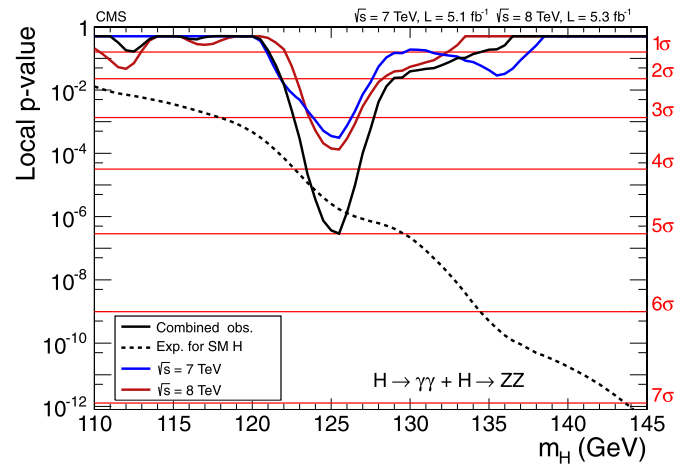


Fig. 16. The observed local p -value for decay modes with high mass-resolution channels, $\gamma\gamma$ and ZZ , as a function of the SM Higgs boson mass. The dashed line shows the expected local p -values for a SM Higgs boson with a mass m_H .

7.1. Significance of the observed excess

The consistency of the observed excess with the background-only hypothesis may be judged from Fig. 14, which shows a scan of the local p -value for the 7 and 8 TeV data sets and their combination. The 7 and 8 TeV data sets exhibit an excess of 3.2σ and 3.8σ significance, respectively, for a Higgs boson mass of approximately 125 GeV. In the overall combination the significance is 5.0σ for $m_H = 125.5$ GeV. Fig. 15 gives the local p -value for the five decay modes individually and displays the expected overall p -value.

The largest contributors to the overall excess in the combination are the $\gamma\gamma$ and ZZ decay modes. They both have very good mass resolution, allowing good localization of the invariant mass of a putative resonance responsible for the excess. Their combined significance reaches 5.0σ (Fig. 16). The WW decay mode has an exclusion sensitivity comparable to the $\gamma\gamma$ and ZZ decay modes but does not have a good mass resolution. It has an excess with local significance 1.6σ for $m_H \sim 125$ GeV. When added to the $\gamma\gamma$ and ZZ decay modes, the combined significance becomes 5.1σ . Adding the $\tau\tau$ and bb channels in the combination, the final significance becomes 5.0σ . Table 6 summarises the expected and observed local p -values for a SM Higgs boson mass hypothesis of 125.5 GeV for the various combinations of channels.

Table 6

The expected and observed local p -values, expressed as the corresponding number of standard deviations of the observed excess from the background-only hypothesis, for $m_H = 125.5$ GeV, for various combinations of decay modes.

Decay mode/combination	Expected (σ)	Observed (σ)
$\gamma\gamma$	2.8	4.1
ZZ	3.8	3.2
$\tau\tau + bb$	2.4	0.5
$\gamma\gamma + ZZ$	4.7	5.0
$\gamma\gamma + ZZ + WW$	5.2	5.1
$\gamma\gamma + ZZ + WW + \tau\tau + bb$	5.8	5.0

The global p -value for the search range 115–130 (110–145) GeV is calculated using the method suggested in Ref. [115], and corresponds to 4.6σ (4.5σ). These results confirm the very low probability for an excess as large as or larger than that observed to arise from a statistical fluctuation of the background. The excess constitutes the observation of a new particle with a mass near 125 GeV, manifesting itself in decays to two photons or to ZZ . These two decay modes indicate that the new particle is a boson; the two-photon decay implies that its spin is different from one [135,136].

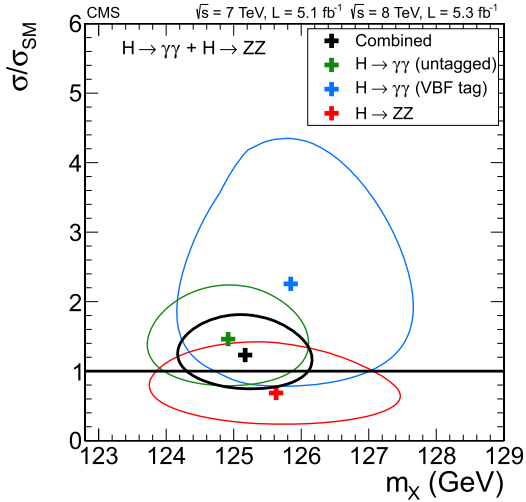


Fig. 17. The 68% CL contours for the signal strength $\sigma/\sigma_{\text{SM}}$ versus the boson mass m_χ for the untagged $\gamma\gamma$, $\gamma\gamma$ with VBF-like dijet, 4ℓ , and their combination. The symbol $\sigma/\sigma_{\text{SM}}$ denotes the production cross section times the relevant branching fractions, relative to the SM expectation. In this combination, the relative signal strengths for the three decay modes are constrained by the expectations for the SM Higgs boson.

7.2. Mass of the observed boson

The mass m_χ of the observed boson is determined using the $\gamma\gamma$ and ZZ decay modes, with the former dominating the precision of the measurement. The calibration of the energy scale in the $\gamma\gamma$ decay mode is achieved with reference to the known Z boson mass, as described in Section 5.1. There are two main sources of systematic uncertainty: (i) imperfect simulation of the differences between electrons and photons and (ii) the need to extrapolate from m_Z to $m_\chi \approx 125$ GeV. The systematic uncertainties are evaluated by making comparisons between data and simulated samples of $Z \rightarrow ee$ and $H \rightarrow \gamma\gamma$ ($m_H = 90$ GeV). The two uncertainties, which together amount to 0.5%, are assumed to be fully correlated between all the $\gamma\gamma$ event categories in the 7 and 8 TeV data. For the $ZZ \rightarrow 4\ell$ decay mode the energy scale (for electrons) and momentum scale (for muons) are calibrated using the leptonic decays of the Z boson, with an assigned uncertainty of 0.4%.

Fig. 17 shows the two-dimensional 68% CL regions for the signal strength $\sigma/\sigma_{\text{SM}}$ versus m_χ for the three channels (untagged $\gamma\gamma$, dijet-tagged $\gamma\gamma$, and $ZZ \rightarrow 4\ell$). The combined 68% CL contour shown in Fig. 17 assumes that the relative event yields among the three channels are those expected from the standard model, while the overall signal strength is a free parameter.

To extract the value of m_χ in a model-independent way, the signal yields of the three channels are allowed to vary independently. Thus the expected event yields in these channels are scaled by independent factors, while the signal is assumed to be due to a particle with a unique mass m_χ . The combined best-fit mass is $m_\chi = 125.3 \pm 0.4(\text{stat.}) \pm 0.5(\text{syst.})$ GeV.

7.3. Compatibility with the SM Higgs boson hypothesis

A first test of the compatibility of the observed boson with the SM Higgs boson is provided by examination of the best-fit value for the common signal strength $\sigma/\sigma_{\text{SM}}$, obtained in a combination of all search channels. Fig. 18 shows a scan of the overall $\sigma/\sigma_{\text{SM}}$ obtained in the combination of all channels versus a hypothesised Higgs boson mass m_H . The band corresponds to the $\pm 1\sigma$ uncertainty (statistical and systematic). The excesses seen in the 7 TeV and 8 TeV data, and in their combination, around 125 GeV are

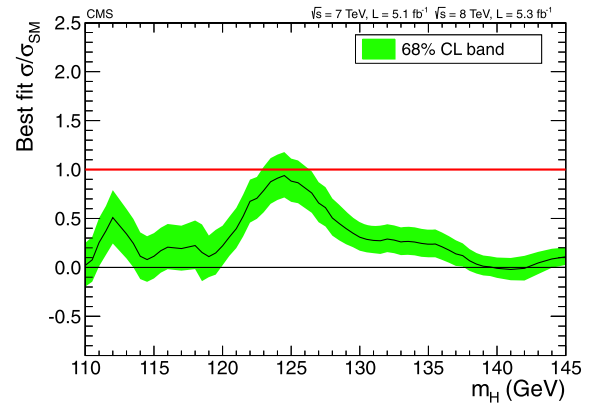


Fig. 18. The observed best-fit signal strength $\sigma/\sigma_{\text{SM}}$ as a function of the SM Higgs boson mass in the range 110–145 GeV for the combined 7 and 8 TeV data sets. The symbol $\sigma/\sigma_{\text{SM}}$ denotes the production cross section times the relevant branching fractions, relative to the SM expectation. The band corresponds to the ± 1 standard deviation uncertainty in $\sigma/\sigma_{\text{SM}}$.

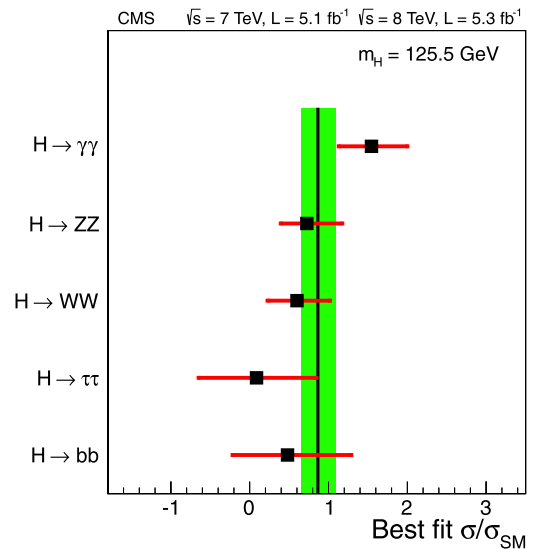


Fig. 19. Values of $\sigma/\sigma_{\text{SM}}$ for the combination (solid vertical line) and for individual decay modes (points). The vertical band shows the overall $\sigma/\sigma_{\text{SM}}$ value 0.87 ± 0.23 . The symbol $\sigma/\sigma_{\text{SM}}$ denotes the production cross section times the relevant branching fractions, relative to the SM expectation. The horizontal bars indicate the ± 1 standard deviation uncertainties in the $\sigma/\sigma_{\text{SM}}$ values for individual modes; they include both statistical and systematic uncertainties.

consistent with unity within the $\pm 1\sigma$ uncertainties. The observed $\sigma/\sigma_{\text{SM}}$ value for an excess at 125.5 GeV in a combination of all data is 0.87 ± 0.23 . The different decay channels and data sets have been examined for self-consistency. Fig. 19 shows the measured values of $\sigma/\sigma_{\text{SM}}$ results obtained for the different decay modes. These results are consistent, within uncertainties, with the expectations for the SM Higgs boson.

8. Conclusions

Results are presented from searches for the standard model Higgs boson in proton–proton collisions at $\sqrt{s} = 7$ and 8 TeV in the CMS experiment at the LHC, using data samples corresponding to integrated luminosities of up to 5.1 fb^{-1} at 7 TeV and 5.3 fb^{-1} at 8 TeV. The search is performed in five decay modes: $\gamma\gamma$, ZZ , W^+W^- , $\tau^+\tau^-$, and $b\bar{b}$. An excess of events is observed above the expected background, with a local significance of 5.0σ , at a mass near 125 GeV, signalling the production of a new par-

ticle. The expected local significance for a standard model Higgs boson of that mass is 5.8σ . The global p -value in the search range of 115–130 (110–145) GeV corresponds to 4.6σ (4.5σ). The excess is most significant in the two decay modes with the best mass resolution, $\gamma\gamma$ and ZZ , and a fit to these signals gives a mass of $125.3 \pm 0.4(\text{stat.}) \pm 0.5(\text{syst.})$ GeV. The decay to two photons indicates that the new particle is a boson with spin different from one. The results presented here are consistent, within uncertainties, with expectations for the standard model Higgs boson. The collection of further data will enable a more rigorous test of this conclusion and an investigation of whether the properties of the new particle imply physics beyond the standard model.

Acknowledgements

We congratulate our colleagues in the CERN accelerator departments for the excellent performance of the LHC machine. We thank the computing centres in the Worldwide LHC computing Grid for the provisioning and excellent performance of computing infrastructure essential to our analyses. We gratefully acknowledge the contributions of the technical staff at CERN and other CMS institutes. We also thank the administrative staff at CERN and the other CMS institutes and acknowledge support from BMWF and FWF (Austria); FNRS and FWO (Belgium); CNPq, CAPES, FAPERJ, and FAPESP (Brazil); MES (Bulgaria); CERN; CAS, MoST, and NSFC (China); COLCIENCIAS (Colombia); MSES (Croatia); RPF (Cyprus); MEYS (Czech Republic); MoER, SF0690030s09 and ERDF (Estonia); Academy of Finland, MEC, and HIP (Finland); CEA and CNRS/IN2P3 (France); BMBF, DFG, and HGF (Germany); GSRT (Greece); OTKA and NKTH (Hungary); DAE and DST (India); IPM (Iran); SFI (Ireland); INFN (Italy); NRF and WCU (Republic of Korea); LAS (Lithuania); CINVESTAV, CONACYT, SEP, and UASLP-FAI (Mexico); MSI (New Zealand); PAEC (Pakistan); MSHE and NSC (Poland); FCT (Portugal); JINR (Armenia, Belarus, Georgia, Ukraine, Uzbekistan); MON, RosAtom, RAS and RFBR (Russia); MSTD (Serbia); SEIDI and CPAN (Spain); Swiss Funding Agencies (Switzerland); NSC (Taipei); TUBITAK and TAEK (Turkey); NASU (Ukraine); STFC (United Kingdom); DOE and NSF (USA). Individuals have received support from the Marie-Curie programme and the European Research Council (European Union); the Leventis Foundation; the A.P. Sloan Foundation; the Alexander von Humboldt Foundation; the Austrian Science Fund (FWF); the Belgian Federal Science Policy Office; the Fonds pour la Formation à la Recherche dans l'Industrie et dans l'Agriculture (FRIA-Belgium); the Agentschap voor Innovatie door Wetenschap en Technologie (IWT-Belgium); the Council of Science and Industrial Research, India; the Compagnia di San Paolo (Torino); and the HOMING PLUS programme of Foundation for Polish Science, cofinanced from European Union, Regional Development Fund.

Open access

This article is published Open Access at sciencedirect.com. It is distributed under the terms of the Creative Commons Attribution License 3.0, which permits unrestricted use, distribution, and reproduction in any medium, provided the original authors and source are credited.

References

- [1] F. Englert, R. Brout, Phys. Rev. Lett. 13 (1964) 321, <http://dx.doi.org/10.1103/PhysRevLett.13.321>.
- [2] P.W. Higgs, Phys. Lett. 12 (1964) 132, [http://dx.doi.org/10.1016/0031-9163\(64\)91136-9](http://dx.doi.org/10.1016/0031-9163(64)91136-9).
- [3] P.W. Higgs, Phys. Rev. Lett. 13 (1964) 508, <http://dx.doi.org/10.1103/PhysRevLett.13.508>.
- [4] G.S. Guralnik, C.R. Hagen, T.W.B. Kibble, Phys. Rev. Lett. 13 (1964) 585, <http://dx.doi.org/10.1103/PhysRevLett.13.585>.
- [5] P.W. Higgs, Phys. Rev. 145 (1966) 1156, <http://dx.doi.org/10.1103/PhysRev.145.1156>.
- [6] T.W.B. Kibble, Phys. Rev. 155 (1967) 1554, <http://dx.doi.org/10.1103/PhysRev.155.1554>.
- [7] S.L. Glashow, Nucl. Phys. 22 (1961) 579, [http://dx.doi.org/10.1016/0029-5582\(61\)90469-2](http://dx.doi.org/10.1016/0029-5582(61)90469-2).
- [8] S. Weinberg, Phys. Rev. Lett. 19 (1967) 1264, <http://dx.doi.org/10.1103/PhysRevLett.19.1264>.
- [9] A. Salam, in: N. Svartholm (Ed.), Elementary Particle Physics: Relativistic Groups and Analyticity, Almqvist & Wiskell, 1968, p. 367, proceedings of the eighth Nobel symposium.
- [10] J.M. Cornwall, D.N. Levin, G. Tiktopoulos, Phys. Rev. Lett. 30 (1973) 1268, <http://dx.doi.org/10.1103/PhysRevLett.30.1268>.
- [11] J.M. Cornwall, D.N. Levin, G. Tiktopoulos, Phys. Rev. D 10 (1974) 1145, <http://dx.doi.org/10.1103/PhysRevD.10.1145>, also Erratum, <http://dx.doi.org/10.1103/PhysRevD.11.972>.
- [12] C.H. Llewellyn Smith, Phys. Lett. B 46 (1973) 233, [http://dx.doi.org/10.1016/0370-2693\(73\)90692-8](http://dx.doi.org/10.1016/0370-2693(73)90692-8).
- [13] B.W. Lee, C. Quigg, H.B. Thacker, Phys. Rev. D 16 (1977) 1519, <http://dx.doi.org/10.1103/PhysRevD.16.1519>.
- [14] ALEPH, CDF, D0, DELPHI, L3, OPAL, SLD Collaborations, the LEP Electroweak Working Group, the Tevatron Electroweak Working Group, and the SLD Electroweak and Heavy Flavour Groups, Precision electroweak measurements and constraints on the standard model, CERN PH-EP-2010-095, at this time, the most up-to-date Higgs boson mass constraints come from <http://lepewwg.web.cern.ch/LEPEWWG/plots/winter2012/>, arXiv:1012.2367, 2010, <http://cdsweb.cern.ch/record/1313716>.
- [15] ALEPH, DELPHI, L3, OPAL Collaborations, and LEP Working Group for Higgs Boson Searches, Phys. Lett. B 565 (2003) 61, arXiv:hep-ex/0306033, [http://dx.doi.org/10.1016/S0370-2693\(03\)00614-2](http://dx.doi.org/10.1016/S0370-2693(03)00614-2).
- [16] CDF and D0 Collaborations, Phys. Rev. Lett. 104 (2010) 061802, <http://dx.doi.org/10.1103/PhysRevLett.104.061802>.
- [17] CDF Collaboration, Phys. Rev. Lett. (2012), submitted for publication, arXiv:1207.1707.
- [18] CDF and D0 Collaborations, Phys. Rev. Lett. 109 (2012) 071804, <http://dx.doi.org/10.1103/PhysRevLett.109.071804>.
- [19] D0 Collaboration, Phys. Rev. Lett. (2012), submitted for publication, arXiv:1207.6631.
- [20] L. Evans, P. Bryant (Eds.), LHC Machine, JINST 3 (2008) S08001, <http://dx.doi.org/10.1088/1748-0221/3/08/S08001>.
- [21] S. Chatrchyan, et al., Phys. Lett. B 710 (2012) 26, arXiv:1202.1488, <http://dx.doi.org/10.1016/j.physletb.2012.02.064>.
- [22] G. Aad, et al., Phys. Rev. D 86 (2012) 032003, arXiv:1207.0319, <http://dx.doi.org/10.1103/PhysRevD.86.032003>.
- [23] LHC Higgs Cross Section Working Group, in: S. Dittmaier, C. Mariotti, G. Passarino, R. Tanaka (Eds.), Handbook of LHC Higgs Cross Sections: 1. Inclusive Observables, CERN, Geneva, 2011, arXiv:1101.0593, <http://cdsweb.cern.ch/record/1318996>.
- [24] S. Chatrchyan, et al., Phys. Lett. B 710 (2012) 403, arXiv:1202.1487, <http://dx.doi.org/10.1016/j.physletb.2012.03.003>.
- [25] S. Chatrchyan, et al., Phys. Rev. Lett. 108 (2012) 111804, arXiv:1202.1997, <http://dx.doi.org/10.1103/PhysRevLett.108.111804>.
- [26] S. Chatrchyan, et al., Phys. Lett. B 710 (2012) 91, arXiv:1202.1489, <http://dx.doi.org/10.1016/j.physletb.2012.02.076>.
- [27] S. Chatrchyan, et al., Phys. Lett. B 713 (2012) 68, arXiv:1202.4083, <http://dx.doi.org/10.1016/j.physletb.2012.05.028>.
- [28] S. Chatrchyan, et al., Phys. Lett. B 710 (2012) 284, arXiv:1202.4195, <http://dx.doi.org/10.1016/j.physletb.2012.02.085>.
- [29] M. Della Negra, et al., in: G. Jarlskog, D. Rein (Eds.), Proceedings of the Large Hadron Collider Workshop, Aachen, Germany, 1990, p. 467, CERN 90-10-V-3/ECFA 90-133-V-3, <http://cdsweb.cern.ch/record/215299/files/CERN-90-10-V-3.pdf>.
- [30] M. Della Negra, et al., Letter of intent by the CMS Collaboration for a general purpose detector at the LHC, Tech. Rep. CERN-LHCC-92-03, CERN-LHCC-I-1, CERN, 1992, <https://cdsweb.cern.ch/record/290808>.
- [31] N. Ellis, T.S. Virdee, Ann. Rev. Nucl. Part. Sci. 44 (1994) 609, <http://dx.doi.org/10.1146/annurev.ns.44.120194.003141>.
- [32] S. Chatrchyan, et al., The CMS experiment at the CERN LHC, JINST 3 (2008) S08004, <http://dx.doi.org/10.1088/1748-0221/3/08/S08004>.
- [33] CMS Collaboration, b-jet identification in the CMS experiment, CMS Physics Analysis Summary CMS-PAS-BTV-11-004, 2012, <https://cdsweb.cern.ch/record/1427247>.
- [34] V. Khachatryan, et al., Phys. Rev. D 83 (2011) 112004, arXiv:1012.5545, <http://dx.doi.org/10.1103/PhysRevD.83.112004>.
- [35] CMS Collaboration, Particle-flow event reconstruction in CMS and performance for jets, taus, and E_{miss} , CMS Physics Analysis Summary CMS-PAS-PFT-09-001, 2009, <http://cdsweb.cern.ch/record/1194487>.

- [36] CMS Collaboration, Commissioning of the particle-flow event reconstruction with the first LHC collisions recorded in the CMS detector, CMS Physics Analysis Summary CMS-PAS-PFT-10-001, 2010, <http://cdsweb.cern.ch/record/1247373>.
- [37] M. Cacciari, G.P. Salam, G. Soyez, JHEP 0804 (2008) 063, <http://dx.doi.org/10.1088/1126-6708/2008/04/063>.
- [38] M. Cacciari, G.P. Salam, Phys. Lett. B 659 (2008) 119, <http://dx.doi.org/10.1016/j.physletb.2007.09.077>.
- [39] M. Cacciari, G.P. Salam, G. Soyez, JHEP 0804 (2008) 005, <http://dx.doi.org/10.1088/1126-6708/2008/04/005>.
- [40] M. Cacciari, G.P. Salam, G. Soyez, Eur. Phys. J. C 72 (2012) 1896, arXiv:1111.6097, <http://dx.doi.org/10.1140/epjc/s10052-012-1896-2>.
- [41] S. Chatrchyan, et al., JINST 6 (2011) 11002, arXiv:1107.4277, <http://dx.doi.org/10.1088/1748-0221/6/11/P11002>.
- [42] S. Chatrchyan, et al., JINST 6 (2011) 9001, arXiv:1106.5048, <http://dx.doi.org/10.1088/1748-0221/6/09/P09001>.
- [43] CMS Collaboration, Commissioning of the particle-flow event reconstruction with leptons from J/ψ and W decays at 7 TeV, CMS Physics Analysis Summary CMS-PAS-PFT-10-003, 2010, <http://cdsweb.cern.ch/record/1279347>.
- [44] CMS Collaboration, Electron reconstruction and identification at $\sqrt{s} = 7$ TeV, CMS Physics Analysis Summary CMS-PAS-EGM-10-004, 2010, <http://cdsweb.cern.ch/record/1299116>.
- [45] S. Baffioni, C. Charlot, F. Ferri, D. Futyan, P. Meridiani, et al., Eur. Phys. J. C 49 (2007) 1099, <http://dx.doi.org/10.1140/epjc/s10052-006-0175-5>.
- [46] W. Adam, R. Fruhwirth, A. Strandlie, T. Todorov, J. Phys. G 31 (2005) N9, <http://dx.doi.org/10.1088/0954-3889/31/9/N01>.
- [47] CMS Collaboration, Absolute calibration of the luminosity measurement at CMS: Winter 2012 update, CMS Physics Analysis Summary CMS-PAS-SMP-12-008, 2012, <https://cdsweb.cern.ch/record/1434360>.
- [48] S. van der Meer, Calibration of the effective beam height in the ISR, Tech. Rep. CERN-ISR-PO-68-31, CERN, Geneva, 1968, <https://cdsweb.cern.ch/record/296752>.
- [49] J.R. Ellis, M.K. Gaillard, D.V. Nanopoulos, Nucl. Phys. B 106 (1976) 292, [http://dx.doi.org/10.1016/0550-3213\(76\)90382-5](http://dx.doi.org/10.1016/0550-3213(76)90382-5).
- [50] H.M. Georgi, S.L. Glashow, M.E. Machacek, D.V. Nanopoulos, Phys. Rev. Lett. 40 (1978) 692, <http://dx.doi.org/10.1103/PhysRevLett.40.692>.
- [51] S.L. Glashow, D.V. Nanopoulos, A. Yildiz, Phys. Rev. D 18 (1978) 1724, <http://dx.doi.org/10.1103/PhysRevD.18.1724>.
- [52] R.N. Cahn, S.D. Ellis, R. Kleiss, W.J. Stirling, Phys. Rev. D 35 (1987) 1626, <http://dx.doi.org/10.1103/PhysRevD.35.1626>.
- [53] J.F. Gunion, G.L. Kane, J. Wudka, Nucl. Phys. B 299 (1988) 231, [http://dx.doi.org/10.1016/0550-3213\(88\)90284-2](http://dx.doi.org/10.1016/0550-3213(88)90284-2).
- [54] D.L. Rainwater, D. Zeppenfeld, JHEP 9712 (1997) 005, arXiv:hep-ph/9712271, <http://dx.doi.org/10.1088/1126-6708/1997/12/005>.
- [55] D.L. Rainwater, D. Zeppenfeld, K. Hagiwara, Phys. Rev. D 59 (1998) 014037, arXiv:hep-ph/9808468, <http://dx.doi.org/10.1103/PhysRevD.59.014037>.
- [56] D.L. Rainwater, D. Zeppenfeld, Phys. Rev. D 60 (1999) 113004, arXiv:hep-ph/9906218, <http://dx.doi.org/10.1103/PhysRevD.60.113004>, also Erratum, <http://dx.doi.org/10.1103/PhysRevD.61.099901>.
- [57] A. Djouadi, M. Spira, P.M. Zerwas, Phys. Lett. B 264 (1991) 440, [http://dx.doi.org/10.1016/0370-2693\(91\)90375-Z](http://dx.doi.org/10.1016/0370-2693(91)90375-Z).
- [58] S. Dawson, Nucl. Phys. B 359 (1991) 283, [http://dx.doi.org/10.1016/0550-3213\(91\)90061-2](http://dx.doi.org/10.1016/0550-3213(91)90061-2).
- [59] M. Spira, A. Djouadi, D. Graudenz, P.M. Zerwas, Nucl. Phys. B 453 (1995) 17, arXiv:hep-ph/9504378, [http://dx.doi.org/10.1016/0550-3213\(95\)00379-7](http://dx.doi.org/10.1016/0550-3213(95)00379-7).
- [60] R.V. Harlander, W.B. Kilgore, Phys. Rev. Lett. 88 (2002) 201801, arXiv:hep-ph/0201206, <http://dx.doi.org/10.1103/PhysRevLett.88.201801>.
- [61] C. Anastasiou, K. Melnikov, Nucl. Phys. B 646 (2002) 220, arXiv:hep-ph/0207004, [http://dx.doi.org/10.1016/S0550-3213\(02\)00837-4](http://dx.doi.org/10.1016/S0550-3213(02)00837-4).
- [62] V. Ravindran, J. Smith, W.L. van Neerven, Nucl. Phys. B 665 (2003) 325, arXiv:hep-ph/0302135, [http://dx.doi.org/10.1016/S0550-3213\(03\)00457-7](http://dx.doi.org/10.1016/S0550-3213(03)00457-7).
- [63] S. Catani, D. de Florian, M. Grazzini, P. Nason, JHEP 0307 (2003) 028, <http://dx.doi.org/10.1088/1126-6708/2003/07/028>.
- [64] U. Aglietti, R. Bonciani, G. Degrassi, A. Vicini, Phys. Lett. B 595 (2004) 432, arXiv:hep-ph/0404071, <http://dx.doi.org/10.1016/j.physletb.2004.06.063>.
- [65] G. Degrassi, F. Maltoni, Phys. Lett. B 600 (2004) 255, arXiv:hep-ph/0407249, <http://dx.doi.org/10.1016/j.physletb.2004.09.008>.
- [66] S. Actis, G. Passarino, C. Sturm, S. Uccirati, Phys. Lett. B 670 (2008) 12, arXiv:0809.1301, <http://dx.doi.org/10.1016/j.physletb.2008.10.018>.
- [67] C. Anastasiou, R. Boughezal, F. Petriello, JHEP 0904 (2009) 003, arXiv:0811.3458, <http://dx.doi.org/10.1088/1126-6708/2009/04/003>.
- [68] D. de Florian, M. Grazzini, Phys. Lett. B 674 (2009) 291, arXiv:0901.2427, <http://dx.doi.org/10.1016/j.physletb.2009.03.033>.
- [69] J. Baglio, A. Djouadi, JHEP 1103 (2011) 055, arXiv:1012.0530, [http://dx.doi.org/10.1007/JHEP03\(2011\)055](http://dx.doi.org/10.1007/JHEP03(2011)055).
- [70] D. de Florian, M. Grazzini, Higgs production at the LHC: updated cross sections at $\sqrt{s} = 8$ TeV, arXiv:1206.4133, 2012.
- [71] G. Bozzi, S. Catani, D. de Florian, M. Grazzini, Nucl. Phys. B 737 (2006) 73, arXiv:hep-ph/0508068, <http://dx.doi.org/10.1016/j.nuclphysb.2005.12.022>.
- [72] D. de Florian, G. Ferrera, M. Grazzini, D. Tommasini, JHEP 1111 (2011) 064, [http://dx.doi.org/10.1007/JHEP11\(2011\)064](http://dx.doi.org/10.1007/JHEP11(2011)064).
- [73] G. Passarino, C. Sturm, S. Uccirati, Nucl. Phys. B 834 (2010) 77, arXiv:1001.3360, <http://dx.doi.org/10.1016/j.nuclphysb.2010.03.013>.
- [74] I.W. Stewart, F.J. Tackmann, Phys. Rev. D 85 (2012) 034011, arXiv:1107.2117, <http://dx.doi.org/10.1103/PhysRevD.85.034011>.
- [75] A. Djouadi, J. Kalinowski, M. Spira, Comput. Phys. Commun. 108 (1998) 56, arXiv:hep-ph/9704448, [http://dx.doi.org/10.1016/S0010-4655\(97\)00123-9](http://dx.doi.org/10.1016/S0010-4655(97)00123-9).
- [76] A. Djouadi, J. Kalinowski, M. Muhlleitner, M. Spira, in: The Les Houches 2009 workshop on TeV colliders: The tools and Monte Carlo working group summary report, arXiv:1003.1643, 2010.
- [77] A. Bredenstein, A. Denner, S. Dittmaier, M.M. Weber, Phys. Rev. D 74 (2006) 013004, arXiv:hep-ph/0604011, <http://dx.doi.org/10.1103/PhysRevD.74.013004>.
- [78] A. Bredenstein, A. Denner, S. Dittmaier, M.M. Weber, JHEP 0702 (2007) 080, arXiv:hep-ph/0611234, <http://dx.doi.org/10.1088/1126-6708/2007/02/080>.
- [79] S. Actis, G. Passarino, C. Sturm, S. Uccirati, Nucl. Phys. B 811 (2009) 182, arXiv:0809.3667, <http://dx.doi.org/10.1016/j.nuclphysb.2008.11.024>.
- [80] A. Denner, S. Heinemeyer, I. Puljak, D. Rebuszi, M. Spira, Eur. Phys. J. C 71 (2011) 1753, arXiv:1107.5909, <http://dx.doi.org/10.1140/epjc/s10052-011-1753-8>.
- [81] M. Ciccolini, A. Denner, S. Dittmaier, Phys. Rev. Lett. 99 (2007) 161803, arXiv:0707.0381, <http://dx.doi.org/10.1103/PhysRevLett.99.161803>.
- [82] M. Ciccolini, A. Denner, S. Dittmaier, Phys. Rev. D 77 (2008) 013002, arXiv:0710.4749, <http://dx.doi.org/10.1103/PhysRevD.77.013002>.
- [83] T. Figy, C. Oleari, D. Zeppenfeld, Phys. Rev. D 68 (2003) 073005, arXiv:hep-ph/0306109, <http://dx.doi.org/10.1103/PhysRevD.68.073005>.
- [84] K. Arnold, M. Bahr, G. Bozzi, F. Campanario, C. Englert, et al., Comput. Phys. Commun. 180 (2009) 1661, arXiv:0811.4559, <http://dx.doi.org/10.1016/j.cpc.2009.03.006>.
- [85] P. Bolzoni, F. Maltoni, S.-O. Moch, M. Zaro, Phys. Rev. Lett. 105 (2010) 011801, arXiv:1003.4451, <http://dx.doi.org/10.1103/PhysRevLett.105.011801>.
- [86] T. Han, S. Willenbrock, Phys. Lett. B 273 (1991) 167, [http://dx.doi.org/10.1016/0370-2693\(91\)90572-8](http://dx.doi.org/10.1016/0370-2693(91)90572-8).
- [87] O. Brein, A. Djouadi, R. Harlander, Phys. Lett. B 579 (2004) 149, arXiv:hep-ph/0307206, <http://dx.doi.org/10.1016/j.physletb.2003.10.112>.
- [88] M.L. Ciccolini, S. Dittmaier, M. Krämer, Phys. Rev. D 68 (2003) 073003, arXiv:hep-ph/0306234, <http://dx.doi.org/10.1103/PhysRevD.68.073003>.
- [89] R. Hamberg, W.L. van Neerven, T. Matsuura, Nucl. Phys. B 359 (1991) 343, [http://dx.doi.org/10.1016/0550-3213\(91\)90064-5](http://dx.doi.org/10.1016/0550-3213(91)90064-5).
- [90] A. Denner, S. Dittmaier, S. Kallweit, A. Muck, EW corrections to Higgs strahlung at the Tevatron and the LHC with HAWK, arXiv:1112.5258, 2011.
- [91] G. Ferrera, M. Grazzini, F. Tramontano, Phys. Rev. Lett. 107 (2011) 152003, arXiv:1107.1164, <http://dx.doi.org/10.1103/PhysRevLett.107.152003>.
- [92] W. Beenakker, S. Dittmaier, M. Kramer, B. Plumper, M. Spira, et al., Phys. Rev. Lett. 87 (2001) 201805, arXiv:hep-ph/0107081, <http://dx.doi.org/10.1103/PhysRevLett.87.201805>.
- [93] W. Beenakker, S. Dittmaier, M. Kramer, B. Plumper, M. Spira, et al., Nucl. Phys. B 653 (2003) 151, arXiv:hep-ph/0211352, [http://dx.doi.org/10.1016/S0550-3213\(03\)00044-0](http://dx.doi.org/10.1016/S0550-3213(03)00044-0).
- [94] S. Dawson, L.H. Orr, L. Reina, D. Wackerth, Phys. Rev. D 67 (2003) 071503, arXiv:hep-ph/0211438, <http://dx.doi.org/10.1103/PhysRevD.67.071503>.
- [95] S. Dawson, C. Jackson, L.H. Orr, L. Reina, D. Wackerth, Phys. Rev. D 68 (2003) 034022, arXiv:hep-ph/0305087, <http://dx.doi.org/10.1103/PhysRevD.68.034022>.
- [96] M. Botje, J. Butterworth, A. Cooper-Sarkar, A. de Roeck, J. Feltesse, et al., The PDF4LHC Working Group interim recommendations, arXiv:1101.0538, 2011.
- [97] S. Alekhin, S. Alioli, R.D. Ball, V. Bertone, J. Blumlein, et al., The PDF4LHC Working Group interim report, arXiv:1101.0536, 2011.
- [98] H.-L. Lai, M. Guzzi, J. Huston, Z. Li, P.M. Nadolsky, et al., Phys. Rev. D 82 (2010) 074024, arXiv:1007.2241, <http://dx.doi.org/10.1103/PhysRevD.82.074024>.
- [99] A.D. Martin, W.J. Stirling, R.S. Thorne, G. Watt, Eur. Phys. J. C 63 (2009) 189, arXiv:0901.0002, <http://dx.doi.org/10.1140/epjc/s10052-009-1072-5>.
- [100] R.D. Ball, et al., Nucl. Phys. B 849 (2011) 296, arXiv:1101.1300, <http://dx.doi.org/10.1016/j.nuclphysb.2011.03.021>.
- [101] C. Anastasiou, S. Buehler, F. Herzog, A. Lazopoulos, JHEP 1204 (2012) 004, arXiv:1202.3638, [http://dx.doi.org/10.1007/JHEP04\(2012\)004](http://dx.doi.org/10.1007/JHEP04(2012)004).
- [102] LHC Higgs Cross Section Working Group, in: S. Dittmaier, C. Mariotti, G. Passarino, R. Tanaka (Eds.), Handbook of LHC Higgs Cross Sections: 2. Differential Distributions, CERN, Geneva, 2012, arXiv:1201.3084.
- [103] S. Agostinelli, et al., Nucl. Instrum. Meth. A 506 (2003) 250, [http://dx.doi.org/10.1016/S0168-9002\(03\)01368-8](http://dx.doi.org/10.1016/S0168-9002(03)01368-8).
- [104] S. Alioli, P. Nason, C. Oleari, E. Re, JHEP 0904 (2009) 002, <http://dx.doi.org/10.1088/1126-6708/2009/04/002>.
- [105] P. Nason, C. Oleari, JHEP 1002 (2010) 037, [http://dx.doi.org/10.1007/JHEP02\(2010\)037](http://dx.doi.org/10.1007/JHEP02(2010)037).
- [106] T. Sjöstrand, S. Mrenna, P.Z. Skands, JHEP 0605 (2006) 026, <http://dx.doi.org/10.1088/1126-6708/2006/05/026>.
- [107] G. Bozzi, S. Catani, D. de Florian, M. Grazzini, Phys. Lett. B 564 (2003) 65, [http://dx.doi.org/10.1016/S0370-2693\(03\)00656-7](http://dx.doi.org/10.1016/S0370-2693(03)00656-7).

- [108] C. Anastasiou, K. Melnikov, F. Petriello, Nucl. Phys. B 724 (2005) 197, <http://dx.doi.org/10.1016/j.nuclphysb.2005.06.036>.
- [109] C. Anastasiou, S. Bucherer, Z. Kunszt, JHEP 0910 (2009) 068, <http://dx.doi.org/10.1088/1126-6708/2009/10/068>.
- [110] S. Gieseke, D. Grellscheid, K. Hamilton, A. Ribon, P. Richardson, et al., Herwig++ 2.0 Release Note, arXiv:hep-ph/0609306, 2006.
- [111] J. Alwall, P. Demin, S. de Visscher, R. Frederix, M. Herquet, et al., JHEP 0709 (2007) 028, arXiv:0706.2334, <http://dx.doi.org/10.1088/1126-6708/2007/09/028>.
- [112] ATLAS and CMS Collaborations, LHC Higgs Combination Group, Procedure for the LHC Higgs boson search combination in Summer 2011, Tech. Rep. ATL-PHYS-PUB 2011-11, CMS NOTE 2011/005, 2011, <http://cdsweb.cern.ch/record/1379837>.
- [113] T. Junk, Nucl. Instrum. Meth. A 434 (1999) 435, [http://dx.doi.org/10.1016/S0168-9002\(99\)00498-2](http://dx.doi.org/10.1016/S0168-9002(99)00498-2).
- [114] A.L. Read, J. Phys. G 28 (2002) 2693, <http://dx.doi.org/10.1088/0954-3899/28/10/313>.
- [115] E. Gross, O. Vitells, Eur. Phys. J. C 70 (2010) 525, arXiv:1005.1891, <http://dx.doi.org/10.1140/epjc/s10052-010-1470-8>.
- [116] G. Cowan, K. Cranmer, E. Gross, O. Vitells, Eur. Phys. J. C 71 (2011) 1554, arXiv:1007.1727, <http://dx.doi.org/10.1140/epjc/s10052-011-1554-0>.
- [117] L. Moneta, K. Belasco, K. Cranmer, S. Kreiss, et al., in: 13th Int. Workshop on Advanced Computing and Analysis Techniques in Physics Research (ACAT2010), 2010, PoS ACAT:057, arXiv:1009.1003, http://pos.sissa.it/archive/conferences/093/057/ACAT2010_057.pdf.
- [118] C.J. Seez, T.S. Virdee, L. Di Lella, R.H. Kleiss, Z. Kunszt, W.J. Stirling, in: G. Jarlskog, D. Rein (Eds.), Proceedings of the Large Hadron Collider Workshop, Aachen, Germany, 1990, p. 474, CERN 90-10-V-2/ECFA 90-133-V-2, <http://cdsweb.cern.ch/record/220524>.
- [119] B.P. Roe, H.-J. Yang, J. Zhu, Y. Liu, I. Stancu, et al., Nucl. Instrum. Meth. A 543 (2005) 577, <http://dx.doi.org/10.1016/j.nima.2004.12.018>.
- [120] H. Voss, A. Höcker, J. Stelzer, F. Tegenfeldt, in: XI Int. Workshop on Advanced Computing and Analysis Techniques in Physics Research, 2007, PoS ACAT:040, arXiv:physics/0703039, http://pos.sissa.it/archive/conferences/050/040/ACAT_040.pdf.
- [121] R.J. Barlow, J. Comp. Phys. 72 (1987) 202, [http://dx.doi.org/10.1016/0021-9991\(87\)90078-7](http://dx.doi.org/10.1016/0021-9991(87)90078-7).
- [122] M. Della Negra, D. Froidevaux, K. Jakobs, R. Kinnunen, R. Kleiss, A. Nisati, T. Sjöstrand, in: G. Jarlskog, D. Rein (Eds.), Proceedings of the Large Hadron Collider Workshop, Aachen, Germany, 1990, p. 509, CERN 90-10-V-2/ECFA 90-133-V-2, <http://cdsweb.cern.ch/record/215298>.
- [123] N. Cabibbo, A. Maksymowicz, Phys. Rev. B 137 (1965) 438, <http://dx.doi.org/10.1103/PhysRev.137.B438>, also Erratum, <http://dx.doi.org/10.1103/PhysRev.168.1926>.
- [124] Y. Gao, A.V. Gritsan, Z. Guo, K. Melnikov, M. Schulze, et al., Phys. Rev. D 81 (2010) 075022, arXiv:1001.3396, <http://dx.doi.org/10.1103/PhysRevD.81.075022>.
- [125] A. De Rijula, J. Lykken, M. Pierini, C. Rogan, M. Spiropulu, Phys. Rev. D 82 (2010) 013003, arXiv:1001.5300, <http://dx.doi.org/10.1103/PhysRevD.82.013003>.
- [126] S. Chatrchyan, et al., JHEP 1204 (2012) 036, arXiv:1202.1416, [http://dx.doi.org/10.1007/JHEP04\(2012\)036](http://dx.doi.org/10.1007/JHEP04(2012)036).
- [127] S.Y. Choi, D.J. Miller, M.M. Muhlleitner, P.M. Zerwas, Phys. Lett. B 553 (2003) 61, arXiv:hep-ph/0210077, [http://dx.doi.org/10.1016/S0370-2693\(02\)03191-X](http://dx.doi.org/10.1016/S0370-2693(02)03191-X).
- [128] S. Chatrchyan, et al., JHEP 1110 (2011) 132, [http://dx.doi.org/10.1007/JHEP10\(2011\)132](http://dx.doi.org/10.1007/JHEP10(2011)132).
- [129] V.D. Barger, G. Bhattacharya, T. Han, B.A. Kniehl, Phys. Rev. D 43 (1991) 779, <http://dx.doi.org/10.1103/PhysRevD.43.779>.
- [130] M. Dittmar, H.K. Dreiner, Phys. Rev. D 55 (1997) 167, arXiv:hep-ph/9608317, <http://dx.doi.org/10.1103/PhysRevD.55.167>.
- [131] S. Chatrchyan, et al., JINST 7 (2011) P01001, <http://dx.doi.org/10.1088/1748-0221/7/01/P01001>.
- [132] S. Chatrchyan, et al., Phys. Rev. Lett. 106 (2011) 231801, arXiv:1104.1619, <http://dx.doi.org/10.1103/PhysRevLett.106.231801>.
- [133] A. Denner, S. Dittmaier, S. Kallweit, A. Muck, JHEP 1203 (2012) 075, arXiv:1112.5142, [http://dx.doi.org/10.1007/JHEP03\(2012\)075](http://dx.doi.org/10.1007/JHEP03(2012)075).
- [134] J. Gallicchio, M.D. Schwartz, Phys. Rev. Lett. 105 (2010) 022001, arXiv:1001.5027, <http://dx.doi.org/10.1103/PhysRevLett.105.022001>.
- [135] L.D. Landau, Dokl. Akad. Nauk 60 (1948) 207.
- [136] C.N. Yang, Phys. Rev. 77 (1950) 242, <http://dx.doi.org/10.1103/PhysRev.77.242>.

CMS Collaboration

S. Chatrchyan, V. Khachatryan, A.M. Sirunyan, A. Tumasyan

Yerevan Physics Institute, Yerevan, Armenia

W. Adam, E. Aguilo, T. Bergauer, M. Dragicevic, J. Erö, C. Fabjan¹, M. Friedl, R. Frühwirth¹, V.M. Ghete, J. Hammer, M. Hoch, N. Hörmann, J. Hrubec, M. Jeitler¹, W. Kiesenhofer, V. Knünz, M. Krammer¹, I. Krätschmer, D. Liko, W. Majerotto, I. Mikulec, M. Pernicka[†], B. Rahbaran, C. Rohringer, H. Rohringer, R. Schöfbeck, J. Strauss, F. Szoncsó, A. Taurok, W. Waltenberger, G. Walzel, E. Widl, C.-E. Wulz¹

Institut für Hochenergiephysik der OeAW, Wien, Austria

V. Chekhovsky, I. Emeliantchik, A. Litomin, V. Makarenko, V. Mossolov, N. Shumeiko, A. Solin, R. Stefanovitch, J. Suarez Gonzalez

National Centre for Particle and High Energy Physics, Minsk, Belarus

A. Fedorov, M. Korzhik, O. Missevitch, R. Zuyevski

Research Institute for Nuclear Problems, Minsk, Belarus

M. Bansal, S. Bansal, W. Beaumont, T. Cornelis, E.A. De Wolf, D. Druzhkin, X. Janssen, S. Luyckx, L. Mucibello, S. Ochesanu, B. Roland, R. Rougny, M. Selvaggi, Z. Staykova, H. Van Haevermaet, P. Van Mechelen, N. Van Remortel, A. Van Spilbeeck

Universiteit Antwerpen, Antwerpen, Belgium

F. Blekman, S. Blyweert, J. D'Hondt, O. Devroede, R. Gonzalez Suarez, R. Goorens, A. Kalogeropoulos, M. Maes, A. Olbrechts, S. Tavernier, W. Van Doninck, L. Van Lancker, P. Van Mulders, G.P. Van Onsem, I. Villella

Vrije Universiteit Brussel, Brussel, Belgium

B. Clerbaux, G. De Lentdecker, V. Dero, J.P. Dewulf, A.P.R. Gay, T. Hreus, A. Léonard, P.E. Marage, A. Mohammadi, T. Reis, S. Rugovac, L. Thomas, C. Vander Velde, P. Vanlaer, J. Wang, J. Wickens

Université Libre de Bruxelles, Bruxelles, Belgium

V. Adler, K. Beernaert, A. Cimmino, S. Costantini, G. Garcia, M. Grunewald, B. Klein, J. Lellouch, A. Marinov, J. McCartin, A.A. Ocampo Rios, D. Ryckbosch, N. Strobbe, F. Thyssen, M. Tytgat, S. Walsh, E. Yazgan, N. Zaganidis

Ghent University, Ghent, Belgium

S. Basegmez, G. Bruno, R. Castello, L. Ceard, J. De Favereau De Jeneret, C. Delaere, P. Demin, T. du Pree, D. Favart, L. Forthomme, A. Giammanco², G. Grégoire, J. Hollar, V. Lemaitre, J. Liao, O. Militaru, C. Nuttens, D. Pagano, A. Pin, K. Piotrkowski, N. Schul, J.M. Vizan Garcia

Université Catholique de Louvain, Louvain-la-Neuve, Belgium

N. Belyi, T. Caeberts, E. Daubie, G.H. Hammad

Université de Mons, Mons, Belgium

G.A. Alves, L. Brito, M. Correa Martin Junior, T. Martins, M.E. Pol, M.H.G. Souza

Centro Brasileiro de Pesquisas Fisicas, Rio de Janeiro, Brazil

W.L. Aldá Júnior, W. Carvalho, A. Custódio, E.M. Da Costa, D. De Jesus Damiao, C. De Oliveira Martins, S. Fonseca De Souza, D. Matos Figueiredo, L. Mundim, H. Nogima, V. Oguri, W.L. Prado Da Silva, A. Santoro, A. Sznajder, A. Vilela Pereira

Universidade do Estado do Rio de Janeiro, Rio de Janeiro, Brazil

T.S. Anjos³, C.A. Bernardes³, F.A. Dias⁴, T.R. Fernandez Perez Tomei, E.M. Gregores³, R.L. Iope, C. Lagana, S.M. Lietti, F. Marinho, P.G. Mercadante³, S.F. Novaes, Sandra S. Padula

Instituto de Fisica Teorica, Universidade Estadual Paulista, Sao Paulo, Brazil

L. Dimitrov, V. Genchev⁵, P. Iaydjiev⁵, S. Piperov, M. Rodozov, S. Stoykova, G. Sultanov, V. Tcholakov, R. Trayanov, I. Vankov, M. Vutova

Institute for Nuclear Research and Nuclear Energy, Sofia, Bulgaria

C. Roumenin, D. Uzunova, R. Zahariev

Institute of System Engineering and Robotics, Sofia, Bulgaria

A. Dimitrov, R. Hadjiiska, V. Kozhuharov, L. Litov, B. Pavlov, P. Petkov

University of Sofia, Sofia, Bulgaria

J.G. Bian, G.M. Chen, H.S. Chen, K.L. He, C.H. Jiang, W.G. Li, D. Liang, S. Liang, X. Meng, G. Sun, H.S. Sun, J. Tao, J. Wang, X. Wang, Z. Wang, H. Xiao, M. Xu, M. Yang, J. Zang, X. Zhang, Z. Zhang, Z. Zhang, W.R. Zhao, Z. Zhu

Institute of High Energy Physics, Beijing, China

C. Asawatangtrakuldee, Y. Ban, J. Cai, S. Guo, Y. Guo, W. Li, H.T. Liu, S. Liu, Y. Mao, S.J. Qian, H. Teng, D. Wang, Y.L. Ye, L. Zhang, B. Zhu, W. Zou

State Key Lab. of Nucl. Phys. and Tech., Peking University, Beijing, China

C. Avila, J.P. Gomez, B. Gomez Moreno, A.F. Osorio Oliveros, J.C. Sanabria

Universidad de Los Andes, Bogota, Colombia

N. Godinovic, D. Lelas, R. Plestina⁶, D. Polic, I. Puljak⁵

Technical University of Split, Split, Croatia

Z. Antunovic, M. Kovac

University of Split, Split, Croatia

V. Brigljevic, S. Duric, K. Kadija, J. Luetic, S. Morovic

Institute Rudjer Boskovic, Zagreb, Croatia

A. Attikis, M. Galanti, G. Mavromanolakis, J. Mousa, C. Nicolaou, F. Ptochos, P.A. Razis

University of Cyprus, Nicosia, Cyprus

M. Finger, M. Finger Jr.

Charles University, Prague, Czech Republic

A. Aly, Y. Assran⁷, A. Awad, S. Elgammal⁸, A. Ellithi Kamel⁹, S. Khalil⁸, M.A. Mahmoud¹⁰, A. Mahrous, A. Radi^{11,12}

Academy of Scientific Research and Technology of the Arab Republic of Egypt, Egyptian Network of High Energy Physics, Cairo, Egypt

A. Hektor, M. Kadastik, K. Kannike, M. Müntel, M. Raidal, L. Rebane, A. Strumia, A. Tiko

National Institute of Chemical Physics and Biophysics, Tallinn, Estonia

P. Eerola, G. Fedi, M. Voutilainen

Department of Physics, University of Helsinki, Helsinki, Finland

E. Anttila, J. Härkönen, A. Heikkinen, V. Karimäki, H.M. Katajisto, R. Kinnunen, M.J. Kortelainen, M. Kotamäki, T. Lampén, K. Lassila-Perini, S. Lehti, T. Lindén, P. Luukka, T. Mäenpää, T. Peltola, E. Tuominen, J. Tuominiemi, E. Tuovinen, D. Ungaro, T.P. Vanhala, L. Wendland

Helsinki Institute of Physics, Helsinki, Finland

K. Banzuzi, A. Karjalainen, A. Korpela, T. Tuuva

Lappeenranta University of Technology, Lappeenranta, Finland

M. Anfreville, M. Besancon, S. Choudhury, M. Dejardin, D. Denegri, B. Fabbro, J.L. Faure, F. Ferri, S. Ganjour, F.X. Gentit, A. Givernaud, P. Gras, G. Hamel de Monchenault, P. Jarry, F. Kircher, M.C. Lemaire, E. Locci, J. Malcles, I. Mandjavidze, A. Nayak, J.P. Pansart, J. Rander, J.M. Reymond, A. Rosowsky, I. Shreyber, M. Titov, P. Verrecchia

DSM/IRFU, CEA/Saclay, Gif-sur-Yvette, France

J. Badier, S. Baffioni, F. Beaudette, E. Becheva, L. Benhabib, L. Bianchini, M. Bluj¹³, C. Broutin, P. Busson, M. Cerutti, D. Chamont, C. Charlot, N. Daci, T. Dahms, M. Dalchenko, L. Dobrzynski, Y. Geerebaert, R. Granier de Cassagnac, M. Haguenaue, P. Hennion, G. Milleret, P. Miné, C. Mironov, I.N. Naranjo, M. Nguyen, C. Ochando, P. Paganini, T. Romanteau, D. Sabes, R. Salerno, A. Sartirana, Y. Sirois, C. Thiebaut, C. Veelken, A. Zabi

Laboratoire Leprince-Ringuet, Ecole Polytechnique, IN2P3–CNRS, Palaiseau, France

J.-L. Agram¹⁴, J. Andrea, A. Besson, D. Bloch, D. Bodin, J.-M. Brom, M. Cardaci, E.C. Chabert, C. Collard, E. Conte¹⁴, F. Drouhin¹⁴, C. Ferro, J.-C. Fontaine¹⁴, D. Gelé, U. Goerlach, C. Goetzmann, L. Gross, D. Huss, P. Juillot, E. Kieffer, A.-C. Le Bihan, J. Pansanel, Y. Patois, P. Van Hove

Institut Pluridisciplinaire Hubert Curien, Université de Strasbourg, Université de Haute Alsace Mulhouse, CNRS/IN2P3, Strasbourg, France

D. Boutigny, D. Mercier

Centre de Calcul de l'Institut National de Physique Nucleaire et de Physique des Particules, CNRS/IN2P3, Villeurbanne, France, Villeurbanne, France

G. Baulieu, S. Beauceron, N. Beaupere, M. Bedjidian, O. Bondu, G. Boudoul, S. Brochet, J. Chasserat, R. Chierici⁵, C. Combaret, D. Contardo, P. Depasse, H. El Mamouni, J. Fay, S. Gascon, N. Giraud, M. Gouzevitch, R. Haroutunian, B. Ille, T. Kurca, M. Lethuillier, N. Lumb, H. Mathez, L. Mirabito, S. Perries, L. Sgandurra, V. Sordini, Y. Tschudi, M. Vander Donckt, P. Verdier, S. Viret

Université de Lyon, Université Claude Bernard Lyon 1, CNRS-IN2P3, Institut de Physique Nucléaire de Lyon, Villeurbanne, France

V. Roinishvili, L. Rurua

E. Andronikashvili Institute of Physics, Academy of Science, Tbilisi, Georgia

N. Amaglobeli, I. Bagaturia, B. Chiladze, R. Kvatadze, D. Lomidze, R. Shanidze, Z. Tsamalaidze¹⁵

Institute of High Energy Physics and Informatization, Tbilisi State University, Tbilisi, Georgia

R. Adolphi, G. Anagnostou, C. Autermann, S. Beranek, R. Brauer, W. Braunschweig, B. Calpas, M. Edelhoff, L. Feld, N. Heracleous, O. Hindrichs, R. Jussen, W. Karpinski, K. Klein, K. Lübelmeyer, J. Merz, A. Ostapchuk, D. Pandoulas, A. Perieanu, F. Raupach, J. Sammet, S. Schael, D. Schmitz, A. Schultz von Dratzig, R. Siedling, D. Sprenger, H. Weber, B. Wittmer, M. Wlochal, V. Zhukov¹⁶

RWTH Aachen University, I. Physikalisches Institut, Aachen, Germany

M. Ata, P. Biallass, J. Caudron, E. Dietz-Laursonn, D. Duchardt, M. Erdmann, R. Fischer, A. Güth, T. Hebbeker, C. Heidemann, G. Hilgers, K. Hoepfner, C. Hof, T. Klimkovich, D. Klingebiel, P. Kreuzer, C. Magass, M. Merschmeyer, A. Meyer, M. Olschewski, P. Papacz, B. Philipps, H. Pieta, H. Reithler, S.A. Schmitz, L. Sonnenschein, M. Sowa, J. Steggemann, D. Teyssier, M. Weber

RWTH Aachen University, III. Physikalisches Institut A, Aachen, Germany

M. Bontenackels, V. Cherepanov, Y. Erdogan, G. Flügge, H. Geenen, M. Geisler, W. Haj Ahmad, F. Hoehle, B. Kargoll, T. Kress, Y. Kuessel, J. Lingemann⁵, A. Nowack, L. Perchalla, O. Pooth, P. Sauerland, A. Stahl, M.H. Zoeller

RWTH Aachen University, III. Physikalisches Institut B, Aachen, Germany

M. Aldaya Martin, J. Behr, W. Behrenhoff, U. Behrens, M. Bergholz¹⁷, A. Bethani, K. Borras, A. Burgmeier, A. Cakir, L. Calligaris, A. Campbell, E. Castro, F. Costanza, D. Dammann, C. Diez Pardos, G. Eckerlin, D. Eckstein, A. Flossdorf, G. Flucke, A. Geiser, I. Glushkov, P. Goettlicher, A. Grebenyuk, P. Gunnellini, S. Habib, J. Hauk, G. Hellwig, H. Jung, M. Kasemann, P. Katsas, C. Kleinwort, H. Kluge, A. Knutsson, M. Krämer, D. Krücker, E. Kuznetsova, W. Lange, B. Lewendel, W. Lohmann¹⁷, B. Lutz, R. Mankel, I. Marfin, M. Marienfeld, I.-A. Melzer-Pellmann, A.B. Meyer, J. Mnich, C. Muhl, A. Mussgiller, S. Naumann-Emme, O. Novgorodova, J. Olzem, A. Parenti, H. Perrey, A. Petrukhin, D. Pitzl, A. Raspereza, P.M. Ribeiro Cipriano, C. Riedl, E. Ron, C. Rosemann, M. Rosin, J. Salfeld-Nebgen, R. Schmidt¹⁷, T. Schoerner-Sadenius, N. Sen, A. Spiridonov, M. Stein, J. Tomaszewska, D. Volyanskyy, R. Walsh, C. Wissing, C. Youngman

Deutsches Elektronen-Synchrotron, Hamburg, Germany

V. Blobel, J. Draeger, H. Enderle, J. Erfle, U. Gebbert, M. Görner, T. Hermanns, R.S. Höing, K. Kaschube, G. Kaussen, H. Kirschenmann, R. Klanner, J. Lange, B. Mura, F. Nowak, T. Peiffer, N. Pietsch, D. Rathjens, C. Sander, H. Schettler, P. Schleper, E. Schlieckau, A. Schmidt, M. Schröder, T. Schum, M. Seidel, J. Sibille¹⁸, V. Sola, H. Stadie, G. Steinbrück, J. Thomsen, L. Vanelderden

University of Hamburg, Hamburg, Germany

C. Barth, J. Bauer, J. Berger, P. Blüm, C. Böser, V. Buege, Z.Y. Chen, S. Chowdhury, T. Chwalek, D. Daeuwel, W. De Boer, A. Descroix, A. Dierlamm, G. Dirkes, M. Fahrner, M. Feindt, U. Felzmann, M. Frey, A. Furgeri,

I. Gebauer, A. Gessler, J. Gruschke, M. Guthoff⁵, C. Hackstein, F. Hartmann, F. Hauler, T. Hauth⁵, S. Heier, S.M. Heindl, M. Heinrich, A. Heiss, H. Held, K.H. Hoffmann, S. Honc, U. Husemann, M. Imhof, C. Jung, S. Junghans, I. Katkov¹⁶, U. Kerzel, D. Knoblauch, J.R. Komaragiri, M. Kräber, T. Kuhr, T. Liamsuwan, P. Lobelle Pardo, D. Martschei, A. Menchikov, X. Mol, D. Mörmann, S. Mueller, Th. Müller, D. Neuberger, M.B. Neuland, M. Niegel, A. Nürnberg, O. Oberst, A. Oehler, T. Ortega Gomez, J. Ott, C. Piasecki, A. Poschlad, G. Quast, K. Rabbertz, F. Ratnikov, N. Ratnikova, M. Renz, S. Röcker, F. Roederer, A. Sabellek, C. Saout, A. Scheurer, D. Schieferdecker, P. Schieferdecker, F.-P. Schilling, M. Schmanau, G. Schott, W. Schwerdtfeger, H.J. Simonis, A. Skiba, F.M. Stober, A. Theel, W.H. Thümmel, D. Troendle, A. Trunov, R. Ulrich, J. Wagner-Kuhr, S. Wayand, M. Weber, T. Weiler, M. Zeise, E.B. Ziebarth, M. Zvada

Institut für Experimentelle Kernphysik, Karlsruhe, Germany

G. Daskalakis, T. Gerasis, S. Kesisoglou, A. Kyriakis, D. Loukas, I. Manolakos, A. Markou, C. Markou, C. Mavrommatis, E. Ntomari

Institute of Nuclear Physics "Demokritos", Aghia Paraskevi, Greece

L. Gouskos, A. Panagiotou, N. Saoulidou

University of Athens, Athens, Greece

I. Evangelou, C. Foudas, P. Kokkas, N. Manthos, I. Papadopoulos, V. Patras, F.A. Triantis

University of Ioánnina, Ioánnina, Greece

G. Bencze, C. Hajdu, P. Hidas, D. Horvath¹⁹, F. Sikler, V. Veszpremi, G. Vesztergombi²⁰, P. Zalan

KFKI Research Institute for Particle and Nuclear Physics, Budapest, Hungary

N. Beni, S. Czellar, A. Fenyvesi, J. Molnar, J. Palinkas, Z. Szillasi

Institute of Nuclear Research ATOMKI, Debrecen, Hungary

J. Karancsi, P. Raics, Z.L. Trocsanyi, B. Ujvari, G. Zilizi

University of Debrecen, Debrecen, Hungary

S.B. Beri, V. Bhandari, V. Bhatnagar, N. Dhingra, R. Gupta, M. Kaur, J.M. Kohli, M.Z. Mehta, N. Nishu, L.K. Saini, A. Sharma, J.B. Singh

Panjab University, Chandigarh, India

Ashok Kumar, Arun Kumar, S. Ahuja, A. Bhardwaj, S. Chatterji, B.C. Choudhary, P. Gupta, S. Malhotra, M. Naimuddin, K. Ranjan, V. Sharma, R.K. Shivpuri

University of Delhi, Delhi, India

S. Banerjee, S. Bhattacharya, S. Dutta, B. Gomber, Sa. Jain, Sh. Jain, R. Khurana, S. Sarkar, M. Sharan

Saha Institute of Nuclear Physics, Kolkata, India

A. Abdulsalam, R.K. Choudhury, D. Dutta, M. Ghodgaonkar, S. Kailas, S.K. Kataria, V. Kumar, P. Mehta, A.K. Mohanty⁵, L.M. Pant, P. Shukla, A. Topkar

Bhabha Atomic Research Centre, Mumbai, India

T. Aziz, S. Chendvankar, P.V. Deshpande, S.N. Ganguli, S. Ganguly, M. Guchait²¹, A. Gurtu²², M. Maity²³, K. Mazumdar, G.B. Mohanty, B. Parida, M.R. Patil, R. Raghavan, K. Sudhakar, N. Wickramage

Tata Institute of Fundamental Research – EHEP, Mumbai, India

B.S. Acharya, S. Banerjee, S. Bheesette, S. Dugad, S.D. Kalmani, M.R. Krishnaswamy, V.R. Lakkireddi, N.K. Mondal, V.S. Narasimham, N. Panyam, P. Verma

Tata Institute of Fundamental Research – HECR, Mumbai, India

F. Ardalan, H. Arfaei²⁴, H. Bakhshiansohi, S.M. Etesami²⁵, A. Fahim²⁴, M. Hashemi, A. Jafari, M. Khakzad, M. Mohammadi Najafabadi, S. Paktinat Mehdiabadi, B. Safarzadeh²⁶, M. Zeinali

Institute for Research in Fundamental Sciences (IPM), Tehran, Iran

M. Abbrescia^{a,b}, L. Barbone^{a,b}, C. Calabria^{a,b,5}, S.S. Chhibra^{a,b}, A. Colaleo^a, D. Creanza^{a,c}, N. De Filippis^{a,c,5}, M. De Palma^{a,b}, G. De Robertis^a, G. Donvito^a, L. Fiore^a, G. Iaselli^{a,c}, F. Loddo^a, G. Maggi^{a,c}, M. Maggi^a, N. Manna^{a,b}, B. Marangelli^{a,b}, S. My^{a,c}, S. Natali^{a,b}, S. Nuzzo^{a,b}, N. Pacifico^a, A. Pompili^{a,b}, G. Pugliese^{a,c}, A. Ranieri^a, F. Romano^{a,c}, G. Selvaggi^{a,b}, L. Silvestris^a, G. Singh^{a,b}, V. Spinoso^a, R. Venditti^{a,b}, P. Verwilligen, G. Zito^a

^a INFN Sezione di Bari, Bari, Italy

^b Università di Bari, Bari, Italy

^c Politecnico di Bari, Bari, Italy

G. Abbiendi^a, A.C. Benvenuti^a, D. Bonacorsi^{a,b}, S. Braibant-Giacomelli^{a,b}, L. Brigliadori^{a,b}, P. Capiluppi^{a,b}, A. Castro^{a,b}, F.R. Cavallo^a, M. Cuffiani^{a,b}, G.M. Dallavalle^a, F. Fabbri^a, A. Fanfani^{a,b}, D. Fasanella^{a,b}, P. Giacomelli^a, C. Grandi^a, L. Guiducci^{a,b}, S. Marcellini^a, G. Masetti^a, M. Meneghelli^{a,b,5}, A. Montanari^a, F.L. Navarria^{a,b}, F. Odorici^a, A. Perrotta^a, F. Primavera^{a,b}, A.M. Rossi^{a,b}, T. Rovelli^{a,b}, G.P. Siroli^{a,b}, R. Travaglini^{a,b}

^a INFN Sezione di Bologna, Bologna, Italy

^b Università di Bologna, Bologna, Italy

S. Albergo^{a,b}, G. Cappello^{a,b}, M. Chiorboli^{a,b}, S. Costa^{a,b}, F. Noto^a, R. Potenza^{a,b}, M.A. Saizu^{a,27}, A. Tricomi^{a,b}, C. Tuve^{a,b}

^a INFN Sezione di Catania, Catania, Italy

^b Università di Catania, Catania, Italy

G. Barbagli^a, V. Ciulli^{a,b}, C. Civinini^a, R. D'Alessandro^{a,b}, E. Focardi^{a,b}, S. Frosali^{a,b}, E. Gallo^a, C. Genta^a, S. Gozzi^{a,b}, M. Meschini^a, S. Paoletti^a, G. Parrini^a, R. Ranieri^a, G. Sguazzoni^a, A. Tropiano^{a,b}

^a INFN Sezione di Firenze, Firenze, Italy

^b Università di Firenze, Firenze, Italy

L. Benussi, S. Bianco, S. Colafranceschi²⁸, F. Fabbri, D. Piccolo

INFN Laboratori Nazionali di Frascati, Frascati, Italy

P. Fabbriatore, S. Farinon, M. Greco, R. Musenich, S. Tosi

INFN Sezione di Genova, Genova, Italy

A. Benaglia^{a,b}, L. Carbone^a, P. D'Angelo^a, F. De Guio^{a,b}, L. Di Matteo^{a,b,5}, P. Dini^a, F.M. Farina^{a,b}, S. Fiorendi^{a,b}, S. Gennai^{a,5}, A. Ghezzi^{a,b}, S. Malvezzi^a, R.A. Manzoni^{a,b}, A. Martelli^{a,b}, A. Massironi^{a,b}, D. Menasce^a, L. Moroni^a, P. Negri^{a,b,†}, M. Paganoni^{a,b}, D. Pedrini^a, A. Pullia^{a,b}, S. Ragazzi^{a,b}, N. Redaelli^a, S. Sala^a, T. Tabarelli de Fatis^{a,b}

^a INFN Sezione di Milano-Bicocca, Milano, Italy

^b Università di Milano-Bicocca, Milano, Italy

S. Buontempo^a, C.A. Carrillo Montoya^a, N. Cavallo^{a,29}, A. De Cosa^{a,b,5}, O. Dogangun^{a,b}, F. Fabozzi^{a,29}, A.O.M. Iorio^{a,b}, L. Lista^a, S. Meola^{a,30}, M. Merola^a, P. Paolucci^{a,5}

^a INFN Sezione di Napoli, Napoli, Italy

^b Università di Napoli "Federico II", Napoli, Italy

P. Azzi^a, N. Bacchetta^{a,5}, M. Bellato^a, M. Benettoni^a, M. Biasotto^{a,31}, D. Bisello^{a,b},
 A. Branca^{a,5}, R. Carlin^{a,b}, P. Checchia^a, T. Dorigo^a, U. Dosselli^a, F. Fanzago^a, F. Gasparini^{a,b},
 U. Gasparini^{a,b}, P. Giubilato^{a,b}, F. Gonella^a, A. Gozzelino^a, M. Gulmini^{a,31}, K. Kanishchev^{a,c},
 S. Lacaprara^a, I. Lazzizzera^{a,c}, M. Loretì^a, M. Margoni^{a,b}, G. Maron^{a,31}, M. Mazzucato^a,
 A.T. Meneguzzo^{a,b}, F. Montecassiano^a, M. Passaseo^a, J. Pazzini^{a,b}, M. Pegoraro^a, N. Pozzobon^{a,b},
 P. Ronchese^{a,b}, F. Simonetto^{a,b}, E. Torassa^a, M. Tosi^{a,b}, S. Vanini^{a,b}, S. Ventura^a, P. Zotto^{a,b},
 G. Zumerle^{a,b}

^a INFN Sezione di Padova, Padova, Italy

^b Università di Padova, Padova, Italy

^c Università di Trento (Trento), Padova, Italy

U. Berzano^a, M. Gabusi^{a,b}, S.P. Ratti^{a,b}, C. Riccardi^{a,b}, P. Torre^{a,b}, P. Vitulo^{a,b}

^a INFN Sezione di Pavia, Pavia, Italy

^b Università di Pavia, Pavia, Italy

M. Biasini^{a,b}, G.M. Bilei^a, L. Fanò^{a,b}, P. Lariccia^{a,b}, A. Lucaroni^{a,b,5}, G. Mantovani^{a,b}, M. Menichelli^a,
 A. Nappi^{a,b,†}, D. Passeri^{a,b}, P. Placidi^{a,b}, F. Romeo^{a,b}, A. Saha^a, A. Santocchia^{a,b}, L. Servoli^a,
 A. Spiezia^{a,b}, S. Taroni^{a,b}, M. Valdata^{a,b}

^a INFN Sezione di Perugia, Perugia, Italy

^b Università di Perugia, Perugia, Italy

F. Angelini^a, S. Arezzini^a, P. Azzurri^{a,c}, G. Bagliesi^a, A. Basti^a, R. Bellazzini^a, J. Bernardini^a, T. Boccali^a,
 F. Bosi^a, A. Brez^a, G. Broccolo^{a,c}, F. Calzolari^a, A. Carboni^a, R. Castaldi^a, C. Cerri^a, A. Ciampa^a,
 R.T. D’Agnolo^{a,c,5}, R. Dell’Orso^a, F. Fiori^{a,b,5}, L. Foà^{a,c}, A. Giassi^a, S. Giusti^a, A. Kraan^a, L. Latronico^a,
 F. Ligabue^{a,c}, S. Linari^a, T. Lomtadze^a, L. Martini^{a,32}, M. Massa^a, M.M. Massai^a, E. Mazzone^a,
 A. Messineo^{a,b}, A. Moggi^a, F. Palla^a, F. Raffaelli^a, A. Rizzi^{a,b}, G. Sanguinetti^a, G. Segneri^a,
 A.T. Serban^{a,33}, P. Spagnolo^a, G. Spandre^a, P. Squillacioti^{a,5}, R. Tenchini^a, G. Tonelli^{a,b}, A. Venturi^a,
 P.G. Verdini^a

^a INFN Sezione di Pisa, Pisa, Italy

^b Università di Pisa, Pisa, Italy

^c Scuola Normale Superiore di Pisa, Pisa, Italy

S. Baccaro^{a,34}, L. Barone^{a,b}, A. Bartoloni^a, F. Cavallari^a, I. Dafinei^a, D. Del Re^{a,b}, M. Diemoz^a, C. Fanelli,
 M. Grassi^{a,b,5}, E. Longo^{a,b}, P. Meridiani^{a,5}, F. Micheli^{a,b}, S. Nourbakhsh^{a,b}, G. Organtini^{a,b},
 R. Paramatti^a, S. Rahatlou^{a,b}, M. Sigamani^a, L. Soffi^{a,b}, I.G. Talamo^a

^a INFN Sezione di Roma, Roma, Italy

^b Università di Roma “La Sapienza”, Roma, Italy

N. Amapane^{a,b}, R. Arcidiacono^{a,c}, S. Argiro^{a,b}, M. Arneodo^{a,c}, C. Biino^a, N. Cartiglia^a, M. Costa^{a,b},
 N. Demaria^a, C. Mariotti^{a,5}, S. Maselli^a, E. Migliore^{a,b}, V. Monaco^{a,b}, M. Musich^{a,5}, M.M. Obertino^{a,c},
 N. Pastrone^a, M. Pelliccioni^a, C. Peroni^{a,b}, A. Potenza^{a,b}, A. Romero^{a,b}, M. Ruspà^{a,c}, R. Sacchi^{a,b},
 A. Solano^{a,b}, A. Staiano^a

^a INFN Sezione di Torino, Torino, Italy

^b Università di Torino, Torino, Italy

^c Università del Piemonte Orientale (Novara), Torino, Italy

F. Ambroglini^{a,b}, S. Belforte^a, V. Candelise^{a,b}, M. Casarsa^a, F. Cossutti^a, G. Della Ricca^{a,b}, B. Gobbo^a,
 C. Kavka^a, M. Marone^{a,b,5}, D. Montanino^{a,b,5}, A. Penzo^a, A. Schizzi^{a,b}

^a INFN Sezione di Trieste, Trieste, Italy

^b Università di Trieste, Trieste, Italy

T.Y. Kim, S.K. Nam

Kangwon National University, Chunchon, Republic of Korea

S. Chang, J. Chung, S.W. Ham, D. Han, J. Kang, D.H. Kim, G.N. Kim, J.E. Kim, K.S. Kim, D.J. Kong, M.W. Lee, Y.D. Oh, H. Park, S.R. Ro, D. Son, D.C. Son, J.S. Suh

Kyungpook National University, Daegu, Republic of Korea

J.Y. Kim, Zero J. Kim, S. Song

Chonnam National University, Institute for Universe and Elementary Particles, Kwangju, Republic of Korea

S. Choi, D. Gyun, B. Hong, M. Jo, Y. Jo, M. Kang, H. Kim, T.J. Kim, K.S. Lee, D.H. Moon, S.K. Park, K.S. Sim

Korea University, Seoul, Republic of Korea

M. Choi, G. Hahn, S. Kang, H. Kim, J.H. Kim, C. Park, I.C. Park, S. Park, G. Ryu

University of Seoul, Seoul, Republic of Korea

Y. Choi, Y.K. Choi, J. Goh, M.S. Kim, E. Kwon, B. Lee, J. Lee, S. Lee, H. Seo, I. Yu

Sungkyunkwan University, Suwon, Republic of Korea

M. Janulis, A. Juodagalvis, R. Naujikas

Vilnius University, Vilnius, Lithuania

H. Castilla-Valdez, E. De La Cruz-Burelo, I. Heredia-de La Cruz, R. Lopez-Fernandez, R. Magaña Villalba, J. Martínez-Ortega, A. Sánchez-Hernández, L.M. Villaseñor-Cendejas

Centro de Investigacion y de Estudios Avanzados del IPN, Mexico City, Mexico

S. Carrillo Moreno, F. Vazquez Valencia

Universidad Iberoamericana, Mexico City, Mexico

H.A. Salazar Ibarguen

Benemerita Universidad Autonoma de Puebla, Puebla, Mexico

E. Casimiro Linares, A. Morelos Pineda, M.A. Reyes-Santos

Universidad Autónoma de San Luis Potosí, San Luis Potosí, Mexico

P. Allfrey, D. Krofcheck

University of Auckland, Auckland, New Zealand

A.J. Bell, N. Bernardino Rodrigues, A.P.H. Butler, P.H. Butler, R. Doesburg, D. Pfeiffer, S. Reucroft, H. Silverwood, J.C. Williams

University of Canterbury, Christchurch, New Zealand

M. Ahmad, M.H. Ansari, M.I. Asghar, J. Butt, H.R. Hoorani, S. Khalid, W.A. Khan, T. Khurshid, S. Qazi, M.A. Shah, M. Shoaib

National Centre for Physics, Quaid-I-Azam University, Islamabad, Pakistan

H. Bialkowska, B. Boimska, T. Frueboes, R. Gokieli, L. Gosciolo, M. Górski, M. Kazana, I.M. Kudla, K. Nawrocki, K. Romanowska-Rybinska, M. Szleper, G. Wrochna, P. Zalewski

National Centre for Nuclear Research, Swierk, Poland

G. Brona, K. Bunkowski, M. Cwiok, H. Czyrkowski, R. Dabrowski, W. Dominik, K. Doroba, A. Kalinowski, M. Konecki, J. Krolikowski, W. Oklinski, K. Pozniak³⁵, W. Zabolotny³⁵, P. Zych

Institute of Experimental Physics, Faculty of Physics, University of Warsaw, Warsaw, Poland

G. Kasprowicz, R. Romaniuk

Warsaw University of Technology, Institute of Electronic Systems, Warsaw, Poland

R. Alemany-Fernandez, N. Almeida, P. Bargassa, A. David, P. Faccioli, P.G. Ferreira Parracho, M. Gallinaro, P.Q. Ribeiro, J. Seixas, J. Silva, J. Varela, P. Vischia

Laboratório de Instrumentação e Física Experimental de Partículas, Lisboa, Portugal

S. Afanasiev, I. Belotelov, P. Bunin, Y. Ershov, M. Gavrilenko, A. Golunov, I. Golutvin, N. Gorbounov, I. Gorbunov, I. Gramenitski, V. Kalagin, A. Kamenev, V. Karjavin, V. Konoplyanikov, V. Korenkov, G. Kozlov, A. Kurenkov, A. Lanev, A. Makankin, A. Malakhov, I. Melnitchenko, V.V. Mitsyn, P. Moisenz, D. Oleynik, A. Orlov, V. Palichik, V. Perelygin, A. Petrosyan, M. Savina, R. Semenov, S. Shmatov, S. Shulha, A. Skachkova, N. Skatchkov, V. Smetannikov, V. Smirnov, D. Smolin, E. Tikhonenko, S. Vasil'ev, A. Volodko, A. Zarubin, V. Zhiltsov

Joint Institute for Nuclear Research, Dubna, Russia

S. Evstyukhin, V. Golovtsov, Y. Ivanov, V. Kim, P. Levchenko, V. Murzin, V. Oreshkin, I. Smirnov, V. Sulimov, L. Uvarov, S. Vavilov, A. Vorobyev, An. Vorobyev

Petersburg Nuclear Physics Institute, Gatchina (St. Petersburg), Russia

Yu. Andreev, A. Anisimov, A. Dermenev, S. Gninenko, N. Golubev, D. Gorbunov, A. Karneyeu, M. Kirsanov, N. Krasnikov, V. Matveev, A. Pashenkov, G. Pivovarov, V.E. Postoev, V. Rubakov, V. Shirinyants, A. Solovey, D. Tlisov, A. Toropin, S. Troitsky

Institute for Nuclear Research, Moscow, Russia

V. Epshteyn, M. Erofeeva, V. Gavrillov, V. Kaftanov[†], I. Kiselevich, V. Kolosov, A. Konoplyannikov, M. Kossov, Y. Kozlov, A. Krokhotin, D. Litvintsev, N. Lychkovskaya, A. Oulianov, V. Popov, G. Safronov, S. Semenov, N. Stepanov, V. Stolin, E. Vlasov, V. Zaytsev, A. Zhokin

Institute for Theoretical and Experimental Physics, Moscow, Russia

A. Belyaev, E. Boos, V. Bunichev, A. Demiyarov, M. Dubinin⁴, L. Dudko, A. Ershov, A. Gribushin, V. Ilyin, A. Kaminskiy³⁶, V. Klyukhin, O. Kodolova, V. Korotkikh, A. Kryukov, I. Lokhtin, A. Markina, S. Obraztsov, M. Perfilov, S. Petrushanko, A. Popov, A. Proskuryakov, L. Sarycheva[†], V. Savrin, A. Snigirev, I. Vardanyan

Moscow State University, Moscow, Russia

V. Andreev, M. Azarkin, I. Dremin, M. Kirakosyan, A. Leonidov, G. Mesyats, S.V. Rusakov, A. Vinogradov

P.N. Lebedev Physical Institute, Moscow, Russia

I. Azhgirey, I. Bayshev, S. Bitiukov, V. Grishin⁵, V. Kachanov, A. Kalinin, D. Konstantinov, A. Korablev, V. Krychkine, A. Levine, V. Petrov, A. Ryabov, R. Ryutin, A. Sobol, V. Talov, L. Tourtchanovitch, S. Troshin, N. Tyurin, A. Uzunian, A. Volkov

State Research Center of Russian Federation, Institute for High Energy Physics, Protvino, Russia

P. Adzic³⁷, M. Djordjevic, M. Ekmedzic, D. Krpic³⁷, J. Milosevic, N. Smiljkovic, M. Zupan

University of Belgrade, Faculty of Physics and Vinca Institute of Nuclear Sciences, Belgrade, Serbia

M. Aguilar-Benitez, J. Alcaraz Maestre, P. Arce, C. Battilana, E. Calvo, M. Cerrada, M. Chamizo Llatas, N. Colino, B. De La Cruz, A. Delgado Peris, D. Domínguez Vázquez, C. Fernandez Bedoya, J.P. Fernández Ramos, A. Ferrando, J. Flix, M.C. Fouz, P. Garcia-Abia, O. Gonzalez Lopez, S. Goy Lopez, J.M. Hernandez, M.I. Josa, G. Merino, J. Puerta Pelayo, A. Quintario Olmeda, I. Redondo, L. Romero, J. Santaolalla, M.S. Soares, C. Willmott

Centro de Investigaciones Energéticas Medioambientales y Tecnológicas (CIEMAT), Madrid, Spain

C. Albajar, G. Codispoti, J.F. de Trocóniz

Universidad Autónoma de Madrid, Madrid, Spain

H. Brun, J. Cuevas, J. Fernandez Menendez, S. Folgueras, I. Gonzalez Caballero, L. Lloret Iglesias, J. Piedra Gomez

Universidad de Oviedo, Oviedo, Spain

J.A. Brochero Cifuentes, I.J. Cabrillo, A. Calderon, S.H. Chuang, J. Duarte Campderros, M. Felcini³⁸, M. Fernandez, G. Gomez, J. Gonzalez Sanchez, A. Graziano, C. Jorda, A. Lopez Virto, J. Marco, R. Marco, C. Martinez Rivero, F. Matorras, F.J. Munoz Sanchez, T. Rodrigo, A.Y. Rodríguez-Marrero, A. Ruiz-Jimeno, L. Scodellaro, M. Sobron Sanudo, I. Vila, R. Vilar Cortabitarte

Instituto de Física de Cantabria (IFCA), CSIC-Universidad de Cantabria, Santander, Spain

D. Abbaneo, P. Aspell, E. Auffray, G. Auzinger, M. Bachtis, J. Baechler, P. Baillon, A.H. Ball, D. Barney, J.F. Benitez, C. Bernet⁶, W. Bialas, G. Bianchi, P. Bloch, A. Bocci, A. Bonato, C. Botta, H. Breuker, D. Campi, T. Camporesi, E. Cano, G. Cerminara, A. Charkiewicz, T. Christiansen, J.A. Coarasa Perez, B. Curé, D. D'Enterria, A. Dabrowski, J. Daguin, A. De Roeck, S. Di Guida, M. Dobson, N. Dupont-Sagorin, A. Elliott-Peisert, M. Eppard, B. Frisch, W. Funk, A. Gaddi, M. Gastal, G. Georgiou, H. Gerwig, M. Giffels, D. Gigi, K. Gill, D. Giordano, M. Girone, M. Giunta, F. Glege, R. Gomez-Reino Garrido, P. Govoni, S. Gowdy, R. Guida, J. Gutleber, M. Hansen, P. Harris, C. Hartl, J. Harvey, B. Hegner, A. Hinzmann, A. Honma, V. Innocente, P. Janot, K. Kaadze, E. Karavakis, K. Kloukinas, K. Kousouris, P. Lecoq, Y.-J. Lee, P. Lenzi, R. Loos, C. Lourenço, N. Magini, T. Mäki, M. Malberti, L. Malgeri, M. Mannelli, A. Marchioro, J. Marques Pinho Noite, L. Masetti, F. Meijers, S. Mersi, E. Meschi, L. Moneta, M.U. Mozer, M. Mulders, P. Musella, A. Onnela, T. Orimoto, L. Orsini, J.A. Osborne, E. Palencia Cortezon, E. Perez, L. Perrozzi, P. Petagna, A. Petrilli, A. Petrucci, A. Pfeiffer, M. Pierini, M. Pimiä, D. Piparo, G. Polese, H. Postema, L. Quertenmont, A. Racz, W. Reece, D. Ricci, J. Rodrigues Antunes, G. Rolandi³⁹, C. Rovelli⁴⁰, M. Rovere, V. Ryjov, H. Sakulin, D. Samyn, F. Santanastasio, C. Schäfer, C. Schwick, A. Sciaba, I. Segoni, S. Sekmen, A. Sharma, P. Siegrist, P. Silva, M. Simon, P. Sphicas^{*,41}, D. Spiga, B.G. Taylor, P. Tropea, J. Troska, A. Tsirou, F. Vasey, L. Veillet, G.I. Veres²⁰, P. Vichoudis, J.R. Vlimant, P. Wertelaers, H.K. Wöhri, S.D. Worm⁴², W.D. Zeuner

CERN, European Organization for Nuclear Research, Geneva, Switzerland

W. Bertl, K. Deiters, W. Erdmann, D. Feichtinger, K. Gabathuler, R. Horisberger, Q. Ingram, H.C. Kaestli, S. König, D. Kotlinski, U. Langenegger, B. Meier, F. Meier, D. Renker, T. Rohe, T. Sakhelashvili⁴³

Paul Scherrer Institut, Villigen, Switzerland

L. Bäni, F. Behner, B. Betev, B. Blau, P. Bortignon, M.A. Buchmann, B. Casal, N. Chanon, Z. Chen, D.R. Da Silva Di Calafiori, S. Dambach⁴⁴, G. Davatz, A. Deisher, G. Dissertori, M. Dittmar, L. Djambazov, M. Donegà, M. Dünser, C. Eggel⁴⁴, J. Eugster, G. Faber, K. Freudenreich, C. Grab, W. Hintz, D. Hits, H. Hofer, O. Holme, I. Horvath, P. Lecomte, W. Lustermann, C. Marchica⁴⁴, A.C. Marini, P. Martinez Ruiz del Arbol, N. Mohr, F. Moortgat, C. Nägeli⁴⁴, P. Nef, F. Nessi-Tedaldi, F. Pandolfi, L. Pape, F. Pauss, M. Peruzzi, T. Punz, F.J. Ronga, U. Röser, M. Rossini, L. Sala, A.K. Sanchez, M.-C. Sawley, D. Schinzel, A. Starodumov⁴⁵, B. Stieger, H. Suter, M. Takahashi, L. Tauscher[†], A. Thea, K. Theofilatos, D. Treille, P. Trüb⁴⁴, S. Udriot, C. Urscheler, G. Viertel, H.P. von Gunten, R. Wallny, H.A. Weber, L. Wehrli, J. Weng, S. Zelepoukine⁴⁶

Institute for Particle Physics, ETH Zurich, Zurich, Switzerland

C. Amsler⁴⁷, V. Chiochia, S. De Visscher, C. Favaro, M. Ivova Rikova, B. Millan Mejias, P. Otiougova, P. Robmann, H. Snoek, S. Tupputi, M. Verzetti

Universität Zürich, Zurich, Switzerland

Y.H. Chang, K.H. Chen, W.T. Chen, A. Go, C.M. Kuo, S.W. Li, W. Lin, M.H. Liu, Z.K. Liu, Y.J. Lu, D. Mekterovic, A.P. Singh, R. Volpe, J.H. Wu, S.S. Yu

National Central University, Chung-Li, Taiwan

P. Bartalini, P. Chang, Y.H. Chang, Y.W. Chang, Y. Chao, K.F. Chen, C. Dietz, Z. Gao⁵, U. Grundler, W.-S. Hou, Y. Hsiung, K.Y. Kao, Y.J. Lei, J.J. Liao, S.W. Lin, R.-S. Lu, D. Majumder, E. Petrakou, X. Shi, J.G. Shiu, Y.M. Tzeng, K. Ueno, Y. Velikzhanin, X. Wan, C.C. Wang, M. Wang, J.T. Wei, P. Yeh

National Taiwan University (NTU), Taipei, Taiwan

B. Asavapibhop, N. Srimanobhas

Chulalongkorn University, Bangkok, Thailand

A. Adiguzel, M.N. Bakirci⁴⁸, S. Cerci⁴⁹, C. Dozen, I. Dumanoglu, E. Eskut, S. Girgis, G. Gokbulut, E. Gurpinar, I. Hos, E.E. Kangal, T. Karaman, G. Karapinar⁵⁰, A. Kayis Topaksu, G. Onengut, K. Ozdemir, S. Ozturk⁵¹, A. Polatoz, K. Sogut⁵², D. Sunar Cerci⁴⁹, B. Tali⁴⁹, H. Topakli⁴⁸, L.N. Vergili, M. Vergili

Cukurova University, Adana, Turkey

I.V. Akin, T. Aliev, B. Bilin, M. Deniz, H. Gamsizkan, A.M. Guler, K. Ocalan, A. Ozpineci, M. Serin, R. Sever, U.E. Surat, M. Zeyrek

Middle East Technical University, Physics Department, Ankara, Turkey

M. Deliomeroğlu, E. Gülmez, B. Isildak⁵³, M. Kaya⁵⁴, O. Kaya⁵⁴, S. Ozkorucuklu⁵⁵, N. Sonmez⁵⁶

Bogazici University, Istanbul, Turkey

K. Cankocak

Istanbul Technical University, Istanbul, Turkey

B. Grynyov

Institute of Single Crystals of National Academy of Science, Kharkov, Ukraine

L. Levchuk, S. Lukyanenko, D. Soroka, P. Sorokin

National Scientific Center, Kharkov Institute of Physics and Technology, Kharkov, Ukraine

M.K.H. Ahmad, A. Branson, R. McClatchey, M. Odeh, J. Shamdasani, K. Soomro

Centre for Complex Cooperative Systems, University of the West of England, Bristol, United Kingdom

T. Barrass, F. Bostock, J.J. Brooke, E. Clement, D. Cussans, H. Flacher, R. Frazier, J. Goldstein, M. Grimes, G.P. Heath, H.F. Heath, L. Kreczko, W. Laceso, S. Metson, D.M. Newbold⁴², K. Nirunpong, A. Poll, S. Senkin, V.J. Smith, T. Williams

University of Bristol, Bristol, United Kingdom

L. Basso⁵⁷, E. Bateman, K.W. Bell, A. Belyaev⁵⁷, C. Brew, R.M. Brown, B. Camanzi, D.J.A. Cockerill, J.F. Connolly[†], J.A. Coughlan, L.G. Denton, P.S. Flower, M.J. French, R.J.S. Greenhalgh, R.N.J. Halsall, K. Harder, S. Harper, J.A. Hill, J. Jackson, B.W. Kennedy, A.L. Lintern, A.B. Lodge, E. Olaiya, M.R. Pearson, D. Petyt, B.C. Radburn-Smith, C.H. Shepherd-Themistocleous, B.J. Smith, M. Sproston, R. Stephenson, I.R. Tomalin, M.J. Torbet, J.H. Williams[†], W.J. Womersley

Rutherford Appleton Laboratory, Didcot, United Kingdom

R. Bainbridge, G. Ball, J. Ballin, D. Bauer, R. Beuselinck, O. Buchmuller, D. Colling, N. Cripps, M. Cutajar, P. Dauncey, G. Davies, M. Della Negra, W. Ferguson, J. Fulcher, D. Futyan, A. Gilbert, A. Guneratne Bryer, G. Hall, Z. Hatherell, J. Hays, G. Iles, M. Jarvis, J. Jones, G. Karapostoli, M. Kenzie, J. Leaver, L. Lyons,

A.-M. Magnan, J. Marrouche, B. Mathias, D.G. Miller, R. Nandi, J. Nash, A. Nikitenko⁴⁵, M. Noy, A. Papageorgiou, J. Pela, M. Pesaresi, K. Petridis, M. Pioppi⁵⁸, D. Rand, D.M. Raymond, S. Rogerson, A. Rose, M.J. Ryan, C. Seez, P. Sharp[†], A. Sparrow, M. Stoye, A. Tapper, C. Timlin, S. Tourneur, M. Vazquez Acosta, T. Virdee, S. Wakefield, N. Wardle, T. Whyntie, M. Wingham, O. Zorba

Imperial College, London, United Kingdom

M. Chadwick, J.E. Cole, P.R. Hobson, A. Khan, P. Kyberd, D. Leggat, D. Leslie, W. Martin, I.D. Reid, P. Symonds, L. Teodorescu, M. Turner

Brunel University, Uxbridge, United Kingdom

J. Dittmann, K. Hatakeyama, H. Liu, T. Scarborough

Baylor University, Waco, USA

O. Charaf, C. Henderson, P. Rumerio

The University of Alabama, Tuscaloosa, USA

A. Avetisyan, T. Bose, E. Carrera Jarrin, C. Fantasia, E. Hazen, A. Heister, J.St. John, P. Lawson, D. Lazic, J. Rohlf, D. Sperka, L. Sulak, F. Varela Rodriguez, S. Wu

Boston University, Boston, USA

J. Alimena, S. Bhattacharya, D. Cutts, Z. Demiragli, A. Ferapontov, A. Garabedian, U. Heintz, R. Hooper, S. Jabeen, G. Kukartsev, E. Laird, G. Landsberg, M. Luk, M. Narain, D. Nguyen, M. Segala, T. Sinthuprasith, T. Speer, K.V. Tsang, Z. Unalan

Brown University, Providence, USA

R. Breedon, G. Breto, M. Calderon De La Barca Sanchez, M. Case, S. Chauhan, M. Chertok, J. Conway, R. Conway, P.T. Cox, J. Dolen, R. Erbacher, M. Gardner, G. Grim, J. Gunion, B. Holbrook, W. Ko, A. Kopecky, R. Lander, F.C. Lin, T. Miceli, P. Murray, M. Nikolic, D. Pellett, F. Ricci-tam, J. Rowe, B. Rutherford, M. Searle, J. Smith, M. Squires, M. Tripathi, R. Vasquez Sierra, R. Yohay

University of California, Davis, Davis, USA

V. Andreev, K. Arisaka, D. Cline, R. Cousins, J. Duris, S. Erhan, P. Everaerts, C. Farrell, J. Hauser, M. Ignatenko, C. Jarvis, J. Kubic, S. Otwinowski, C. Plager, G. Rakness, P. Schlein[†], P. Traczyk, V. Valuev, M. Weber, X. Yang, Y. Zheng

University of California, Los Angeles, Los Angeles, USA

J. Babb, R. Clare, M.E. Dinardo, J. Ellison, J.W. Gary, F. Giordano, G. Hanson, G.Y. Jeng⁵⁹, J.G. Layter, H. Liu, O.R. Long, A. Luthra, H. Nguyen, S. Paramesvaran, B.C. Shen[†], J. Sturdy, S. Sumowidagdo, R. Wilken, S. Wimpenny

University of California, Riverside, Riverside, USA

W. Andrews, J.G. Branson, G.B. Cerati, M. Cinquilli, S. Cittolin, D. Evans, F. Golf, A. Holzner, R. Kelley, M. Lebourgeois, J. Letts, I. Macneill, B. Mangano, T. Martin, A. Mrak-Tadel, S. Padhi, C. Palmer, G. Petrucciani, M. Pieri, M. Sani, I. Sfiligoi, V. Sharma, S. Simon, E. Sudano, M. Tadel, Y. Tu, A. Vartak, S. Wasserbaech⁶⁰, F. Würthwein, A. Yagil, J. Yoo

University of California, San Diego, La Jolla, USA

D. Barge, R. Bellan, C. Campagnari, M. D'Alfonso, T. Danielson, K. Flowers, P. Geffert, J. Incandela, C. Justus, P. Kalavase, S.A. Koay, D. Kovalskyi, V. Krutelyov, S. Kyre, S. Lowette, G. Magazzu, N. Mccoll, V. Pavlunin, F. Rebassoo, J. Ribnik, J. Richman, R. Rossin, D. Stuart, W. To, C. West, D. White

University of California, Santa Barbara, Santa Barbara, USA

D. Adamczyk, A. Apresyan, A. Barczyk, A. Bornheim, J. Bunn, Y. Chen, G. Denis, E. Di Marco, J. Duarte, P. Galvez, M. Gataullin, D. Kcira, I. Legrand, V. Litvine, Y. Ma, Z. Maxa, A. Mott, A. Mughal, D. Nae, H.B. Newman, S. Ravot, C. Rogan, S.G. Rozsa, S. Shevchenko, K. Shin, M. Spiropulu, C. Steenberg, M. Thomas, V. Timciuc, F. van Lingen, J. Veverka, B.R. Voicu, R. Wilkinson, S. Xie, Y. Yang, L. Zhang, K. Zhu, R.Y. Zhu

California Institute of Technology, Pasadena, USA

B. Akgun, V. Azzolini, A. Calamba, R. Carroll, T. Ferguson, Y. Iiyama, D.W. Jang, S.Y. Jun, Y.F. Liu, M. Paulini, J. Russ, N. Terentyev, H. Vogel, I. Vorobiev

Carnegie Mellon University, Pittsburgh, USA

J.P. Cumalat, B.R. Drell, W.T. Ford, A. Gaz, B. Heyburn, D. Johnson, E. Luiggi Lopez, U. Nauenberg, J.G. Smith, K. Stenson, K.A. Ulmer, S.R. Wagner, S.L. Zang

University of Colorado at Boulder, Boulder, USA

L. Agostino, J. Alexander, A. Chatterjee, N. Eggert, L.K. Gibbons, B. Heltsley, A. Khukhunaishvili, B. Kreis, V. Kuznetsov, N. Mirman, G. Nicolas Kaufman, J.R. Patterson, D. Riley, A. Ryd, E. Salvati, S. Stroiney, W. Sun, W.D. Teo, J. Thom, J. Thompson, J. Tucker, J. Vaughan, Y. Weng, L. Winstrom, P. Wittich

Cornell University, Ithaca, USA

D. Winn

Fairfield University, Fairfield, USA

S. Abdullin, M. Albert, M. Albrow, J. Anderson, G. Apollinari, M. Atac[†], W. Badgett, J.A. Bakken, B. Baldin, K. Banicz, L.A.T. Bauerdick, A. Beretvas, J. Berryhill, P.C. Bhat, M. Binkley[†], F. Borchering, K. Burkett, J.N. Butler, V. Chetluru, H.W.K. Cheung, F. Chlebana, S. Cihangir, W. Dagenhart, G. Derylo, C. Dumitrescu, D. Dykstra, D.P. Eartly, J.E. Elias[†], V.D. Elvira, G. Eulisse, D. Evans, D. Fagan, I. Fisk, S. Foulkes, J. Freeman, I. Gaines, Y. Gao, P. Garton, L. Giacchetti, E. Gottschalk, D. Green, Y. Guo, O. Gutsche, A. Hahn, J. Hanlon, R.M. Harris, J. Hirschauer, B. Holzman, B. Hooberman, J. Howell, C.h. Huang, D. Hufnagel, S. Jindariani, M. Johnson, C.D. Jones, U. Joshi, E. Juska, B. Kilminster, B. Klima, S. Kunori, S. Kwan, K. Larson, C. Leonidopoulos, J. Linacre, D. Lincoln, R. Lipton, J.A. Lopez Perez, S. Los, J. Lykken, K. Maeshima, J.M. Marraffino, S. Maruyama, D. Mason, P. McBride, T. McCauley, K. Mishra, S. Moccia, R.K. Mommsen, S. Mrenna, Y. Musienko⁶¹, S. Muzaffar, C. Newman-Holmes, V. O'Dell, I. Osborne, J. Pivarski, S. Popescu²⁷, R. Pordes, O. Prokofyev, V. Rapsevicius, A. Ronzhin, P. Rossman, S. Ryu, E. Sexton-Kennedy, S. Sharma, T.M. Shaw, R.P. Smith[†], A. Soha, W.J. Spalding, L. Spiegel, W. Tanenbaum, L. Taylor, R. Thompson, A. Tiradani, S. Tkaczyk, N.V. Tran, L. Tuura, L. Uplegger, E.W. Vaandering, R. Vidal, J. Whitmore, W. Wu, F. Yang, J. Yarba, J.C. Yun, T. Zimmerman

Fermi National Accelerator Laboratory, Batavia, USA

D. Acosta, P. Avery, V. Barashko, D. Bourilkov, M. Chen, T. Cheng, S. Das, M. De Gruttola, G.P. Di Giovanni, D. Dobur, S. Dolinsky, A. Drozdetskiy, R.D. Field, M. Fisher, Y. Fu, I.K. Furic, J. Gartner, L. Gorn, D. Holmes, J. Hugon, B. Kim, J. Konigsberg, A. Korytov, A. Kropivnitskaya, T. Kypreos, J.F. Low, A. Madorsky, K. Matchev, P. Milenovic⁶², G. Mitselmakher, L. Muniz, M. Park, R. Remington, A. Rinkevicius, B. Scurlock, N. Skhirtladze, M. Snowball, J. Stasko, J. Yelton, M. Zakaria

University of Florida, Gainesville, USA

V. Gaultney, S. Hewamanage, L.M. Lebolo, S. Linn, P. Markowitz, G. Martinez, J.L. Rodriguez

Florida International University, Miami, USA

T. Adams, A. Askew, M. Bertoldi, J. Bochenek, J. Chen, W.G.D. Dharmaratna, B. Diamond, S.V. Gleyzer, J. Haas, S. Hagopian, V. Hagopian, M. Jenkins, K.F. Johnson, H. Prosper, S. Tentindo, V. Veeraraghavan, M. Weinberg

Florida State University, Tallahassee, USA

M.M. Baarmand, B. Dorney, M. Hohlmann, H. Kalakhety, R. Ralich, I. Vodopiyanov, F. Yumiceva

Florida Institute of Technology, Melbourne, USA

M.R. Adams, I.M. Anghel, L. Apanasevich, Y. Bai, V.E. Bazterra, R.R. Betts, I. Bucinskaite, J. Callner, R. Cavanaugh, M.H. Chung, O. Evdokimov, E.J. Garcia-Solis, L. Gauthier, C.E. Gerber, D.J. Hofman, R. Hollis, A. Iordanova, S. Khalatyan, G.J. Kunde⁶³, F. Lacroix, M. Malek, C. O'Brien, C. Silkworth, C. Silvestre, A. Smoron, D. Strom, P. Turner, N. Varelas

University of Illinois at Chicago (UIC), Chicago, USA

U. Akgun, E.A. Albayrak, A.S. Ayan, B. Bilki⁶⁴, W. Clarida, P. Debbins, F. Duru, F.D. Ingram, E. McCliment, J.-P. Merlo, H. Mermerkaya⁶⁵, A. Mestvirishvili, M.J. Miller, A. Moeller, J. Nachtman, C.R. Newsom, E. Norbeck, J. Olson, Y. Onel, F. Ozok⁶⁶, I. Schmidt, S. Sen, P. Tan, E. Tiras, J. Wetzel, T. Yetkin, K. Yi

The University of Iowa, Iowa City, USA

B.A. Barnett, B. Blumenfeld, S. Bolognesi, D. Fehling, G. Giurgiu, A.V. Gritsan, Z.J. Guo, G. Hu, P. Maksimovic, S. Rappoccio, M. Swartz, A. Whitbeck

Johns Hopkins University, Baltimore, USA

P. Baringer, A. Bean, G. Benelli, D. Coppage, O. Grachov, R.P. Kenny Iii, M. Murray, D. Noonan, V. Radicci, S. Sanders, R. Stringer, G. Tinti, J.S. Wood, V. Zhukova

The University of Kansas, Lawrence, USA

A.F. Barfuss, T. Bolton, I. Chakaberia, A. Ivanov, S. Khalil, M. Makouski, Y. Maravin, S. Shrestha, I. Svintradze

Kansas State University, Manhattan, USA

J. Gronberg, D. Lange, D. Wright

Lawrence Livermore National Laboratory, Livermore, USA

A. Baden, R. Bard, M. Boutemour, B. Calvert, S.C. Eno, J.A. Gomez, T. Grassi, N.J. Hadley, R.G. Kellogg, M. Kirn, T. Kolberg, Y. Lu, M. Marionneau, A.C. Mignerey, K. Pedro, A. Peterman, K. Rossato, A. Skuja, J. Temple, M.B. Tonjes, S.C. Tonwar, T. Toole, E. Twedt

University of Maryland, College Park, USA

A. Apyan, G. Bauer, J. Bendavid, W. Busza, E. Butz, I.A. Cali, M. Chan, V. Dutta, G. Gomez Ceballos, M. Goncharov, K.A. Hahn, Y. Kim, M. Klute, K. Krajczar⁶⁷, A. Levin, P.D. Luckey, T. Ma, S. Nahn, C. Paus, D. Ralph, C. Roland, G. Roland, M. Rudolph, G.S.F. Stephans, F. Stöckli, K. Sumorok, K. Sung, D. Velicanu, E.A. Wenger, R. Wolf, B. Wyslouch, M. Yang, Y. Yilmaz, A.S. Yoon, M. Zanetti

Massachusetts Institute of Technology, Cambridge, USA

D. Bailleux, S.I. Cooper, P. Cushman, B. Dahmes, A. De Benedetti, R. Egeland, G. Franzoni, A. Gude, J. Haupt, A. Inyakin, S.C. Kao, K. Klapoetke, Y. Kubota, J. Mans, N. Pastika, R. Rusack, A. Singovsky, N. Tambe, J. Turkewitz

University of Minnesota, Minneapolis, USA

L.M. Cremaldi, R. Kroeger, L. Perera, R. Rahmat, J. Reidy, D.A. Sanders, D. Summers

University of Mississippi, University, USA

G. Attebury, E. Avdeeva, K. Bloom, B. Bockelman, S. Bose, D.R. Claes, A. Dominguez, M. Eads, J. Keller, I. Kravchenko, J. Lazo-Flores, C. Lundstedt, H. Malbouisson, S. Malik, R. Snihur, G.R. Snow, D. Swanson

University of Nebraska-Lincoln, Lincoln, USA

U. Baur, A. Godshalk, I. Iashvili, S. Jain, A. Kharchilava, A. Kumar, S.P. Shipkowski, K. Smith

State University of New York at Buffalo, Buffalo, USA

G. Alverson, E. Barberis, D. Baumgartel, M. Chasco, J. Haley, J. Moromisato, D. Nash, J. Swain, D. Trocino, E. Von Goeler, D. Wood, J. Zhang

Northeastern University, Boston, USA

A. Anastassov, B. Gobbi, A. Kubik, L. Lusito, N. Odell, R.A. Ofierzynski, B. Pollack, A. Pozdnyakov, M. Schmitt, S. Stoynev, M. Velasco, S. Won

Northwestern University, Evanston, USA

L. Antonelli, B. Baumbaugh, D. Berry, A. Brinkerhoff, K.M. Chan, A.H. Heering, M. Hildreth, C. Jessop, D.J. Karmgard, N. Kellams, J. Kolb, K. Lannon, W. Luo, S. Lynch, N. Marinelli, D.M. Morse, T. Pearson, M. Planer, R. Ruchti, J. Slaunwhite, N. Valls, M. Wayne, M. Wolf, A. Woodard

University of Notre Dame, Notre Dame, USA

B. Bylsma, L.S. Durkin, C. Hill, R. Hughes, K. Kotov, T.Y. Ling, D. Puigh, M. Rodenburg, C.J. Rush, V. Sehgal, C. Vuosalo, G. Williams, B.L. Winer

The Ohio State University, Columbus, USA

N. Adam, E. Berry, P. Elmer, D. Gerbaudo, V. Halyo, P. Hebda, J. Hegeman, A. Hunt, P. Jindal, D. Lopes Pegna, P. Lujan, D. Marlow, T. Medvedeva, M. Mooney, J. Olsen, P. Piroué, X. Quan, A. Raval, H. Saka, D. Stickland, C. Tully, J.S. Werner, T. Wildish, Z. Xie, S.C. Zenz, A. Zuranski

Princeton University, Princeton, USA

J.G. Acosta, M. Bonnett Del Alamo, E. Brownson, X.T. Huang, A. Lopez, H. Mendez, S. Oliveros, J.E. Ramirez Vargas, A. Zatserklyaniy

University of Puerto Rico, Mayaguez, USA

E. Alagoz, K. Arndt, V.E. Barnes, D. Benedetti, G. Bolla, D. Bortoletto, A. Bujak, M. De Mattia, A. Everett, L. Gutay, Z. Hu, M. Jones, O. Koybasi, M. Kress, A.T. Laasanen, J. Lee, N. Leonardo, C. Liu, V. Maroussov, P. Merkel, D.H. Miller, J. Miyamoto, N. Neumeister, C. Rott, A. Roy, I. Shipsey, D. Silvers, A. Svyatkovskiy, M. Vidal Marono, H.D. Yoo, J. Zablocki, Y. Zheng

Purdue University, West Lafayette, USA

S. Guragain, N. Parashar

Purdue University Calumet, Hammond, USA

A. Adair, C. Boulahouache, V. Cuplov, K.M. Ecklund, F.J.M. Geurts, S.J. Lee, W. Li, J.H. Liu, M. Matveev, B.P. Padley, R. Redjimi, J. Roberts, A. Tumanov, P. Yepes, J. Zabel

Rice University, Houston, USA

B. Betchart, A. Bodek, H. Budd, Y.S. Chung, R. Covarelli, P. de Barbaro, R. Demina, Y. Eshaq, T. Ferbel, A. Garcia-Bellido, G. Ginther, P. Goldenzweig, Y. Gotra, J. Han, A. Harel, S. Korjenevski, D.C. Miner, D. Orbaker, W. Sakumoto, P. Slattery, D. Vishnevskiy, M. Zielinski

University of Rochester, Rochester, USA

A. Bhatti, R. Ciesielski, L. Demortier, K. Goulios, G. Lungu, S. Malik, C. Mesropian

The Rockefeller University, New York, USA

S. Arora, A. Barker, J.P. Chou, C. Contreras-Campana, E. Contreras-Campana, D. Duggan, D. Ferencek, Y. Gershtein, R. Gray, E. Halkiadakis, D. Hidas, A. Lath, S. Panwalkar, M. Park, R. Patel, V. Rekovic, J. Robles, K. Rose, S. Salur, S. Schnetzer, C. Seitz, S. Somalwar, R. Stone, S. Thomas

Rutgers, the State University of New Jersey, Piscataway, USA

G. Cerizza, M. Hollingsworth, G. Raghianti, S. Spanier, Z.C. Yang, A. York

University of Tennessee, Knoxville, USA

O. Bouhali, R. Eusebi, W. Flanagan, J. Gilmore, T. Kamon⁶⁸, V. Khotilovich, R. Montalvo, C.N. Nguyen, I. Osipenkov, Y. Pakhotin, A. Perloff, J. Roe, A. Safonov, T. Sakuma, S. Sengupta, I. Suarez, A. Tatarinov, D. Toback

Texas A&M University, College Station, USA

N. Akchurin, J. Damgov, C. Dragoiu, P.R. Duderu, C. Jeong, K. Kovitanggoon, S.W. Lee, T. Libeiro, Y. Roh, A. Sill, I. Volobouev, R. Wigmans

Texas Tech University, Lubbock, USA

E. Appelt, A.G. Delannoy, D. Engh, C. Florez, W. Gabella, S. Greene, A. Gurrola, W. Johns, P. Kurt, C. Maguire, A. Melo, M. Sharma, P. Sheldon, B. Snook, S. Tuo, J. Velkovska

Vanderbilt University, Nashville, USA

D. Andelin, M.W. Arenton, M. Balazs, S. Boutle, S. Conetti, B. Cox, B. Francis, J. Goodell, R. Hirosky, A. Ledovskoy, C. Lin, C. Neu, D. Phillips II, J. Wood

University of Virginia, Charlottesville, USA

S. Gollapinni, R. Harr, P.E. Karchin, C. Kottachchi Kankanamge Don, P. Lamichhane, M. Mattson, C. Milstène, A. Sakharov

Wayne State University, Detroit, USA

M. Anderson, D. Belknap, J.N. Bellinger, L. Borrello, D. Bradley, D. Carlsmith, M. Cepeda, I. Crotty⁵, S. Dasu, F. Feyzi, E. Friis, T. Gorski, L. Gray, K.S. Grogg, M. Grothe, R. Hall-Wilton, M. Herndon, A. Hervé, P. Klabbers, J. Klukas, J. Lackey, A. Lanaro, C. Lazaridis, J. Leonard, R. Loveless, S. Lusin⁵, M. Magrans de Abril, W. Maier, A. Mohapatra, I. Ojalvo, F. Palmonari, G.A. Pierro, D. Reeder, I. Ross, A. Savin, W.H. Smith, J. Swanson, D. Wenman

University of Wisconsin, Madison, USA

* Corresponding author.

† Deceased.

¹ Also at Vienna University of Technology, Vienna, Austria.

² Also at National Institute of Chemical Physics and Biophysics, Tallinn, Estonia.

³ Also at Universidade Federal do ABC, Santo Andre, Brazil.

⁴ Also at California Institute of Technology, Pasadena, USA.

⁵ Also at CERN, European Organization for Nuclear Research, Geneva, Switzerland.

⁶ Also at Laboratoire Leprince-Ringuet, Ecole Polytechnique, IN2P3–CNRS, Palaiseau, France.

⁷ Also at Suez Canal University, Suez, Egypt.

⁸ Also at Zewail City of Science and Technology, Zewail, Egypt.

- ⁹ Also at Cairo University, Cairo, Egypt.
- ¹⁰ Also at Fayoum University, El-Fayoum, Egypt.
- ¹¹ Also at British University, Cairo, Egypt.
- ¹² Now at Ain Shams University, Cairo, Egypt.
- ¹³ Also at National Centre for Nuclear Research, Swierk, Poland.
- ¹⁴ Also at Université de Haute-Alsace, Mulhouse, France.
- ¹⁵ Also at Joint Institute for Nuclear Research, Dubna, Russia.
- ¹⁶ Also at Moscow State University, Moscow, Russia.
- ¹⁷ Also at Brandenburg University of Technology, Cottbus, Germany.
- ¹⁸ Also at The University of Kansas, Lawrence, USA.
- ¹⁹ Also at Institute of Nuclear Research ATOMKI, Debrecen, Hungary.
- ²⁰ Also at Eötvös Loránd University, Budapest, Hungary.
- ²¹ Also at Tata Institute of Fundamental Research – HECR, Mumbai, India.
- ²² Now at King Abdulaziz University, Jeddah, Saudi Arabia.
- ²³ Also at University of Visva-Bharati, Santiniketan, India.
- ²⁴ Also at Sharif University of Technology, Tehran, Iran.
- ²⁵ Also at Isfahan University of Technology, Isfahan, Iran.
- ²⁶ Also at Plasma Physics Research Center, Science and Research Branch, Islamic Azad University, Teheran, Iran.
- ²⁷ Also at Horia Hulubei National Institute of Physics and Nuclear Engineering (IFIN-HH), Bucharest, Romania.
- ²⁸ Also at Facoltà Ingegneria Università di Roma, Roma, Italy.
- ²⁹ Also at Università della Basilicata, Potenza, Italy.
- ³⁰ Also at Università degli Studi Guglielmo Marconi, Roma, Italy.
- ³¹ Also at Laboratori Nazionali di Legnaro dell' INFN, Legnaro, Italy.
- ³² Also at Università degli Studi di Siena, Siena, Italy.
- ³³ Also at University of Bucharest, Faculty of Physics, Bucuresti-Magurele, Romania.
- ³⁴ Also at ENEA – Casaccia Research Center, S. Maria di Galeria, Italy.
- ³⁵ Also at Warsaw University of Technology, Institute of Electronic Systems, Warsaw, Poland.
- ³⁶ Also at INFN Sezione di Padova; Università di Padova; Università di Trento (Trento), Padova, Italy.
- ³⁷ Also at Faculty of Physics of University of Belgrade, Belgrade, Serbia.
- ³⁸ Also at University of California, Los Angeles, Los Angeles, USA.
- ³⁹ Also at Scuola Normale e Sezione dell'INFN, Pisa, Italy.
- ⁴⁰ Also at INFN Sezione di Roma; Università di Roma "La Sapienza", Roma, Italy.
- ⁴¹ Also at University of Athens, Athens, Greece.
- ⁴² Also at Rutherford Appleton Laboratory, Didcot, United Kingdom.
- ⁴³ Also at Institute of High Energy Physics and Informatization, Tbilisi State University, Tbilisi, Georgia.
- ⁴⁴ Also at Paul Scherrer Institut, Villigen, Switzerland.
- ⁴⁵ Also at Institute for Theoretical and Experimental Physics, Moscow, Russia.
- ⁴⁶ Also at University of Wisconsin, Madison, USA.
- ⁴⁷ Also at Albert Einstein Center for Fundamental Physics, Bern, Switzerland, BERN, SWITZERLAND.
- ⁴⁸ Also at Gaziosmanpasa University, Tokat, Turkey.
- ⁴⁹ Also at Adiyaman University, Adiyaman, Turkey.
- ⁵⁰ Also at Izmir Institute of Technology, Izmir, Turkey.
- ⁵¹ Also at The University of Iowa, Iowa City, USA.
- ⁵² Also at Mersin University, Mersin, Turkey.
- ⁵³ Also at Ozyegin University, Istanbul, Turkey.
- ⁵⁴ Also at Kafkas University, Kars, Turkey.
- ⁵⁵ Also at Suleyman Demirel University, Isparta, Turkey.
- ⁵⁶ Also at Ege University, Izmir, Turkey.
- ⁵⁷ Also at School of Physics and Astronomy, University of Southampton, Southampton, United Kingdom.
- ⁵⁸ Also at INFN Sezione di Perugia; Università di Perugia, Perugia, Italy.
- ⁵⁹ Also at University of Sydney, Sydney, Australia.
- ⁶⁰ Also at Utah Valley University, Orem, USA.
- ⁶¹ Also at Institute for Nuclear Research, Moscow, Russia.
- ⁶² Also at University of Belgrade, Faculty of Physics and Vinca Institute of Nuclear Sciences, Belgrade, Serbia.
- ⁶³ Also at Los Alamos National Laboratory, Los Alamos, USA.
- ⁶⁴ Also at Argonne National Laboratory, Argonne, USA.
- ⁶⁵ Also at Erzincan University, Erzincan, Turkey.
- ⁶⁶ Also at Mimar Sinan University, Istanbul, Istanbul, Turkey.
- ⁶⁷ Also at KFKI Research Institute for Particle and Nuclear Physics, Budapest, Hungary.
- ⁶⁸ Also at Kyungpook National University, Daegu, Republic of Korea.